Title
Developing MitoPunch Mitochondrial Transfer to Enable Stable Transplantation of Human Mitochondrial DNA

Author
Sercel, Alexander John

Publication Date
2021

Peer reviewed|Thesis/dissertation

UNIVERSITY OF CALIFORNIA

Los Angeles

Developing MitoPunch Mitochondrial Transfer to Enable Stable Transplantation of Human Mitochondrial DNA

A dissertation submitted in partial satisfaction of the requirements for the degree Doctor of Philosophy in Molecular Biology

by

Alexander John Sercel

2021

ABSTRACT OF THE DISSERTATION

Developing MitoPunch Mitochondrial Transfer

to Enable Stable Transplantation

of Human Mitochondrial DNA

by

Alexander John Sercel

Doctor of Philosophy in Molecular Biology

University of California, Los Angeles, 2021

Professor Michael Alan Teitell, Chair

Mitochondria, often considered simple cellular powerhouses that generate ATP by oxidative phosphorylation, are essential organelles found in all nucleated mammalian cells that play integral roles in apoptosis, Ca^{2+} signaling, reactive oxygen species generation, metabolism, and other critical cellular processes. Mitochondria are unique among organelles in that they contain multiple copies of their own genome (mtDNA) that is replicated and translated independently of the nuclear DNA (nDNA). Mitochondrial function is dependent upon the compatibility of the gene products of these two genomes and the coordination of their gene expression, and the current lack of methods to edit the mtDNA presents a major roadblock to dissecting the contribution of mtDNA sequence to cell fitness. There exist techniques to specify mtDNA-

nDNA combinations in mammalian cells by delivery of isolated mitochondria into mtDNA depleted cells, however these approaches are technically challenging or restricted to a narrow range of manipulatable cell types. Novel methods that facilitate isolated mitochondrial transfer and generation of stable isolated mitochondrial recipient (SIMR) cells with known mtDNA-nDNA pairings are crucial to enable studies of mitonuclear communication, metabolism, and cell fate determination. To overcome these limitations we developed MitoPunch, a high-throughput, easily-assembled, pressure-driven mitochondrial transfer platform that can generate SIMR cell lines from mitochondria isolated from cell lines and donor tissue and a wide range of mtDNA depleted transformed or replication-limited cells. In this dissertation we present the method to construct and implement the MitoPunch apparatus, data demonstrating the generation of SIMR clones from mtDNA-depleted transformed and primary cell lines using MitoPunch, and a proof of principle pipeline for engineering induced pluripotent stem cells and differentiated cell types from SIMR clones produced using MitoPunch. The results found in this thesis suggest that MitoPunch enables for the first time the high throughput generation of stable mtDNA specified cell lines for use in detailed molecular studies of mtDNA-nDNA interactions.

The dissertation of Alexander John Sercel is approved.

Stephen Lawrence Zipursky

Orian Shirihai

Thomas G. Graeber

Bennett G. Novitch

Michael Alan Teitell, Committee Chair

University of California, Los Angeles

2021

This dissertation is dedicated to my many teachers

who have helped me become myself.

Table of Contents

List of Figures

Chapter 2: More than a powerplant: the influence of mitochondrial transfer on the epigenome

Chapter 3: Stable transplantation of human mitochondrial DNA by high-throughput, pressurized isolated mitochondrial delivery

Acknowledgements

Completing my dissertation has been anything but an individual effort, and I owe a great debt of gratitude to many individuals for their support and input throughout the past six years.

I first want to thank my advisor, Dr. Michael Teitell, for the guidance, encouragement, and intellectual freedom he provided throughout my thesis work. Mike pushed me to think rigorously and independently and taught me first-hand the value of reaching across disciplines to do great science. I would also like to thank my PhD thesis committee, Dr. Lawrence Zipursky, Dr. Orian Shirihai, Dr. Thomas Graeber, and Dr. Bennett Novitch for their key feedback on my work.

Next, I want to thank every member of the Teitell laboratory who I have had the great pleasure of working with. Thank you to Fasih Ahsan, Junior Torres, Amy Yu, Alexander Napior, Dr. Lynnea Waters, Dr. Laura Jimenez, Emma Dawson, Garret Guyot, Dr. Diane Kim, Dr. Dian Huang, Thang Nguyen, Vivian Lu, and Dr. Jason Hong. I am especially grateful to Dr. Alexander Patananan for his mentorship and collaboration throughout my thesis work. I would also like to specifically thank Stephanie Kennedy for the countless ways she has helped me grow and for always lending me a strong shoulder to lean on when the going was hard. I additionally want to thank my dear friends, Mark Crawford, Melissa Anderson, Steven Shushnar, Andy Vong, and Kayla Valpey, who have kept me sane and grounded throughout my time at UCLA.

Lastly, thank you to my family for their constant love and support. I want to give special thanks to my parents, Dr. Joel and Cynthia Sercel, for providing me with an incredible intellectual and moral foundation that has enabled all that I have done. Everything I have accomplished I owe to you. Finally, I want to thank my two brothers and closest friends, Christopher and Nicholas Sercel, for continually inspiring me to do and be my very best.

Chapter 2 was originally published in Current Opinion in Physiology. Alexander N. Patananan, Alexander J. Sercel, and Michael A. Teitell. 2018. More than a powerplant: the influence of mitochondrial transfer on the epigenome. Current Opinion in Physiology volume 3, pages 16-24 (2017). It is accessible online with the DOI: https://doi.org/10.1016/j.cophys.2017.11.006. It is reprinted here with permission by Elsevier. This work was conducted under the direction and in the laboratory of MAT. ANP and AJS were supported by NIH NRSA Grants CA009120 and GM007185, respectively. MAT was supported by AFOSR Grant FA9550-15-1-0406; NIH Grants GM114188, GM073981, and CA185189; and by a California Institute for Regenerative Medicine grant, RT3-07678. We also acknowledged the Library of Science and Medical Illustrations (http://www.somersault1824.com/)

Chapter 3 was originally published in eLife. Alexander J. Sercel*, Alexander N. Patananan*, Tianxing Man, Ting-Hsiang Wu, Amy K. Yu, Garret W. Guyot, Sharooz Rabizadeh, Kayvan R. Niazi, Pei-Yu Chiou, and Michael A. Teitell. 2021. Stable transplantation of human mitochondrial DNA by high-throughput, pressurized isolated mitochondrial delivery. eLife volume 10, e6102. It is accessible online with the DOI: https://doi.org/10.7554/eLife.63102. It is reprinted here with permission under the Creative Commons Attribution 4.0 International License (CC BY 4.0

https://creativecommons.org/licenses/by/4.0/legalcode). AJS was supported by NIH NRSA Grants CA009120 and GM007185. This work was conducted under the direction and in the laboratory of MAT. ANP was supported by NIH NRSA Grant CA009120 and AHA Grant 18POST34080342. AKY was supported by NI NRSA Grant GM007185. P-.Y. Chiou was supported by the NIH (R01GM114188) and by the Air Force Office of Scientific Research (FA9550-15-1-0406). M.A.T. was supported by the Air Force Office of Scientific Research (FA9550-15-1-0406), the NIH (R01GM114188, R01GM073981, R01CA185189, R21CA227480, R01GM127985, and P30CA016042), and CIRM (RT3-07678).

Chapter 4 was originally published in STAR Protocols. Alexander J. Sercel, Alexander J. Napior, Alexander N. Patananan, Ting-Hsiang Wu, Pei-Yu Chiou, Michael A. Teitell. 2021. Generating stable isolated mitochondrial recipient clones in mammalian cells using MitoPunch mitochondrial transfer. Volume 2, Issue 4. It is accessible online at DOI: https://doi.org/10.1016/j.xpro.2021.100850. It is reprinted here with permission under the Creative Commons License Attribution-NonCommercial-NoDerivatives 4.0 International License (CC BY-NC-ND 4.0 https://creativecommons.org/licenses/by-nc-nd/4.0/legalcode). This work was conducted under the direction and in the laboratory of MAT. A.J.S. was supported by the NIH (T32GM007185 and T32CA009120). A.N.P. was supported by the NIH (T32CA009120) and American Heart Association (18POST34080342). P.-Y.C. was supported by the NSF (CBET 1404080), the NIH (RO1GM114188), and the Air Force Office of Scientific Research (FA9550-15-1-0406). M.A.T. was supported by the Air Force Office of Scientific Research (FA9550-15-1-0406), the Department of Defense (W81XWH2110139), the NIH

(R01GM114188, R01GM073981, R01CA185189, R21CA227480, R01GM127985, and P30CA016042), and CIRM (RT3-07678).

Chapter 5 was originally published in Scientific Reports. Emma R. Dawson, Alexander N. Patananan, Alexander J. Sercel, and Michael A. Teitell. 2020. Stable retention of chloramphenicol-resistant mtDNA to rescue metabolically impaired cells. Volume 10, 14328. It is accessible online at DOI: https://doi.org/10.1038/s41598-020-71199-0. It is reprinted here with permission under the Creative Commons Attribution 4.0 International License (CC BY 4.0 https://creativecommons.org/licenses/by/4.0/legalcode). This work was conducted under the direction and in the laboratory of MAT. E.R.D. was supported by the NIH (GM55052 and 5T34GM008563). A.N.P. was supported by the NIH (T32CA009120) and American Heart Association (18POST34080342). A.J.S. was supported by the NIH (T32GM007185 and T32CA009120). M.A.T. was supported by the Air Force Office of Scientific Research (FA9550-15-1-0406), the NIH (R01GM114188, R01GM073981, R01CA185189, R21CA227480, R01GM127985, and P30CA016042), and by CIRM (RT3-07678).

Chapter 6 was originally published in Trends in Cell Biology. Alexander J. Sercel*, Natasha M. Carlson*, Alexander N. Patananan, and Michael A. Teitell. Mitochondrial DNA Dynamics in Reprogramming to Pluripotency. 2021. Volume 31, number 4. It is accessible online at DOI: https://doi.org/10.1016/j.tcb.2020.12.009. It is reprinted here with permission under the Creative Commons License Attribution-NonCommercial-NoDerivatives 4.0 International License (CC BY-NC-ND 4.0 https://creativecommons.org/licenses/by-nc-nd/4.0/legalcode). A.J.S. was supported by two NIH National Research Service Award fellowships (T32GM007185

and T32CA009120). N.M.C was supported by the California Institute for Regenerative Medicine Grant EDUC2-08411. A.N.P. was supported by the NIH (T32CA009120) and American Heart Association (18POST34080342). M.A.T. was supported by the Air Force Office of Scientific Research (FA9550-15-1-0406), the NIH (R01GM114188, R01GM073981, R01CA185189, R21CA227480, R01GM127985, and P30CA016042), and by CIRM (RT3-07678).

Chapter 7 was originally published in Cell Reports. Alexander N. Patananan*, Alexander J. Sercel*, Ting-Hsiang Wu, Fasih M. Ahsan, Alejandro Torres, Jr., Stephanie A.L. Kennedy, Amy Vandiver, Amanda J. Collier, Artin Mehrabi, Jon Van Lew, Lise Zakin,
Noe Rodriguez, Marcos Sixto, Wael Tadros, Adam Lazar, Peter A. Sieling, Thang L. Nguyen, Emma R. Dawson, Daniel Braas, Justin Golovato, Luis Cisneros, Charles Vaske, Kathrin Plath, Shahrooz Rabizadeh, Kayvan R. Niazi, Pei-Yu Chiou, and Michael A. Teitell. 2020. Volume 33, number 108562. It is accessible online at DOI: https://doi.org/10.1016/j.celrep.2020.108562. It is reprinted here with permission under the Creative Commons License Attribution-NonCommercial-NoDerivatives 4.0 International License (CC BY-NC-ND 4.0 https://creativecommons.org/licenses/by-nc-nd/4.0/legalcode). This work was conducted under the direction and in the laboratory of MAT. A.N.P. was supported by the NIH (T32CA009120) and American Heart Association (18POST34080342). A.J.S. was supported by the NIH (T32GM007185 and T32CA009120). K.P. was supported by the Broad Center of Regenerative Medicine and Stem Cell Research at UCLA, the David Geffen School of Medicine, the NIH (P01GM099134), and a Faculty Scholar grant from the HHMI. M.A.T. was supported by the Air Force Office of Scientific Research (FA9550-15-1-0406), the NIH (R01GM114188,

R01GM073981, R01CA185189, R21CA227480, R01GM127985, and P30CA016042), and CIRM (RT3-07678).

Vita

Education

2015-Present: **University of California, Los Angeles**

- Doctoral Candidate, Molecular Biology Interdepartmental Training Program (MBIDP)
- Thesis Advisor: Michael Teitell MD, PhD

2011-2015: **University of California, Santa Barbara**

- Bachelor of Arts in Biology from the College of Creative Studies
- Graduated with Highest Honors, overall GPA 3.92
- Studied abroad at Lund University, Sweden

Publications

Sercel AJ*, Patananan AN*, Man T, Wu T-H, Yu AK, Guyot GW, Rabizadeh S, Niazi KR, Chiou P-Y, Teitell MA. (2021). Stable transplantation of human mitochondrial DNA by high-throughput, pressurized isolated mitochondrial delivery. eLife. doi: 10.7554/eLife.63102. PMCID: PMC7864630

Sercel AJ*, Carlson N*, Patananan AN, Teitell MA (2020). Mitochondrial DNA Dynamics in Reprogramming to Pluripotency. Trends in Cell Biology. doi: 10.1016/j.tcb.2020.12.009. PMID: 33422359

Patananan AN*, **Sercel AJ***, Wu T-H*, Ahsan FM, Torres AJ, Kennedy SA, Vandiver A, Collier AJ, Mehrabi A, Van Lew J, Zakin L, Rodriguez N, Sixto M, Tadros W, Lazar A, Sieling PA, Nguyen TL, Dawson ER, Braas D, Golovato J, Cisneros L, Vaske C, Plath K, Rabizadeh S, Niazi KR, Chiou P-Y, Teitell MA. (2020) Pressure-Driven Mitochondrial Transfer Pipeline Generates Mammalian Cells of Desired Genetic Combinations and Fates. Cell Reports 33, 108562. doi: 10.1016/j.celrep.2020.108562. PMID: 33378680

Dawson ER, Patananan AN, **Sercel AJ**, and Teitell MA (2020) Stable retention of chloramphenicol-resistant mtDNA to rescue metabolically impaired cells. Scientific Reports 10, 14328. doi: 10.1038/s41598-020-71199-0. PMCID: PMC7459123

Patananan AN, **Sercel AJ**, Teitell MA. (2018) More than a powerplant: the influence of mitochondrial transfer on the epigenome. Current Opinion in Physiology, 3:16-24. doi: 10.1016/j.cophys.2017.11.006. PMCID: PMC5937705

Ganguly P, Do TD, Larini L, LaPointe NE, **Sercel AJ**, Shade MF, Feinstein SC, Bowers MT, Shea JE. (2015) Tau assembly: the dominant role of PHF6 (VQIVYK) in microtubule binding region repeat R3. J. Phys. Chem B. 119(13):4582-93. doi: 10.1021/acs.jpcb.5b00175. PMCID: PMC4428543

*Authors contributed equally

Presentations

Sercel, A.J., Patananan, A.N., et al. (2020). Efficient and stable rescue of respiration in mtDNA deficient cells using a high throughput mitochondrial transfer platform. Oral presentation at the UCLA MBIDP Virtual Retreat: September 25-27 2020

Sercel, A.J., Patananan, A.N., et al. (2019). Efficient and stable rescue of respiration in mtDNA deficient cells using a high throughput mitochondrial transfer platform. Poster presentation at the UCLA Mito Symposium: November 8, 2019

Sercel AJ, Patananan, AN, et al. (2019). Efficient and stable rescue of respiration in mtDNA deficient cells using a high throughput mitochondrial transfer platform. Poster presentation at the Mitochondrial Biogenesis and Dynamics in Health and Disease Conference, Palm Springs, California: May 19-24, 2019

Sercel AJ, Patananan, AN, et al. (2018). Efficient and stable rescue of respiration in mtDNA deficient cells using a high throughput mitochondrial transfer platform. Poster presentation at the UCLA Mito Symposium, Los Angeles, California: November 2, 2018

Sercel AJ, Patananan, AN, et al. (2018). A novel mitochondrial transfer platform efficiently and stably rescues respiration in mtDNA-deficient cells. Poster presentation at the Cell Symposia: Multifaceted Mitochondria, Paradise Point, San Diego, California: June 4-6, 2018

Sercel AJ, Patananan AN, Wu T-H, et al. (2018) A novel mitochondrial transfer platform efficiently and stably rescues respiration in mtDNA-deficient cells. Poster presentation at the UCLA MBIDP Retreat, Ventura, California: March 17-18, 2018

Sercel AJ, Patananan AN, Wu T-H, et al. (2018). A novel mitochondrial transfer tool for metabolic engineering. Poster presentation at the UCLA MBIDP Retreat, Ventura, California: April 22-23, 2017

Grants and Awards

2018-2021:	T32CA009120, UCLA Tumor Immunology Training Program
2019:	UCLA Grad Slam Finalist
2016-2018:	T32GM007185, UCLA Cellular and Molecular Biology Training Program
2016:	UCLA Entering Mentoring Training Program Awardee
2016:	UCLA Ethics Case Study Competition Awardee
2015:	UCSB New Venture Competition, Second Place
2015:	UCSB New Venture Competition, Elings Prize Recipient
2014:	UCSB Undergraduate Research and Creative Activities Awardee
2014:	Caltech Amgen Scholar

Chapter 1: Introduction

Mitochondria and mitochondrial DNA

Mitochondria, thought to have originated from an ancient symbiosis between an endosymbiotic a-proteobacteria and its Asgard Archaea host, are organelles essential to eukaryotic life present in dozens to thousands of copies in every nucleated mammalian cell (Roger et al., 2017). Unique among mammalian organelles, mitochondria contain up to thousands of copies of their own 16,569 bp circular, maternally inherited genome (mtDNA) which is replicated independently of the nuclear genome (nDNA) (Giles et al., 1980). Mitochondria generate up to 90 percent of cellular ATP by oxidative phosphorylation (OXPHOS) driven by the mitochondrial electron transport chain (ETC) (Harris and Das, 1991). Far from simple biochemical powerplants, mitochondria play crucial roles in cellular metabolism through their involvement in the production, degradation, and/or regulation of tricarboxylic acid (TCA) cycle metabolites (Martinez-Reyes and Chandel, 2020), reactive oxygen species (ROS) (Ott et al., 2007), fatty acids (Holloway et al., 2009), and one-carbon metabolic intermediates (Bao et al., 2016) among other pathways (Chen et al., 2016).

Mitochondria are composed of more than 1000 proteins encoded between the nDNA and the mtDNA (Calvo and Mootha, 2010). In humans, the mtDNA codes for only 37 genes including 13 proteins directly required for OXPHOS and linked to metabolite biosynthesis. Proper mitochondrial function depends upon the joint function of the gene products of the mtDNA and the nDNA (Wolff et al., 2014), and mutations to mitochondrial proteins in either genome can impact mitochondrial metabolism and OXPHOS and cause disease in humans (Wallace, 2018). 1 in 200 people are carriers of mtDNA disease-related mutations, however, mtDNA mutations lead to pathology in only 1 in 5000 people (Patananan et al., 2016). The majority of

individuals harboring such mtDNA mutations do not exhibit pathologic phenotypes due to the high copy number of mtDNA in each nucleated mammalian cell (Alston et al., 2017). Because each cell can contain up to hundreds of individual copies of the mtDNA, the deleterious effects of mutant mtDNA can be compensated for by functional, wildtype mtDNA present alongside the mutant (Stefano et al., 2017). The phenomenon of a heterogeneous population of mtDNA within a single cell is known as heteroplasmy (Nissanka and Moraes, 2020), and the proportion of the total mtDNA made up by a specific mtDNA sequence is called the heteroplasmic ratio (Sercel et al., 2021a). In this way, the heteroplasmic ratio of a specific mtDNA variant can dictate the nature and degree of its impact on mitochondrial function in a cell, organ, or patient (Grady et al., 2018; Kandel et al., 2017; Picard et al., 2014; Pinti et al., 2019).

mtDNA editing

A critical roadblock to basic studies of mtDNA and nDNA coordination and translational application of gene therapy to diseases of the mtDNA is the inability to edit the mtDNA within mammalian cells (Patananan et al., 2016). Zinc finger endonucleases and TALENs specific for the mtDNA can reduce levels of specific mtDNA sequences in heteroplasmic cells and even animals when engineered with mitochondria-targeting leader sequences (Bacman et al., 2018; Gammage et al., 2018), but they suffer from low efficiency and the inability to knock-in desired gene sequences. This is potentially due to the multi-copy nature of mitochondria and the mtDNA and the double membrane structure of the mitochondria making efficient delivery of genome editing reagents to all copies of the mtDNA technically difficult or impossible. CRISPR-Cas based DNA editing has sparked a revolution in nuclear genetic engineering, however, its

dependance on guide RNA, which cannot be imported into the mitochondria, renders it ineffective for mtDNA editing (Falkenberg and Hirano, 2020). Additionally, it has been thought that mitochondria lack the robust DNA repair mechanisms found in the nucleus that enable recovery from double strand DNA breaks, however, this point is debated (Bohr and Anson, 1999; Stein and Sia, 2017; Zinovkina, 2018). These factors together make targeting DNA editing enzymes to the matrices of a cell's entire mitochondrial population technically challenging and altering the mtDNA sequence with conventional means nearly impossible. An exciting new approach to edit specific nucleotides in the mtDNA using a bacterial cytidine deaminase toxin enables a limited repertoire of point mutations; however, it is hindered by low efficiency (Mok et al., 2020).

Mitochondrial transfer

As a result of the current impasse to mtDNA editing, flexible 'reverse genetics' experiments to measure the effect of specific mtDNA sequences and heteroplasmies on mitochondrial and cellular metabolism and activity are not feasible outside of a highly limited repertoire of model combinations (Ishikawa and Nakada, 2021). A growing body of work demonstrates that transfer of mitochondria between cells occurs *in vitro* and *in vivo* and provides a potential path around this roadblock (Patananan et al., 2016; Singh et al., 2017). Such transfer events can result from direct cell-to-cell delivery of mitochondria via tunneling nanotubes, release of mitochondria packaged in extracellular vesicles uptaken by recipient cells, or coincubation of isolated mitochondria with recipient cells (Hayakawa et al., 2016; Kitani et al., 2014; Spees et al., 2006). While the mechanisms controlling these phenomena are unknown, several reports suggest

mitochondrial transfer as a protective mechanism against cellular stress (Paliwal et al., 2018; Shanmughapriya et al., 2020).

In many of these reports, mitochondrial recipient cells show alterations in metabolism and behavior following mitochondrial transfer, however most of these studies observe only temporary changes to cellular or organ function (Jiang et al., 2016; Kesner et al., 2016; Kitani et al., 2014). A minority of these reports have coincubated isolated mitochondria with cells depleted of mtDNA (ρ0) and observed rescue of ρ0 respiration and stable retention of the exogenous mtDNA, potentially enabling a path to specify the mtDNA and nDNA in cells as an alternative to mtDNA editing (Clark and Shay, 1982; Patel et al., 2017). However, these approaches require large quantities of donor material or the presence of a selection marker on the exogenous mtDNA which drastically restricts the diversity of mtDNA that can be used for such mtDNA transplantation experiments.

The efficiency of ρ0 cell rescue by isolated mitochondrial transfer is increased by using methods that deliver mitochondria directly into the recipient cell cytoplasm instead of relying on cellular uptake mechanisms, such as membrane disruption (King and Attardi, 1988; Wu et al., 2016) or cell fusion with enucleated cytoplasts (cybridization) (Wilkins et al., 2014). While more efficient than coincubating recipient cells with isolated mitochondria, these methods are typically laborious, technically challenging, and dependent upon immortalized cancer cells as mitochondrial recipients which reduces physiologic relevance of the resulting rescue clones. One exciting recent study generated a single clone expressing desired mtDNA and nDNA along with 11 false-positive clones using cybrid fusion with primary, Hayflick-limited cells,

however, the reproducibility and applicability of this approach to other mtDNA-nDNA combinations is unknown (Wong et al., 2017). More efficient methods to specify the mtDNA-nDNA sequences in a wide variety of cell types are necessary to enable detailed studies of mitochondrial function and disease in mammalian systems.

MitoPunch

To overcome these limitations, we developed a simple, high-throughput device called MitoPunch capable of transferring isolated mitochondria into ~1 x 10^5 adherent cells simultaneously (Sercel et al., 2021b). Briefly, ρ0 recipient cells are seeded on a polyethylene terephthalate (PET) filter membrane containing 3 μm holes. This filter is pressed against a polydimethylsiloxane (PDMS) reservoir filled with a suspension of isolated mitochondria to create a seal. MitoPunch employs a solenoid-activated plunger which strikes the PDMS reservoir to pressurize the mitochondrial suspension, generating small perforations in the recipient cell membranes through the holes in the PET filter which allow isolated mitochondria directly into the recipient cell cytoplasm. This direct access to the cytoplasm and endogenous mitochondrial network is the key to facilitating efficient stable transplantation of exogenous mtDNA into recipient cells. Following MitoPunch transfer, recipient cells are collected and subjected to a restrictive medium selection for ~7 d, after which stable isolated mitochondrial recipient (SIMR) clones with rescued mtDNA content and respiration emerge which can be counted to measure rescue efficiency or isolated for further analysis.

MitoPunch is an enabling technology for generating dozens to hundreds of SIMR clones from a wide range of starting materials. We have successfully produced SIMR cell lines from

transformed and replication limited ρ0 recipient cells using mitochondria isolated from wildtype and mtDNA mutant cell lines, human donor peripheral blood mononuclear cells, and freshly dissected mouse organs. Moreover, MitoPunch can generate heteroplasmic SIMR clones if the transferred mitochondrial isolate is prepared by mixing mitochondria isolated from different cell sources. The following chapters of this thesis document the impact of mitochondrial metabolism and mtDNA heteroplasmy on cell fate and function, the development of the MitoPunch apparatus for generating SIMR clones from a wide range of cell and tissue sources, and the application of MitoPunch to investigating and engineering mtDNA-nDNA interactions.

Chapter summaries

Chapter 2 of this thesis is a detailed review of the metabolites produced by the mitochondria that influence the state of the epigenome. This chapter provides a metabolic context for how mitochondrial function regulates cell fate and function, and how mitochondrial transfer, both *in vitro* and *in vivo*, can influence epigenetic marks. The work was previously published in the form of a Review in the journal Current Opinion in Physiology in 2018 by the laboratory of Dr. Michael Teitell.

Chapter 3 of this thesis describes the mechanism, function, and application of the MitoPunch apparatus and was previously published as a Tools and Resources article entitled "Stable transplantation of human mitochondrial DNA by high-throughput, pressurized isolated mitochondrial delivery" in the journal eLife in 2021 by the laboratory of Dr. Michael Teitell. This work demonstrates the unique utility of MitoPunch by comparing it to coincubation with

isolated mitochondria and another published pressure-driven mitochondrial transfer method, MitoCeption (Caicedo et al., 2015).

Chapter 4 of this thesis is a detailed protocol for fabricating, constructing, and implementing the MitoPunch apparatus including instructions for selecting, quantifying, and isolating SIMR clones. This work has been submitted as a manuscript entitled "Generating stable isolated mitochondrial recipient clones in mammalian cells using MitoPunch mitochondrial transfer" to the journal STAR Protocols and is currently in revision.

Chapter 5 of this thesis extends the application of MitoPunch from transferring isolated mitochondria into ρ0 recipient cells to using MitoPunch to replace mutant mtDNA with respiration-competent wildtype mtDNA without mtDNA depletion. This work shows that transfer of wildtype mtDNA-containing isolated mitochondria into mtDNA mutant recipient cells followed by uridine-depletion selection alone does not yield SIMR clones. However, transfer of mitochondria bearing a resistance marker to the antibiotic chloramphenicol into mtDNA mutant cells followed by selection with uridine-deplete, chloramphenicol supplemented medium does yield SIMR clones bearing only the respiration-competent, chloramphenicol-resistant mtDNA. This study was published as an Article in the journal Scientific Reports in 2020 by the laboratory of Dr. Michael Teitell.

Chapter 6 of this thesis is a literature review and meta-analysis of the field of induced pluripotent stem cell (iPSC) mitochondria and mtDNA heteroplasmy. The work is focused on the significance of mitochondrial metabolism and heteroplasmy on iPSC fate and function and

the phenomenon of heteroplasmic shifts between somatic cell and iPSC fate through reprogramming. This review includes a meta-analysis of studies that have quantified changes in heteroplasmy between somatic cells and the iPSCs derived from them and highlights the paucity of detailed work investigating this phenomenon. This chapter was previously published as a Review entitled "Mitochondrial DNA Dynamics in Reprogramming to Pluripotency" in the journal Trends in Cell Biology in 2020 by the laboratory of Dr. Michael Teitell.

Chapter 7 of this thesis describes work demonstrating MitoPunch as a key part of a pipeline to generate iPSC lines containing specified mtDNA and nDNA combinations. In this study, we generate SIMR clones from three ρ0 human fibroblast lines using mitochondria isolated from human donor peripheral blood mononuclear cells and from the HEK293T cell line, reprogram them to iPSC fate, differentiate them to a mesenchymal stem cell fate, and finally demonstrate the functionality of the SIMR mesenchymal stem cells by differentiating them into adipocytes, osteoblasts, and chondrocytes. We measured the whole transcriptome of these SIMR lines at fibroblast, iPSC, and mesenchymal stem cell fates and compared the transcript abundance to unmanipulated controls. We observed large differences in gene expression between SIMR and parental lines at the fibroblast fate which were almost completely resolved following reprogramming and differentiation. This study demonstrates the utility of MitoPunch as a tool for manipulating the mtDNA genotype of iPSCs for basic research and potential clinical application and shows that SIMR cell transcription is aberrant prior to reprogramming and differentiation. This work was published as a Resource entitled "Pressure-Driven Mitochondrial Transfer Pipeline Generates Mammalian Cells of Desired Genetic Combinations and Fates" in the journal Cell Reports in 2020 by the laboratory of Dr. Michael Teitell.

References

Alston, C.L., Rocha, M.C., Lax, N.Z., Turnbull, D.M., and Taylor, R.W. (2017). The genetics and pathology of mitochondrial disease. J Pathol *241*, 236-250.

Bacman, S.R., Kauppila, J.H.K., Pereira, C.V., Nissanka, N., Miranda, M., Pinto, M., Williams, S.L., Larsson, N.G., Stewart, J.B., and Moraes, C.T. (2018). MitoTALEN reduces mutant mtDNA load and restores tRNA(Ala) levels in a mouse model of heteroplasmic mtDNA mutation. Nat Med *24*, 1696-1700.

Bao, X.R., Ong, S.E., Goldberger, O., Peng, J., Sharma, R., Thompson, D.A., Vafai, S.B., Cox, A.G., Marutani, E., Ichinose, F., et al. (2016). Mitochondrial dysfunction remodels one-carbon metabolism in human cells. Elife *5*.

Bohr, V.A., and Anson, R.M. (1999). Mitochondrial DNA repair pathways. J Bioenerg Biomembr *31*, 391-398.

Caicedo, A., Fritz, V., Brondello, J.M., Ayala, M., Dennemont, I., Abdellaoui, N., de Fraipont, F., Moisan, A., Prouteau, C.A., Boukhaddaoui, H., et al. (2015). MitoCeption as a new tool to assess the effects of mesenchymal stem/stromal cell mitochondria on cancer cell metabolism and function. Sci Rep *5*, 9073.

Calvo, S.E., and Mootha, V.K. (2010). The mitochondrial proteome and human disease. Annu Rev Genomics Hum Genet *11*, 25-44.

Chen, W.W., Freinkman, E., Wang, T., Birsoy, K., and Sabatini, D.M. (2016). Absolute Quantification of Matrix Metabolites Reveals the Dynamics of Mitochondrial Metabolism. Cell *166*, 1324-1337 e1311.

Clark, M.A., and Shay, J.W. (1982). Mitochondrial transformation of mammalian cells. Nature *295*, 605-607.

Falkenberg, M., and Hirano, M. (2020). Editing the Mitochondrial Genome. N Engl J Med *383*, 1489-1491.

Gammage, P.A., Viscomi, C., Simard, M.L., Costa, A.S.H., Gaude, E., Powell, C.A., Van Haute, L., McCann, B.J., Rebelo-Guiomar, P., Cerutti, R., et al. (2018). Genome editing in mitochondria corrects a pathogenic mtDNA mutation in vivo. Nat Med *24*, 1691-1695.

Giles, R.E., Blanc, H., Cann, H.M., and Wallace, D.C. (1980). Maternal inheritance of human mitochondrial DNA. Proc Natl Acad Sci U S A *77*, 6715-6719.

Grady, J.P., Pickett, S.J., Ng, Y.S., Alston, C.L., Blakely, E.L., Hardy, S.A., Feeney, C.L., Bright, A.A., Schaefer, A.M., Gorman, G.S., et al. (2018). mtDNA heteroplasmy level and copy number indicate disease burden in m.3243A>G mitochondrial disease. EMBO Mol Med *10*.

Harris, D.A., and Das, A.M. (1991). Control of mitochondrial ATP synthesis in the heart. Biochem J *280 (Pt 3)*, 561-573.

Hayakawa, K., Esposito, E., Wang, X., Terasaki, Y., Liu, Y., Xing, C., Ji, X., and Lo, E.H. (2016). Transfer of mitochondria from astrocytes to neurons after stroke. Nature *535*, 551-555.

Holloway, G.P., Bonen, A., and Spriet, L.L. (2009). Regulation of skeletal muscle mitochondrial fatty acid metabolism in lean and obese individuals. Am J Clin Nutr *89*, 455S-462S.

Ishikawa, K., and Nakada, K. (2021). Attempts to understand the mechanisms of mitochondrial diseases: The reverse genetics of mouse models for mitochondrial disease. Biochim Biophys Acta Gen Subj *1865*, 129835.

Jiang, D., Gao, F., Zhang, Y., Wong, D.S., Li, Q., Tse, H.F., Xu, G., Yu, Z., and Lian, Q. (2016). Mitochondrial transfer of mesenchymal stem cells effectively protects corneal epithelial cells from mitochondrial damage. Cell Death Dis *7*, e2467.

Kandel, J., Picard, M., Wallace, D.C., and Eckmann, D.M. (2017). Mitochondrial DNA 3243A>G heteroplasmy is associated with changes in cytoskeletal protein expression and cell mechanics. J R Soc Interface *14*.

Kesner, E.E., Saada-Reich, A., and Lorberboum-Galski, H. (2016). Characteristics of Mitochondrial Transformation into Human Cells. In Sci Rep (Springer Science and Business Media LLC), p. 26057.

King, M.P., and Attardi, G. (1988). Injection of mitochondria into human cells leads to a rapid replacement of the endogenous mitochondrial DNA. Cell *52*, 811-819.

Kitani, T., Kami, D., Matoba, S., and Gojo, S. (2014). Internalization of isolated functional mitochondria: involvement of macropinocytosis. J Cell Mol Med *18*, 1694-1703.

Martinez-Reyes, I., and Chandel, N.S. (2020). Mitochondrial TCA cycle metabolites control physiology and disease. Nat Commun *11*, 102.

Mok, B.Y., de Moraes, M.H., Zeng, J., Bosch, D.E., Kotrys, A.V., Raguram, A., Hsu, F., Radey, M.C., Peterson, S.B., Mootha, V.K., et al. (2020). A bacterial cytidine deaminase toxin enables CRISPR-free mitochondrial base editing. Nature *583*, 631-637.

Nissanka, N., and Moraes, C.T. (2020). Mitochondrial DNA heteroplasmy in disease and targeted nuclease-based therapeutic approaches. EMBO Rep *21*, e49612.

Ott, M., Gogvadze, V., Orrenius, S., and Zhivotovsky, B. (2007). Mitochondria, oxidative stress and cell death. Apoptosis *12*, 913-922.

Paliwal, S., Chaudhuri, R., Agrawal, A., and Mohanty, S. (2018). Regenerative abilities of mesenchymal stem cells through mitochondrial transfer. J Biomed Sci *25*, 31.

Patananan, A.N., Wu, T.H., Chiou, P.Y., and Teitell, M.A. (2016). Modifying the Mitochondrial Genome. Cell Metab *23*, 785-796.

Patel, D., Rorbach, J., Downes, K., Szukszto, M.J., Pekalski, M.L., and Minczuk, M. (2017). Macropinocytic entry of isolated mitochondria in epidermal growth factor-activated human osteosarcoma cells. In Sci Rep (Springer Science and Business Media LLC).

Picard, M., Zhang, J., Hancock, S., Derbeneva, O., Golhar, R., Golik, P., O'Hearn, S., Levy, S., Potluri, P., Lvova, M., et al. (2014). Progressive increase in mtDNA 3243A>G heteroplasmy causes abrupt transcriptional reprogramming. Proc Natl Acad Sci U S A *111*, E4033-4042.

Pinti, M.V., Fink, G.K., Hathaway, Q.A., Durr, A.J., Kunovac, A., and Hollander, J.M. (2019). Mitochondrial dysfunction in type 2 diabetes mellitus: an organ-based analysis. Am J Physiol Endocrinol Metab *316*, E268-E285.

Roger, A.J., Munoz-Gomez, S.A., and Kamikawa, R. (2017). The Origin and Diversification of Mitochondria. Curr Biol *27*, R1177-R1192.

Sercel, A.J., Carlson, N.M., Patananan, A.N., and Teitell, M.A. (2021a). Mitochondrial DNA Dynamics in Reprogramming to Pluripotency. Trends Cell Biol *31*, 311-323.

Sercel, A.J., Patananan, A.N., Man, T., Wu, T.H., Yu, A.K., Guyot, G.W., Rabizadeh, S., Niazi, K.R., Chiou, P.Y., and Teitell, M.A. (2021b). Stable transplantation of human mitochondrial DNA by high-throughput, pressurized isolated mitochondrial delivery. Elife *10*.

Shanmughapriya, S., Langford, D., and Natarajaseenivasan, K. (2020). Inter and Intracellular mitochondrial trafficking in health and disease. Ageing Res Rev *62*, 101128.

Singh, B., Modica-Napolitano, J.S., and Singh, K.K. (2017). Defining the momiome: Promiscuous information transfer by mobile mitochondria and the mitochondrial genome. Semin Cancer Biol *47*, 1-17.

Spees, J.L., Olson, S.D., Whitney, M.J., and Prockop, D.J. (2006). Mitochondrial transfer between cells can rescue aerobic respiration. Proc Natl Acad Sci U S A *103*, 1283-1288.

Stefano, G.B., Bjenning, C., Wang, F., Wang, N., and Kream, R.M. (2017). Mitochondrial Heteroplasmy. Adv Exp Med Biol *982*, 577-594.

Stein, A., and Sia, E.A. (2017). Mitochondrial DNA repair and damage tolerance. Front Biosci (Landmark Ed) *22*, 920-943.

Wallace, D.C. (2018). Mitochondrial genetic medicine. Nat Genet *50*, 1642-1649.

Wilkins, H.M., Carl, S.M., and Swerdlow, R.H. (2014). Cytoplasmic hybrid (cybrid) cell lines as a practical model for mitochondriopathies. Redox Biol *2*, 619-631.

Wolff, J.N., Ladoukakis, E.D., Enriquez, J.A., and Dowling, D.K. (2014). Mitonuclear interactions: evolutionary consequences over multiple biological scales. Philos Trans R Soc Lond B Biol Sci *369*, 20130443.

Wong, R.C.B., Lim, S.Y., Hung, S.S.C., Jackson, S., Khan, S., Van Bergen, N.J., De Smit, E., Liang, H.H., Kearns, L.S., Clarke, L., et al. (2017). Mitochondrial replacement in an iPSC model of Leber's hereditary optic neuropathy. Aging (Albany NY) *9*, 1341-1350.

Wu, T.H., Sagullo, E., Case, D., Zheng, X., Li, Y., Hong, J.S., TeSlaa, T., Patananan, A.N., McCaffery, J.M., Niazi, K., et al. (2016). Mitochondrial Transfer by Photothermal Nanoblade Restores Metabolite Profile in Mammalian Cells. Cell Metab *23*, 921-929.

Zinovkina, L.A. (2018). Mechanisms of Mitochondrial DNA Repair in Mammals. Biochemistry (Mosc) *83*, 233-249.

Chapter 2: More than a powerplant: the influence of mitochondrial transfer on the epigenome

Available online at www.sciencedirect.com

ScienceDirect

Current Opinion in Physiology

More than a powerplant: the influence of mitochondrial transfer on the epigenome

Alexander N Patananan[1], Alexander J Sercel[2] and Michael A Teitell[1,2,3,4]

Each cell in the human body, with the exception of red blood cells, contains multiple copies of mitochondria that house their own genetic material, the maternally inherited mitochondrial DNA. Mitochondria are the cell's powerplant due to their massive ATP generation. However, the mitochondrion is also a hub for metabolite production from the TCA cycle, fatty acid beta-oxidation, and ketogenesis. In addition to producing macromolecules for biosynthetic reactions and cell replication, several mitochondrial intermediate metabolites serve as cofactors or substrates for epigenome modifying enzymes that regulate chromatin structure and impact gene expression. Here, we discuss connections between mitochondrial metabolites and enzymatic writers and erasers of chromatin modifications. We do this from the unique perspective of cell-to-cell mitochondrial transfer and its potential impact on mitochondrial replacement therapies.

Addresses
[1] Department of Pathology and Laboratory Medicine, David Geffen School of Medicine, University of California, Los Angeles, Los Angeles, CA 90095, USA
[2] Molecular Biology Interdepartmental Program, University of California, Los Angeles, Los Angeles, CA 90095, USA
[3] Jonsson Comprehensive Cancer Center, David Geffen School of Medicine, University of California, Los Angeles, Los Angeles, CA 90095, USA
[4] Department of Pediatrics and Bioengineering, Eli and Edythe Broad Center of Regenerative Medicine and Stem Cell Research, and California NanoSystems Institute, University of California, Los Angeles, Los Angeles, CA 90095, USA

Corresponding author: Teitell, Michael A (mteitell@mednet.ucla.edu)

Current Opinion in Physiology 2018, **3**:16–24

This review comes from a themed issue on **Mitochondria biology**

Edited by **John Elrod** and **Åsa Gustafsson**

For a complete overview see the Issue and the Editorial

Available online 11th December 2017

https://doi.org/10.1016/j.cophys.2017.11.006

Introduction

Considered to originate from an endosymbiotic α-proteobacteria in an ancient cellular host, modern mitochondria occur in dozens to thousands of copies per nucleated mammalian cell and are essential to eukaryotic life. Mitochondria are considered powerplants because they produce up to 90 percent of cellular ATP [1]. However, they are also hubs of metabolic activity and are involved in the production, breakdown, and/or regulation of reactive oxygen species (ROS), fatty acids, one-carbon metabolic intermediates, tricarboxylic acid (TCA) cycle metabolites, and ketone bodies. These metabolites provide cell type-specific and situational control over gene expression by fueling the addition of chemical groups, or epigenetic marks, to DNA or its associated proteins. These marks affect electrostatic and hydrophobic interactions within chromatin, influencing transcription factor or repressor binding and enhancing (euchromatin) or repressing (heterochromatin) gene expression (Figure 1).

In addition to approximately 1500 different mitochondrial proteins encoded in the nucleus [2], each mitochondrion contains multiple copies of a small, maternally inherited genome, the mitochondrial DNA (mtDNA). In humans, mtDNA is a compact 16,569 bp circular genome coding for 37 genes directly required for oxidative phosphorylation (OXPHOS) and linked to metabolite biosynthesis. Although pathogenic mutations to mtDNA affect 1 in 5000 people, 1 in 200 are carriers of mtDNA disease-related mutations but do not exhibit pathology because the deleterious effects of mutant mtDNA can be masked by normal mtDNA [3]. The phenomenon of a single cell carrying a heterogeneous population of normal and pathogenic mtDNA genotypes is known as heteroplasmy, and the heteroplasmic ratio of a specific pathogenic mtDNA to other mtDNA genotypes can dictate the severity of a disease. mtDNA mutations are particularly difficult to treat because modifying the mtDNA is currently impossible, however artificial or natural transfer of whole mitochondria containing mtDNA between cells provides mechanisms for altering metabolism and repairing cell damage [3–9], and may be a viable approach for mtDNA diseases (Figure 2). Studies on establishing mitochondrial replacement therapies (MRTs) that allow women carrying mtDNA mutations to have disease-free children have been performed in Mexico [10•], and proposed for the United States [11] and the United Kingdom [12]. Investigating the role of mitochondrial function and transfer in nuclear gene regulation and cell fate could provide insight for the long-term feasibility of MRTs and for understanding physiological changes resulting from altered mitochondrial activity.

Mitochondrial metabolites and epigenetics

Mitochondria house key metabolic processes including OXPHOS, long-chain fatty acid beta-oxidation, and

Figure 1

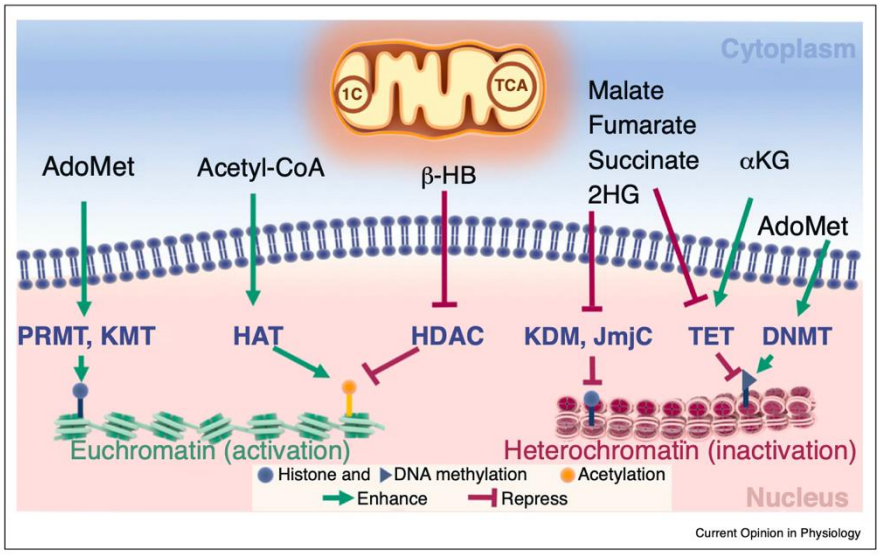

Mitochondrial metabolites influence the epigenome. Mitochondrial metabolites from many pathways, including the one-carbon (1C) and TCA cycles, are cofactors and regulators of the writers and erasers of epigenetic marks. Arginine (PRMT), lysine (KMT), and DNA (DNMT) methyltransferases require *S*-adenosylmethionine (AdoMet) to generate methylation marks, which can either activate or repress transcription. Likewise, histone acetyltransferases (HATs) require acetyl-CoA to acetylate histones and activate transcription. Both methylation and acetylation can be removed by demethylases (KDMs, JmjCs, and TET enzymes) and histone deacetylases (HDACs), respectively. Abbreviations: β-HB, beta-hydroxybutyrate; 2HG, 2-hydroxyglutarate; αKG, alpha-ketoglutarate.

amino acid metabolism along with the urea, one-carbon, and TCA cycles. A recent study identified 346 distinct metabolites produced within the mitochondria alone [13]. These metabolites regulate the enzymes that modify DNA and histones to modulate gene expression [14–17]. Perturbation of individual electron transport chain (ETC) complexes resulting from hereditary mutations in nuclear DNA and mtDNA can generate distinct mitochondrial metabolite and gene transcription profiles [13]. Intriguingly, cells *in vitro* and *in vivo* can donate mitochondria to specific recipient cells, and these donated mitochondria may manipulate cellular metabolism [8], promote tissue repair [18••], or alter disease progression [19]. The exact mechanism(s) by which transferred mitochondria and their specific mtDNA sequences fuel these changes likely go beyond altering cellular ATP concentrations and are discussed here.

Methylation of histones and DNA

DNA methylation at transcriptional start sites usually represses gene expression by altering chromatin structure, inhibiting transcription factor binding, and/or recruiting transcription repressors to methylated nucleotides [20]. However, DNA methylation may also promote transcriptional activation when methylation occurs in a gene body [21]. The most prevalent mammalian DNA modification is 5-methylcytosine in regions of CpG islands that is catalyzed by *de novo* DNA methyltransferases DNMT3A and DNMT3B and sustained through DNA replication by the DNA maintenance methyltransferase, DNMT1 [22]. Histone-tail amino acids are also subject to methylation, which can repress or activate gene expression depending on the residue, number, and epigenetic context of added or removed methyl groups. Histone-tail methylation occurs on any basic residue, but epigenetic modifications to arginine and lysine are most common [23–26].

Methyltransferase activity depends upon mitochondrial function since these enzymes require *S*-adenosylmethionine (AdoMet), which is synthesized by methionine adenosyltransferase from ATP and methionine. One-carbon cycle intermediates are required for AdoMet synthesis, and cells with impaired one-carbon cycling show decreased AdoMet levels and reduced DNA and histone methylation [27,28]. The one-carbon cycle occurs in both the cytosol and mitochondria, however mitochondrial serine catabolism is the predominant source of cellular one carbon metabolites [29]. Serine catabolism requires

Figure 2

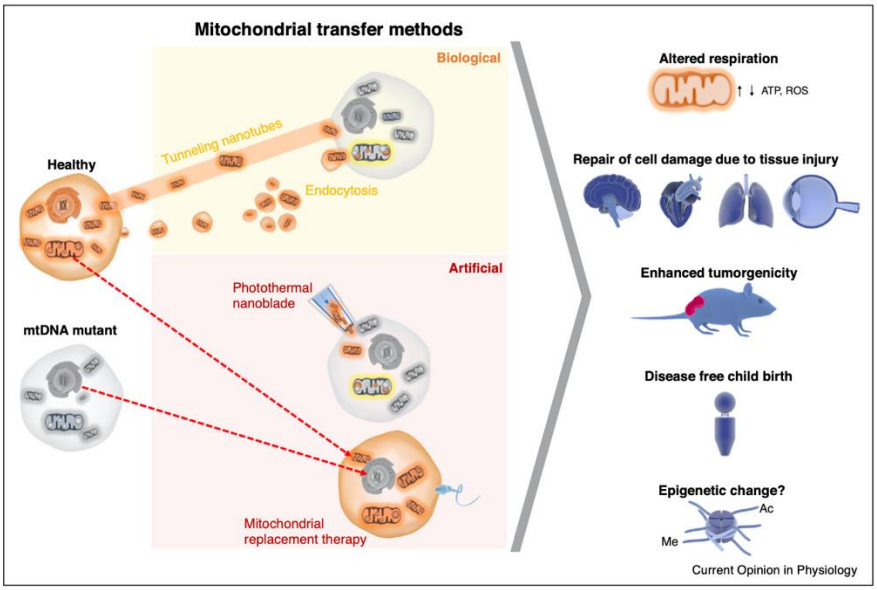

The biological and epigenetic impact of mitochondrial transfer. Transferring mitochondria with specific mtDNA sequences into cell lines of interest helps our understanding of metabolic control of the epigenome and could be developed into therapies for mitochondrial disorders. The transfer of mitochondria from healthy (labeled orange) to metabolically impaired (labeled gray) cells can occur *in vivo* via tunneling nanotubes and endocytosis. Additionally, isolated mitochondria can be transferred using artificial methods, such as the photothermal nanoblade. Several MRTs show promise for treating heritable mtDNA disorders, including somatic cell nuclear transfer followed by *in vitro* fertilization. Both biological and artificial mitochondrial transfer methods have been shown to alter respiration and the functions of astrocytes, cardiomyocytes, lung epithelial and corneal epithelial cells after tissue injury, and tumorgenicity in mouse models. However, mitochondrial transfer results in cells with new mtDNA sequences (highlighted yellow) that may change metabolic processes and the epigenome of cells. MRTs that completely replace a cell's mitochondrial population and initially give rise to disease free children may result in longer term metabolic disturbances, potentially due to non-evolved incompatibilities between nuclear DNA and mtDNA encoded proteins.

coupled respiration and its ATP and NAD+ byproducts, closely tying methylation to respiration and mitochondrial activity [30,31].

DNA and histone methylation marks are removed by Ten-Eleven Translocation (TET) or Jumonji catalytic (JmjC) domain-containing demethylases, respectively [14]. To remove 5-methylcytosine, TET dioxygenases convert 5-methylcytosine to 5-hydroxymethylcytosine, which is further oxidized to 5-formylcytosine and 5-carboxylcytosine before final removal by base excision repair [22,32,33]. Methyl groups on lysine residues in histones are removed by demethylases, of which 27 have been identified [34]. Lysine demethylases may also exhibit some arginine demethylase activity [35,36].

Mitochondrial metabolites and demethylation activities

Several TCA cycle-associated metabolites competitively inhibit demethylase activity and have profound effects on gene expression. Fumarate and succinate accumulate in cells with mutations in fumarate hydratase and succinate dehydrogenase [37], which inhibits TET demethylases and 5-hydroxymethylcytosine formation, reduces histone demethylation, activates the hypoxia inducible pathway [38•,39], and may lead to tumorigenesis [37,40,41••]. 2-hydroxyglutarate (2HG) is a TCA cycle-associated metabolite that can inhibit demethylases, and elevated 2HG levels can promote tumorigenesis [42,43], enhance mTOR signaling, and alter T cell differentiation (Figure 3) [44••,45•]. 2HG occurs as two enantiomers, D-R-2-hydroxyglutarate or L-S-2-hydroxyglutarate, depending on the biosynthetic pathway. D-R-2-hydroxyglutarate generation occurs by neomorphic mutations in isocitrate dehydrogenase 1 and 2 (IDH1/2) [46] or by transamination via glutamate-oxaloacetate transaminase 1 (GOT1) [44••]. Conversely, both hypoxia [47,48] and promiscuous activity of lactate and malate dehydrogenase enzymes at acidic pH [49,50] generate L-R-2-hydroxyglutarate. It is

Figure 3

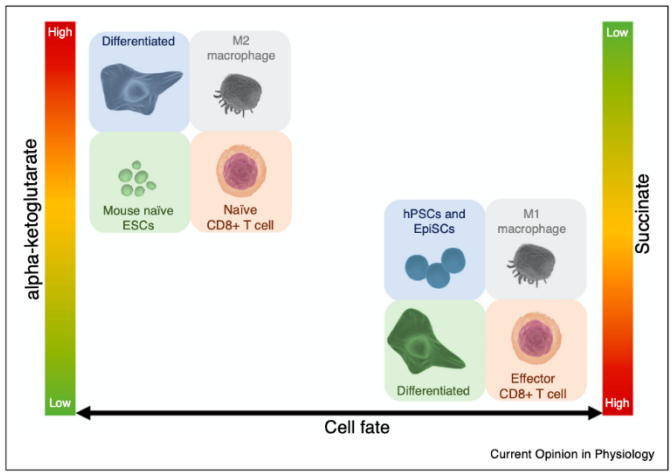

TCA cycle-associated metabolites, epigenetics, and cell fate. The fates of stem cells, T cells, and macrophages are regulated by cellular concentrations of αKG and succinate. These outcomes are at least partially mediated by αKG-dependent dioxygenases, which remove methyl epigenetic marks to alter nuclear gene expression. Activation or inhibition of these enzymes is dictated by high levels of αKG or succinate, respectively, and the resulting changes to the epigenome alter the differentiation and development of cells. Key: ESCs, embryonic stem cells; hPSCs, human pluripotent stem cells; EpiSCs, epiblast stem cells.

unclear whether these enantiomers have different cellular activity as both occur naturally, but a shift to favor L-S-2-hydroxyglutarate appears to result in T cell activation due to histone and DNA demethylation (Figure 3) [45•].

The cellular concentrations of TCA cycle metabolites alpha-ketoglutarate (αKG) and succinate are dependent upon mitochondrial activity and are important regulators of DNA and histone methylation patterning and cell fate. Both TET and JmjC-containing demethylases require O_2, αKG, and complexed iron (II) for activity, and produce succinate and CO_2 as reaction byproducts [14,51]. Adjusting αKG to succinate ratios can cause phenotype switching in cells. In macrophages, a high αKG to succinate ratio causes demethylation of H3K27me3 marks and drives M2 macrophage differentiation for anti-inflammatory and tissue repair responses, whereas a low ratio promotes lipopolysaccharide-sensing M1 macrophages and a pro-inflammatory response (Figure 3) [52•]. Elevated superoxide radicals from superoxide dismutase 2 depletion in stromal precursor cells may impede differentiation by promoting the accumulation of αKG, impairing glycolysis, and enhancing oxidative metabolism [53]. The mechanism(s) by which αKG causes epigenetic changes in this case is unknown, although αKG involvement may suggest a demethylase related activity that requires exploration. Alternatively, the extracellular levels of these metabolites may influence gene expression and cell function by serving as ligands of G-Protein Coupled Receptors (GPCRs). For example, succinate and αKG can bind to GPCR91 and GPCR99, respectively, to regulate cellular functions and tissue physiology [54,55]. Further investigation is needed to determine the extent to which mitochondrial metabolites influence cellular phenotypes by epigenetic modification or through non-canonical signaling pathways.

Finally, naïve mouse embryonic stem cells maintain DNA/histone demethylase function and pluripotency by sustaining an elevated αKG to succinate ratio [56]. Artificially reducing this ratio impairs TET demethylase activity, increases trimethylation and decreases monomethylation of H3K9, K3K27, H3K36, and H4K20, and promotes cell differentiation [56]. In less naïve, primed-state human pluripotent stem cells and mouse epiblast stem cells, elevated αKG levels promote stimulated differentiation [57••]. Furthermore, elevated αKG causes a decrease in H3K4me3 and H3K27me3, while an increased succinate concentration enhances these marks [57••]. These results show that *in vitro*, specific mitochondrial metabolites differentially regulate epigenome modifying enzymes and cellular differentiation depending upon cell state and microenvironment cues (Figure 3). Because these studies often involve the extracellular addition of membrane-permeable derivatives to cells under laboratory conditions, how robust this regulation is *in vivo* needs further study. Additionally, while it is known that the transfer of mitochondria occurs between

cells *in vitro* and *in vivo*, the biological consequences of transfer are unclear and it is unknown whether this process occurs in glycolytic hypoxic stem cells niches, which could alter mitochondrial metabolites and specific patterns of differentiation.

Mitochondrial metabolites and histone acetylation

In addition to methylation, acetylation occurs on histone tail residues, promoting euchromatin conformation and gene activation [58,59]. The twenty-two known HATs use the cofactor acetyl-coenzyme A (acetyl-CoA) to bind acetyl groups to lysine residues [58]. Histone acetylation is dependent upon the availability of acetyl-CoA, which accumulates within the nucleus, cytoplasm, and mitochondria [60]. Mitochondrial acetyl-CoA is made from fatty acid beta-oxidation, from branched-chain amino acids, and from pyruvate, citrate, and acetate via pyruvate decarboxylase, ATP citrate lyase (ACL), and acetyl-CoA synthetase 1 enzymes, respectively [61,62]. Furthermore, not only is TCA cycle generated citrate exported to the cytoplasm or nucleus and converted by ACL into acetyl-CoA, but ACL is also essential for histone acetylation and epigenome remodeling during nutrient sensing and adipocyte differentiation [63–65]. 2HG can enhance histone H3 acetylation by stimulating ACL and histone acetyltransferases (HATs) [42]. Finally, macrophages exposed to IL-4 show enhanced Akt-mTORC1 pathway activity, which increases the production of acetyl-CoA by ACL and results in H3/H4 histone acetylation that, similar to elevated demethylase activity, favors M2 macrophage activation [66].

Acetyl marks are removed by the eighteen histone deacetylases (HDACs), which are divided into four classes. Class I, II, and IV (HDACs 1-11) are Zn^{2+}-dependent, whereas class III HDACs, also known as the sirtuins (SIRT1-7), require NAD+ for activity [58,67,68]. Each class of HDAC is inhibited by different mitochondrial metabolites, which can result in histone H3/H4 tail hyperacetylation [69]. Class I and IIa HDACs are inhibited by the ketone body D-beta-hydroxybutyrate, a metabolic intermediate produced in liver mitochondria by fatty acid beta-oxidation during starvation conditions and when the TCA cycle is unable to produce sufficient amounts of acetyl-CoA [70,71]. This inhibition results in histone hyperacetylation, transcription changes, and activation of oxidative stress transcription factors FOXO3A and MT2, similar to the depletion of HDAC1 and HDAC2 [71,72]. Understanding how mitochondrial function and transfer may influence this regulation requires further study but also seems critical in animal models. Altering histone acetylation and gene expression can improve spatial memory impairment caused by hypoxia [73•] and extend lifespan in the roundworm *Caenorhabditis elegans* [74], although it can also induce tumorgenicity in certain cases [75].

Depletion of the class III HDAC SIRT1 results in increased H3K9 acetylation in hepatocellular carcinoma cells [76]. NAD+ depletion results in hyperacetylation and reduced trimethylation at H3K9 as well as reduced cell proliferation in human cancer models [77]. The simultaneous change in both acetylation and methylation highlights the multilayered regulation of the epigenome by a single metabolite. However, the specific role of mitochondrial NAD+ is currently unknown due to the technical challenges of studying how specific subcellular NAD+ pools influence enzymatic activities [78].

Mitochondrial transfer

mtDNA encoded proteins are essential for OXPHOS and also influence the synthesis of TCA cycle metabolites linked to epigenome modifications. In the extreme example of cells without mtDNA, called rho null (ρ0) cells, respiration is terminated, concentrations of succinate and 2HG are elevated, and αKG, fumarate, malate, and citrate levels are reduced [79•]. These changes in TCA cycle intermediates in mtDNA-deficient cells can reduce H3K9, H3K18, and H3K27 histone acetylation [80]. Additionally, mtDNA depletion increases one-carbon cycle serine metabolism and transsulfuration, and leads to both hypo-methylation and hyper-methylation of CpG islands [81–83,84•]. Although not thoroughly investigated, mtDNA depletion does not result in consistent changes across the epigenome. Rather, these studies suggest that dramatic changes to mitochondrial metabolite concentrations in ρ0 cells may activate and repress gene expression with variability. Further studies are needed to elucidate which metabolites drive patterns of epigenetic modification of specific genes and pathways in response to altered mtDNA levels.

Artificially transferring isolated, functional mitochondria into ρ0 cells rescues OXPHOS and restores the metabolic and transcriptional profiles of the recipient hybrid cells (Figure 2). Wu *et al.* transferred mitochondria from a donor cell line into ρ0 recipient cells using a large cargo delivery device called a photothermal nanoblade and generated three rescue clones that reestablished OXPHOS. Mitochondrial transfer did not fully restore all metabolites, such as 2HG and citrate, to wild-type levels [79•]. Furthermore, one of three examined rescue clones still resembled the ρ0 recipient line's metabolomic profile and TCA cycle gene expression pattern, suggesting that incomplete remodeling of the epigenome occurred despite restoring ETC activity. Latorre-Pellicer *et al.* recently reported that mice with identical nuclear genomes but different mtDNA genotypes exhibit significant differences in metabolic profiles, key cellular pathways, and lifespan [85]. These data suggest that different mtDNA haplotypes may be more or less compatible with different nuclear genotypes, influencing mitochondrial function, altering metabolism in whole organisms, and leading to epigenetic and phenotypic changes [86].

Table 1

Mitochondrial metabolites and their effect on epigenome marks.

Metabolite	Enzyme(s) affected	Enzyme substrate	Effect on enzyme activity	Transcription change
TCA cycle				
αKG	Demethylases	DNA, histones	+	+ or −
Fumarate	Demethylases	DNA, histones	−	+ or −
Succinate	Demethylases	DNA, histones	−	+ or −
Acetyl-CoA	HATs	Histones	+	+
TCA cycle associated				
2HG	Demethylases, acetyltransferases	DNA, histones	−	+ or −
			+	+
Respiration				
NAD+	Sirtuin deacetylases	Histones	+	−
FAD	Demethylases	Histones	+	+ or −
Fatty acid beta-oxidation				
D-beta-hydroxybutyrate	Deacetylases	Histones	−	+
One-carbon cycle associated				
AdoMet	Methyltransferases	DNA, histones	+	+ or −

+, Enhanced; −, Repressed.

In addition to haplotype incompatibility, results from these two studies may also be from epigenetic modifications to the mtDNA itself. Although controversial and initially determined to have no methylation [87] or associated histone proteins, interest in mtDNA epigenetics has increased with evidence suggesting mtDNA contains CpG sites that may be methylated to low levels [88,89] and that DNMT and TET enzymes localize to mitochondria [90–92]. Several publications suggest the accumulation of mtDNA methylation as biomarkers in a wide variety of pathologies involving mitochondrial function, from environmental pollution to aging and cardiovascular disease [88,93,94]. Although mtDNA methylation could modulate transcription like methyl groups in nuclear chromatin, such methylation marks may also regulate the cellular compatibility and tolerance of mtDNA, similarly to how the immune system identifies self from non-self. Further work is needed to determine whether these sporadically reported marks are not artifacts and quantify their biological relevance as any mitochondrial replacement therapy would need to overcome mitochondrial-nuclear compatibility issues.

The transfer of mitochondria between cells is also a biological phenomenon that occurs by endocytosis, tunneling nanotubes, and potentially other uncharacterized pathways in tissue culture and *in vivo* [3] (Figure 2). When non-tumorigenic ρ0 cancer cells are injected into a mouse, they receive mitochondria and mtDNA from the microenvironment, regain OXPHOS, and recover their tumorgenicity [8,9]. Whether this transfer also occurs between the stroma and cancer cells with their endogenous mtDNA intact, which is more relevant to human disease, remains to be clarified. This question has been addressed in non-cancer models showing that mitochondrial transfer modulates metabolism [95], tissue damage repair [96], and disease progression [3,97]. However, these studies often focus on ATP production, ROS levels, or cell viability associated with mitochondrial transfer rather than alterations to global gene expression and the epigenome that may be driving these biological changes.

Brief remarks

Mitochondria are metabolite-generating factories that support biomolecule and epigenome modification. The metabolites formed within mitochondria are substrates for and regulators of the writers and erasers of the epigenome (Table 1). This regulation may extend beyond altering chromatin structure and gene expression in the nucleus. A more complete understanding of mitochondrial-associated metabolism as a driver of epigenome modifications and its relationship to cell-to-cell mitochondrial transfer may provide mechanistic insight for treating a wide variety of diseases, including mtDNA-disorders.

Conflicts of interest

The authors do not have any conflicts of interest to declare.

References and recommended reading

Papers of particular interest, published within the period of review, have been highlighted as:

- • of special interest
- •• of outstanding interest

1. Harris DA, Das AM: **Control of mitochondrial ATP synthesis in the heart**. *Biochem J* 1991, **280**:561-573.
2. Calvo SE, Mootha VK: **The mitochondrial proteome and human disease**. *Annu Rev Genomics Hum Genet* 2010, **11**:25-44.
3. Patananan AN, Wu TH, Chiou PY, Teitell MA: **Modifying the mitochondrial genome**. *Cell Metab* 2016, **23**:785-796.
4. Lightowlers RN, Taylor RW, Turnbull DM: **Mutations causing mitochondrial disease: what is new and what challenges remain?** *Science* 2015, **349**:1494-1499.
5. Weinberg SE, Chandel NS: **Targeting mitochondria metabolism for cancer therapy**. *Nat Chem Biol* 2015, **11**:9-15.

6. Weinberg F, Chandel NS: **Reactive oxygen species-dependent signaling regulates cancer**. *Cell Mol Life Sci* 2009, **66**:3663-3673.

7. Weinberg F, Hamanaka R, Wheaton WW, Weinberg S, Joseph J, Lopez M, Kalyanaraman B, Mutlu GM, Budinger GR, Chandel NS: **Mitochondrial metabolism and ROS generation are essential for Kras-mediated tumorigenicity**. *Proc Natl Acad Sci U S A* 2010, **107**:8788-8793.

8. Tan AS, Baty JW, Dong LF, Bezawork-Geleta A, Endaya B, Goodwin J, Bajzikova M, Kovarova J, Peterka M, Yan B *et al.*: **Mitochondrial genome acquisition restores respiratory function and tumorigenic potential of cancer cells without mitochondrial DNA**. *Cell Metab* 2015, **21**:81-94.

9. Dong LF, Kovarova J, Bajzikova M, Bezawork-Geleta A, Svec D, Endaya B, Sachaphibulkij K, Coelho AR, Sebkova N, Ruzickova A *et al.*: **Horizontal transfer of whole mitochondria restores tumorigenic potential in mitochondrial DNA-deficient cancer cells**. *eLife* 2017, **6**.

10. • Zhang J, Liu H, Luo S, Chavez-Badiola A, Liu Z, Yang M, Munne S, Konstantinidis M, Well D, Huang T: **First live birth using human oocytes reconstituted by spindle nuclear transfer for mitochondrial DNA mutation causing leigh syndrome**. *ASRM Scientific Congress & Expo: Scaling New Heights in Reproductive Medicine: Fertility and Sterility*. 2016:e375.

First example of a human mother carrying a known mtDNA mutation giving birth to a child following three-parent mitochondrial replacement therapy.

11. Reardon S: **US panel greenlights creation of male 'three-person' embryos**. *Nature* 2016, **530**:142.

12. Lyon J: **Sanctioned UK trial of mitochondrial transfer nears**. *JAMA* 2017, **317**:462-464.

13. Chen WW, Freinkman E, Wang T, Birsoy K, Sabatini DM: **Absolute quantification of matrix metabolites reveals the dynamics of mitochondrial metabolism**. *Cell* 2016, **166**:1324-1337 e1311.

14. Aon MA, Cortassa S, Juhaszova M, Sollott SJ: **Mitochondrial health, the epigenome and healthspan**. *Clin Sci* 2016, **130**:1285-1305.

15. Sakamoto A, Hino S, Nagaoka K, Anan K, Takase R, Matsumori H, Ojima H, Kanai Y, Arita K, Nakao M: **Lysine demethylase lsd1 coordinates glycolytic and mitochondrial metabolism in hepatocellular carcinoma cells**. *Cancer Res* 2015, **75**:1445-1456.

16. Tian Y, Garcia G, Bian Q, Steffen KK, Joe L, Wolff S, Meyer BJ, Dillin A: **Mitochondrial stress induces chromatin reorganization to promote longevity and UPR(mt)**. *Cell* 2016, **165**:1197-1208.

17. Guha M, Srinivasan S, Guja K, Mejia E, Garcia-Diaz M, Johnson FB, Ruthel G, Kaufman BA, Rappaport EF, Glineburg MR *et al.*: **Hnrnpa2 is a novel histone acetyltransferase that mediates mitochondrial stress-induced nuclear gene expression**. *Cell Discov* 2016, **2**:16045.

18. •• Hayakawa K, Esposito E, Wang X, Terasaki Y, Liu Y, Xing C, Ji X, Lo EH: **Transfer of mitochondria from astrocytes to neurons after stroke**. *Nature* 2016, **535**:551-555.

Astrocytes release vesicles containing functional mitochondria into their surroundings by a CD38-dependent pathway. These mitochondria are uptaken by neurons to restore ATP production and cell viability following ischemic injury *in vitro* and *in vivo*.

19. Marlein CR, Zaitseva L, Piddock RE, Robinson S, Edwards D, Shafat MS, Zhou Z, Lawes M, Bowles KM, Rushworth SA: **NADPH oxidase-2 derived superoxide drives mitochondrial transfer from bone marrow stromal cells to leukemic blasts**. *Blood* 2017.

20. Chen K, Zhao BS, He C: **Nucleic acid modifications in regulation of gene expression**. *Cell Chem Biol* 2016, **23**:74-85.

21. Lyko F: **The DNA methyltransferase family: a versatile toolkit for epigenetic regulation**. *Nat Rev Genet* 2017.

22. Breiling A, Lyko F: **Epigenetic regulatory functions of DNA modifications: 5-methylcytosine and beyond**. *Epigenetics Chromatin* 2015, **8**:24.

23. Bedford MT, Clarke SG: **Protein arginine methylation in mammals: who, what, and why**. *Mol Cell* 2009, **33**:1-13.

24. Di Lorenzo A, Bedford MT: **Histone arginine methylation**. *FEBS Lett* 2011, **585**:2024-2031.

25. Greer EL, Shi Y: **Histone methylation: a dynamic mark in health, disease and inheritance**. *Nat Rev Genet* 2012, **13**:343-357.

26. Hyun K, Jeon J, Park K, Kim J: **Writing, erasing and reading histone lysine methylations**. *Exp Mol Med* 2017, **49**:e324.

27. Maddocks OD, Labuschagne CF, Adams PD, Vousden KH: **Serine metabolism supports the methionine cycle and DNA/RNA methylation through de novo ATP synthesis in cancer cells**. *Mol Cell* 2016, **61**:210-221.

28. Singhal NK, Li S, Arning E, Alkhayer K, Clements R, Sarcyk Z, Dassanayake RS, Brasch NE, Freeman EJ, Bottiglieri T *et al.*: **Changes in methionine metabolism and histone H3 trimethylation are linked to mitochondrial defects in multiple sclerosis**. *J Neurosci* 2015, **35**:15170-15186.

29. Yang M, Vousden KH: **Serine and one-carbon metabolism in cancer**. *Nat Rev Cancer* 2016, **16**:650-662.

30. Ducker GS, Chen L, Morscher RJ, Ghergurovich JM, Esposito M, Teng X, Kang Y, Rabinowitz JD: **Reversal of cytosolic one-carbon flux compensates for loss of the mitochondrial folate pathway**. *Cell Metab* 2016, **24**:640-641.

31. Meiser J, Tumanov S, Maddocks O, Labuschagne CF, Athineos D, Van Den Broek N, Mackay GM, Gottlieb E, Blyth K, Vousden K *et al.*: **Serine one-carbon catabolism with formate overflow**. *Sci Adv* 2016, **2**:e1601273.

32. Wu H, Zhang Y: **Reversing DNA methylation: mechanisms, genomics, and biological functions**. *Cell* 2014, **156**:45-68.

33. Hardwick JS, Ptchelkine D, El-Sagheer AH, Tear I, Singleton D, Phillips SEV, Lane AN, Brown T: **5-Formylcytosine does not change the global structure of DNA**. *Nat Struct Mol Biol* 2017, **24**:544-552.

34. Cloos PAC, Christensen J, Agger K, Helin K: **Erasing the methyl mark: histone demethylases at the center of cellular differentiation and disease**. *Gene Dev* 2008, **22**:1115-1140.

35. Walport LJ, Hopkinson RJ, Chowdhury R, Schiller R, Ge W, Kawamura A, Schofield CJ: **Arginine demethylation is catalysed by a subset of JmjC histone lysine demethylases**. *Nat Commun* 2016, **7**.

36. Blanc RS, Richard S: **Arginine methylation: the coming of age**. *Mol Cell* 2017, **65**:8-24.

37. Hoekstra AS, de Graaff MA, Briaire-de Bruijn IH, Ras C, Seifar RM, van Minderhout I, Cornelisse CJ, Hogendoorn PCW, Breuning MH, Suijker J *et al.*: **Inactivation of SDH and FH cause loss of 5hmC and increased H3K9me3 in paraganglioma/pheochromocytoma and smooth muscle tumors**. *Oncotarget* 2015, **6**:38777-38788.

38. • Wentzel JF, Lewies A, Bronkhorst AJ, van Dyk E, du Plessis LH, Pretorius PJ: **Exposure to high levels of fumarate and succinate leads to apoptotic cytotoxicity and altered global DNA methylation profiles in vitro**. *Biochimie* 2017, **135**:28-34.

Exposure to high concentrations of succinate causes cells to elevate levels of pro-apoptotic caspase 3 and/or caspase 7, and exposure to elevated fumarate levels causes DNA fragmentation. Increasing levels of either succinate or fumarate leads to global DNA hypermethylation.

39. Frezza C, Pollard PJ, Gottlieb E: **Inborn and acquired metabolic defects in cancer**. *J Mol Med* 2011, **89**:213-220.

40. Xiao M, Yang H, Xu W, Ma S, Lin H, Zhu H, Liu L, Liu Y, Yang C, Xu Y *et al.*: **Inhibition of alpha-KG-dependent histone and DNA demethylases by fumarate and succinate that are accumulated in mutations of FH and SDH tumor suppressors**. *Gene Dev* 2012, **26**:1326-1338.

41. •• Sciacovelli M, Goncalves E, Johnson TI, Zecchini VR, da Costa ASH, Gaude E, Drubbel AV, Theobald SJ, Abbo SR, Tran MGB *et al.*: **Fumarate is an epigenetic modifier that elicits epithelial-to-mesenchymal transition**. *Nature* 2016, **537**:544-547.

Elevated levels of fumarate or loss of fumarate hydratase inhibits demethylation of the anti-metastatic miRNA cluster mir-200ba429, driving cells into an epithelial-to-mesenchymal-transition and a more metastatic phenotype.

42. Karlstaedt A, Zhang X, Vitrac H, Harmancey R, Vasquez H, Wang JH, Goodell MA, Taegtmeyer H: **Oncometabolite d-2-hydroxyglutarate impairs alpha-ketoglutarate dehydrogenase and contractile function in rodent heart**. *Proc Natl Acad Sci USA* 2016, **113**:10436-10441.

43. Janke R, Iavarone AT, Rine J: **Oncometabolite d-2-hydroxyglutarate enhances gene silencing through inhibition of specific H3K36 histone demethylases**. *eLife* 2017, **6**.

44. •• Xu T, Stewart KM, Wang X, Liu K, Xie M, Kyu Ryu J, Li K, Ma T, Wang H, Ni L *et al.*: **Metabolic control of TH17 and induced Treg cell balance by an epigenetic mechanism**. *Nature* 2017, **548**:228-233.

Development of T helper 17 (T_H17) cells requires accumulation of 2HG from cellular αKG pools to promote Foxp3 hypermethylation and transcriptional repression. The small molecule (aminooxy)acetic acid inhibits GOT1, reducing αKG production and 2HG levels, reprogramming differentiation of T_H17 cells to an induced regulatory T cell state.

45. • Tyrakis PA, Palazon A, Macias D, Lee KL, Phan AT, Velica P, You J, Chia GS, Sim J, Doedens A *et al.*: **S-2-hydroxyglutarate regulates CD8(+) T-lymphocyte fate**. *Nature* 2016, **540**:236-241.

2HG accumulates in two enantiomers, S-2-hydroxygluatarate and R-2-hydroxyglutarate, in healthy cells. CD8+ T cells show an increase in the S-2-hydroxygluatarate to R-2-hydroxyglutarate ratio upon TCR triggering, which is responsible for modulating global histone and DNA methylation to form activated effector T cells.

46. Ward PS, Patel J, Wise DR, Abdel-Wahab O, Bennett BD, Coller HA, Cross JR, Fantin VR, Hedvat CV, Perl AE *et al.*: **The common feature of leukemia-associated IDH1 and IDH2 mutations is a neomorphic enzyme activity converting alpha-ketoglutarate to 2-hydroxyglutarate**. *Cancer Cell* 2010, **17**:225-234.

47. Oldham WM, Clish CB, Yang Y, Loscalzo J: **Hypoxia-mediated increases in L-2-hydroxyglutarate coordinate the metabolic response to reductive stress**. *Cell Metab* 2015, **22**:291-303.

48. Intlekofer AM, Dematteo RG, Venneti S, Finley LW, Lu C, Judkins AR, Rustenburg AS, Grinaway PB, Chodera JD, Cross JR *et al.*: **Hypoxia induces production of L-2-hydroxyglutarate**. *Cell Metab* 2015, **22**:304-311.

49. Intlekofer AM, Wang B, Liu H, Shah H, Carmona-Fontaine C, Rustenburg AS, Salah S, Gunner MR, Chodera JD, Cross JR *et al.*: **L-2-hydroxyglutarate production arises from noncanonical enzyme function at acidic pH**. *Nat Chem Biol* 2017, **13**:494-500.

50. Nadtochiy SM, Schafer X, Fu D, Nehrke K, Munger J, Brookes PS: **Acidic ph is a metabolic switch for 2-hydroxyglutarate generation and signaling**. *J Biol Chem* 2016, **291**:20188-20197.

51. Filipp FV: **Crosstalk between epigenetics and metabolism-yin and yang of histone demethylases and methyltransferases in cancer**. *Brief Funct Genomics* 2017.

52. • Liu PS, Wang H, Li X, Chao T, Teav T, Christen S, Di Conza G, Cheng WC, Chou CH, Vavakova M *et al.*: **Alpha-ketoglutarate orchestrates macrophage activation through metabolic and epigenetic reprogramming**. *Nat Immunol* 2017.

αKG enhances M2 macrophage activation by promoting fatty acid beta-oxidation and Jmjd3-dependent epigenetic remodeling of M2 genes. Reducing the αKG/succinate ratio enhances the M1 proinflammatory macrophage phenotype.

53. Singh K, Krug L, Basu A, Meyer P, Treiber N, Beken SV, Wlaschek M, Kochanek S, Bloch W, Geiger H *et al.*: **Alpha-ketoglutarate curbs differentiation and induces cell death in mesenchymal stromal precursors with mitochondrial dysfunction**. *Stem Cells* 2017, **35**:1704-1718.

54. Husted AS, Trauelsen M, Rudenko O, Hjorth SA, Schwartz TW: **GPCR-mediated signaling of metabolites**. *Cell Metab* 2017, **25**:777-796.

55. He WH, Miao FJP, Lin DCH, Schwandner RT, Wang ZL, Gao JH, Chen JL, Tian H, Ling L: **Citric acid cycle intermediates as ligands for orphan g-protein-coupled receptors**. *Nature* 2004, **429**:188-193.

56. Carey BW, Finley LW, Cross JR, Allis CD, Thompson CB: **Intracellular alpha-ketoglutarate maintains the pluripotency of embryonic stem cells**. *Nature* 2015, **518**:413-416.

57. •• TeSlaa T, Chaikovsky AC, Lipchina I, Escobar SL, Hochedlinger K, Huang J, Graeber TG, Braas D, Teitell MA: **Alpha-ketoglutarate accelerates the initial differentiation of primed human pluripotent stem cells**. *Cell Metab* 2016, **24**:485-493.

Primed human pluripotent stem cells and mouse epiblast stem cells undergo accelerated differentiation when the αKG/succinate ratio is increased. Additional αKG induces global histone and DNA demethylation, leading to a more differentiated phenotype.

58. Drazic A, Myklebust LM, Ree R, Arnesen T: **The world of protein acetylation**. *Biochim Biophys Acta* 2016, **1864**:1372-1401.

59. Tessarz P, Kouzarides T: **Histone core modifications regulating nucleosome structure and dynamics**. *Nat Rev Mol Cell Biol* 2014, **15**:703-708.

60. Padmanabhan K, Billaud M: **Desynchronization of circadian clocks in cancer: a metabolic and epigenetic connection**. *Front Endocrinol* 2017, **8**.

61. Choudhary C, Weinert BT, Nishida Y, Verdin E, Mann M: **The growing landscape of lysine acetylation links metabolism and cell signalling**. *Nat Rev Mol Cell Biol* 2014, **15**:536-550.

62. Pietrocola F, Galluzzi L, Bravo-San Pedro JM, Madeo F, Kroemer G: **Acetyl coenzyme A: a central metabolite and second messenger**. *Cell Metab* 2015, **21**:805-821.

63. Wellen KE, Hatzivassiliou G, Sachdeva UM, Bui TV, Cross JR, Thompson CB: **ATP-citrate lyase links cellular metabolism to histone acetylation**. *Science* 2009, **324**:1076-1080.

64. Deb DK, Chen Y, Sun J, Wang Y, Li YC: **ATP-citrate lyase is essential for high glucose-induced histone hyperacetylation and fibrogenic gene upregulation in mesangial cells**. *Am J Physiol Renal Physiol* 2017, **313**:F423-F429.

65. Carrer A, Parris JL, Trefely S, Henry RA, Montgomery DC, Torres A, Viola JM, Kuo YM, Blair IA, Meier JL *et al.*: **Impact of a high-fat diet on tissue acyl-CoA and histone acetylation levels**. *J Biol Chem* 2017, **292**:3312-3322.

66. Covarrubias AJ, Aksoylar HI, Yu J, Snyder NW, Worth AJ, Iyer SS, Wang J, Ben-Sahra I, Byles V, Polynne-Stapornkul T *et al.*: **Akt-mTORC1 signaling regulates Acly to integrate metabolic input to control of macrophage activation**. *eLife* 2016, **5**.

67. Delcuve GP, Khan DH, Davie JR: **Roles of histone deacetylases in epigenetic regulation: emerging paradigms from studies with inhibitors**. *Clin Epigenetics* 2012, **4**:5.

68. Ryall JG, Cliff T, Dalton S, Sartorelli V: **Metabolic reprogramming of stem cell epigenetics**. *Cell Stem Cell* 2015, **17**:651-662.

69. Drogaris P, Villeneuve V, Pomies C, Lee EH, Bourdeau V, Bonneil E, Ferbeyre G, Verreault A, Thibault P: **Histone deacetylase inhibitors globally enhance H3/H4 tail acetylation without affecting H3 lysine 56 acetylation**. *Sci Rep* 2012, **2**:220.

70. Dedkova EN, Blatter LA: **Role of beta-hydroxybutyrate, its polymer poly-beta-hydroxybutyrate and inorganic polyphosphate in mammalian health and disease**. *Front Physiol* 2014, **5**:260.

71. Shimazu T, Hirschey MD, Newman J, He W, Shirakawa K, Le Moan N, Grueter CA, Lim H, Saunders LR, Stevens RD *et al.*: **Suppression of oxidative stress by beta-hydroxybutyrate, an endogenous histone deacetylase inhibitor**. *Science* 2013, **339**:211-214.

72. Kong G, Huang Z, Ji W, Wang X, Liu J, Wu X, Huang Z, Li R, Zhu Q: **The ketone metabolite beta-hydroxybutyrate attenuates oxidative stress in spinal cord injury by suppression of class I histone deacetylases**. *J Neurotrauma* 2017.

73. • Zhao M, Huang X, Cheng X, Lin X, Zhao T, Wu L, Yu X, Wu K, Fan M, Zhu L: **Ketogenic diet improves the spatial memory impairment caused by exposure to hypobaric hypoxia through increased acetylation of histones in rats**. *PLOS ONE* 2017, **12**: e0174477.

Rats fed a ketogenic diet show enhanced blood concentration of beta-hydroxybutyrate and rescued hypobaric hypoxia-induced spatial

memory impairment. This neuro-reparative effect is mediated by the beta-hydroxybutyrate inhibition of histone deacetylases, resulting in increased acetylation of histones H3 and H4.

74. Edwards C, Canfield J, Copes N, Rehan M, Lipps D, Bradshaw PC: **D-beta-hydroxybutyrate extends lifespan in *C. elegans***. *Aging (Milano)* 2014, **6**:621-644.

75. Huang CK, Chang PH, Kuo WH, Chen CL, Jeng YM, Chang KJ, Shew JY, Hu CM, Lee WH: **Adipocytes promote malignant growth of breast tumours with monocarboxylate transporter 2 expression via beta-hydroxybutyrate**. *Nat Commun* 2017, **8**.

76. Zhang B, Chen J, Cheng AS, Ko BC: **Depletion of sirtuin 1 (SIRT1) leads to epigenetic modifications of telomerase (TERT) gene in hepatocellular carcinoma cells**. *PLOS ONE* 2014, **9**:e84931.

77. Del Nagro C, Xiao Y, Rangell L, Reichelt M, O'Brien T: **Depletion of the central metabolite NAD leads to oncosis-mediated cell death**. *J Biol Chem* 2014, **289**:35182-35192.

78. Matilainen O, Quiros PM, Auwerx J: **Mitochondria and epigenetics crosstalk in homeostasis and stress**. *Trends Cell Biol* 2017, **27**:453-463.

79. • Wu TH, Sagullo E, Case D, Zheng X, Li Y, Hong JS, TeSlaa T, Patananan AN, McCaffery JM, Niazi K *et al.*: **Mitochondrial transfer by photothermal nanoblade restores metabolite profile in mammalian cells**. *Cell Metab* 2016, **23**:921-929.
Cells lacking mtDNA show impaired respiration and robust differences in metabolite profiles compared to parent cells. Restored respiration and metabolite levels occur when mtDNA-deficient cells obtain mtDNA by isolated mitochondrial transfer.

80. Martinez-Reyes I, Diebold LP, Kong H, Schieber M, Huang H, Hensley CT, Mehta MM, Wang TY, Santos JH, Woychik R *et al.*: **TCA cycle and mitochondrial membrane potential are necessary for diverse biological functions**. *Mol Cell* 2016, **61**:199-209.

81. Minocherhomji S, Tollefsbol TO, Singh KK: **Mitochondrial regulation of epigenetics and its role in human diseases**. *Epigenetics* 2012, **7**:326-334.

82. Smiraglia DJ, Kazhiyur-Mannar R, Oakes CC, Wu YZ, Liang P, Ansari T, Su J, Rush LJ, Smith LT, Yu L *et al.*: **Restriction landmark genomic scanning (RLGS) spot identification by second generation virtual RLGS in multiple genomes with multiple enzyme combinations**. *BMC Genomics* 2007, **8**:446.

83. Smiraglia DJ, Kulawiec M, Bistulfi GL, Gupta SG, Singh KK: **A novel role for mitochondria in regulating epigenetic modification in the nucleus**. *Cancer Biol Ther* 2008, **7**:1182-1190.

84. • Bao XR, Ong SE, Goldberger O, Peng J, Sharma R, Thompson DA, Vafai SB, Cox AG, Marutani E, Ichinose F *et al.*: **Mitochondrial dysfunction remodels one-carbon metabolism in human cells**. *eLife* 2016, **5**.
mtDNA depletion causes enhanced serine biosynthesis and transsulferation by ATF4. Damaging the ETC reduces the production of formate from serine. Serine depletion in these cells causes growth defects, which are rescued by serine supplementation in the culture media.

85. Latorre-Pellicer A, Moreno-Loshuertos R, Lechuga-Vieco AV, Sanchez-Cabo F, Torroja C, Acin-Perez R, Calvo E, Aix E, Gonzalez-Guerra A, Logan A *et al.*: **Mitochondrial and nuclear DNA matching shapes metabolism and healthy ageing**. *Nature* 2016, **535**:561-565.

86. Betancourt AM, King AL, Fetterman JL, Millender-Swain T, Finley RD, Oliva CR, Crowe DR, Ballinger SW, Bailey SM: **Mitochondrial–nuclear genome interactions in non-alcoholic fatty liver disease in mice**. *Biochem J* 2014, **461**:223-232.

87. Dawid IB: **5-Methylcytidylic acid: absence from mitochondrial DNA of frogs and hela cells**. *Science* 1974, **184**:80-81.

88. Mawlood SK, Dennany L, Watson N, Dempster J, Pickard BS: **Quantification of global mitochondrial DNA methylation levels and inverse correlation with age at two CpG sites**. *Aging (Milano)* 2016, **8**:636-641.

89. Liu B, Du Q, Chen L, Fu G, Li S, Fu L, Zhang X, Ma C, Bin C: **CpG methylation patterns of human mitochondrial DNA**. *Sci Rep* 2016, **6**:23421.

90. Shock LS, Thakkar PV, Peterson EJ, Moran RG, Taylor SM: **DNA methyltransferase 1, cytosine methylation, and cytosine hydroxymethylation in mammalian mitochondria**. *Proc Natl Acad Sci USA* 2011, **108**:3630-3635.

91. Wong M, Gertz B, Chestnut BA, Martin LJ: **Mitochondrial DNMT3A and DNA methylation in skeletal muscle and CNS of transgenic mouse models of ALS**. *Front Cell Neurosci* 2013, **7**:279.

92. Bellizzi D, D'Aquila P, Scafone T, Giordano M, Riso V, Riccio A, Passarino G: **The control region of mitochondrial DNA shows an unusual CpG and non-CpG methylation pattern**. *DNA Res* 2013, **20**:537-547.

93. Baccarelli AA, Byun HM: **Platelet mitochondrial DNA methylation: a potential new marker of cardiovascular disease**. *Clin Epigenetics* 2015, **7**.

94. Iacobazzi V, Castegna A, Infantino V, Andria G: **Mitochondrial DNA methylation as a next-generation biomarker and diagnostic tool**. *Mol Genet Metab* 2013, **110**:25-34.

95. Melcher M, Danhauser K, Seibt A, Degistirici O, Baertling F, Kondadi AK, Reichert AS, Koopman WJH, Willems P, Rodenburg RJ *et al.*: **Modulation of oxidative phosphorylation and redox homeostasis in mitochondrial NDUFS4 deficiency via mesenchymal stem cells**. *Stem Cell Res Ther* 2017, **8**:150.

96. Jiang D, Gao F, Zhang Y, Wong DS, Li Q, Tse HF, Xu G, Yu Z, Lian Q: **Mitochondrial transfer of mesenchymal stem cells effectively protects corneal epithelial cells from mitochondrial damage**. *Cell Death Dis* 2016, **7**:e2467.

97. Moschoi R, Imbert V, Nebout M, Chiche J, Mary D, Prebet T, Saland E, Castellano R, Pouyet L, Collette Y *et al.*: **Protective mitochondrial transfer from bone marrow stromal cells to acute myeloid leukemic cells during chemotherapy**. *Blood* 2016, **128**:253-264.

Chapter 3: Stable transplantation of human mitochondrial DNA by high-throughput, pressurized isolated mitochondrial delivery

eLife

TOOLS AND RESOURCES

Stable transplantation of human mitochondrial DNA by high-throughput, pressurized isolated mitochondrial delivery

Alexander J Sercel[1†], Alexander N Patananan[2†], Tianxing Man[3], Ting-Hsiang Wu[4,5], Amy K Yu[1], Garret W Guyot[2], Shahrooz Rabizadeh[4,5,6,7], Kayvan R Niazi[4,5,7,8], Pei-Yu Chiou[3,7,8], Michael A Teitell[1,2,7,8,9,10,11]*

[1]Molecular Biology Interdepartmental Doctoral Program, University of California, Los Angeles, Los Angeles, United States; [2]Department of Pathology and Laboratory Medicine, David Geffen School of Medicine, University of California, Los Angeles, Los Angeles, United States; [3]Department of Mechanical and Aerospace Engineering, University of California, Los Angeles, Los Angeles, United States; [4]NanoCav, LLC, Culver City, United States; [5]NantBio, Inc, and ImmunityBio, Inc, Culver City, United States; [6]NantOmics, LLC, Culver City, United States; [7]California NanoSystems Institute, University of California, Los Angeles, Los Angeles, United States; [8]Department of Bioengineering, University of California, Los Angeles, Los Angeles, United States; [9]Eli and Edythe Broad Center of Regenerative Medicine and Stem Cell Research University of California, Los Angeles, Los Angeles, United States; [10]Department of Pediatrics, David Geffen School of Medicine, University of California, Los Angeles, Los Angeles, United States; [11]Jonsson Comprehensive Cancer Center, David Geffen School of Medicine, University of California, Los Angeles, Los Angeles, United States

***For correspondence:** mteitell@mednet.ucla.edu

[†]These authors contributed equally to this work

Competing interest: See page 16

Funding: See page 17

Received: 15 September 2020
Accepted: 12 January 2021
Published: 13 January 2021

Reviewing editor: Simon C Johnson, University of Washington, United States

Abstract Generating mammalian cells with specific mitochondrial DNA (mtDNA)–nuclear DNA (nDNA) combinations is desirable but difficult to achieve and would be enabling for studies of mitochondrial-nuclear communication and coordination in controlling cell fates and functions. We developed 'MitoPunch', a pressure-driven mitochondrial transfer device, to deliver isolated mitochondria into numerous target mammalian cells simultaneously. MitoPunch and MitoCeption, a previously described force-based mitochondrial transfer approach, both yield stable isolated mitochondrial recipient (SIMR) cells that permanently retain exogenous mtDNA, whereas coincubation of mitochondria with cells does not yield SIMR cells. Although a typical MitoPunch or MitoCeption delivery results in dozens of immortalized SIMR clones with restored oxidative phosphorylation, only MitoPunch can produce replication-limited, non-immortal human SIMR clones. The MitoPunch device is versatile, inexpensive to assemble, and easy to use for engineering mtDNA–nDNA combinations to enable fundamental studies and potential translational applications.

Introduction

Mitochondrial DNA (mtDNA) and nuclear DNA (nDNA) genome coordination regulates metabolism, epigenome modifications, and other processes vital for mammalian cell survival and activity (***Patananan et al., 2018***; ***Ryan and Hoogenraad, 2007***; ***Singh et al., 2017***). Together, these

eLife digest Mitochondria are specialized structures within cells that generate vital energy and biological building blocks. Mitochondria have a double membrane and contain many copies of their own circular DNA (mitochondrial DNA), which include the blueprints to create just thirteen essential mitochondrial proteins.

Like all genetic material, mitochondrial DNA can become damaged or mutated, and these changes can be passed on to offspring. Some of these alterations are linked to severe and debilitating diseases. Both the double membrane of the mitochondria and their high number of DNA copies make treating such diseases difficult. A successful therapy must be capable of correcting almost every copy of mitochondrial DNA. However, the multiple copies of mitochondrial DNA create a problem for genetic research as current techniques are unable to reliably introduce particular mitochondrial mutations to all types of human cells to investigate how they may alter cell function.

Sercel, Patananan et al. have developed a method to deliver new mitochondria into thousands of cells at the same time. This technique, called MitoPunch, uses a pressure-driven device to propel mitochondria taken from donor cells into recipient cells without mitochondrial DNA to reestablish their function. Using human cancer cells and healthy skin cells that lack mitochondrial DNA, Sercel, Patananan et al. showed that cells that received mitochondria retained the new mitochondrial DNA. The technique uses readily accessible parts, meaning it can be performed quickly and inexpensively in any laboratory. It further only requires a small amount of donor starting material, meaning that even precious samples with limited material could be used as mitochondrial donors.

This new technique has several important potential applications for mitochondrial DNA research. It could be used in the lab to create large numbers of cell lineswith known mutations in the mitochondrial DNA to establish new systems that test drugs or probe the interaction between mitochondrial and nuclear DNA. It could be used to study a broad spectrum of biological questions since mitochondrial function is essential for several processes required for life. Critically, it could also be used as a starting point to develop next-generation therapies capable of treating inherited mitochondrial genetic diseases in severely affected patients.

genomes encode >1100 mitochondrial proteins, with only 13 essential electron transport chain (ETC) proteins encoded within the mtDNA (***Calvo and Mootha, 2010***). The mitochondrial proteins encoded in the mtDNA and the nDNA must be compatible to support mitochondrial ETC activity. Mutations in mtDNA can impair the ETC by altering nDNA co-evolved ETC complex protein interactions, causing defective cellular respiration and debilitating diseases (***Greaves et al., 2012***). Furthermore, the coordination of these two genomes to transcribe, translate, and potentially modify appropriate levels of their respective gene products to maintain energetic and metabolic homeostasis is essential to the proper functioning of the ETC (***Wolff et al., 2014***). As a result, methods that enable pairing of specific mtDNA and nDNA genotypes in tractable systems are key to understanding the basic biology of mitonuclear interactions and their implications for health and disease.

Our current inability to edit mtDNA sequences is a roadblock for many studies and potential applications. For example, endonucleases targeted to the mitochondrion inefficiently eliminate and cannot alter mtDNA sequences (***Bacman et al., 2018***). An exciting new bacterial cytidine deaminase toxin generates a limited repertoire of point mutations in the mtDNA; however, its efficiency remains low and it is unable to knock-in new gene sequences (***Mok et al., 2020***). Mitochondrial transfer between cells in vitro and in vivo provides a potential path forward for transplanting existing mtDNA sequences; however, the mechanisms controlling such transfers remain unknown (***Dong et al., 2017***; ***Torralba et al., 2016***). Isolated mitochondrial transfer has been used to deliver mitochondria to a range of recipient cell types in vitro and even in vivo (***Caicedo et al., 2015***; ***Emani et al., 2017***; ***Kitani et al., 2014***); however, most studies using these methods observe only short-term changes to cell or organ performance and function. A small number of these studies have coincubated mitochondria with recipient cells and observed permanent retention of the exogenous mtDNA in mtDNA-deficient (so-called 'ρ0') cells using large doses of mitochondria or antibiotic selection

schemes (**Clark and Shay, 1982**; **Patel et al., 2017**), although these approaches may not be possible when mitochondrial donor material is limited or does not possess a suitable selection marker.

Methods that deliver mitochondria directly into ρ0 cells can increase stable mitochondrial transfer efficiency and employ a wider range of mitochondrial donor sources. Such methods include membrane disruption (**King and Attardi, 1988**; **Wu et al., 2016**) or fusion with enucleated cytoplasts (**Wilkins et al., 2014**). However, these methods are typically laborious, low-throughput, or depend on cancerous, immortal recipient cells lacking physiologic mitochondrial activity. An interesting recent study did report one desired mtDNA–nDNA clone and 11 false-positive clones using cybrid fusion with replication-limited cells, an achievement hampered by a low generation rate with unknown reproducibility or generalizability (**Wong et al., 2017**).

There exist clinically relevant methods to replace the mtDNA of human cells, such as somatic cell nuclear transfer and pronuclear transfer that involve delivering nuclear genetic material from patients with mtDNA diseases into enucleated oocytes with non-mutant mtDNA genotypes (**Hyslop et al., 2016**; **Tachibana et al., 2013**). These methods hold potential for replacing deleterious mtDNA for the unborn, but they are technically challenging, low-throughput, dependent on high-quality patient samples, and prone to contamination by mutant mtDNA from the affected nuclear source material (**Kang et al., 2016**). Higher-throughput techniques that exchange non-native for resident mtDNAs in non-immortal somatic cells in tissue culture could enable studies of mtDNA–nDNA interactions and replace deleterious mtDNAs within cells with therapeutic potential (**Patananan et al., 2016**). Thus, a higher throughput, reproducible, and versatile mtDNA transfer approach to generate multiple desired 'stable isolated mitochondrial recipient' (SIMR) clones in replication-limited cells remains essential for statistically valid studies and potential translation of mitochondrial transplantation.

Results

MitoPunch mechanism uses fluid pressure to disrupt the plasma membrane

We developed 'MitoPunch' as a simple, high-throughput mitochondrial transfer device consisting of a lower polydimethylsiloxane (PDMS) reservoir loaded with a suspension of isolated mitochondria, covered by a polyethylene terephthalate (PET) filter seeded with ~1 × 10^5 adherent cells (**Figure 1A**, **Figure 1—figure supplement 1**). MitoPunch uses a solenoid-activated plunger to transfer isolated mitochondria in a holding chamber by force into the cytosol of mammalian cells. Upon actuation, a mechanical plunger deforms the PDMS from below, which, as calculated by numerical simulation, generates pressure up to 28 kPa inside the PDMS chamber, propelling the suspension through numerous 3 μm pores in the PET filter. This pressure cuts the plasma membrane of recipient cells sitting atop the pores and delivers mitochondria into the cytoplasm of the cut cells (**Figure 1B**). To assess performance, we compared MitoPunch to mitochondrial coincubation (**Kitani et al., 2014**) and to MitoCeption (**Caicedo et al., 2015**), a method that uses centripetal force generated in a centrifuge to localize mitochondria to recipient mammalian cells (**Figure 1C**). In MitoCeption, a 1500 × *g* centripetal force draws isolated mitochondria to a recipient cell monolayer. We calculate that the suspended mitochondria exert a pressure of ~1.6 Pa on recipient cell membranes (**Figure 1D**) (see Materials and methods).

Mitochondrial delivery into transformed and primary cells

We isolated and delivered dsRed-labeled mitochondria from ~1.5 × 10^7 HEK293T cells (**Miyata et al., 2014**) into ~1 × 10^5 143BTK– ρ0 osteosarcoma cells and replication-limited BJ ρ0 foreskin fibroblasts in technical triplicate and measured the fraction of recipient cells positive for dsRed fluorescence by ImageStreamx MarkII imaging flow cytometry (**Figure 2A**). We define technical replication as independently performed mitochondrial deliveries using the same isolated mitochondrial preparation into recipient cells of the same passage. For 143BTK– ρ0 cells at ~2 hr post-delivery, imaging flow cytometry showed that MitoPunch yielded the lowest fraction of dsRed-positive cells compared to coincubation or MitoCeption. Similarly, for BJ ρ0 recipient cells, MitoPunch yielded the lowest fraction of dsRed-positive cells compared to coincubation or MitoCeption, although at lower levels relative to 143BTK– ρ0 recipients. This measurement assesses colocalization of mitochondria with recipient cells, and not necessarily the occurrence or mechanism of

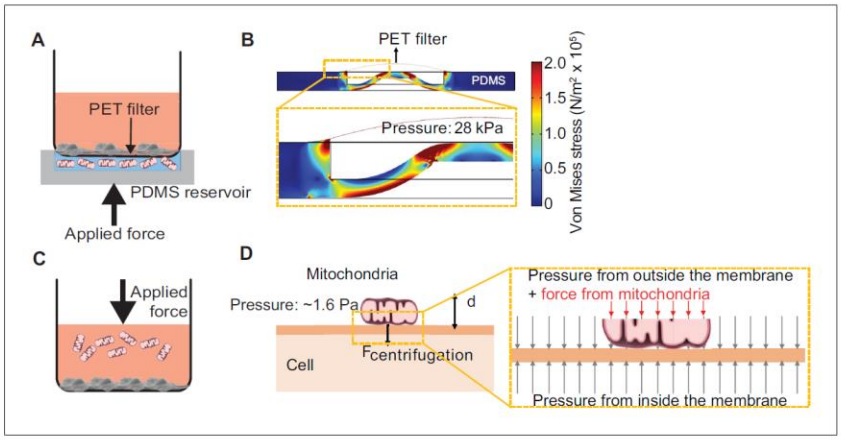

Figure 1. Pressure simulations of mitochondrial transfer tools. (**A**) Schematic of MitoPunch apparatus. Recipient cells (1×10^5) are seeded on a porous polyester (PET) membrane ~24 hr before delivery. A freshly isolated suspension of mitochondria in 1× Dulbecco's Phosphate Buffered Saline (DPBS) with calcium and magnesium, pH 7.4, is loaded into the polydimethylsiloxane (PDMS) chamber and the filter insert is sealed over the PDMS before activation of the mechanical plunger to pressurize the apparatus and deliver the mitochondrial suspension into recipient cells. (**B**) Numerical simulation showing the pressure inside the PDMS chamber reaching 28 kPa with piston activation. COMSOL file used to model MitoPunch pressure is available in ***Figure 1—source data 1***. (**C**) Schematic of MitoCeption technique. Recipient cells (1×10^5) are seeded on wells of a 6-well dish ~24 hr before delivery. A freshly isolated suspension of mitochondria in 1× DPBS with calcium and magnesium, pH 7.4, is pipetted into the cell medium before the plate is centrifuged at 1500 × *g* for 15 min at 4˚C. The plate is incubated in a 37˚C incubator for 2 hr before being centrifuged again at 1500 × g for 15 min at 4˚C. (**D**) MitoCeption pressure model and calculated pressure exerted by isolated mitochondria on recipient cells during delivery.
The online version of this article includes the following source data and figure supplement(s) for figure 1:

Source data 1. Numerical simulation of MitoPunch pressure generation during mitochondrial delivery.
Figure supplement 1. Annotated MitoPunch apparatus.

internalization of delivered mitochondria. These data suggest that the method of delivery and target cell type affect the efficiency of initiating mitochondria–recipient cell interactions.

We quantified the number of discreet dsRed-spots in each cell ~2 hr following delivery from this data (***George et al., 2004***; ***Figure 2B*** and ***Figure 2—figure supplement 1***). ImageStream spot count analysis of 143BTK– ρ0 recipient cells showed MitoPunch delivered a lower mean and median number of dsRed spots per cell than coincubation or MitoCeption. MitoPunch transfers into BJ ρ0 recipient cells yielded fewer mean spots/cell compared to coincubation and MitoCeption with an equivalent median number of spots/cell for MitoPunch and MitoCeption and slightly more for coincubation. Next, we used confocal microscopy to observe dsRed mitochondrial fluorescence in 143BTK– ρ0 recipients fixed 15 min post-transfer, which we chose for its robust mitochondrial acquisition (***Figure 2C***). We visualized mitochondrial localization with confocal microscopy by detecting dsRed protein from the donor mitochondria, shown in red, and labeling the recipient cell plasma membranes with either CellMask Green (coincubation and MitoCeption) or wheat germ agglutinin (MitoPunch), shown in green. Following MitoPunch, mitochondrial dsRed appeared to localize to pores in the filter insert and within the cytoplasm of cells, whereas coincubation and MitoCeption uniformly coated recipient cells with mitochondria, with greater mitochondrial association with recipient cells following MitoCeption. While all three methods initiate physical interactions between mitochondria and recipient cells, MitoPunch delivers mitochondria to the basal membranes of recipient cells at regions associated with the PET membrane pores, compared to a diffuse membrane association pattern seen with coincubation and MitoCeption.

To investigate the capacity of these methods to disrupt recipient cell plasma membranes, we delivered the membrane impermeant dye propidium iodide (PI) by coincubation, MitoPunch, and MitoCeption to measure membrane disruption from delivery and quantified uptake by flow cytometry (***Figure 2D***; ***Novickij et al., 2017***). Delivery into 143BTK– ρ0 cells by MitoPunch and MitoCeption

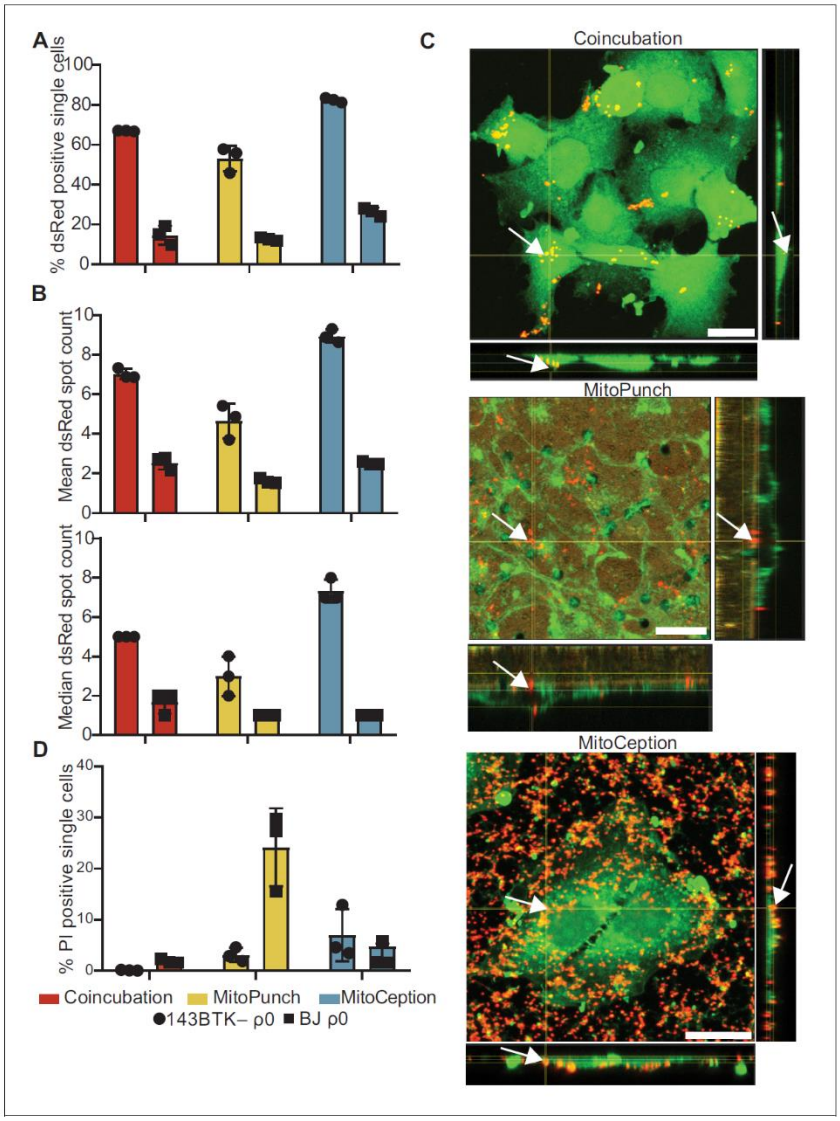

Figure 2. MitoPunch delivers isolated mitochondria to recipient cells. (**A**) Quantification of flow cytometry results measuring the association of dsRed mitochondria with 143BTK– ρ0 and BJ ρ0 single recipient cells following mitochondrial transfer. (**B**) Mean and median dsRed spot count quantification of ImageStream data. (**C**) Sequential Z-stacks of confocal microscopy of 143BTK– ρ0 cells delivered isolated HEK293T-derived dsRed mitochondria by coincubation, MitoPunch, and MitoCeption and fixed 15 min following transfer. Arrows indicate representative mitochondria interacting with recipient cells. Transferred dsRed mitochondria are labeled in red. Plasma membranes are labeled in green, stained with CellMask Green plasma membrane stain in coincubation and MitoCeption and with wheat germ agglutinin plasma membrane stain in MitoPunch. Scale bars indicate 15 µm. (**D**) Quantification of flow cytometry measurements of fluorescence in 143BTK– ρ0 and BJ ρ0 single cells following propidium iodide transfer by coincubation, MitoPunch, and MitoCeption. Error bars represent SD of three technical replicates in all figures.
The online version of this article includes the following figure supplement(s) for figure 2:

Figure 2 continued on next page

Figure 2 continued

Figure supplement 1. Mitochondrial spot quantification.

resulted in similar percentages of PI-positive recipient cells, and both were greater than coincubation. Interestingly, BJ ρ0 cells showed comparable fractions of PI-positive cells to the 143BTK– ρ0 after coincubation and MitoCeption. However, MitoPunch yielded an approximately fivefold increase in the PI-positive fraction compared to all other conditions. These data show that MitoPunch and MitoCeption disrupt the plasma membranes of recipient cells for potential mitochondrial transfer, and the degree of disruption is cell type and delivery method dependent.

Stable retention of transplanted mtDNA

After verifying mitochondrial interaction with recipient cells by coincubation, MitoPunch, and MitoCeption, we next determined whether these methods result in permanent retention of exogenous mtDNA to generate SIMR cells. ρ0 cells cannot synthesize pyrimidines and therefore cannot proliferate or survive without supplemented uridine because of ETC impairment, so we used nucleotide-free medium prepared with dialyzed fetal bovine serum (SIMR selection medium) to select for SIMR cells with transplanted mtDNA and restored ETC activity (***Grégoire et al., 1984***; ***Figure 3A and B***).

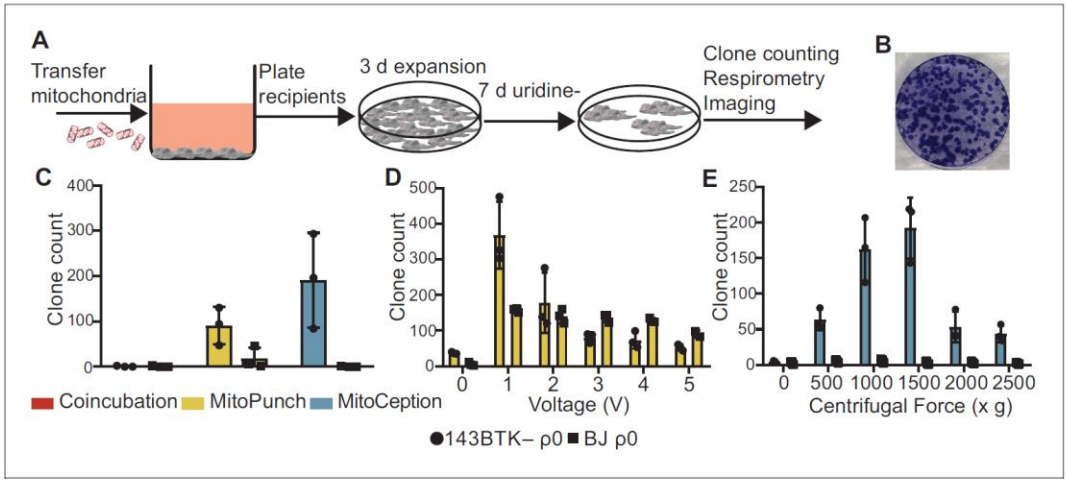

Figure 3. Stable retention of transplanted mitochondrial DNA (mtDNA) into transformed and replication-limited cells. (**A**) Workflow for stable isolated mitochondrial recipient (SIMR) cell generation by mitochondrial transfer into ρ0 cells. (**B**) Representative fixed and crystal violet stained 10 cm plate image following MitoPunch and SIMR cell selection used for SIMR clone generation quantification. (**C**) Quantification of crystal violet stained 143BTK– ρ0 and BJ ρ0 SIMR clones. Error bars represent SD of three technical replicates. (**D**) Quantification of crystal violet stained 143BTK– ρ0 and BJ ρ0 SIMR clones formed by MitoPunch actuated with indicated voltages after uridine-free selection. Error bars represent SD of three technical replicates with the exception of BJ ρ0 5 V transfer, which shows two replicates. (**E**) Quantification of crystal violet stained 143BTK– ρ0 and BJ ρ0 SIMR clones formed by MitoCeption with indicated centripetal forces after uridine-free selection. Error bars represent SD of three technical replicates.
The online version of this article includes the following figure supplement(s) for figure 3:

Figure supplement 1. Verification of surviving mitochondrial donor cells following mitochondrial isolation.
Figure supplement 2. MitoPunch generates stable isolated mitochondrial recipient (SIMR) clones in immortalized mouse cells.
Figure supplement 3. Quantification of MitoPunch reproducibility.
Figure supplement 4. Quantification of MitoPunch reproducibility relative to mitochondrial mass transferred.
Figure supplement 5. Quantification of stable isolated mitochondrial recipient (SIMR) generation efficiency by delivering different masses of isolated mitochondria.
Figure supplement 6. Quantification of MitoPunch stable isolated mitochondrial recipient (SIMR) generation by serial deliveries using one isolated mitochondrial aliquot.

BJ ρ0 cells survive longer under this selection scheme compared to the 143BTK– ρ0 (data not shown), so we included an additional selection phase by culturing these cells in nucleotide-free, glucose-free, galactose supplemented medium (galactose selection medium) (***Robinson et al., 1992***). We isolated and transferred HEK293T dsRed mitochondria into 143BTK– ρ0 and BJ ρ0 cells by coincubation, MitoPunch, and MitoCeption, performed SIMR selection in cell-type appropriate medium for 7 days, and quantified the number of viable clones by crystal violet staining (***Figure 3C***). Coincubation did not generate SIMR clones in 143BTK– ρ0 cells, in contrast to MitoPunch and MitoCeption, which each generated dozens of clones. BJ ρ0 cells with delivered HEK293T mitochondria by coincubation or MitoCeption did not form SIMR clones. MitoPunch generated numerous SIMR clones in both cell types, although fewer BJ ρ0 SIMR clones than in 143BTK– ρ0 cells, whereas MitoCeption only generated clones in 143BTK– ρ0 cells and was unable to form stable clones in replication-limited BJ cells. To assess the risk of mitochondrial donor cells surviving disruption during mitochondrial isolation and generating false positive SIMR clones, we performed three independent mitochondrial isolations, plated an aliquot from each isolation representing mitochondria isolated from ~1.5×10^7 HEK293T dsRed cells on 10 cm dishes, and carried these plates through the 10-day selection with SIMR selection medium before crystal violet staining for visual assessment (***Figure 3—figure supplement 1***). We observed no cell growth on any of the three plates, indicating a minimal incidence of donor cell survival through the mitochondrial isolation protocol.

We next investigated whether differences in SIMR clone generation between 143BTK– ρ0 and BJ ρ0 cells were driven by sensitivity to differences in delivery pressure. We developed a MitoPunch device with adjustable plunger acceleration modulated by changing the circuit voltage (ImmunityBio). We generated independent voltage titration curves in 1 V increments (0 V – 5 V) for each cell type in technical triplicate at each voltage and used the same mitochondrial preparation for all samples for each cell type. All prior experiments in this study are controlled by delivering DPBS with calcium and magnesium to recipient cells by MitoPunch, but here we included a 0 V condition in which the seeded filter insert was positioned atop the PDMS reservoir and pressed against an aliquot of isolated mitochondrial suspension similar to deliveries with force, but without actuating the piston. We achieved maximum 143BTK– ρ0 SIMR clone generation with this tunable MitoPunch at 1 V, with a sharp reduction to background with increasing voltage (***Figure 3D***). The BJ ρ0 recipient also showed maximal SIMR generation at 1 V, with a shallow decline in SIMR generation efficiency to 5 V. Surprisingly, the 0 V condition consistently yielded a few SIMR clones in the 143 BTK– ρ0 recipients and inconsistently in the BJ ρ0 recipients. This result suggests that the pressure generated by sealing the filter insert against the PDMS reservoir is sufficient to generate SIMR clones at a low frequency. For all forthcoming MitoPunch trials we use the variable voltage MitoPunch device set to 1 V.

We performed a similar force titration with MitoCeption by varying the maximum centripetal force, using a common mitochondrial preparation for all samples of both cell types. In 143BTK– ρ0 cells, we observed maximum clone generation at 1000 × *g* and 1500 × *g*, and we did not generate BJ ρ0 SIMR clones greater than the 0 × *g* background at any acceleration tested (***Figure 3E***). This background, present in both 143BTK– ρ0 and BJ ρ0 conditions at 0 × *g*, is likely from rare un-lysed donor cells from mitochondrial preparations directly pipetted into the culture medium of recipient cells during MitoCeption. We have infrequently observed imperfect donor cell lysis , usually in larger mitochondrial preparations, that results in rare, persistant dsRed fluorescent colonies as observed by fluorescence microscopy. True SIMR clones cannot produce the dsRed protein from donor mitochondria and lose fluorescence with time over selection, while these persistent dsRed colonies maintain their fluorescence over the same period (data not shown). Despite this occasional low-level contaminating donor cell background, MitoCeption yielded a strong dose-dependent response in SIMR clone generation from 143BTK– ρ0 recipients above the background. Additionally, MitoPunch deliveries into B16 ρ0 mouse melanoma cells (***Tan et al., 2015***) yielded maximal SIMR generation at a different voltage than in the human cell lines tested, showing that optimal mitochondrial delivery pressure may be cell type dependent (***Figure 3—figure supplement 2***). These data suggest that MitoPunch is uniquely able to generate SIMR clones in replication-limited fibroblasts and SIMR generation efficiency depends on delivery pressure.

We next quantified the reproducibility of our mitochondrial preparation technique and the MitoPunch procedure by performing triplicate MitoPunch transfers using three independent mitochondrial preparations from equal numbers of HEK293T dsRed biological replicate populations (***Figure 3—figure supplements 3*** and ***4***). We define biological replication here as mitochondrial

preparations derived from independently cultured populations of mitochondrial donor cells. Mitochondrial preparations 1, 2, and 3 (same as those pictured in ***Figure 3—figure supplement 1***) generated consistent protein concentrations, and each preparation yielded dozens of SIMR clones in all three technical replicate MitoPunch deliveries with the exception of Prep 3, which resulted in two lower efficiency replicates. We quantified the number of SIMR clones generated per microgram of mitochondrial mass loaded into the MitoPunch apparatus and observed a similar trend. These results showed that our mitochondrial isolation technique produced consistent levels of isolated mitochondrial mass and that the MitoPunch technique yielded high numbers of SIMR clones.

To enable desirable mtDNA–nDNA clone generation using limited starting material, such as mitochondria from rare cell subpopulations, we determined the minimal mass of mitochondrial isolate required to generate SIMR clones. We performed coincubation, MitoPunch, and MitoCeption transfers into ~1 $\times$ 10^5 143BTK– ρ0 recipient cells using decreasing concentrations of dsRed mitochondria isolated from HEK293T cells and plated half of the recipient cell population on 10 cm plates. We observed a similar dose-dependent relationship between mitochondrial mass delivered and SIMR clones observed for MitoPunch and MitoCeption across 0.16 µg, 1.6 µg, and 16 µg total mitochondrial protein suspended in 120 µL of 1$\times$ DPBS, pH 7.4 transfer buffer (***Figure 3—figure supplement 5***). These results showed that although MitoPunch and MitoCeption generate SIMR clones from transformed recipient cells with similar efficiency per microgram of mitochondrial isolate delivered, the differences inherent to the two protocols rendered direct comparisons of their relative efficiencies less meaningful.

Moving the seeded PET filter from a 12-well dish to the MitoPunch apparatus often resulted in excess medium being carried to the PDMS reservoir. Combined with the small volume of mitochondrial preparation delivered to the recipient cells, we observed that MitoPunch resulted in diluted residual mitochondrial isolate left in the reservoir post-transfer. In the interest of conserving mitochondrial material, we tested whether a used 120 µL aliquot of isolated mitochondria can be applied to repeated MitoPunch transfers to generate SIMR clones (***Figure 3—figure supplement 6***). We performed 11 sequential deliveries into 143BTK– ρ0 cells using one aliquot of mitochondrial isolate and found maximal SIMR clone generation from the first and second deliveries, after which we observe a sharp reduction in SIMR cell formation and inconsistent SIMR generation rate up to the 11th transfer. These data showed that multiple MitoPunch transfers can be performed using a single aliquot of mitochondrial suspension when material is limited.

SIMR cells rescue ρ0 mitochondrial respiration and network morphology

Finally, we measured mitochondrial function in SIMR cells by quantifying the rate of oxygen consumption and assessing mitochondrial morphology. We isolated three independent 143BTK– ρ0 SIMR clones generated by MitoPunch or MitoCeption transfer of isolated HEK293T mitochondria and measured each clone's oxygen consumption rate (OCR) using a Seahorse Extracellular Flux Analyzer mitochondrial stress test (***Figure 4A***, ***Figure 4—figure supplement 1***). To determine whether SIMR clone respiration remained stable through time, we grew the clones through two freeze/thaw cycles in uridine supplemented medium and measured cellular respiration. We found that one MitoCeption clone lost its respiratory capacity and one MitoPunch clone was not viable after freezing and thawing (data not shown). In the remaining clones, basal and maximal respiration, spare respiratory capacity, and ATP generation remained stable throughout both freeze-thaw cycles. We have performed numerous similar experiments using a range of recipients and mitochondrial donors and observed successful clone viability after freeze-thaw (data not shown).

We then immunostained the freeze-thawed SIMR clones with anti-TOM20 and anti-double-stranded DNA (dsDNA) antibodies to detect mitochondria and mtDNA content, respectively, by confocal microscopy (***Figure 4B*** and ***Figure 4—figure supplement 2***). The MitoCeption clone that lost respiratory capacity showed a fragmented mitochondrial network with no detectable mtDNA (***Figure 4—figure supplement 2***), whereas the other SIMR clones generated by MitoPunch and MitoCeption contained mtDNA with filamentous mitochondrial network morphologies. These data show that the majority of 143BTK– ρ0 SIMR clones generated by either MitoPunch or MitoCeption have retained mtDNA, restored respiratory profiles, and filamentous mitochondrial network morphologies.

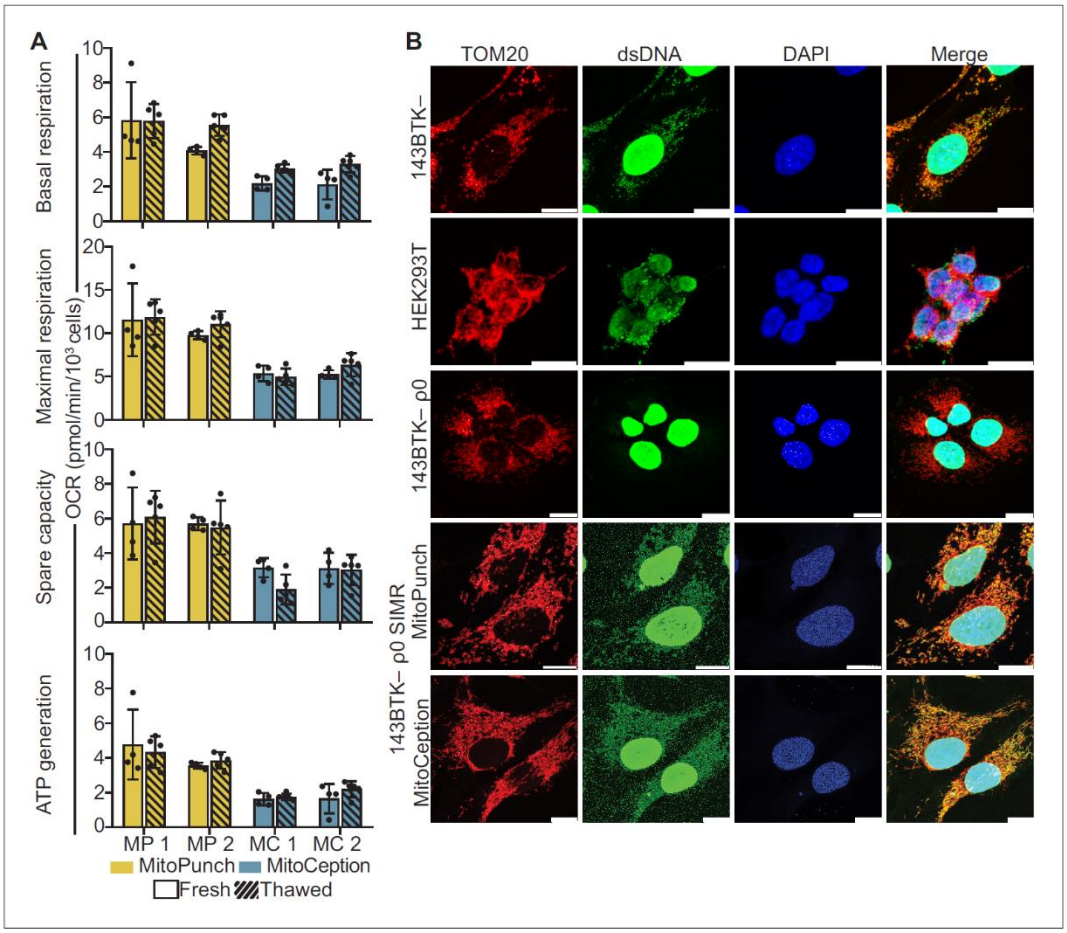

Figure 4. Mitochondrial DNA (mtDNA) transplantation rescues ρ0 mitochondrial phenotypes. (**A**) Oxygen consumption rate (OCR) quantification of basal and maximal respiration, spare respiratory capacity, and ATP generation from two independent 143BTK– ρ0 + HEK293T stable isolated mitochondrial recipient (SIMR) clones generated by MitoPunch and MitoCeption. Cross-hatched data indicate clones that were frozen and thawed twice each. Error bars represent SD of four technical replicates for fresh SIMR cell measurements and five for thawed SIMR cell measurements. (**B**) Confocal microscopy of representative 143BTK– ρ0 + HEK293T SIMR clones compared to 143BTK– parental, HEK293T dsRed mitochondrial donor, and 143BTK– ρ0 controls. Mitochondria were stained with anti-TOM20 antibody and labeled red, double-stranded DNA was stained with anti-dsDNA antibody and labeled green, and cell nuclei were stained with NucBlue (Hoechst 33342) and labeled blue. Scale bars indicate 15 μm.
The online version of this article includes the following figure supplement(s) for figure 4:

Figure supplement 1. Schematic of the Seahorse Mito Stress Test.
Figure supplement 2. Confocal microscopy of stable isolated mitochondrial recipient (SIMR) lines.

Discussion

Stability of the mitochondrial genome is essential for studying the long-term effects of mtDNA–nDNA interactions and for potential therapeutic applications of mitochondrial transfer. MitoPunch generates up to hundreds of SIMR clones in both transformed and Hayflick-limited recipient cells by exerting a pressure sufficient to perforate mammalian cell membranes in regions small enough to be

repaired within minutes, which sustains cell viability and resumed cell growth and proliferation (**Boye et al., 2017**). We have generated SIMR clones by MitoPunch with mitochondria isolated by a commercially available kit, as performed here, as well as by using standard mitochondrial isolation buffers. Additionally, we achieved similar results by disrupting mitochondrial donor cells using Dounce homogenization (data not shown) but found the commercially available kit with syringe disruption is advantageous due to its ease of use, reproducibility, and a reduced number of steps to isolate mitochondria. We generated dozens of SIMR clones by MitoPunch and MitoCeption using these mitochondrial isolation methods and anticipate that other mitochondrial preparation techniques will also yield SIMR clones.

Interestingly, we do not observe SIMR clone generation by coincubation in our study. Few reports show limited stable clone formation by coincubation techniques, but these studies used up to 100-fold higher levels of exogenous mitochondria in coincubation experiments than required for MitoPunch or MitoCeption in our hands, or antibiotic selection schemes to achieve stable mitochondrial transfer (**Clark and Shay, 1982**; **Patel et al., 2017**). High levels of mitochondrial protein are easily isolated from fast-growing immortalized cell lines but may not be available when using human donor-derived or other limiting starting material. Additionally, mitochondrial donor cells of interest nearly exclusively lack antibiotic selection markers, making such selection schemes unfeasible. Particularly in those cases, the greatly enhanced SIMR generation capacity of MitoPunch and MitoCeption is strongly enabling for generating desired mtDNA–nDNA combinations.

The distinct mechanisms and procedures of MitoPunch and MitoCeption make direct comparisons of their relative efficiencies challenging. Despite this, our results demonstrate that both techniques generate SIMR clones from ρ0 transformed cells in a mitochondrial dose-dependent fashion and can be readily adopted by laboratories studying mtDNA–nDNA interactions. Strikingly, in the cell types we have tested, we find that only MitoPunch generates SIMR clones from ρ0 primary, non-immortal cells. Studies in our laboratory suggest that the transcriptome and metabolome of replication-limited SIMR clones differ significantly from un-manipulated control clones but can be recovered and reset to un-manipulated control levels by cellular reprogramming to induced pluripotent stem cells and subsequent differentiation (**Patananan et al., 2020**). These results indicate that SIMR clone generation in replication-limited, reprogrammable cells is crucial for studies of mtDNA–nDNA interactions involving mitochondrial transplantation into ρ0 cells, and that MitoPunch is uniquely capable of efficiently generating enough clones for statistically valid studies in such work. We have circumvented the need for ρ0 recipient cells by using the MitoPunch technology to completely replace mutant mtDNA in mouse cells without mtDNA depletion. This was done by delivering mitochondria containing mtDNA with a chloramphenicol resistant point mutation and selecting for SIMR clones containing only rescue mtDNA using antibiotic supplemented nucleotide-free medium (**Dawson et al., 2020**). However, this workflow is dependent upon using antibiotic resistant mitochondrial donor cells and is not applicable to investigating the full spectrum of mtDNA sequences required for robust studies of mtDNA–nDNA interactions. Future work with MitoPunch and other isolated mitochondrial transfer modalities will be improved by developing techniques to avoid fully depleting the mtDNA of recipient cells of interest before generating SIMR clones for downstream analysis and applications.

Materials and methods

Key resources table

Reagent type (species) or resource	Designation	Source or reference	Identifiers	Additional information
Cell line (*Homo sapiens*)	143 BTK– ρ0 osteosarcoma	**Patananan et al., 2020**, ATCC	Cat. #CRL-8303; RRID:CVCL_9W36	
Cell line (*Homo sapiens*)	143 BTK– osteosarcoma	ATCC	Cat. #CRL-8303; RRID:CVCL_9W36	
Cell line (*Homo sapiens*)	BJ ρ0 foreskin fibroblast (male)	**Patananan et al., 2020** ATCC	Cat. #CRL-2522; RRID:CVCL_3653	

Continued on next page

Continued

Reagent type (species) or resource	Designation	Source or reference	Identifiers	Additional information
Cell line (*Homo sapiens*)	HEK293T dsRed	***Miyata et al., 2014***		A gift from the laboratory of Dr. Carla Koehler
Cell line (*M. musculus*)	B16 ρ0 melanoma	***Dong et al., 2017***		A gift from the laboratory of Dr. Michael Berridge
Cell line (*M. musculus*)	L929 fibroblasts	ATCC	Cat. #CCLI-1	
Antibody	Anti-TOMM20 (Rabbit monoclonal)	Abcam	Cat. #ab78547 RRID:AB_2043078	IF(1:1000)
Antibody	Anti-dsDNA (Mouse monoclonal)	Abcam	Cat. #ab27156 RRID:AB_470907	IF(1:1000)
Antibody	Anti-rabbit IgG (Donkey polyclonal)	Thermo Fisher Scientific	Cat. #A-31573 RRID:AB_2536183	IF(1:100)
Antibody	Anti-mouse IgG (Donkey polyclonal)	Thermo Fisher Scientific	Cat. #A-21202 RRID:AB_141607	IF(1:100)
Commercial assay or kit	Qproteome Mitochondria Isolation kit	Qiagen	Cat. #37612	
Commercial assay or kit	BCA protein assay	Thermo Fisher	Cat. #23225	
Chemical compound, drug	Propidium iodide	Thermo Fisher Scientific	Cat. #P1304MP	
Chemical compound, drug	Accutase	Thermo Fisher Scientific	Cat. #A1110501	
Chemical compound, drug	16% paraformaldehyde	Thermo Fisher Scientific	Cat. #28906	
Chemical compound, drug	Triton-X 100	Sigma	Cat. #X100	
Chemical compound, drug	ProLong Gold Antifade Mountant with DAPI	Invitrogen	Cat. #P3691	
Chemical compound, drug	ProLong Glass Antifade Mountant with NucBlue Stain	Thermo Fisher Scientific	Cat. #P36985	
Chemical compound, drug	Uridine	Thermo Fisher Scientific	Cat. #AC140770250	
Chemical compound, drug	Galactose	Sigma-Aldrich	Cat. #G5388-100G	
Chemical compound, drug	CellMask Green PM	Molecular Probes	Cat. #C37608	
Chemical compound, drug	Alexa Fluor 488 conjugated Wheat Germ Agglutinin	Invitrogen	Cat. #W11261	
Chemical compound, drug	Crystal violet	Thermo Fisher Scientific	Cat. #C581-25	
Software, algorithm	Wave 2.6.2	Agilent	RRID:SCR_014526	
Software, algorithm	FlowJo 10.6.2	BD Biosciences	RRID:SCR_008520	
Software, algorithm	IDEAS 6.2	Luminex		
Software, algorithm	Multiphysics 5.3	COMSOL	RRID:SCR_014767	
Software, algorithm	Imaris Viewer 9.5.1	Oxford Instruments	RRID:SCR_007370	
Software, algorithm	Imaris File Converter 9.5.1	Oxford Instruments	RRID:SCR_007370	
Software, algorithm	Prism v.8	Graphpad	RRID:SCR_002798	
Software, algorithm	LAS X Lite 3.7.1.21655	Leica		
Software, algorithm	FIJI	***Schindelin et al., 2012***		
Other	Dialyzed FBS	Life Technologies	Cat#26400–044	

Continued on next page

Continued

Reagent type (species) or resource	Designation	Source or reference	Identifiers	Additional information
Other	12–well 3.0 µm Transparent PET Membrane	Corning	Cat#353181	
Other	Glass coverslips	Zeiss	Cat#474030–9000	
Other	V3 96-well plate	Agilent	Cat#101085–004	
Other	Variable voltage MitoPunch apparatus	ImmunityBio		Inquiries regarding this device can be made to the corresponding author

Cell culture conditions

Human ρ0 cells were grown in DMEM (Fisher Scientific, Waltham, MA, Cat. # MT10013CM) supplemented with 10% FBS, non-essential amino acids (Gibco, Waltham, MA, Cat. #11140–050), GlutaMax (Thermo Fisher Scientific, Waltham, MA, Cat. # 35050–061), penicillin and streptomycin (VWR, Radnor, PA, Cat. # 45000–652), and 50 mg/L uridine (Thermo Fisher Scientific, Cat. # AC140770250). All other human cell lines were grown in DMEM (Fisher Scientific, Cat. # MT10013CM) supplemented with 10% FBS, non-essential amino acids, GlutaMax, and penicillin and streptomycin. B16 ρ0 cells were grown in RPMI (Thermo Fisher Scientific, Cat. # MT-10–040 CM) supplemented with 10% FBS, non-essential amino acids, GlutaMax, penicillin and streptomycin, pyruvate (Corning, Corning, NY, Cat. # 25000 CI), and 50 mg/L uridine. L929 cells were grown in RPMI supplemented with 10% FBS, non-essential amino acids, GlutaMax, penicillin and streptomycin, and pyruvate. All mammalian cells were cultured in a humidified incubator maintained at 37˚C and 5% CO_2. The following cells were used in this study: HEK293T dsRed (female), 143BTK– (female), 143BTK– ρ0 (female), BJ ρ0 (male), B16 (male), and L929 (male). We have not formally identified these cell lines; however, we have sequenced their mitochondrial and nuclear DNA for polymorphisms and find unique sequences which we use for genotyping our cultures (unpublished data). BJ ρ0 cells were used as mitochondrial recipients within three passages of thaw for all mitochondrial transfer experiments in this work to avoid the onset of senescence. All lines were routinely tested for mycoplasma with negative results.

Mitochondrial isolation

Mitochondria were isolated from ~1.5 × 10^7 mitochondrial donor cells per mitochondrial transfer using the Qproteome Mitochondrial Isolation Kit (Qiagen, Hilden, Germany, Cat. #37612) with slight alterations to the manufacturers protocol. Mitochondrial donor cells were harvested using a cell scraper (Fisher Scientific, Cat. # 08-100-241) and collected in 50 mL conical tubes at approximately 6 × 10^7 cells per tube (Thermo Scientific, Cat. #12-565-271). Cells were pelleted by centrifugation at 500 × *g* for 10 min at 4˚C and washed with DPBS before pelleting again by centrifugation at 500 × *g* for 10 min at 4˚C. Cells were resuspended at 1 × 10^7 cells/mL in ice-cold Lysis Buffer with Protease Inhibitor Solution and incubated for 10 min at 4˚C in 2 mL tubes on an end-over-end shaker. Lysates were centrifuged at 1000 × *g* for 10 min at 4˚C and supernatant was aspirated. Pellets were resuspended in 1.5 mL ice-cold Disruption Buffer with Protease Inhibitor Solution and mechanical disruption was accomplished by 10 passes through a 26 G blunt ended needle (VWR, Radnor, PA, Cat. # 89134–164) attached to a 3 mL syringe (VWR, Cat. # BD309657). The subsequent lysates were centrifuged at 1000 × *g* for 10 min at 4˚C and the supernatants were transferred to new 2 mL tubes. The resultant supernatants were centrifuged again at 1000 × *g* for 10 min at 4˚C to remove any remaining intact cells, and the supernatants were transferred to clean 1.5 mL tubes. These supernatants were centrifuged at 6000 × *g* for 10 min at 4˚C and the supernatants were aspirated. The resulting mitochondrial pellets were resuspended in mitochondrial storage buffer and pelleted by centrifugation at 6000 × *g* for 20 min at 4˚C. The isolated mitochondrial pellets were resuspended in 120 µL per transfer replicate 1× DPBS with calcium and magnesium (Thermo Fisher Scientific, Cat. # 14040133) immediately prior to mitochondrial transfer and kept on ice.

Mitochondrial coincubation

~1 × 10^5 143BTK– ρ0 or BJ ρ0 cells were seeded into wells of 6-well dishes ~ 24 hr prior to delivery. Mitochondria isolated from ~1.5 × 10^7 HEK293T dsRed cells resuspended in 120 µL 1× DPBS with calcium and magnesium were pipetted into the culture medium of each well containing recipient cells and incubated at 37˚C and 5% CO_2 for 2 hr. Cells were then released from the dish using Accutase (Thermo Fisher Scientific, Cat. # A1110501) and seeded into 10 cm plates for SIMR cell selection or harvested for additional analyses.

MitoPunch apparatus construction

A 5 V solenoid (Sparkfun, Boulder, CO, Cat. # ROB-11015) is screwed into a threaded plug (Thor Labs, Newton, NJ, Cat. # SM1PL) and inserted into a bottom plate (Thor Labs, Cat. # CP02T) (***Figure 1—figure supplement 1***). The solenoid is regulated by a Futurlec mini board (Futurlec, New York, NY, Cat. # MINIPOWER) and powered by a MEAN WELL power supply (MEAN WELL, New Taipei City, Taiwan, Cat. # RS-35–12). Optomechanical assembly rods (Thor Labs, Cat. # ER3) are inserted into the bottom plate. The middle and top plates (Thor Labs, Cat. # CP02) are threaded through the assembly rods. The middle plate is fitted with a retaining ring, which supports an aluminum washer (outer diameter, 25 mm; inner diameter, 10 mm). The middle plate is secured along the assembly rods using the included screws. The retaining ring is adjusted such that the top surface of the washer is at the same height as the piston surface in its retracted state. A flexible PDMS (10:1 ratio of Part A base: Part B curing agent) (Fisher Scientific, Cat. #NC9644388) reservoir consisting of a bottom layer (25 mm diameter, 0.67 mm height) bonded to an upper ring (outer diameter, 25 mm; inner diameter, 10 mm; height, 1.30 mm) is placed on top of the washer. This reservoir can contain up to ~120 µL of liquid. To perform MitoPunch delivery, a 3 µm membrane transwell insert (Corning, Cat. # 353181) seeded with 1 × 10^5 adherent cells is lowered through the top plate and rested atop one retaining ring. The insert is secured to the top plate by an additional retaining ring. This assembly is lowered until the base of the insert contacts the top surface of the PDMS reservoir and is secured in place with screws to form a tight seal. In addition, a variable voltage version of this device based on the same principles with identical delivery procedures as MitoPunch, but with tunable plunger acceleration achieved by varying actuator voltage, was engineered by ImmunityBio and is available upon request to the corresponding author. Optimal MitoPunch delivery voltage for individual cell lines is determined empirically by performing a voltage-response curve in technical triplicate across a range of voltages from 1 V to 5 V using the piston acceleration control software.

Seeding cells for MitoPunch mitochondrial transfer

Filter inserts with 3 µm pores (Corning, Cat. # 353181) are placed in wells of a 12-well dish. 1.5 mL warm uridine supplemented medium is dispensed in the wells outside of the filter insert, and 1 × 10^5 adherent cells suspended in 0.5 mL warm uridine supplemented medium are seeded within the filter inserts and placed in a humidified incubator maintained at 37˚C and 5% CO_2 1 day prior to mitochondrial delivery.

MitoPunch mitochondrial transfer

Following mitochondrial isolation, the MitoPunch apparatus is sterilized with 70% ethanol and entered into the biological safety cabinet and an autoclaved PDMS reservoir is placed in the device as indicated in ***Figure 1—figure supplement 1***. The PDMS reservoir is washed 3× with 120 µL sterile DPBS with calcium and magnesium after being set in the MitoPunch apparatus. 120 µL mitochondrial suspension from ~1 × 10^7 donor cells in DPBS with calcium and magnesium is loaded into the PDMS reservoir. Mitochondrial transfer is performed by securing the seeded membrane to the PDMS reservoir and actuating the solenoid for 3 s. The mechanical plunger strikes the middle of the PDMS chamber, displacing the base layer by ~1.3 mm. This displacement pressurizes the mitochondrial suspension and propels it through the membrane and into the cells (***Figure 1B***). Once the solenoid has returned to its starting position, the insert is removed from the apparatus, placed back in the 12-well dish in its original medium, and incubated at 37˚C and 5% CO_2 for 2 hr. Cells were then released from the dish using Accutase and seeded into 10 cm plates for SIMR cell selection or harvested for additional analyses.

Collecting mitochondrial recipient cells following MitoPunch transfer

Following MitoPunch mitochondrial transfer and 2 hr incubation, medium is aspirated from within the transwell filter with care taken not to disrupt the cells on the membrane, and then from outside and underneath the filter insert. The well and insert are washed 1× with DPBS (0.5 mL inside the insert and 1 mL outside the insert) with DPBS aspirated as before. Cells are released from the membrane by 5 min incubation at 37˚C and 5% CO_2 with Accutase (0.5 mL inside the insert and 1 mL outside the insert). Following incubation, the cells are suspended in the Accutase within the filter insert using a P1000 pipette, being careful not to puncture the PET membrane, and directly pipetted into 10 cm plates with 10 mL warm uridine supplemented medium.

MitoCeption

As described previously (***Caicedo et al., 2015***), 1 × 10^5 recipient cells were seeded in each well of a 6-well dish and incubated at 37˚C and 5% CO_2 overnight. Mitochondrial isolate from ~1 × 10^7 donor cells suspended in 1× DPBS with calcium and magnesium was pipetted into the well and the plate was centrifuged at 1500 × *g* for 15 min at 4˚C. Cells were removed from the centrifuge and incubated for 2 hr at 37˚C and 5% CO_2 before being centrifuged a second time at 1500 × *g* for 15 min at 4˚C. Cells were then released from the dish using Accutase and seeded into 10 cm plates for SIMR cell selection or harvested for additional analyses.

The pressure generated by the MitoCeption method was estimated by calculating the force exerted per unit area of the cell membrane during centrifugation. The force induced by the centrifugation of a single mitochondrion on the cell membrane was equal to the centripetal force of the mitochondria under the acceleration of 1500 × *g* minus the buoyancy force,

$$F_{centrifugation} = (m_{mito} - m_{water}) * a$$

where m_{mito} and m_{water} are the mass of mitochondria and water, and a is the acceleration rate of centrifugation. The equivalent pressure induced by mitochondria during centrifugation was approximated by

$$p = \frac{F_{centrifugation}}{S} = \frac{(m_{mito} - m_{water}) * a}{S} = \frac{(\rho_{mito} - \rho_{water}) Va}{S} \approx (\rho_{mito} - \rho_{water}) * a * d$$

where ρ_{mito} (1.1 g/cm^3) and ρ_{water} (1.0 g/cm^3) are the density of mitochondria and water, V and S are the volume and cross-sectional area of mitochondria, and d is the thickness of a mitochondrion (~1 μm). Using values for the geometry and properties of a mitochondrion, the pressure induced by MitoCeption centrifugation was ~1.6 Pa.

Numerical simulation of MitoPunch internal pressure

The finite element method (COMSOL Inc, Burlington, MA, Multiphysics 5.3) was used to simulate the pressure inside the MitoPunch PDMS chamber. We constructed the simulation geometry according to real device dimensions. Piston movement was applied as initial displacement in the y direction. Considering the incompressibility of the aqueous medium inside the PDMS chamber, the volume of the chamber was maintained constant while solving for the stress distribution of all the materials.

SIMR clone isolation

Mitochondrial recipient and vehicle delivery control 143BTK– ρ0 cells were grown in complete medium supplemented with 50 mg/L uridine for 3 days following mitochondria or vehicle transfer. After 3 days, the medium was changed to SIMR selection medium (complete medium with 10% dialyzed FBS (Life Technologies, Carlsbad, CA, Cat. # 26400–044)) and medium was exchanged daily. After the vehicle delivery control sample died and clones emerged on mitochondrial transfer plates (~7 days SIMR selection medium), clones were isolated using cloning rings or plates were fixed and stained with crystal violet for counting.

Mitochondrial recipient and vehicle delivery control BJ ρ0 and B16 ρ0 cells were grown in complete media supplemented with 50 mg/L uridine for 3 days following mitochondria transfer. After 3 days, the medium was changed to SIMR selection medium and exchanged daily. On day 5 post-delivery, cells were shifted to galactose selection medium (glucose-free, galactose-containing

medium [DMEM without glucose, Gibco, Cat. # 11966025] supplemented with 10% dialyzed FBS and 4.5 g/L galactose [Sigma-Aldrich, Cat. #G5388-100G]). After the vehicle delivery control sample died and clones emerged on mitochondrial transfer plates (~36 hr in galactose selection medium), clones were isolated using cloning rings or plates were fixed and stained with crystal violet for counting.

Crystal violet staining and clone counting

Media was aspirated from 10 cm plates before fixation with 1 mL freshly diluted 4% paraformaldehyde in 1× DPBS for 15 min at RT. Fixative was removed and 1 mL 0.5% w/v crystal violet solution (Thermo Fisher Scientific, Cat. # C581-25) dissolved in 20% methanol in water was applied to each plate and incubated for 30 min at RT. Crystal violet was removed and plates were washed 2× with deionized water before drying overnight at RT. Dried plates were photographed and crystal violet stained clones were counted manually using FIJI (***Schindelin et al., 2012***).

Imaging flow cytometry

Mitochondria were transferred to recipient cells, which were harvested and collected in 1.5 mL tubes. Samples were centrifuged 5 min at 1000 × *g*, supernatant was aspirated, and cells were washed 3× with 0.5 mL 1× DPBS, pH 7.4. The DPBS was aspirated and cells were fixed in 100 µL freshly diluted 4% paraformaldehyde (Thermo Fisher Scientific, Cat. # 28906) for 15 min on ice. Fixative was diluted with 1 mL of 1× DPBS, pH 7.4, and 5% FBS and centrifuged for 10 min at 500 × *g*. Supernatant was removed and cells resuspended in 1× DPBS, pH 7.4, with 5% FBS. Imaging flow cytometry was performed using an ImageStream MarkII platform and analyzed using the IDEAS 6.2 software package (Luminex, Austin, TX).

Confocal microscopy

1×10^5 cells were plated in 6-well dishes with 2 mL of media on glass coverslips (Zeiss, Oberkochen, Germany, Cat. # 474030–9000) ~24 hr prior to sample preparation. Medium was aspirated and samples were fixed with 0.5 mL freshly diluted 4% paraformaldehyde in 1× DPBS, pH 7.4 pipetted onto samples and incubated for 15 min at RT. Paraformaldehyde was removed and samples were washed 3× with 5 min 1× DPBS incubations. Samples were then permeabilized by 10 min RT incubation in 0.1% Triton-X 100 (Sigma, St. Louis, MO, Cat. # X100). Permeabilized samples were washed 3× with 1× DPBS and then incubated for 1 hr at RT with 2% bovine serum albumin (BSA) dissolved in 1× DPBS blocking buffer. Blocking buffer was aspirated and cells incubated for 1 hr at RT with a 1:1000 dilution of primary antibodies in 2% BSA blocking buffer against dsDNA (Abcam, Cambridge, United Kingdom, Cat. # ab27156) and TOM20 protein (Abcam, Cat. # ab78547), and then washed 3× with 5 min 1× DPBS incubations. Cells were then incubated with secondary antibodies (Invitrogen, Cat. # A31573 and A21202) diluted 1:100 in 2% BSA blocking buffer protected from light for 1 hr at RT. After incubation with secondary antibodies, samples were washed 3× with 5 min 1× DPBS incubations and mounted on microscope slides.

To mount, samples were removed from the 6-well dish and rinsed by dipping in deionized water, dried with a Kimwipe, and mounted using ProLong Gold Antifade Mountant with DAPI (Invitrogen, Carlsbad, CA, Cat. # P3691) or ProLong Glass Antifade Mountant with NucBlue Stain (Thermo Fisher Scientific, Cat # P36985) on microscope slides (VWR, Cat. # 48311–601). Samples were dried at RT protected from light for 48 hr prior to confocal imaging with a Leica SP8 confocal microscope (Leica, Wetzlar, Germany) and later analyzed with either LAS X Lite 3.7.1.21655 (Leica) for two-dimensional image preparation or Imaris File Converter 9.5.1 (Oxford Instruments, Abingdon, United Kingdom) and Imaris Viewer 9.5.1 (Oxford Instruments) for Z-stack analysis.

To perform confocal imaging on cells immediately following mitochondrial transfer, 1×10^5 cells were plated in 6-well dishes with 2 mL of media on glass coverslips for coincubation and MitoCeption or seeded onto 12-well filter inserts as described above for MitoPunch ~24 hr prior to delivery. Immediately prior to mitochondrial transfer, coincubation and MitoCeption samples were stained with 1× CellMask Green PM (Molecular Probes, Eugene, OR, Cat. # C37608) diluted in warm medium for 10 min and washed twice in DPBS, and MitoPunch samples were stained with 5 µg/mL Alexa Fluor 488 conjugated Wheat Germ Agglutinin (Invitrogen, Cat. # W11261) diluted in warm media for 10 min and washed twice in DPBS. Following delivery, culture medium was removed and 1

mL freshly diluted 4% paraformaldehyde in 1× DPBS, pH 7.4, was pipetted onto samples and incubated for 15 min at RT. Paraformaldehyde was aspirated and samples were washed 3× with 1× DPBS, pH 7.4. Samples were further washed with DPBS 3× with 5 min RT incubation per wash. MitoPunch filters were removed from the plastic insert using an inverted P1000 pipette tip. Samples were mounted and imaged as described above.

OCR measurements

OCR measurements were performed using a Seahorse XFe96 Extracellular Flux Analyzer (Agilent, Santa Clara, CA). 2×10^4 cells were seeded into each well of a V3 96-well plate (Agilent, Cat. # 101085–004) and cultured 24 hr before measuring OCR. The Agilent Seahorse mitochondrial stress test was used to quantify OCR for basal respiration and respiration following the sequential addition of the mitochondrial inhibitors oligomycin, carbonyl cyanide-p-trifluoromethoxyphenylhydrazone (FCCP), and antimycin A. Data were analyzed using the Wave 2.6.2 software package (Agilent).

PI staining, delivery, and flow cytometry

Cells (1×10^5) were plated for delivery and incubated overnight. Media was changed to FluorBrite DMEM media (ThermoFisher Scientific, Cat. # A1896701) with 3 µM PI (Thermo Fisher Scientific, Cat. # P1304MP) immediately before transfer. MitoCeption and coincubation were carried out as described above, and MitoPunch was performed with PI FluorBrite medium loaded into the PDMS reservoir and incubated for 15 min at 37˚C and 5% CO_2. All samples were washed with 1× DPBS and collected using Accutase. Samples were collected in flow cytometry tubes and centrifuged 5 min at 500 × *g*. Samples were washed with 1× DPBS with 5% FBS three times and analyzed on a BD Fortessa flow cytometer (BD Biosciences, San Jose, CA) and data were processed using FlowJo 10.6.2 (BD Biosciences).

Quantification and statistical analysis

All information pertaining to experimental replication are found in the figure legends. Mitochondrial transfer experiments were performed in technical triplicate to enable calculation of standard deviation unless otherwise indicated, and oxygen consumption measurements were collected in technical quadruplicate or quintuplicate indicated in the legend of ***Figure 4***. Investigators were blinded for SIMR colony counting analysis. All column heights represent the mean of technical triplicate results unless noted otherwise. All error bars in this manuscript represent standard deviation of three technical replicates unless otherwise specified in the figure legend.

Acknowledgements

We thank Rebeca Acin-Perez, Linsey Stiles, and Orian Shirihai of the UCLA Metabolomics Core for help with Seahorse XF Analyzer assays. We thank Zoran Galic, Alejandro Garcia, and Salem Haile of the UCLA Jonsson Comprehensive Cancer Center Flow Cytometry Core Laboratory and Felecia Codrea, Jessica Scholes, and Jeffrey Calimlim of the UCLA Broad Stem Cell Research Center Flow Cytometry Core for assistance with cellular analysis. We thank Laurent Bentolila and Matthew J Schibler of the UCLA Advanced Light Microscopy/Spectroscopy core for assistance with confocal microscopy. We also thank Emma Dawson, Lynnea Waters, Natasha Carlson, and Christopher Sercel for critical feedback and assistance with this manuscript.

Additional information

Competing interests

Ting-Hsiang Wu: T.-H.W. was an employee of NanoCav, LLC, and is currently employed by NantBio, Inc and ImmunityBio, Inc. Shahrooz Rabizadeh: S.R. is a board member of NanoCav, LLC, and employed by NantBio, Inc, ImmunityBio, Inc, and NantOmics, LLC. Kayvan R Niazi: K.R.N. is a board member of NanoCav, LLC, and employed by NantBio, Inc and ImmunityBio, Inc. Pei-Yu Chiou: P.-Y. C. is a co-founder, board member, shareholder, and consultant for NanoCav, LLC, a private start-up company working on mitochondrial transfer techniques and applications. Michael A Teitell: M.A.T. is

a co-founder, board member, shareholder, and consultant for NanoCav, LLC, a private start-up company working on mitochondrial transfer techniques and applications. The other authors declare that no competing interests exist.

Funding

Funder	Grant reference number	Author
National Institutes of Health	T32CA009120	Alexander J Sercel Alexander N Patananan
National Institutes of Health	T32GM007185	Alexander J Sercel
American Heart Association	18POST34080342	Alexander N Patananan
National Institutes of Health	T32GM008042	Amy K Yu
National Science Foundation	CBET 1404080	Pei-Yu Chiou
National Institutes of Health	R01GM114188	Pei-Yu Chiou Michael A Teitell
Air Force Office of Scientific Research	FA9550-15-1-0406	Pei-Yu Chiou Michael A Teitell
National Institutes of Health	R01GM073981	Michael A Teitell
National Institutes of Health	R01CA185189	Michael A Teitell
National Institutes of Health	R21CA227480	Michael A Teitell
National Institutes of Health	P30CA016042	Michael A Teitell
CIRM	RT3-07678	Michael A Teitell

The funders had no role in study design, data collection and interpretation, or the decision to submit the work for publication.

Author contributions

Alexander J Sercel, Conceptualization, Data curation, Formal analysis, Funding acquisition, Validation, Investigation, Visualization, Methodology, Writing - original draft, Project administration; Alexander N Patananan, Conceptualization, Funding acquisition, Validation, Investigation, Methodology, Writing - review and editing; Tianxing Man, Software, Formal analysis, Investigation, Methodology; Ting-Hsiang Wu, Software, Methodology; Amy K Yu, Formal analysis, Investigation; Garret W Guyot, Investigation; Shahrooz Rabizadeh, Kayvan R Niazi, Funding acquisition; Pei-Yu Chiou, Software, Funding acquisition, Methodology; Michael A Teitell, Conceptualization, Supervision, Funding acquisition, Methodology, Writing - review and editing

Author ORCIDs

Alexander J Sercel https://orcid.org/0000-0002-0749-2162
Alexander N Patananan https://orcid.org/0000-0001-9458-9968
Michael A Teitell https://orcid.org/0000-0002-4495-8750

Decision letter and Author response

Decision letter https://doi.org/10.7554/eLife.63102.sa1
Author response https://doi.org/10.7554/eLife.63102.sa2

Additional files

Supplementary files

- Transparent reporting form

Data availability

Figure 1-source data 1. Numerical simulation of MitoPunch pressure generation during mitochondrial delivery. Cited in the legend of Figure 1.

References

Bacman SR, Kauppila JHK, Pereira CV, Nissanka N, Miranda M, Pinto M, Williams SL, Larsson NG, Stewart JB, Moraes CT. 2018. MitoTALEN reduces mutant mtDNA load and restores $tRNA^{Ala}$ levels in a mouse model of heteroplasmic mtDNA mutation. *Nature Medicine* **24**:1696–1700. DOI: https://doi.org/10.1038/s41591-018-0166-8, PMID: 30250143

Boye TL, Maeda K, Pezeshkian W, Sønder SL, Haeger SC, Gerke V, Simonsen AC, Nylandsted J. 2017. Annexin A4 and A6 induce membrane curvature and constriction during cell membrane repair. *Nature Communications* **8**:1623. DOI: https://doi.org/10.1038/s41467-017-01743-6, PMID: 29158488

Caicedo A, Fritz V, Brondello JM, Ayala M, Dennemont I, Abdellaoui N, de Fraipont F, Moisan A, Prouteau CA, Boukhaddaoui H, Jorgensen C, Vignais ML. 2015. MitoCeption as a new tool to assess the effects of mesenchymal stem/stromal cell mitochondria on Cancer cell metabolism and function. *Scientific Reports* **5**: 9073. DOI: https://doi.org/10.1038/srep09073, PMID: 25766410

Calvo SE, Mootha VK. 2010. The mitochondrial proteome and human disease. *Annual Review of Genomics and Human Genetics* **11**:25–44. DOI: https://doi.org/10.1146/annurev-genom-082509-141720, PMID: 20690818

Clark MA, Shay JW. 1982. Mitochondrial transformation of mammalian cells. *Nature* **295**:605–607. DOI: https://doi.org/10.1038/295605a0, PMID: 7057918

Dawson ER, Patananan AN, Sercel AJ, Teitell MA. 2020. Stable retention of chloramphenicol-resistant mtDNA to rescue metabolically impaired cells. *Scientific Reports* **10**:14328. DOI: https://doi.org/10.1038/s41598-020-71199-0, PMID: 32868785

Dong LF, Kovarova J, Bajzikova M, Bezawork-Geleta A, Svec D, Endaya B, Sachaphibulkij K, Coelho AR, Sebkova N, Ruzickova A, Tan AS, Kluckova K, Judasova K, Zamecnikova K, Rychtarcikova Z, Gopalan V, Andera L, Sobol M, Yan B, Pattnaik B, et al. 2017. Horizontal transfer of whole mitochondria restores tumorigenic potential in mitochondrial DNA-deficient Cancer cells. *eLife* **6**:e22187. DOI: https://doi.org/10.7554/eLife.22187, PMID: 28195532

Emani SM, Piekarski BL, Harrild D, Del Nido PJ, McCully JD. 2017. Autologous mitochondrial transplantation for dysfunction after ischemia-reperfusion injury. *The Journal of Thoracic and Cardiovascular Surgery* **154**:286–289. DOI: https://doi.org/10.1016/j.jtcvs.2017.02.018, PMID: 28283239

George TC, Basiji DA, Hall BE, Lynch DH, Ortyn WE, Perry DJ, Seo MJ, Zimmerman CA, Morrissey PJ. 2004. Distinguishing modes of cell death using the ImageStream multispectral imaging flow cytometer. *Cytometry Part A* **59A**:237–245. DOI: https://doi.org/10.1002/cyto.a.20048

Greaves LC, Reeve AK, Taylor RW, Turnbull DM. 2012. Mitochondrial DNA and disease. *The Journal of Pathology* **226**:274–286. DOI: https://doi.org/10.1002/path.3028, PMID: 21989606

Grégoire M, Morais R, Quilliam MA, Gravel D. 1984. On auxotrophy for pyrimidines of respiration-deficient chick embryo cells. *European Journal of Biochemistry* **142**:49–55. DOI: https://doi.org/10.1111/j.1432-1033.1984.tb08249.x, PMID: 6086342

Hyslop LA, Blakeley P, Craven L, Richardson J, Fogarty NM, Fragouli E, Lamb M, Wamaitha SE, Prathalingam N, Zhang Q, O'Keefe H, Takeda Y, Arizzi L, Alfarawati S, Tuppen HA, Irving L, Kalleas D, Choudhary M, Wells D, Murdoch AP, et al. 2016. Towards clinical application of pronuclear transfer to prevent mitochondrial DNA disease. *Nature* **534**:383–386. DOI: https://doi.org/10.1038/nature18303, PMID: 27281217

Kang E, Wu J, Gutierrez NM, Koski A, Tippner-Hedges R, Agaronyan K, Platero-Luengo A, Martinez-Redondo P, Ma H, Lee Y, Hayama T, Van Dyken C, Wang X, Luo S, Ahmed R, Li Y, Ji D, Kayali R, Cinnioglu C, Olson S, et al. 2016. Mitochondrial replacement in human oocytes carrying pathogenic mitochondrial DNA mutations. *Nature* **540**:270–275. DOI: https://doi.org/10.1038/nature20592, PMID: 27919073

King MP, Attardi G. 1988. Injection of mitochondria into human cells leads to a rapid replacement of the endogenous mitochondrial DNA. *Cell* **52**:811–819. DOI: https://doi.org/10.1016/0092-8674(88)90423-0, PMID: 3349520

Kitani T, Kami D, Matoba S, Gojo S. 2014. Internalization of isolated functional mitochondria: involvement of macropinocytosis. *Journal of Cellular and Molecular Medicine* **18**:1694–1703. DOI: https://doi.org/10.1111/jcmm.12316, PMID: 24912369

Miyata N, Steffen J, Johnson ME, Fargue S, Danpure CJ, Koehler CM. 2014. Pharmacologic rescue of an enzyme-trafficking defect in primary hyperoxaluria 1. *PNAS* **111**:14406–14411. DOI: https://doi.org/10.1073/pnas.1408401111, PMID: 25237136

Mok BY, de Moraes MH, Zeng J, Bosch DE, Kotrys AV, Raguram A, Hsu F, Radey MC, Peterson SB, Mootha VK, Mougous JD, Liu DR. 2020. A bacterial cytidine deaminase toxin enables CRISPR-free mitochondrial base editing. *Nature* **583**:631–637. DOI: https://doi.org/10.1038/s41586-020-2477-4, PMID: 32641830

Novickij V, Dermol J, Grainys A, Kranjc M, Miklavčič D. 2017. Membrane permeabilization of mammalian cells using bursts of high magnetic field pulses. *PeerJ* **5**:e3267. DOI: https://doi.org/10.7717/peerj.3267, PMID: 28462057

Patananan AN, Wu TH, Chiou PY, Teitell MA. 2016. Modifying the mitochondrial genome. *Cell Metabolism* **23**: 785–796. DOI: https://doi.org/10.1016/j.cmet.2016.04.004, PMID: 27166943

Patananan AN, Sercel AJ, Teitell MA. 2018. More than a powerplant: the influence of mitochondrial transfer on the epigenome. *Current Opinion in Physiology* **3**:16–24. DOI: https://doi.org/10.1016/j.cophys.2017.11.006, PMID: 29750205

Patananan AN, Sercel AJ, Wu TH, Ahsan FM, Torres AJ, Kennedy SAL, Vandiver A, Collier AJ, Mehrabi A, Van Lew J, Zakin L, Rodriguez N, Sixto M, Tadros W, Lazar A, Sieling PA, Nguyen TL, Dawson ER, Braas D,

Golovato J, et al. 2020. Pressure-Driven mitochondrial transfer pipeline generates mammalian cells of desired genetic combinations and fates. *Cell Reports* **29**:108562. DOI: https://doi.org/10.1016/j.celrep.2020.108562

Patel D, Rorbach J, Downes K, Szukszto MJ, Pekalski ML, Minczuk M. 2017. Macropinocytic entry of isolated mitochondria in epidermal growth factor-activated human osteosarcoma cells. *Scientific Reports* **7**:12886. DOI: https://doi.org/10.1038/s41598-017-13227-0

Robinson BH, Petrova-Benedict R, Buncic JR, Wallace DC. 1992. Nonviability of cells with oxidative defects in galactose medium: a screening test for affected patient fibroblasts. *Biochemical Medicine and Metabolic Biology* **48**:122–126. DOI: https://doi.org/10.1016/0885-4505(92)90056-5, PMID: 1329873

Ryan MT, Hoogenraad NJ. 2007. Mitochondrial-nuclear communications. *Annual Review of Biochemistry* **76**:701–722. DOI: https://doi.org/10.1146/annurev.biochem.76.052305.091720, PMID: 17227225

Schindelin J, Arganda-Carreras I, Frise E, Kaynig V, Longair M, Pietzsch T, Preibisch S, Rueden C, Saalfeld S, Schmid B, Tinevez JY, White DJ, Hartenstein V, Eliceiri K, Tomancak P, Cardona A. 2012. Fiji: an open-source platform for biological-image analysis. *Nature Methods* **9**:676–682. DOI: https://doi.org/10.1038/nmeth.2019, PMID: 22743772

Singh B, Modica-Napolitano JS, Singh KK. 2017. Defining the momiome: promiscuous information transfer by mobile mitochondria and the mitochondrial genome. *Seminars in Cancer Biology* **47**:1–17. DOI: https://doi.org/10.1016/j.semcancer.2017.05.004, PMID: 28502611

Tachibana M, Amato P, Sparman M, Gutierrez NM, Tippner-Hedges R, Ma H, Kang E, Fulati A, Lee HS, Sritanaudomchai H, Masterson K, Larson J, Eaton D, Sadler-Fredd K, Battaglia D, Lee D, Wu D, Jensen J, Patton P, Gokhale S, et al. 2013. Human embryonic stem cells derived by somatic cell nuclear transfer. *Cell* **153**:1228–1238. DOI: https://doi.org/10.1016/j.cell.2013.05.006, PMID: 23683578

Tan AS, Baty JW, Dong LF, Bezawork-Geleta A, Endaya B, Goodwin J, Bajzikova M, Kovarova J, Peterka M, Yan B, Pesdar EA, Sobol M, Filimonenko A, Stuart S, Vondrusova M, Kluckova K, Sachaphibulkij K, Rohlena J, Hozak P, Truksa J, et al. 2015. Mitochondrial genome acquisition restores respiratory function and tumorigenic potential of Cancer cells without mitochondrial DNA. *Cell Metabolism* **21**:81–94. DOI: https://doi.org/10.1016/j.cmet.2014.12.003, PMID: 25565207

Torralba D, Baixauli F, Sánchez-Madrid F. 2016. Mitochondria know no boundaries: mechanisms and functions of intercellular mitochondrial transfer. *Frontiers in Cell and Developmental Biology* **4**:107. DOI: https://doi.org/10.3389/fcell.2016.00107, PMID: 27734015

Wilkins HM, Carl SM, Swerdlow RH. 2014. Cytoplasmic hybrid (cybrid) cell lines as a practical model for mitochondriopathies. *Redox Biology* **2**:619–631. DOI: https://doi.org/10.1016/j.redox.2014.03.006, PMID: 25460729

Wolff JN, Ladoukakis ED, Enríquez JA, Dowling DK. 2014. Mitonuclear interactions: evolutionary consequences over multiple biological scales. *Philosophical Transactions of the Royal Society B: Biological Sciences* **369**:20130443. DOI: https://doi.org/10.1098/rstb.2013.0443

Wong RCB, Lim SY, Hung SSC, Jackson S, Khan S, Van Bergen NJ, De Smit E, Liang HH, Kearns LS, Clarke L, Mackey DA, Hewitt AW, Trounce IA, Pébay A. 2017. Mitochondrial replacement in an iPSC model of Leber's hereditary optic neuropathy. *Aging* **9**:1341–1350. DOI: https://doi.org/10.18632/aging.101231, PMID: 28455970

Wu TH, Sagullo E, Case D, Zheng X, Li Y, Hong JS, TeSlaa T, Patananan AN, McCaffery JM, Niazi K, Braas D, Koehler CM, Graeber TG, Chiou PY, Teitell MA. 2016. Mitochondrial transfer by photothermal nanoblade restores metabolite profile in mammalian cells. *Cell Metabolism* **23**:921–929. DOI: https://doi.org/10.1016/j.cmet.2016.04.007, PMID: 27166949

Figures and figure supplements

Stable transplantation of human mitochondrial DNA by high-throughput, pressurized isolated mitochondrial delivery

Alexander J Sercel *et al*

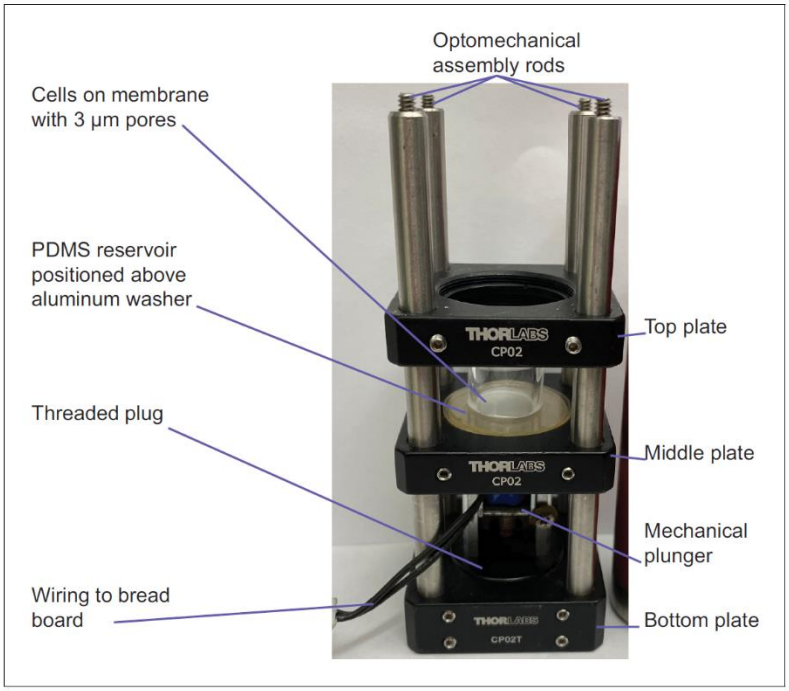

Figure 1—figure supplement 1. Annotated MitoPunch apparatus. Annotated image of the MitoPunch apparatus. Labeled parts are described in the Materials and methods to assist with construction of the apparatus.

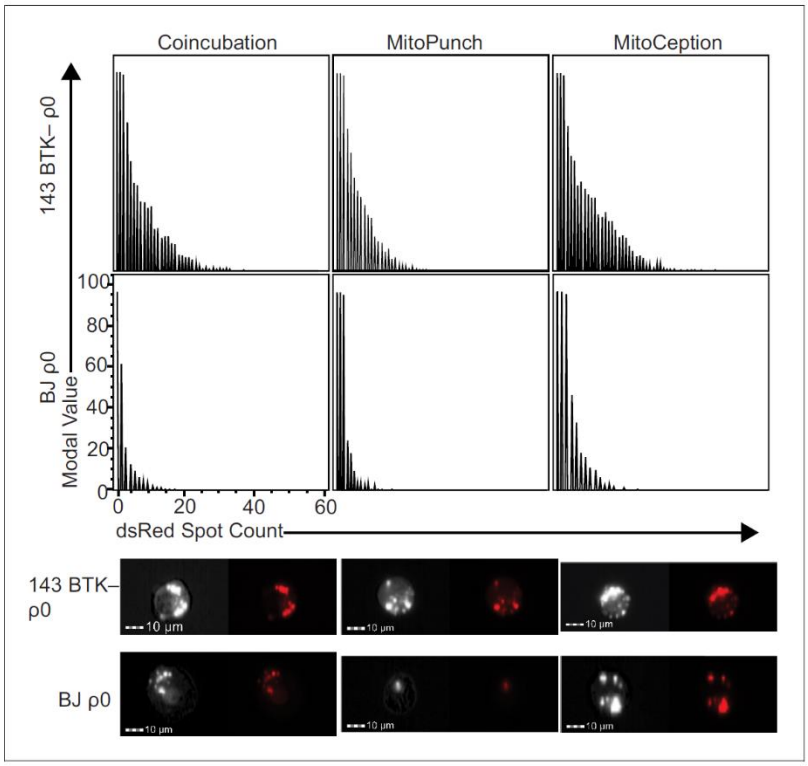

Figure 2—figure supplement 1. Mitochondrial spot quantification. Representative spot count distributions, bright-field images, and PE channel fluorescent images from ImageStream imaging flow cytometry representing the number of dsRed spots associated with 143BTK– ρ0 and BJ ρ0 cells 2 hr after mitochondrial transfer by coincubation, MitoPunch, and MitoCeption. Imaging flow cytometry data is represented as histograms normalized to the mode of each data set. Scale bars indicate 10 µm.

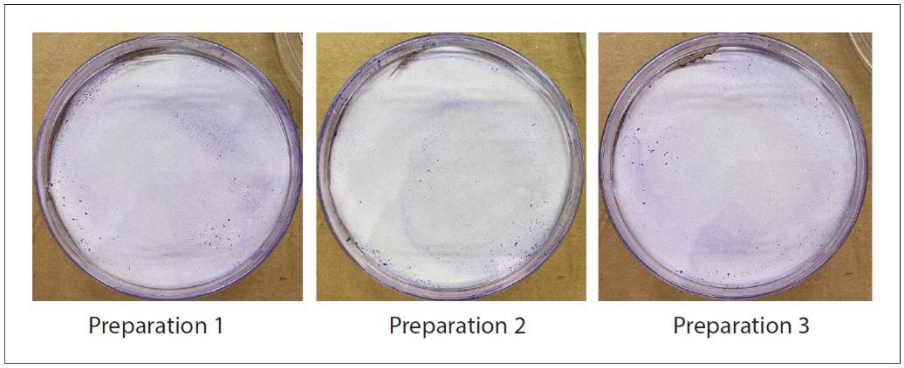

Figure 3—figure supplement 1. Verification of surviving mitochondrial donor cells following mitochondrial isolation. Images of three crystal violet stained 10 cm plates seeded with isolated mitochondria from ~1.5 × 10^7 HEK293T dsRed donor cells taken from three independent mitochondrial isolations following dialyzed medium selection. Pictures were taken on a circular white disk matted within a cardboard frame for clarity.

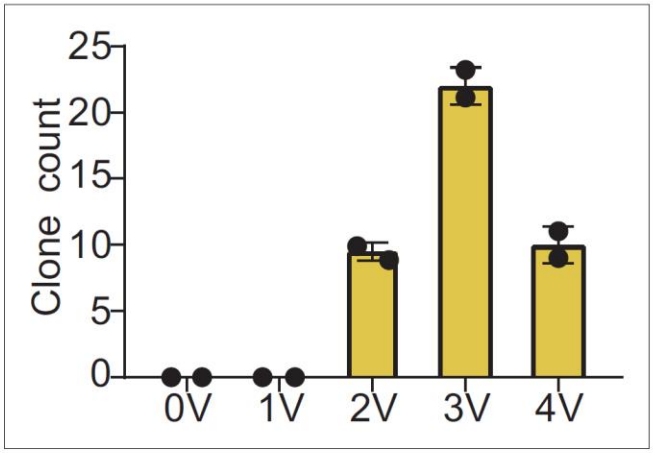

Figure 3—figure supplement 2. MitoPunch generates stable isolated mitochondrial recipient (SIMR) clones in immortalized mouse cells. Quantification of crystal violet stained B16 ρ0 SIMR clones formed by MitoPunch transfer of isolated L929 mitochondria actuated with indicated voltages after SIMR cell selection. Error bars indicate the range between the technical duplicates.

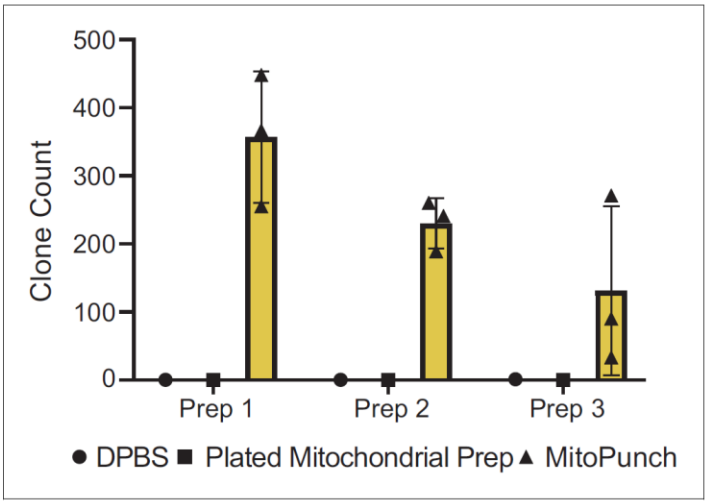

Figure 3—figure supplement 3. Quantification of MitoPunch reproducibility. Quantification of crystal violet stained 143BTK– ρ0 stable isolated mitochondrial recipient (SIMR) clones generated in technical triplicate from three independent HEK293T dsRed mitochondrial donor cell preparations plotted alongside technical singlet DPBS delivery and plated mitochondrial preparation controls (***Figure 3—figure supplement 1***).

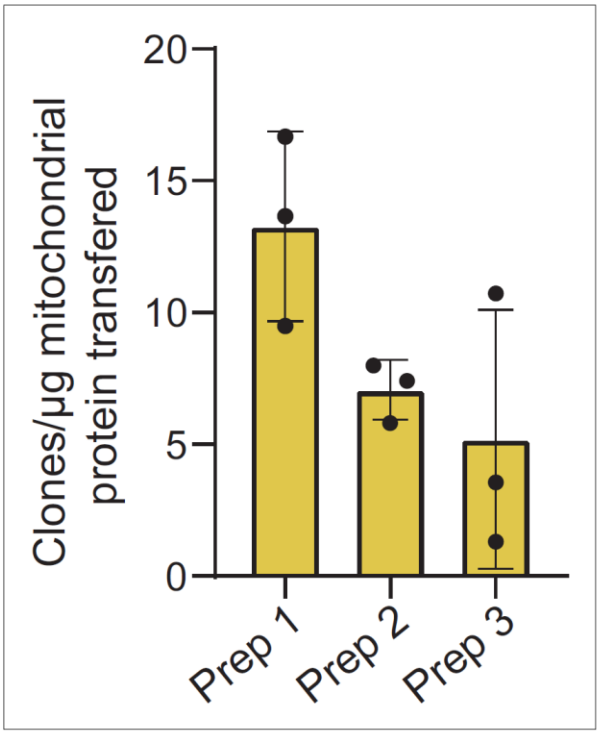

Figure 3—figure supplement 4. Quantification of MitoPunch reproducibility relative to mitochondrial mass transferred. Quantification of crystal violet stained 143BTK– ρ0 stable isolated mitochondrial recipient (SIMR) clones generated in technical triplicate from three independent HEK293T dsRed mitochondrial donor cell preparations plotted as number of SIMR clones generated per µg isolated mitochondrial protein loaded into the polydimethylsiloxane (PDMS) reservoir.

The mass of isolated mitochondria per 120 µL of isolated mitochondrial suspension for the three preparations are as follows: Prep 1–27 µg, Prep 2–33 µg, Prep 3–25 µg.

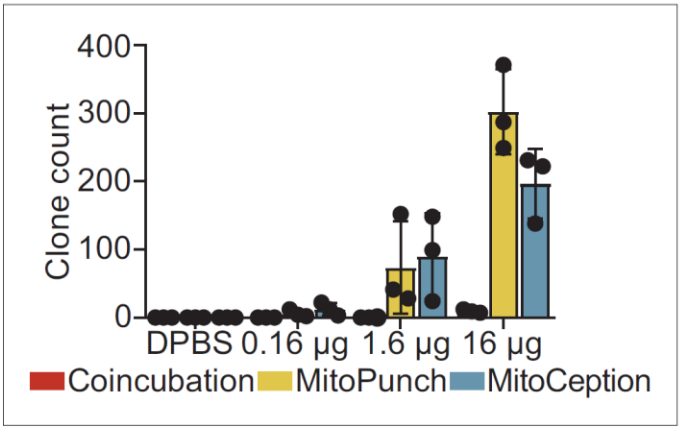

Figure 3—figure supplement 5. Quantification of stable isolated mitochondrial recipient (SIMR) generation efficiency by delivering different masses of isolated mitochondria. Quantification of crystal violet stained 143BTK– ρ0 SIMR clones using indicated concentrations of mitochondrial suspension following 7 days of culture in SIMR selection medium. Error bars represent SD of three technical replicates.

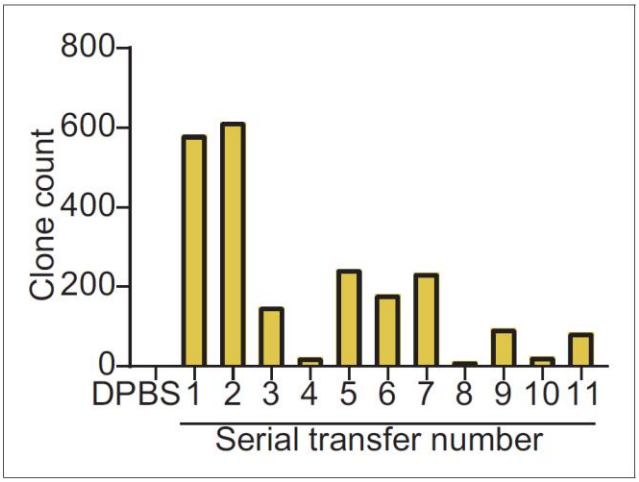

Figure 3—figure supplement 6. Quantification of MitoPunch stable isolated mitochondrial recipient (SIMR) generation by serial deliveries using one isolated mitochondrial aliquot. Quantification of crystal violet stained SIMR clones formed by serial MitoPunch deliveries of HEK293T dsRed mitochondria into 143BTK– ρ0 recipient cells using the same used mitochondrial sample remaining in the polydimethylsiloxane (PDMS) reservoir after the preceding delivery.

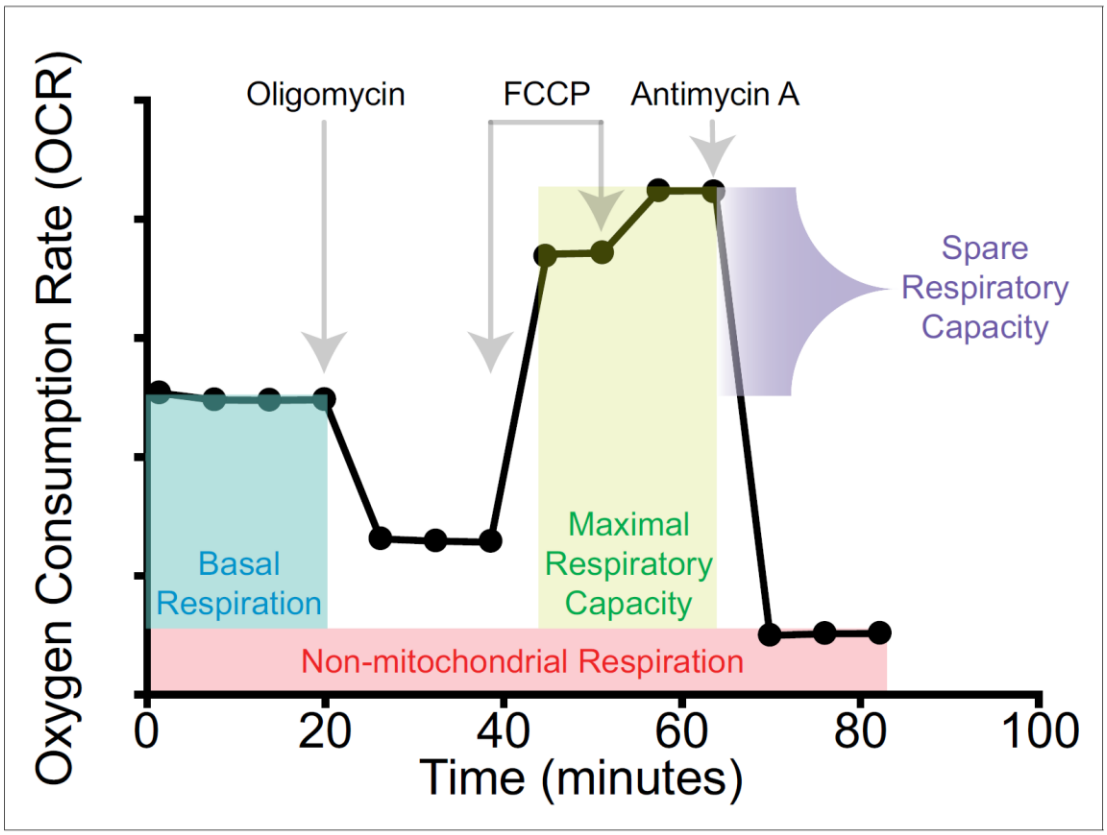

Figure 4—figure supplement 1. Schematic of the Seahorse Mito Stress Test. Annotated plot of oxygen consumption as a function of time, including the identity and timing of drugs injected over the course of a Seahorse Mito Stress Test measurement. Annotations indicate how OXPHOS parameters presented in ***Figure 4A*** are quantified.

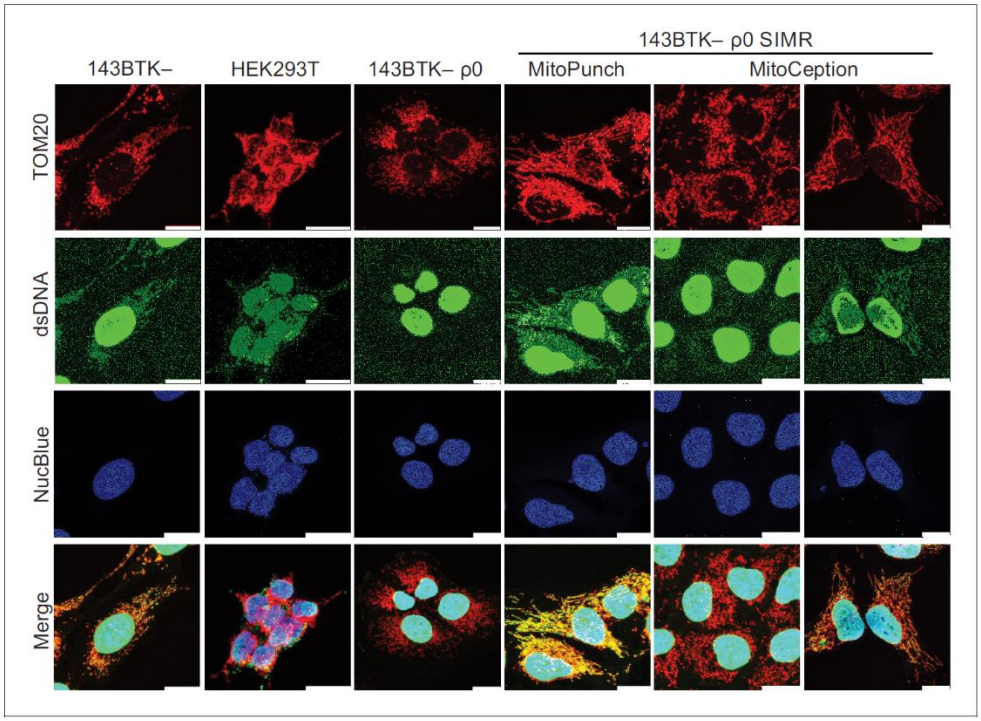

Figure 4—figure supplement 2. Confocal microscopy of stable isolated mitochondrial recipient (SIMR) lines. Confocal microscopy of SIMR clones formed in 143BTK– ρ0 cells with 143BTK– parental, HEK293T dsRed mitochondrial donor, and 143BTK– ρ0 controls. The MitoCeption SIMR clone data on the left represents the SIMR line that lost respiration following freeze-thaw. Mitochondria were stained with anti-TOM20 antibody and labeled red, double-stranded DNA was stained with anti-dsDNA antibody and labeled green, and cell nuclei were stained with NucBlue (Hoechst 33342)and labeled blue. The 143BTK–, 143BTK– ρ0, and HEK293T dsRed control images are the same images used in ***Figure 4B***. Scale bars indicate 15 μm.

Chapter 4: Generating stable isolated mitochondrial recipient clones in mammalian cells using MitoPunch mitochondrial transfer

STAR Protocols

CellPress
OPEN ACCESS

Protocol

Generating stable isolated mitochondrial recipient clones in mammalian cells using MitoPunch mitochondrial transfer

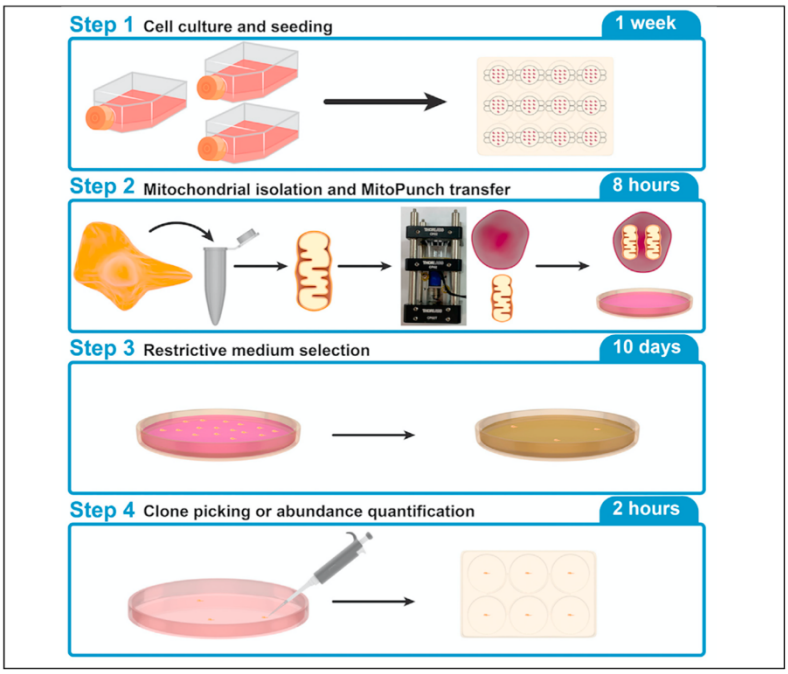

This protocol describes the assembly and use of MitoPunch to deliver mitochondria containing mitochondrial DNA (mtDNA) into cells lacking mtDNA (ρ0 cells). MitoPunch generates stable isolated mitochondrial recipient clones with restored mtDNA and recovered respiration, enabling investigation of mtDNA mutations and mtDNA-nuclear DNA interactions in a range of cell types.

Alexander J. Sercel, Alexander J. Napior, Alexander N. Patananan, Ting-Hsiang Wu, Pei-Yu Chiou, Michael A. Teitell

mteitell@mednet.ucla.edu

Highlights

High-throughput mitochondrial transfer into transformed and primary recipient cells

Selection scheme to isolate stable mtDNA transplant recipient cells

MitoPunch device is easily assembled with minimal engineering expertise

MitoPunch enables new combinations of mitochondrial and nuclear genomes

Sercel et al., STAR Protocols 2, 100850
December 17, 2021
https://doi.org/10.1016/j.xpro.2021.100850

STAR Protocols

CellPress
OPEN ACCESS

Protocol

Generating stable isolated mitochondrial recipient clones in mammalian cells using MitoPunch mitochondrial transfer

Alexander J. Sercel,[1] Alexander J. Napier,[2] Alexander N. Patananan,[2] Ting-Hsiang Wu,[3,4] Pei-Yu Chiou,[5,6,7] and Michael A. Teitell[1,2,6,7,8,9,10,11,12,*]

[1]Molecular Biology Interdepartmental Doctoral Program, University of California, Los Angeles, Los Angeles, CA 90095, USA

[2]Department of Pathology and Laboratory Medicine, David Geffen School of Medicine, University of California, Los Angeles, CA 90095, USA

[3]NanoCav, LLC, Culver City, CA 90230, USA

[4]NantWorks, LLC, Culver City, CA 90230, USA

[5]Department of Mechanical and Aerospace Engineering, University of California, Los Angeles, Los Angeles, CA 90095, USA

[6]California NanoSystems Institute, University of California, Los Angeles, Los Angeles, CA 90095, USA

[7]Department of Bioengineering, University of California, Los Angeles, Los Angeles, CA 90095, USA

[8]Eli and Edythe Broad Center of Regenerative Medicine and Stem Cell Research, University of California, Los Angeles, Los Angeles, CA 90095, USA

[9]Department of Pediatrics, David Geffen School of Medicine, University of California, Los Angeles, Los Angeles, CA 90095, USA

[10]Jonsson Comprehensive Cancer Center, David Geffen School of Medicine, University of California, Los Angeles, Los Angeles, CA 90024, USA

[11]Technical contact

[12]Lead contact

*Correspondence: mteitell@mednet.ucla.edu
https://doi.org/10.1016/j.xpro.2021.100850

SUMMARY

This protocol describes the assembly and use of MitoPunch to deliver mitochondria containing mitochondrial DNA (mtDNA) into cells lacking mtDNA (ρ0 cells). MitoPunch generates stable isolated mitochondrial recipient clones with restored mtDNA and recovered respiration, enabling investigation of mtDNA mutations and mtDNA-nuclear DNA interactions in a range of cell types.
For complete details on the use and execution of this protocol, please refer to Sercel et al. (2021) and Patananan et al. (2020).

BEFORE YOU BEGIN

This protocol describes the process of using MitoPunch to deliver isolated HEK293T mitochondria into 143BTK− ρ0 recipient mammalian cells. We have used MitoPunch to generate stable isolated mitochondrial recipient (SIMR) cell lines with a wide range of both human and mouse cells, of both malignant and primary, non-immortalized origins. Few alterations are necessary to adapt the protocol to different cell lines and cell types, and guidance for doing so is included in the text below.

Construct MitoPunch apparatus

Timing: 30 min

1. Fabricate aluminum washer and 5 V solenoid housing.
   a. Aluminum washer dimensions: outer diameter, 25 mm; inner diameter, 10 mm; thickness, 1.4 mm.

b. Aluminum housing dimensions: rectangular prism of 19.13 mm length, 12.80 mm width, and 30.50 mm height with an internal vertical cutout of 12.65 mm length, 10.20 mm depth, and 19.13 mm height, including two 2 mm diameter screw holes in the bottom of the housing and one 2 mm screw hole on either side of the cutout for securing the 5 V solenoid (Spark Fun, Cat#ROB-11015).

Note: Ensure the 5 V solenoid fits securely in the machined housing. This may require close collaboration with a machinist.

2. Connect mains power cord (Volex, Cat#1725010B1) to the power supply (MEAN WELL, Cat#RS-35-12) by removing the IEC 60320 C13 adapter, striping the wires, and attaching them appropriately to the load (L), neutral (N), and ground hookups.
3. Connect the power supply to the power supply mini board (Futurelec, Cat#MINIPOWER) using a barrel style DC connector with wire leads (McMaster-Carr, Cat#8320N111).
4. Insert hookup wires (Spark Fun, Cat#PRT-08867) into the positive and negative terminals of the mini board, then connect the mini board terminals to the breadboard (Spark Fun, Cat#12615).
5. Install the switch (Spark Fun, Cat#COM-09190) across the DIP ravine on the breadboard and install the jumper wires (Spark Fun, Cat#PRT-00124) to complete the circuit.
6. Connect the JST jumper 2 wire to the breadboard.

Note: See Figure 1 for circuit diagram and image of fully assembled device to assist with the wiring of the apparatus. See Figure 2 for step-by-step assembly of the device.

7. Place the 5 V solenoid into the custom metal casing ensuring that the top of the solenoid is level with the top of the casing, and tighten screws (diameter, 2 mm) to hold it in place.
8. Fit the 5 V solenoid in the casing onto a threaded plug with screws (Thor Labs, Cat#SM1PL) and screw plug into the bottom plate (Thor Labs, Cat#CP02T).
9. Insert 4 optomechanical assembly rods (Thor Labs, Cat#ER3) into the holes in the bottom plate.
   a. With rods flush with the bottom cage plate, secure rods by tightening the screws found next to each rod slot.
10. Remove internal ring from middle cage plate using a spanner wrench (Thor Labs, Cat#SPW602) and slide the middle cage plate (Thor Labs, Cat#CP02) down the assembly rods until the top surface of the middle plate is flush with the top surface of the solenoid.
    a. Reinsert internal ring, tighten, and double check that the top of the middle cage plate is flush with the top of the solenoid.
11. Mount the custom washer atop the middle cage plate and check that the ring stably supports it.
12. Insert the 2-pin JST connector from the breadboard into the MitoPunch 2-pin JST PH connector and test whether the piston actuates when the switch is depressed (see troubleshooting 1).

Assemble polydimethylsiloxane (PDMS) reservoirs

Timing: 6 h

PDMS reservoirs are essential to hold the mitochondrial suspension for delivery into cells using MitoPunch and for delivering the pressure that enables a mitochondrial transfer. PDMS is a biocompatible polymer that is easily fabricated with minimal equipment and expertise (Berthier et al., 2012).

13. Weigh and mix Sylgard 184 PDMS base and curing agent (Dow Corning, Cat#1673921) at a 10:1 ratio.
    a. Prepare a weigh boat on a scale. Tare the scale.
    b. Pour 12 g PDMS base into the weigh boat.

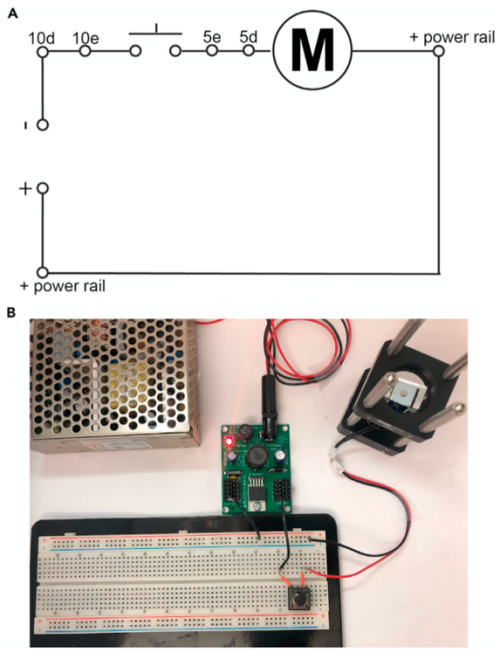

Figure 1. MitoPunch circuit diagram

(A) Circuit diagram of the MitoPunch apparatus. Numbered nodes indicate where wires are inserted into the corresponding breadboard ports.

(B) Image of fully wired and completed MitoPunch apparatus.

c. Tare the scale.
d. Add 1.2 g curing agent into the weigh boat.
e. Mix thoroughly for about 1–2 min with a chemical spatula or similar implement.

Note: PDMS should remain covered until cured to avoid the accumulation of dust and debris.

Note: For visual reference of PDMS fabrication, see Figure 3.

14. Degas PDMS.
    a. Transfer the mixed PDMS into a vacuum desiccator.
    b. Connect a vacuum pump to the desiccator and turn on the pump.
    c. Degas PDMS until all visible air bubbles in the PDMS have disappeared, approximately 30 min.
15. Pour and cure PDMS.
    a. Prepare a clean 10 cm cell culture dish on a scale. Tare the scale.
    b. Pour 6 g of PDMS into the dish. Be careful not to introduce bubbles. If bubbles are generated while pouring, use a 20 µL pipette tip to remove the bubbles or move the dish into the desiccator and repeat degas step.
        i. Repeat with a second 10 cm dish using the remaining PDMS.
    c. Allow PDMS to uniformly coat the dishes (target thickness ~1 mm).
    d. Put the dishes with PDMS into an oven at 65°C for 2–4 h.

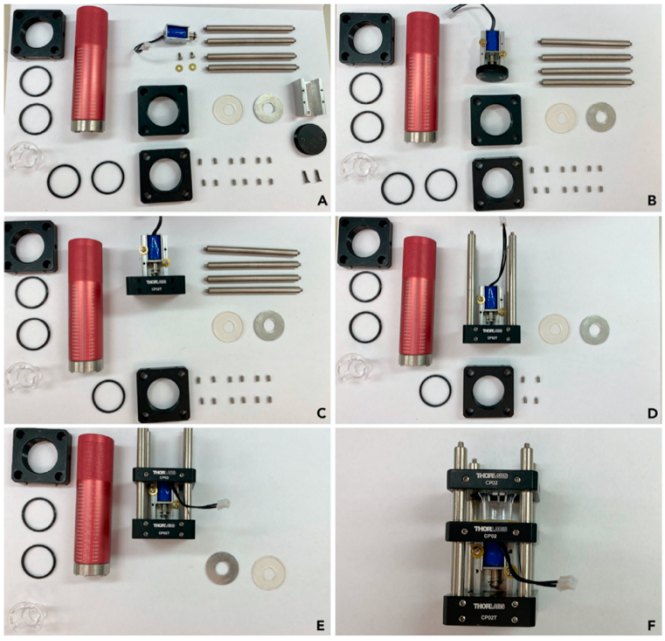

Figure 2. Assembling the MitoPunch apparatus
(A) Layout of all MitoPunch components prior to assembly.
(B) MitoPunch solenoid mounted on the aluminum plug.
(C) Mounted MitoPunch solenoid screwed into base plate.
(D) MitoPunch base plate with optomechanical assembly rods inserted and fixed with screws.
(E) Middle plate mounted flush with the solenoid using screws on the optomechanical assembly rods.
(F) Fully assembled MitoPunch apparatus with top plate lowered onto PDMS reservoir ready for MitoPunch transfer.

⚠ CRITICAL: 10 cm dishes may melt if placed directly on a metal surface in the oven. Place dishes on autoclave safe plastic inside the oven to avoid melting.

16. Hole punch PDMS.
    a. Take the cured PDMS out from the oven and allow to cool to 20°C–25°C.
    b. For the bottom layer, cut out circular PDMS disks with a hole puncher of 25 mm diameter (McMaster-Carr, Cat#3418A25).
    c. For the top layer, cut out circular PDMS disks with a hole puncher of 25 mm diameter. Then use another hole puncher of 10 mm diameter (McMaster-Carr, Cat#3418A1) to remove the center portion and create a PDMS ring.

Note: Prepare an equal number of disks and rings for bonding.

17. Bond PDMS layers.
    a. Remove dust and debris from the PDMS disks and PDMS rings with a piece of removable adhesive tape.
    b. Place the PDMS disks and PDMS rings into an expanded plasma cleaner (Harrick Plasma, Cat#PDC-001) with the clean bonding side face up.
    c. Close the chamber and set the plasma cleaner to high.

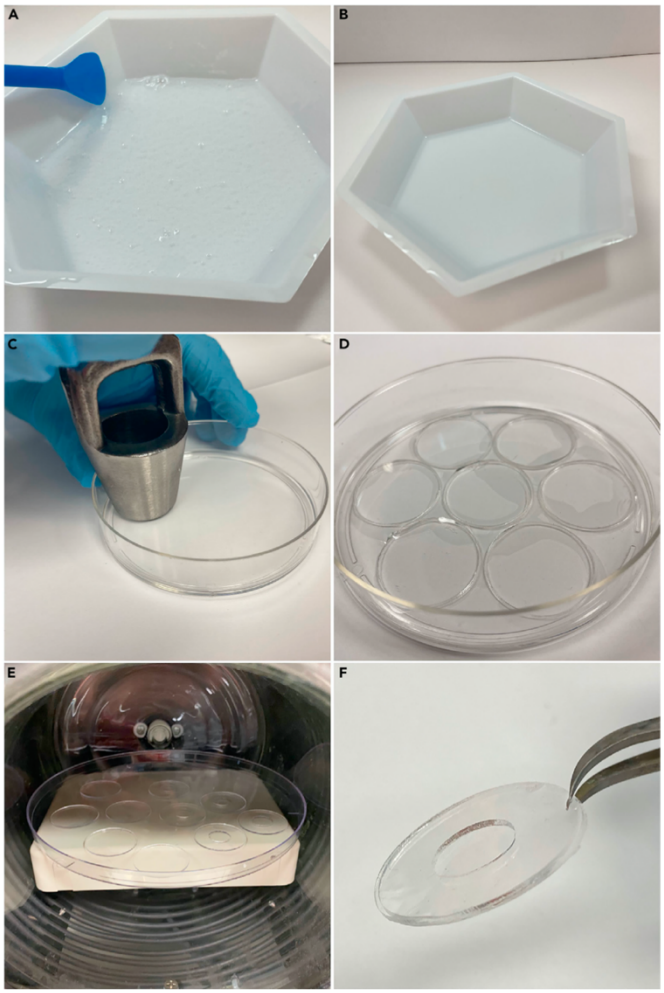

Figure 3. Fabricating PDMS reservoirs for MitoPunch

(A) Uncured PDMS containing bubbles following thorough mixing of the PDMS base and curing agent.
(B) Uncured PDMS following degassing to remove all bubbles.
(C) Punching disks out of a cured layer of PDMS with a hole punch.
(D) Seven punched PDMS disks in a 10 cm dish.
(E) PDMS disks and rings on a 15 cm dish in an oxygen plasma cleaning chamber.
(F) Bonded PDMS reservoir after oxygen plasma treatment.

i. Maintain internal pressure between 300 mTorr and 500 mTorr with the RF level set on high for 1 min.

d. Remove plasma treated PDMS disks and rings from the oxygen plasma chamber.

e. Carefully align and bond the disks and rings by applying firm pressure to ensure the two pieces are sealed together.

Note: Join the two PDMS pieces by pressing the oxygen plasma treated faces together to ensure strong bonding.

f. Heat the bonded PDMS reservoir in the oven at 65°C for at least 2 h to complete bonding.

⚠ CRITICAL: Excess exposure of the oxygen plasma treated faces of the PDMS pieces to air and debris before bonding will result in poor adhesion between the two components. Join the two parts as quickly as possible after oxygen plasma treatment for optimal bonding strength.

Sterilization of MitoPunch components

Timing: 2 h

18. Sterilize a number of PDMS reservoirs equal to the number of MitoPunch replicates to be performed.
    a. Wash reservoirs three times with a 10% bleach solution.
    b. Rinse three times with DI water.
    c. Wash reservoirs three times with a 70% ethanol in water solution.
    d. Rinse three times with DI water.
    e. Package PDMS reservoirs into disposable sterilization pouches.
    f. Autoclave packaged PDMS at 121°C for 30 min.

Note: The wash steps can be completed in a 15 cm dish or a 50 mL conical tube for convenience prior to autoclaving in a disposable sterilization pouch.

19. Sterilize stainless steel forceps.
    a. Wash forceps three times with a 10% bleach solution.
    b. Rinse three times with DI water.
    c. Wash forceps three times with a 70% ethanol in water solution.
    d. Rinse three times with DI water.
    e. Package forceps into a disposable sterilization pouch.
    f. Autoclave packaged forceps at 121°C for 30 min.
20. Sterilize high-vacuum grease.
    a. Apply approximately 4 mL high-vacuum grease to a 5 cm glass petri dish.
    b. Close the glass dish and seal with autoclave tape.
    c. Autoclave high-vacuum grease at 121°C for 30 min.
21. Sterilize glass cloning cylinders.
    a. Place as many cloning cylinders as necessary into a 100 mL glass beaker.
    b. Seal with aluminum foil and apply autoclave tape to the foil top.
    c. Autoclave cloning cylinders at 121°C for 30 min.

Thaw and expand mitochondrial donor and recipient cell lines

Timing: 1 week

22. Thaw mitochondrial donor and recipient cells according to standard protocols for the chosen lines.
    a. Thaw at least 5 d prior to mitochondrial transfer to allow for expansion and mycoplasma testing of cell lines.
23. Expand mitochondrial donor and recipient cell lines.
    a. Expand recipient lines to have 1×10^5 cells per planned MitoPunch replicate.

b. Expand donor cells on T-225 plates until you have one T-225 plate for every two planned MitoPunch replicates, or ~1.5 × 10^6 mitochondrial donor cells for each replicate transfer.

⚠ CRITICAL: Donor cells harvested at high confluence are more likely to cause needle clogging during the mitochondrial isolation. Aim to harvest donor cells at ~80%–90% confluence.

Test recipient cell sensitivity to different SIMR clone selection media conditions

Timing: 7 days

Isolation of SIMR clones following a MitoPunch transfer requires a restrictive medium selection that selectively permits only cells with functional mitochondria to grow. This selection scheme takes advantage of the dependence on electron transport chain activity for *de novo* nucleotide synthesis in mammalian cells (Gregoire et al., 1984). Two selection medium formulations, SIMR selection medium and galactose SIMR selection medium, are used depending on the sensitivity of mitochondrial recipient cells to this selection. SIMR selection medium contains 4.5 g/L glucose, whereas the galactose SIMR selection medium is glucose-free and supplemented with galactose so that glycolysis generates no net ATP (Aguer et al., 2011). Below is a protocol to measure the sensitivity of a chosen ρ0 recipient cell line in these two restrictive mediums in preparation for post-MitoPunch selection.

24. Seed ~2 × 10^4 cells in a 12-well plate with the recipient cell line in uridine-supplemented complete medium.
    a. Incubate ~24 h to allow cells to adhere.

    Note: This seeding density depends upon the growth rate of the chosen recipient cell line. Alter the seeding density such that the cells would reach confluence ~5 d post seeding under normal conditions.

25. Exchange the uridine-supplemented complete medium for 2 mL SIMR selection medium.
    a. Exchange medium with fresh SIMR selection medium daily.
26. Monitor the wells twice daily for 7 d.
    a. Record the time point when cells begin to die.
27. Continue to feed wells and monitor cell viability until all cells have died or 7 d have passed.

    Alternatives: In the event that living cells remain after 7 d, re-plate the experiment as outlined in step 23, and begin with the following alternative protocol.

28. Exchange the uridine-supplemented complete medium for 2 mL galactose SIMR selection medium.
    a. Exchange medium with fresh galactose SIMR selection medium daily.
29. Monitor the wells five times daily for 7 d.
    a. Record the time point when cells begin to die.
30. Continue to feed wells and monitor cell viability until all cells have died or 7 d have passed.

    Note: Galactose SIMR selection medium is far more restrictive than SIMR selection medium and cells can die within hours of first treatment. Careful monitoring of this process is key to timing the selection of MitoPunch experiments to successfully isolate SIMR clones. If cells do not die under either medium, see troubleshooting 2.

Seed mitochondrial recipient cells on PET filters

Timing: 1 days

31. Collect and count mitochondrial recipient cells.
    a. Remove culture medium from recipient cell flasks.
    b. Wash plate with 1X Dulbecco's Phosphate-Buffered Salt Solution (DPBS) (Corning, Cat#21031CV).
    c. Aspirate DPBS and apply StemPro Accutase Cell Dissociation Reagent (Accutase) (Thermo Fisher Scientific, Cat#A1110501).

    Note: Use preferred dissociation reagent for the chosen recipient cell type.

    d. Incubate in 37°C humidified incubator for 5 min.
    e. Resuspend cells in 8.5 mL medium. Transfer cell suspension to 15 mL conical tube.
    f. Centrifuge at 500 × *g* for 5 min, aspirate supernatant, and resuspend in culture medium.
    g. Count cells using a hemocytometer.
    h. Calculate volume of cell suspension needed to seed 1 × 10^5 recipient cells.

32. Seed recipient cells.
    a. Insert 3.0 μm PET filter inserts (Corning, Cat# 353181) into wells of a 12-well dish and dispense 1.5 mL medium to the well outside of the filter insert.
    b. Pipette volume of cell suspension containing 1 × 10^5 cells into filter insert. Add volume of medium to filter insert to bring volume inside filter insert to 500 μL.

⚠ CRITICAL: Ensure even plating of recipient cells on the filter insert for consistent MitoPunch results. See Figure 4A for an example of an evenly seeded well 24 h post-seeding.

KEY RESOURCES TABLE

REAGENT or RESOURCE	SOURCE	IDENTIFIER
Chemicals, peptides, and recombinant proteins		
DMEM w/ 4.5 g/L glucose, sodium pyruvate, and L-glutamine	Corning	Cat#10013CM
DMEM, no glucose	Thermo Fisher Scientific	Cat#11966025
Fetal Bovine Serum	Omega Scientific	Cat#FB-11
Fetal Bovine Serum, dialyzed, US origin	Thermo Fisher Scientific	Cat#26400-044
Penicillin-Streptomycin Solution, 100×	Corning	Cat#30-002-CI
GlutaMAX Supplement	Thermo Fisher Scientific	Cat#35050061
MEM Non-Essential Amino Acids Solution (100X)	Thermo Fisher Scientific	Cat#11140050
Uridine	Acros Organics	Cat#140770250
D-(+)-Galactose	Millipore Sigma	Cat#G5388-100G
Dulbecco's Phosphate-Buffered Salt Solution 1X	Corning	Cat#21031CV
Sodium Pyruvate (100 mM)	Corning	Cat#25000CI
Dulbecco's Phosphate-Buffered Salt Solution, w/ Calcium and Magnesium	Thermo Fisher Scientific	Cat#14040133
StemPro Accutase Cell Dissociation Reagent	Thermo Fisher Scientific	Cat#A1110501
16% Formaldehyde	Thermo Fisher Scientific	Cat#28906
Crystal Violet	Fisher Chemical	Cat#C581-25
Methanol	Fisher Chemical	Cat#A412-4
Critical commercial assays		
Qproteome Mitochondria Isolation Kit	QIAGEN	Cat#37612
Experimental models: Cell lines		
143 BTK– osteosarcoma ρ0; human, female	(Patananan et al., 2020)	N/A
Primary dermal fibroblast normal ρ0; human, male, neonatal	(Patananan et al., 2020)	N/A

(*Continued on next page*)

Continued		
REAGENT or RESOURCE	SOURCE	IDENTIFIER
HEK293T dsRed; human, female	Miyata et al., 2014	N/A
Other		
Breadboard - Full-Size (Bare)	SparkFun	Cat#12615
Solenoid - 5V	SparkFun	Cat#ROB-11015
Momentary Pushbutton Switch - 12mm Square	SparkFun	Cat#COM-09190
Hook-up Stranded Wire - Black (22 AWG)	SparkFun	Cat#PRT-08867
JST Jumper 2 Wire Assembly	SparkFun	Cat#PRT-09914
Jumper Wire Kit - 140pcs	SparkFun	Cat#PRT-00124
Power Supply Mini Board	Futurelec	Cat#MINIPOWER
35W Single Output Switching Power Supply	MEAN WELL	Cat#RS-35-12
Mains Power Cord, NEMA 5-15P to IEC 60320 C13, 2.3 m, 10 A, 125 VAC, Black	Volex	Cat#1725010B1
Push-In Plugs with Wire Leads, 2.1 mm End ID, 12V DC	McMaster-Carr	Cat#8320N111
Spanner Wrench for SM1-Threaded Retaining Rings	Thorlabs	Cat# SPW602
Externally SM1-Threaded Plug	Thorlabs	Cat#SM1PL
SM1-Threaded 30 mm Cage Plate, 0.50" Thick, 2 Retaining Rings, 8–32 Tap	Thorlabs	Cat#CP02T
Cage Assembly Rod, 3" Long, Ø6 mm	Thorlabs	Cat#ER3
SM1-Threaded 30 mm Cage Plate, 0.35" Thick, 2 Retaining Rings, 8–32 Tap	Thorlabs	Cat#CP02
Custom Aluminum Washer	University of California, Los Angeles, Machine Shop	N/A
Custom Aluminum Case	University of California, Los Angeles, Machine Shop	N/A
SYLGARD™ 184 Silicone Elastomer Kit 1.1 KG Kit	Dow Corning	Cat#1673921
Polypropylene Desiccator with Stopcock	Thermo Fisher Scientific	Cat#53100250
230 mm Ceramic Metal Desiccator Plate	Thermo Fisher Scientific	Cat#53120230
10 mm Hole punch	McMaster-Carr	Cat#3418A1
25 mm Hole punch	McMaster-Carr	Cat#3418A25
Expanded Plasma Cleaner	Harrick Plasma	Cat#PDC-001
12–Well 3.0 μm Transparent PET Membrane Cell Culture Inserts	Corning	Cat#353181
26 G Blunt-ended needle	VWR	Cat#89134-164
3 mL Luer-Lok Syringe	BD Biosciences	Cat#309657
High-vacuum grease	Dow Corning	Cat#1597418
Cloning cylinders	Fisher Scientific	Cat# 09-552-21

MATERIALS AND EQUIPMENT

Preparation of complete medium		
Reagent	Final concentration	Amount
DMEM w/ 4.5 g/L glucose, sodium pyruvate, and L-glutamine (Corning, C#10013CM)	-	870 mL
Penicillin Streptomycin solution 100× (Corning, Cat#30-002-CI)	1×	10 mL (from 100× stock)
GlutaMAX Supplement (Thermo Fisher Scientific, Cat#35050061)	1×	10 mL (from 100× stock)
MEM Non-essential Amino Acids 100× (Thermo Fisher Scientific, Cat#11140050)	1×	10 mL (from 100× stock)
Fetal Bovine Serum (FBS) (Omega Scientific, Cat#FB-11)	10%	100 mL
Total	**n/a**	**1000 mL**
Medium can be stored at 4°C for up to 1 month.		

Preparation of uridine-supplemented complete medium		
Reagent	Final concentration	Amount
DMEM w/ 4.5 g/L glucose, sodium pyruvate, and L-glutamine	-	869 mL
Uridine (Acros Organics, Cat#140770250)	50 mg/L	1 mL (from 50 mg/mL stock)
Penicillin Streptomycin solution	1×	10 mL (from 100× stock)
GlutaMAX Supplement	1×	10 mL (from 100× stock)
MEM Non-essential Amino Acids	1×	10 mL (from 100× stock)
Fetal Bovine Serum (FBS)	10%	100 mL
Total	**n/a**	**1000 mL**
Medium can be stored at 4°C for up to 1 month.		

Note: Uridine stocks are prepared and filtered through a 0.22 μm filter in advance then stored at –20°C for up to 1 year.

Preparation of SIMR selection medium		
Reagent	Final concentration	Amount
DMEM w/ 4.5 g/L glucose, sodium pyruvate, and L-glutamine	-	870 mL
Penicillin Streptomycin solution	1×	10 mL (from 100× stock)
GlutaMAX Supplement	1×	10 mL (from 100× stock)
MEM Non-essential Amino Acids	1×	10 mL (from 100× stock)
Dialyzed Fetal Bovine Serum (FBS) (Thermo Fisher Scientific, Cat#26400-044)	10%	100 mL
Total	**n/a**	**1000 mL**
Medium can be stored at 4°C for up to 1 month.		

Preparation of galactose SIMR selection medium		
Reagent	Final concentration	Amount
DMEM, no glucose (Thermo Fisher Scientific, Cat#11966025)	-	430 mL
Galactose (Millipore Sigma, Cat#G5388-100G)	4.5 g/L	2.25 g
Penicillin Streptomycin solution	1×	5 mL (from 100× stock)
GlutaMAX Supplement	1×	5 mL (from 100× stock)
MEM Non-essential Amino Acids	1×	5 mL (from 100× stock)
Sodium Pyruvate (Corning, Cat#25000CI)	1×	5 mL (from 100× stock)
Fetal Bovine Serum (FBS)	10%	50 mL
Total	**n/a**	**500 mL**
Medium can be stored at 4°C for up to 1 month.		

Note: The galactose should be added by dissolving in 40 mL of DMEM and then adding back to the medium before filtering through a 0.22 μm PES filter.

Preparation of paraformaldehyde		
Reagent	Final concentration	Amount
16% Paraformaldehyde (Thermo Fisher Scientific, Cat#28906)	4%	1 mL
Dulbecco's Phosphate-Buffered Salt Solution 1X	-	3 mL
Total	**4%**	**4 mL**
Paraformaldehyde solution should be made freshly before use.		

⚠ CRITICAL: Paraformaldehyde is a toxin and carcinogen that should be handled only in a chemical fume hood for proper ventilation with appropriate PPE including safety glasses, a lab coat, closed-toed shoes, and nitrile gloves. All waste containing paraformaldehyde

should be labeled and disposed of through proper channels. Paraformaldehyde should be stored in a flammable storage cabinet.

Preparation of crystal violet staining solution		
Reagent	Final concentration	Amount
Methanol	20%	20 mL
Deionized water	80%	80 mL
Crystal Violet (Fisher Chemical, Cat#C581-25)	0.5% w/v	5 g
Total	**n/a**	**100 mL**
Crystal violet solution can be kept in the flammable chemical cabinet for up to 6 months.		

⚠ CRITICAL: Crystal violet staining solution contains methanol which is a flammable toxin and should be stored in a flammable storage cabinet. Appropriate PPE including safety glasses, a lab coat, closed-toed shoes, and nitrile gloves should be used when preparing and working with this solution. All waste containing crystal violet staining solution should be labeled and disposed of through proper channels.

STEP-BY-STEP METHOD DETAILS

Mitochondrial preparation

Timing: 2–3 h

MitoPunch requires a freshly isolated stock of cell-free mitochondria for transfer into recipient cells. This protocol uses the Qiagen Qproteome Mitochondrial Isolation Kit (Qiagen, Cat#37612) with minor optimizations for efficiency and purity in this application; however, other mitochondrial isolation methods are also compatible with MitoPunch. Here we define purity as the absence of intact mitochondrial donor cells that escape through the disruption and mitochondrial isolation process. We have measured the purity of our mitochondrial isolates in Figure 3-figure supplement 1 of (Sercel et al., 2021).

1. Harvest mitochondrial donor cells.
   a. Aspirate culture medium from T-225 flasks.
   b. Pipette 20 mL DPBS into each flask.
   c. Release cells from the flasks using a cell scraper.
   d. Suspend scraped cells in DPBS and collect into 50 mL conical tubes.
   e. Centrifuge tubes at 500 × *g* for 10 min at 4°C. Aspirate supernatant.
   f. Wash cell pellets in 10 mL DPBS and centrifuge again at 500 × *g* for 10 min at 4°C. Aspirate supernatant.

⚠ CRITICAL: Keep samples on ice when outside the centrifuge for the remainder of the mitochondrial isolation process.

2. Disrupt mitochondrial donor cells using the Qiagen Qproteome Mitochondrial Isolation Kit.

Note: The buffers used in the following steps are from the Qiagen Qproteome Mitochondrial Isolation Kit and must be handled according to manufacturer protocol.

   a. Resuspend cell pellets in ice-cold Lysis Buffer at a concentration of ~1 × 10^7 cells per 1 mL and transfer to 2 mL tubes.
      i. Prepare Lysis Buffer with 1:100 Protease Inhibitor Solution prior to resuspension.

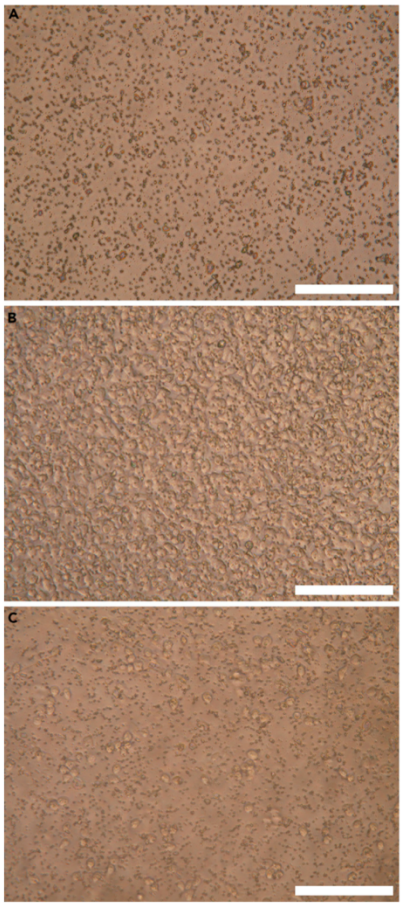

Figure 4. Filter insert seeding and harvesting

(A) Filter insert without cells in DPBS.

(B) Filter insert seeded with 1 × 10^5 143BTK− ρ0 cells imaged after washing with DPBS.

(C) Filter insert seeded with 1 × 10^5 143BTK− ρ0 cells imaged after washing with DPBS and ~7 min incubation with Accutase.

Scale bars represent 200 μm.

b. Incubate on end-over-end shaker for 10 min at 4°C.

Note: Ensure microcentrifuge is chilled to 4°C during this incubation in preparation for the next step.

c. Centrifuge the samples at 1000 × *g* for 10 min at 4°C and aspirate supernatant without disrupting the pellet.

d. Resuspend each cell pellet in 1.5 mL ice cold Disruption Buffer with a 1 mL pipette tip.
   i. Prepare Disruption Buffer with 1:100 Protease Inhibitor Solution prior to resuspension.

e. Disrupt cells using a blunt-ended 26G (VWR, Cat#89134-164) needle attached to a 3 mL Luer-Lok syringe.
   i. Slowly pull the entire lysate into the syringe and expel the volume 10 times, avoiding the formation of bubbles in the suspension.

Note: If clogging of the disruption needle occurs, see troubleshooting 3.

3. Mitochondrial purification.
   a. Centrifuge lysate at 1000 × *g* for 10 min at 4°C and transfer supernatant to a new sterile 1.5 mL tube.

   Optional: Repeat this step to reduce the probability of intact cells contaminating the mitochondrial preparation.

   Note: Pellet will be diffuse and easily disrupted. Take care in removing supernatant to minimize the mass of pellet that is carried over to the next step.

   Note: Supernatants should be combined at this point.

   b. Centrifuge the supernatant at 6000 × *g* for 10 min at 4°C. Carefully aspirate supernatant.

   Note: The pellet now contains isolated mitochondria.

   c. Resuspend the pellet with 1 mL Mitochondrial Storage Buffer using a 1 mL pipette tip and centrifuge at 6000 × *g* for 20 min at 4°C.

   ⚠ CRITICAL: Prepare the MitoPunch apparatus during this centrifugation step to minimize time between resuspension of mitochondrial isolate and MitoPunch transfer as MitoPunch efficiency is negatively impacted by older mitochondrial preparations.

   d. Remove supernatant. The mitochondrial mass should appear as a compact, pin-head-sized pellet at the bottom of the 1.5 mL tube.
   e. Resuspend the mitochondrial pellet in a volume of DPBS with calcium and magnesium (Thermo Fisher Scientific, Cat#14040133) equal to 120 µL times the number of MitoPunch replicates and keep on ice.

MitoPunch mitochondrial transfer

Timing: 1 h

The following instructions describe the process of delivering freshly isolated mitochondria to recipient cells using the MitoPunch apparatus. Briefly, the mechanism by which MitoPunch delivers isolated mitochondria to recipient cells requires pressure generated by a solenoid-driven mechanical plunger. Isolated mitochondria are loaded into a PDMS reservoir to which a cell culture filter insert seeded with recipient cells is sealed. The solenoid is activated which drives the mechanical plunger into the underside of the PDMS reservoir, causing the internal pressure of the reservoir to increase. This increase in pressure forces mitochondrial suspension directly through the pores in the filter insert and into the recipient cell cytoplasm. We have previously quantified the transfer efficiency of MitoPunch by delivering fluorescently labeled isolated mitochondria to 143 BTK− ρ0 and BJ ρ0 recipient cells and measuring the fraction of the recipients positive for the fluorescent marker by imaging flow cytometry (Sercel et al., 2021). We observe ~50% of 143 BTK− ρ0 recipient cells and ~15% of BJ ρ0 recipients as positive for the fluorescent mitochondria. Additionally, we

measured the mean and median number of fluorescent mitochondrial puncta present in recipient cells by imaging flow cytometry. We observed a mean of ~5 and a median of ~3 puncta for 143 BTK− ρ0 recipients and a mean of ~2 and a median of ~1 puncta for BJ ρ0 recipients. Finally, it is important to keep the isolated mitochondrial sample on ice while performing MitoPunch transfers and to minimize the time that isolated mitochondria are kept on ice prior to transfer.

4. Spray 70% ethanol into a tissue and wipe down the MitoPunch apparatus before entering it into a biosafety cabinet.
5. Connect MitoPunch apparatus to breadboard and connect breadboard to power supply (Figure 1B). Connect power supply to the 120 V wall outlet and ensure device has power by testing piston actuation.
6. Remove a sterile PDMS reservoir from an autoclave bag and place on MitoPunch apparatus.
7. Wash PDMS reservoir 3 times with 120 μL DPBS with calcium and magnesium, pipetting up and down 3 times with each wash, being sure to cover the entire surface area of the reservoir.

Note: This step is important to remove any traces of bleach or ethanol from pre-autoclave sterilization and to help the hydrophobic PDMS more readily hold the mitochondrial suspension evenly without pooling into a large droplet.

8. Pipette 120 μL mitochondrial suspension or DPBS control into the PDMS reservoir.
9. Remove 12-well dish of recipient-cell-seeded filter inserts from the incubator and enter it into the biosafety cabinet. Using sterile forceps, remove one filter insert and secure it into the top plate of the MitoPunch apparatus.
   a. To secure, remove the top internal ring from the upper plate of the MitoPunch and place the plastic wings of the filter insert on the remaining ring such that the filter insert is supported within the hole of the top plate. Carefully screw the top internal ring until tight against the filter wings.
10. Lower the top plate along the optomechanical assembly rods such that the filter insert contacts the PDMS reservoir and ensure it is firmly pressed against the PDMS, creating a seal.
11. Actuate the MitoPunch piston using the switch on the breadboard. Leave the piston in the protracted position for 3 s, release the piston switch, remove the filter insert from the apparatus, and replace it in the 12-well dish in its original medium.

⚠ CRITICAL: Apply gentle pressure to the top plate with a hand while actuating the solenoid to maintain a seal between the filter insert and the PDMS.

12. After completing all MitoPunch transfers, place the 12-well dish in a humidified 37°C incubator for 2 h prior to collecting the recipient cells.

Recipient cell collection

Timing: 1 h

Mitochondrial recipient cells need to be harvested and plated on 10 cm dishes after the 2 h incubation that follows mitochondrial transfer for expansion and selection.

13. Aspirate medium from the wells containing filter inserts.
    a. Carefully aspirate medium from within the filter insert, being mindful to not contact the cell layer on the PET membrane.
    b. Aspirate medium from outside the filter insert, making sure to collect the medium retained at the contact point between the bottom of the filter insert and the well.

Note: The PET filter can retain medium and reduce the efficacy of dissociation reagents if not handled properly.

⚠ CRITICAL: Change aspirator tip between samples to avoid contamination of intact cells from the mitochondrial preparation that may be present on the outside of the filter insert.

14. Wash filter inserts with DPBS without calcium and magnesium.
    a. Apply 0.5 mL DPBS gently to the filter insert and 1.5 mL DPBS to the well outside the filter insert.
    b. Carefully aspirate DPBS from within the filter insert and then from outside the insert, being sure to remove any residual liquid retained between the bottom of the filter and the well.

⚠ CRITICAL: Ensure that DPBS reaches both sides of the filter insert.

⚠ CRITICAL: Change aspirator tip between samples to avoid contamination of intact cells from the mitochondrial preparation that may be present on the outside of the filter insert.

15. Apply Accutase dissociation reagent to the filters and incubate for 5 min in a 37°C humidified incubator.
    a. Pipette 0.5 mL Accutase to the filter insert and 1.5 mL to the well outside the insert.

⚠ CRITICAL: Ensure that Accutase reaches both sides of the filter insert.

Note: Visually inspect the plate under an inverted microscope to verify that the cells have released from the filter. If dissociation is incomplete (Figure 4B), return plate to the incubator for 3 min and repeat until cells have released from the membrane (Figure 4C).

16. Once the cells are released from the membrane, apply 0.5 mL uridine-supplemented medium to the filter insert and gently disrupt the cell layer with a 1 mL pipette tip.
    a. Do not draw liquid from outside the filter to reduce the risk of intact mitochondrial donor cell contamination.
17. Pipette the full volume from the filter insert to a 10 cm dish containing 10 mL warm uridine-supplemented complete medium. If few cells are observed in the dish, see troubleshooting 4.
18. Place 10 cm dishes in a 37°C humidified incubator.

SIMR clone selection

Timing: 1 week

Recipient cells need to be cultured in a dialyzed, nucleotide-free selection medium to isolate stable mitochondrial recipient cells. The selection medium is not permissive for ρ0 cells as they are incapable of generating nucleotides *de novo*. A negative ρ0 control is essential for determining the endpoint of the following selection protocol.

19. Incubate the 10 cm dishes of MitoPunch recipient cells in a 37°C humidified incubator with uridine-supplemented complete medium for 3 d following transfer.

⚠ CRITICAL: Monitor confluence daily and do not allow cultures to exceed 80% confluence. If cultures reach >80% confluence, proceed with step 20.

20. Exchange the complete medium for SIMR selection medium.
    a. Exchange the medium daily with 10 mL fresh SIMR selection medium and record the confluence of the ρ0 negative control.

Note: Small colonies will form on the MitoPunch recipient plates and be visible by microscopy typically 3–5 d into SIMR selection medium treatment.

21. Continue daily feeding with SIMR selection medium until the ρ0 control plate is no longer viable, typically 5–7 d under SIMR selection medium treatment.

Note: Proceed to either clone isolation or crystal violet staining as soon as the control plate is no longer viable.

Alternatives: When the recipient cells used were determined to require galactose SIMR selection medium in Test recipient cell sensitivity to different SIMR clone selection media conditions, proceed to step 22.

22. At 5 d post-delivery, feed cells with galactose SIMR selection medium.

Note: Follow selection scheme developed in "Test recipient cell sensitivity to different SIMR clone selection media" for the specific recipient cells used.

a. Selection medium should be exchanged daily and condition of the cells noted.

23. Continue galactose selection until the DPBS control transfer has completely died, up to 7 d post-transfer.
    a. After death of the control, exchange the selection medium for SIMR selection medium to allow clones to grow large enough to harvest.

Note: When selection fails to slow cell growth and induce cell death, see troubleshooting 5. In the event no clones appear after selection, see troubleshooting 6.

SIMR clone harvesting

Timing: 1 h

After the selection process, isolate SIMR clones from 10 cm dishes and passage them onto 6-well dishes for expansion. This must be done before clones overgrow as large clones can merge with neighboring clones or become internally over confluent and die.

24. Select clones for isolation that are not adjacent to or in contact with other clones.

Note: When selecting multiple clones, mark the location of desired clones with a permanent marker or a microscope mounted object marker.

25. Aspirate the medium from the dish and wash with 5 mL of DPBS. Aspirate the DPBS.
26. For each clone to be isolated, coat one side of a cylinder in sterilized high-vacuum grease. Gently adhere each cylinder to the dish and fully encompass one clone within the cylinder.
27. Slowly add 200 μL of Accutase to each cylinder and incubate for 5 min in a 37°C humidified incubator.

⚠ CRITICAL: Watch for any leaks from the bottom of the cylinder while adding dissociation reagent and immediately stop when one appears. Any leaked dissociation reagent can prematurely disrupt other clones adhered to the plate.

28. After incubation, verify that the cells have fully dissociated from the dish under an inverted microscope.
    a. When the cells have not fully dissociated, incubate for another 3 min.
29. Once the cells have fully dissociated, use a micropipettor to move the cell suspension into a well of a 6-well dish containing 2 mL of warm complete medium.

30. Incubate the newly plated clones in a 37°C humidified incubator and continue to expand until ready for use in downstream analysis.

Crystal violet staining

Timing: 2 h

This protocol enables visualization of clone morphology, number, and distribution. Plates treated with this protocol can be stored indefinitely away from light. Additionally, when stain does fade with time, plates can be re-stained with additional crystal violet to increase color saturation for future imaging.

31. Aspirate medium from the plate, taking care to not disturb clones.
32. Apply 1 mL of freshly diluted 4% paraformaldehyde to the dish and tilt the dish to fully coat the surface.
33. Incubate at RT in a chemical fume hood for 15 min.
34. Aspirate the 4% paraformaldehyde from the dish and dispose of in the appropriate chemical waste container.
35. Apply 2 mL of crystal violet solution to each plate and tilt to fully coat. Incubate at RT in the chemical fume hood for 30 min.
36. Remove excess crystal violet using a serological pipette and dispose of it in the appropriate chemical waste container.
37. Rinse each plate twice with DI water to remove excess crystal violet solution.
38. Dry plates upside-down on an absorbent surface to allow any residual crystal violet solution to drip off the plate.
39. Store plates away from light until ready to analyze.

EXPECTED OUTCOMES

Mitochondrial preparations performed as written in this protocol typically yield 60–100 μg of isolated protein per T-225 plate of donor cells. MitoPunch transfer of HEK293T mitochondria into 143BTK− ρ0 cells can generate between dozens to hundreds of independent SIMR clones (Figure 5). Other cell lines used as donor or recipient cells, particularly transferring mutant mtDNA-bearing mitochondria, can reduce the SIMR clone yield (Patananan et al., 2020; Sercel et al., 2021).

LIMITATIONS

Using this protocol, MitoPunch can only deliver isolated mitochondria into adherent cells that can attach to the PET filter membrane. Additionally, MitoPunch is unable to generate SIMR clones in recipient cells that already contain mtDNA unless a secondary antibiotic selection is applied simultaneously with the SIMR restrictive medium scheme (Dawson et al., 2020). The pressure generated by the MitoPunch apparatus as described in this protocol is fixed, and some cell types may require different levels of pressure to generate SIMR clones efficiently (Sercel et al., 2021). MitoPunch delivery into ρ0 primary fibroblasts yields fewer SIMR clones than transfers into transformed ρ0 cells, and SIMR clones isolated from MitoPunch transfer into ρ0 primary fibroblasts can be difficult to expand before the cells reach the Hayflick limit and senesce. Furthermore, mtDNA and nDNA of different haplotypic backgrounds may suffer from biochemical or genetic incompatibilities and reduce the SIMR generation efficiency of MitoPunch transfers using material from such sources. Combinations of mitochondria and recipient cells from different species face incompatibility that prohibits SIMR clone generation. Lastly, isolated donor mitochondria must be freshly isolated prior to every delivery, as extended time in suspension or flash-freezing prior to MitoPunch delivery have a negative effect on SIMR generation efficiency (data not shown).

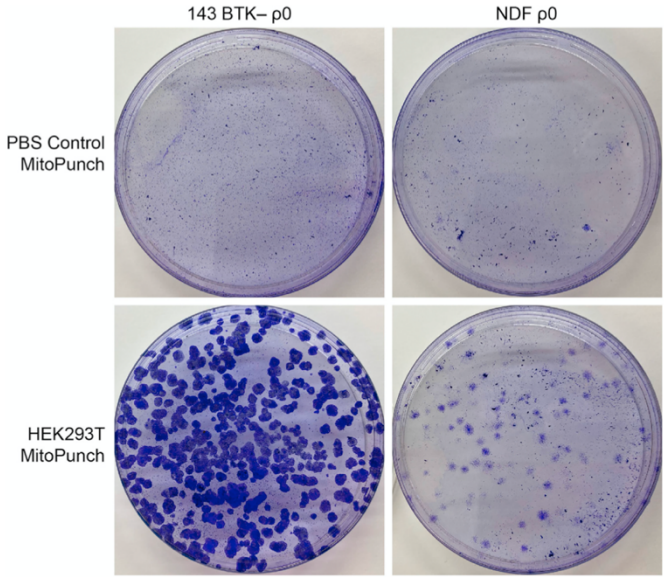

Figure 5. Crystal violet staining of SIMR clones

Images of Crystal Violet stained SIMR clones generated by MitoPunch transfer of HEK293T mitochondria or DPBS with calcium and magnesium vehicle into 143BTK– ρ0 and NDF ρ0 recipient cells on 10 cm dishes after SIMR clone selection.

TROUBLESHOOTING

Problem 1

Construct MitoPunch apparatus: MitoPunch piston is not actuating.

Potential solution

Ensure the electrical wiring of the MitoPunch device is properly connected and remains connected between samples. Always test fire the MitoPunch device before placing the PDMS reservoir on the platform. Additionally, verify that the piston is installed in the correct orientation such that the piston is driven up toward the PDMS reservoir when actuated.

Problem 2

Test recipient cell sensitivity to different SIMR clone selection media conditions: Restrictive medium selection does not reduce cell viability of recipient cells.

Potential solution

When the recipient cells are not completely mtDNA deficient the restrictive media will not effectively induce cell cycle arrest and death. Verify that the recipient cells are ρ0 prior to beginning MitoPunch using qPCR to measure mtDNA copy number and respirometry to quantify mitochondrial electron transport chain activity.

Problem 3

Mitochondrial preparation: Needle clogs persistently during mechanical isolation step of mitochondrial isolation.

Potential solution

Mitochondrial donor cell cultures that reach 100% confluency cause more clogging than cells from plates at lower confluency. Only grow donor cell cultures to 80%–90% confluence before harvesting for mitochondrial isolation.

Problem 4

Recipient cell collection: Few cells are recovered after MitoPunch and collection from filter inserts.

Potential solution

Carefully remove all cell growth medium from inside, outside, and below the PET filter insert. Medium is easily trapped between the bottom surface of the insert and the 12-well culture dish, and this excess medium can impact the efficacy of the dissociation reagent used to collect cells. Additionally, ensure dissociation reagent is applied to both sides of the filter insert as MitoPunch recipient cells grown on the filters extend projections through the pores in the membrane and must be exposed to reagent from both sides for complete dissociation.

Problem 5

SIMR clone selection: Restrictive medium selection does not reduce cell viability of recovered MitoPunch recipient cells.

Potential solution

This problem can be caused by three main factors. The first is allowing the recipient cell cultures to reach 100% confluence before introducing restrictive medium. Begin medium selection before cultures reach 80% confluence. The second is not feeding recipient cell cultures with restrictive medium with sufficient frequency. Apoptotic cells on the dishes will release nucleotides into the medium which can be scavenged by nascent SIMR cells and ρ0 cells alike, leading to constant cell viability throughout the selection process. When daily feeding is insufficient, increase the frequency of media exchange to ensure selection occurs. Third, not all lines are sufficiently sensitive to SIMR selection medium and require galactose SIMR selection medium to induce selection. Follow the steps in Test recipient cell sensitivity to different SIMR clone selection media conditions to determine the sensitivity of the chosen recipient cell line to the selection scheme.

Problem 6

SIMR clone selection: No SIMR clones are observed following MitoPunch and restrictive medium selection.

Potential solution

When no SIMR clones are observed, verify that the mitochondrial isolation yielded coupled mitochondria. Perform a mitochondrial isolation and measure the respiration rate of the mitochondrial isolate using a Seahorse Extracellular Flux Analyzer. When the isolation does not yield coupled mitochondria, verify that the buffers used in the isolation protocol are stored at the appropriate temperatures and are supplemented with protease inhibitor.

RESOURCE AVAILABILITY

Lead contact

Further information and requests for resources and reagents should be directed to and will be fulfilled by the lead contact, Michael A. Teitell (mteitell@mednet.ucla.edu).

Materials availability

This study did not generate new unique reagents. Dimensions of custom fabricated parts necessary to replicate this work are included in the text of this protocol.

Data and code availability

This study did not generate or analyze new code or datasets.

ACKNOWLEDGMENTS

A.J.S. is supported by the NIH (T32GM007185 and T32CA009120). A.N.P. is supported by the NIH (T32CA009120) and American Heart Association (18POST34080342). P.-Y.C. is supported by the NSF (CBET 1404080), the NIH (RO1GM114188), and the Air Force Office of Scientific Research (FA9550-15-1-0406). M.A.T. is supported by the Air Force Office of Scientific Research (FA9550-15-1-0406), the Department of Defense (W81XWH2110139), the NIH (R01GM114188, R01GM073981, R01CA185189, R21CA227480, R01GM127985, and P30CA016042), and CIRM (RT3-07678). We thank Yen-Ju Lin, Xiang Zhang, and Marvin Tan for their assistance with polymer fabrication.

AUTHOR CONTRIBUTIONS

A.J.S. and A.J.N. drafted and edited the manuscript and figures. T.-H.W., P.-Y.C., and M.A.T. developed the core MitoPunch technology. A.J.S., A.N.P., and T.-H.W. optimized and implemented the protocol. P.-Y.C. provided funds and infrastructure to conduct the work. M.A.T. provided funds and infrastructure to conduct the work, edited the manuscript, and advised throughout the optimization of the protocol.

DECLARATION OF INTERESTS

P.-Y.C. and M.A.T. are co-founders, board members, shareholders, and consultants for NanoCav, LLC. Patents related to this technology include (1) Efficient delivery of large cargos into cells on a porous substrate, issued Nov. 12, 2019, US 10,472,651 (UCLA); and (2) Mechanical transfection devices and methods, issued Sep. 1, 2020, US 10,760,040 (NanoCav). The other authors declare no competing interests.

REFERENCES

Aguer, C., Gambarotta, D., Mailloux, R.J., Moffat, C., Dent, R., McPherson, R., and Harper, M.E. (2011). Galactose enhances oxidative metabolism and reveals mitochondrial dysfunction in human primary muscle cells. PLoS One *6*, e28536.

Berthier, E., Young, E.W., and Beebe, D. (2012). Engineers are from PDMS-land, biologists are from polystyrenia. Lab. Chip *12*, 1224–1237.

Dawson, E.R., Patananan, A.N., Sercel, A.J., and Teitell, M.A. (2020). Stable retention of chloramphenicol-resistant mtDNA to rescue metabolically impaired cells. Sci. Rep. *10*, 14328.

Gregoire, M., Morais, R., Quilliam, M.A., and Gravel, D. (1984). On auxotrophy for pyrimidines of respiration-deficient chick embryo cells. Eur. J. Biochem. *142*, 49–55.

Miyata, N., Steffen, J., Johnson, M.E., Fargue, S., Danpure, C.J., and Koehler, C.M. (2014). Pharmacologic rescue of an enzyme-trafficking defect in primary hyperoxaluria 1. Proceedings of the National Academy of Sciences *111*, 14406–14411.

Patananan, A.N., Sercel, A.J., Wu, T.H., Ahsan, F.M., Torres, A., Jr., Kennedy, S.A.L., Vandiver, A., Collier, A.J., Mehrabi, A., Van Lew, J., et al. (2020). Pressure-driven mitochondrial transfer pipeline generates mammalian cells of desired genetic combinations and fates. Cell Rep. *33*, 108562.

Sercel, A.J., Patananan, A.N., Man, T., Wu, T.H., Yu, A.K., Guyot, G.W., Rabizadeh, S., Niazi, K.R., Chiou, P.Y., and Teitell, M.A. (2021). Stable transplantation of human mitochondrial DNA by high-throughput, pressurized isolated mitochondrial delivery. Elife *10*, e63102.

Chapter 5: Stable retention of chloramphenicol-resistant mtDNA to rescue metabolically impaired cells

SCIENTIFIC REPORTS
nature research

OPEN

Stable retention of chloramphenicol-resistant mtDNA to rescue metabolically impaired cells

Emma R. Dawson[1], Alexander N. Patananan[1], Alexander J. Sercel[2] & Michael A. Teitell[1,2,3,4,5,6]✉

The permanent transfer of specific mtDNA sequences into mammalian cells could generate improved models of mtDNA disease and support future cell-based therapies. Previous studies documented multiple biochemical changes in recipient cells shortly after mtDNA transfer, but the long-term retention and function of transferred mtDNA remains unknown. Here, we evaluate mtDNA retention in new host cells using 'MitoPunch', a device that transfers isolated mitochondria into mouse and human cells. We show that newly introduced mtDNA is stably retained in mtDNA-deficient (ρ0) recipient cells following uridine-free selection, although exogenous mtDNA is lost from metabolically impaired, mtDNA-intact (ρ+) cells. We then introduced a second selective pressure by transferring chloramphenicol-resistant mitochondria into chloramphenicol-sensitive, metabolically impaired ρ+ mouse cybrid cells. Following double selection, recipient cells with mismatched nuclear (nDNA) and mitochondrial (mtDNA) genomes retained transferred mtDNA, which replaced the endogenous mutant mtDNA and improved cell respiration. However, recipient cells with matched mtDNA-nDNA failed to retain transferred mtDNA and sustained impaired respiration. Our results suggest that exogenous mtDNA retention in metabolically impaired ρ+ recipients depends on the degree of recipient mtDNA-nDNA co-evolution. Uncovering factors that stabilize exogenous mtDNA integration will improve our understanding of in vivo mitochondrial transfer and the interplay between mitochondrial and nuclear genomes.

Mutations in the multi-copy mitochondrial genome (mtDNA) can impair the biosynthesis of ATP, metabolites, fatty acids, reactive oxygen species, and iron sulfur clusters[1–4]. Even a single nucleotide polymorphism can have profound effects on cellular function and contribute to pathologies including cardiomyopathies, diabetes, autoimmune diseases, neurological disorders, cancer, and even aging[5,6]. The degree of pathology often depends on the ratio of mutant to wild-type mtDNA populations within the same cell, a situation known as heteroplasmy[7]. One in 5,000 people have some degree of a pathological mtDNA disorder, and up to 1 in 8 individuals carry low levels of a mtDNA mutation that can be inherited through the maternal germline[8–11]. Mitochondrial replacement therapy (MRT) aims to prevent transmission of mtDNA disorders from affected mothers to offspring, but limited treatments exist for those already living with a pathological mtDNA mutation[12,13].

Our ability to repair mutant mtDNA and improve metabolically impaired cells would advance disease modeling studies and potential cell-based therapies for mtDNA disorders. Gene therapy and now gene editing is a viable treatment option for some nucleus-encoded disorders[5,14,15]. In contrast, specific mtDNA mutations are difficult to generate or repair because current gene modifying approaches do not work well inside mitochondria.

[1]Department of Pathology and Laboratory Medicine, University of California, Los Angeles, CA 90095, USA. [2]Molecular Biology Interdepartmental Program, University of California, Los Angeles, Los Angeles, CA 90095, USA. [3]Eli and Edythe Broad Center of Regenerative Medicine and Stem Cell Research, University of California, Los Angeles, Los Angeles, CA 90095, USA. [4]California NanoSystems Institute, University of California, Los Angeles, Los Angeles, CA 90095, USA. [5]Department of Pediatrics, David Geffen School of Medicine, University of California, Los Angeles, Los Angeles, CA 90095, USA. [6]Jonsson Comprehensive Cancer Center, David Geffen School of Medicine, University of California, Los Angeles, Los Angeles, CA 90095, USA. ✉email: mteitell@mednet.ucla.edu

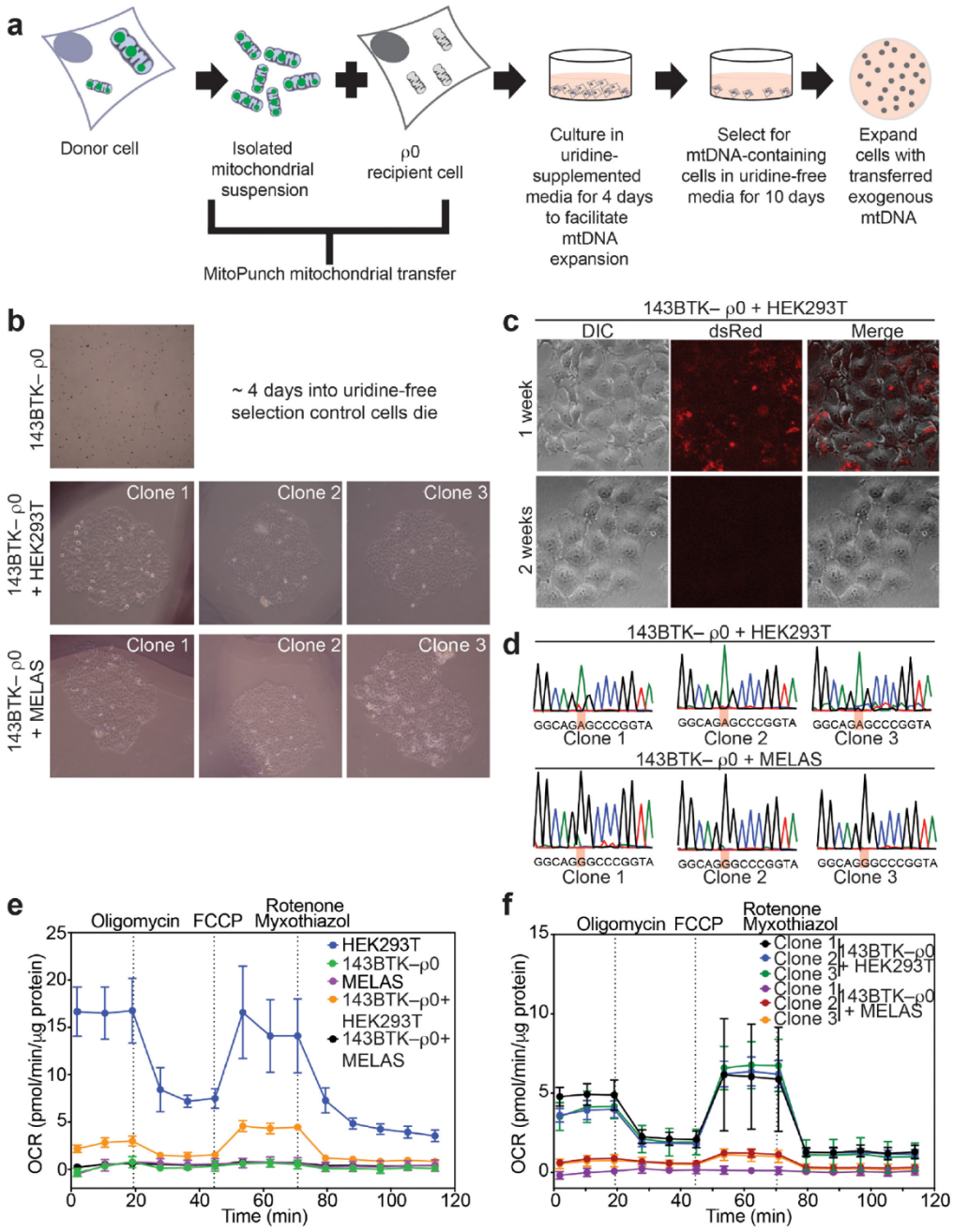
a
Donor cell
Isolated mitochondrial suspension
ρ0 recipient cell
MitoPunch mitochondrial transfer
Culture in uridine-supplemented media for 4 days to facilitate mtDNA expansion
Select for mtDNA-containing cells in uridine-free media for 10 days
Expand cells with transferred exogenous mtDNA
b
143BTK– ρ0
~ 4 days into uridine-free selection control cells die
143BTK– ρ0 + HEK293T
Clone 1
Clone 2
Clone 3
143BTK– ρ0 + MELAS
c
143BTK– ρ0 + HEK293T
DIC
dsRed
Merge
1 week
2 weeks
d
143BTK– ρ0 + HEK293T
GGCAGAGCCCGGTA
143BTK– ρ0 + MELAS
GGCAGGGCCCGGTA
e
Oligomycin
FCCP
Rotenone Myxothiazol
HEK293T
143BTK–ρ0
MELAS
143BTK–ρ0+ HEK293T
143BTK–ρ0+ MELAS
OCR (pmol/min/μg protein)
Time (min)
f
Clone 1 143BTK–ρ0 + HEK293T
Clone 2
Clone 3
Clone 1 143BTK–ρ0 + MELAS
Clone 2
Clone 3

◂**Figure 1.** Stable mitochondrial integration in ρ0 cells. (**a**) Schematic showing selection of ρ0 cell with successfully retained exogenous mtDNA. (**b**) 143BTK- ρ0 cells with transferred HEK293T or MELAS A3243G mitochondria were selected on uridine-deficient media. Approximately 2 weeks after mitochondrial transfer, colonies were imaged on an inverted microscope and 5 × objective. (**c**) 143BTK- ρ0 + dsRed- labeled HEK293T mitochondria were visualized by DIC and fluorescence microscopy 1 and 2 weeks after mitochondrial transfer. (**d**) Sanger sequencing of 3 clones derived from 143BTK− ρ0 cells transferred HEK293T or MELAS mitochondria. Orange highlight denotes mtDNA position 3243. (**e**) Seahorse Extracellular Flux analysis to quantify oxygen consumption rate of bulk culture generated from 143BTK− ρ0 cells transferred HEK293T or MELAS mitochondria. (**f**) Seahorse Extracellular Flux analysis to quantify oxygen consumption rate of clones generated from (**e**). (**e, f**) Oligomycin, FCCP, and rotenone/myxothiazol are an ATP synthase inhibitor, uncoupler, and complex I/III inhibitors, respectively. Each data point represents the average of 3 technical replicates and the error bar denotes standard deviation.

Zinc finger nucleases (ZFNs) and transcription activator-like effector nucleases (TALENs) target and degrade detrimental mtDNAs both in vitro and in vivo, shifting heteroplasmy ratios. However, these modifiers can be challenging to engineer, only degrade pre-existing target mtDNAs, are inefficient with incomplete removal of target mtDNAs, and they cannot generate new mtDNA sequences inside cells[16–23]. To bypass most of these issues, the transfer of mitochondria containing desired mtDNA sequences into cells of interest can generate desirable hybrid cells with unique mtDNA-nDNA pairings. Current mitochondrial transfer approaches for somatic cells include MitoCeption[24], microinjection[25], cell fusion[26], co-culturing[27,28], isolated mitochondrial co-incubation[29], magnetomitotransfer[30], and large cargo delivery platforms[31]. These techniques have in common the provision of mitochondria containing exogenous mtDNA into mtDNA-deficient (ρ0) recipient cells, often followed by selection in uridine-deficient culture medium[32]. ρ0 cells are typically generated using DNA intercalating drugs, such as ethidium bromide, or DNA polymerase chain terminators, such as 2′,3′- dideoxycytidine, to remove recipient cell mtDNA[33,34]. However, these drugs can cause off target nDNA mutations and are not equally effective in removing all endogenous mtDNA from all cell types. In addition, ρ0 mammalian cells do not naturally exist, leading to questions about physiological relevance. An ability to transfer isolated mitochondria and retain exogenous mtDNA in unmodified, endogenous mtDNA containing (ρ+) recipient cells would alleviate many of these potential concerns.

We recently developed a simple mechanical force based hardware device called 'MitoPunch' to transfer isolated mitochondria into mammalian cells. Here, we used MitoPunch to transfer chloramphenicol-resistant (CAP-R) mitochondria into chloramphenicol-sensitive ρ+ recipient cybrid cells that contain mutant mtDNA with impaired respiration. We evaluated whether introduced CAP-R mtDNA into ρ+ recipient cybrid cells was retained or transient and lost when the recipient cell nDNA matched and co-evolved, or was mismatched, with the cybrid cell mtDNA strain, and the resultant effect on respiratory function.

Results

MitoPunch transfer of mitochondria into ρ0 cells. To begin, we used MitoPunch to transfer isolated mitochondria into ρ0 cells, to evaluate the reacquisition of respiratory function or to generate a model of mtDNA disease in a cell system that prior studies indicated should work[24–28,31,35]. ρ0 cells lack a functional electron transport chain (ETC), which blocks dihydroorotate dehydrogenase enzymatic activity and stops endogenous pyrimidine biosynthesis, leading to cell death with time[33,36,37]. Thus, ρ0 cells can only persist in vitro in uridine-supplemented media or in uridine-deficient medium when they reacquire ETC activity. Isolated dsRed-labeled HEK293T[38] or mitochondrial encephalopathy, lactic acidosis, and stroke-like episodes (MELAS) A3243G cybrid[39] mitochondria were MitoPunch transferred into 143BTK− ρ0 osteosarcoma cells in an attempt to generate 143BTK− ρ0 + HEK293T or 143BTK− ρ0 + MELAS hybrid cells, respectively (Fig. 1a). Post-transfer, we grew cells for 4 days in uridine-replete media for recovery, followed by a shift to 10 days of uridine-deficient growth conditions to select for cells with reacquired ETC activity (Fig. 1b). The presence of undisrupted donor cells was minimized by introducing additional centrifugation spins in the mitochondrial isolation procedure and by passing the mitochondrial isolate through a 3 μm filter before reaching the recipient cells, which is an indirect benefit of the MitoPunch transfer pipeline. We isolated three clones from 143BTK− ρ0 + HEK293T or 143BTK− ρ0 + MELAS bulk cultures that contained hundreds or tens of independent colonies, respectively. Since 143BTK− ρ0 + HEK293T cells received dsRed-labeled mitochondria, we could observe the turnover of transferred mitochondria over time, with the label disappearing between one and two weeks after mitochondrial transfer (Fig. 1c). This observation further confirms that there was no whole cell contamination from the mitochondrial donor and is consistent with the predicted turnover rate for mitochondrial proteins[40,41]. Following the 10 day uridine-deficient selection, clones were isolated and expanded. Two months post-transfer, when no original HEK293T or MELAS mitochondrial proteins remained, sequencing of three independent clones of each new hybrid cell type showed persistence of the exogenous mtDNA (Fig. 1d). To assess mitochondrial function, we measured the oxygen consumption rate (OCR) for each bulk culture and each of the six individual clones (Fig. 1e,f). HEK293T cells have a robust respiratory profile, while the 143BTK− ρ0 and MELAS cells have abolished respiration. Compared to 143BTK− ρ0 cells with abolished respiration, 143BTK− ρ0 + HEK293T hybrid cells showed an improved respiratory profile. In contrast, 143BTK− ρ0 + MELAS hybrid cells recapitulated the impaired respiratory profile observed for MELAS patient-derived cells[12,42]. Additionally, we performed qPCR on 143BTK− ρ0 cells containing either MELAS or wild type (WT) transferred mitochondria to compare the restored mtDNA levels to unmodified 143BTK− parental cells (Supplementary Fig. S1). After several weeks of cell culture and freeze–thaw cycles, 143BTK− ρ0 + WT transfers showed mtDNA copy numbers comparable to 143BTK− parent cells. However, 143BTK− ρ0 + MELAS cells maintain a slightly lower mtDNA copy number.

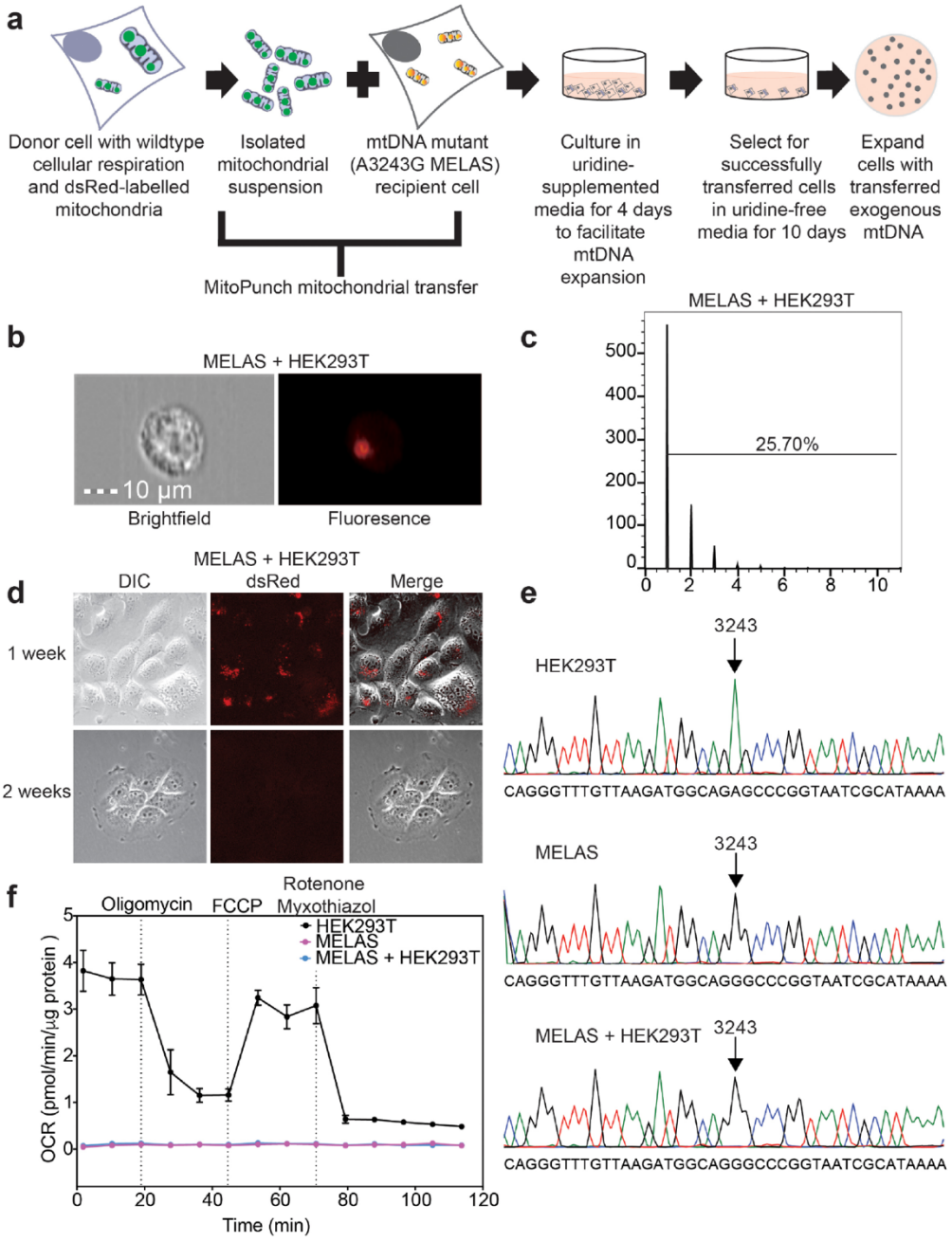
a
Donor cell with wildtype cellular respiration and dsRed-labelled mitochondria
Isolated mitochondrial suspension
mtDNA mutant (A3243G MELAS) recipient cell
MitoPunch mitochondrial transfer
Culture in uridine-supplemented media for 4 days to facilitate mtDNA expansion
Select for successfully transferred cells in uridine-free media for 10 days
Expand cells with transferred exogenous mtDNA
b
MELAS + HEK293T
10 µm
Brightfield
Fluoresence
c
MELAS + HEK293T
25.70%
d
MELAS + HEK293T
DIC
dsRed
Merge
1 week
2 weeks
e
3243
HEK293T
CAGGGTTTGTTAAGATGGCAGAGCCCGGTAATCGCATAAAA
MELAS
CAGGGTTTGTTAAGATGGCAGGGCCCGGTAATCGCATAAAA
MELAS + HEK293T
CAGGGTTTGTTAAGATGGCAGGGCCCGGTAATCGCATAAAA
f
Oligomycin
FCCP
Rotenone
Myxothiazol
HEK293T
MELAS
MELAS + HEK293T
OCR (pmol/min/µg protein)
Time (min)

◂**Figure 2.** Transfer of functional mtDNA is not maintained in ρ + mutant cells. (**a**) Schematic showing selection of ρ + mutant cell with transferred exogenous mtDNA. (**b,c**) Isolated dsRed-labeled HEK293T mitochondria were transferred by MitoPunch into MELAS cybrid cells and immediately analyzed by ImageStream. Brightfield and fluorescence data was collected for 10,000 cells. The number of transferred mitochondria was quantified for each cell. (**d**) MELAS + HEK293T were visualized by DIC and fluorescence microscopy 1 and 2 weeks after mitochondrial transfer. (**e**) Sanger sequencing of HEK293T, MELAS, and MELAS + HEK293T cells. Arrows denote mtDNA position 3243. (**f**) Seahorse Extracellular Flux analysis to quantify oxygen consumption rate of HEK293T, MELAS, and MELAS + HEK293T cells. Oligomycin, FCCP, and rotenone/myxothiazol are an ATP synthase inhibitor, uncoupler, and complex I/III inhibitor, respectively. Each data point represents the average of 3 technical replicates and the error bar denotes standard deviation.

In sum, the MitoPunch mitochondrial transfer and selection pipeline yields permanently retained exogenous mtDNA in a ρ0 recipient cell type, as anticipated, and can model defective respiration that characterizes a typically severe mtDNA disease.

Transferred WT mtDNA is lost from ρ + MELAS cells. We next examined whether MitoPunch transfer could improve the mitochondrial function of ρ + (endogenous mtDNA containing) recipient cells with impaired respiration. As above, we performed MitoPunch transfer of isolated dsRed-labeled HEK293T mitochondria this time into human cybrid cells containing an A3243G MELAS mtDNA mutation (Fig. 2a). Immediately following MitoPunch, we visualized potential MELAS + HEK293T hybrid cells using ImageStream flow cytometry (Fig. 2b) to assess the number of recipient cells with exogenous mitochondria and the number of dsRed-labeled mitochondrial "speckles" per cell. ImageStream data showed that ~ 25% of MitoPunch recipient MELAS cybrid cells acquired 1–6 dsRed speckles per cell, providing a crude estimate of mitochondria transferred (Fig. 2c). We performed an independent experiment and again applied uridine-deficient media selection because MELAS cybrid cells show markedly impaired cellular respiration (Fig. 1e)[24,26,31,35]. Similar to ρ0 recipient cells, exogenous HEK293T mitochondrial proteins remain for one to two weeks post-transfer in selection media (Fig. 2d). However, unlike ρ0 recipients, MELAS cells do not retain exogenous mtDNA beyond 2 months post-transfer, as shown by the continued presence of only the A3243G mtDNA sequence for MELAS + HEK293T bulk cultures containing tens of colonies (Fig. 2e).

We examined a second, independent, MELAS cybrid cell recipient (MELAS2), homoplasmic for A3243G mtDNA, by transferring WT functional mitochondria isolated from donor cells obtained from the same individual. MitoPunch transfer cells underwent selection for four weeks in uridine-deficient media with ~ 50 independent MELAS2 + WT colonies obtained (Supplementary Fig. S1). However, a similar number of independent colonies were also obtained for MitoPunch transfer cells that received 1 × phosphate buffer saline (PBS), pH 7.4, indicating that very low level ETC function in MELAS cybrids is sufficient for survival in uridine-free media selection. We anticipate that ~ 25% of recipient cells obtained WT mtDNA similar to MELAS + HEK293T cells (Fig. 2b,c). However, MELAS2 + WT cells also did not show evidence for exogenous mtDNA after four weeks of selection by sequencing the bulk culture containing ~ 50 independent colonies (Supplementary Fig. S1).

We measured the OCR of MELAS + HEK293T cells in bulk cultures containing tens of independent colonies as a second assessment of retained exogenous mtDNA one month post-transfer. In contrast to transfers into 143BTK− ρ0 recipient cells, MELAS + HEK293T cells replicated the impaired respiratory profile characteristic of the parent MELAS cybrid cells without improved respiration (Fig. 2f). In addition, when isolated MELAS and HEK293T mitochondria were mixed at 1:1 or 10:1 ratios and then MitoPunch transferred into 143BTK− ρ0 recipient cells, we observed significant MELAS mtDNA retention in the 10:1 mixture in addition to the anticipated retention of HEK293T mtDNA (Supplementary Fig. S1). This indicates that the MitoPunch transfer and selection pipeline can generate heteroplasmic clones in addition to homoplasmic clones that may resemble certain physiologic conditions, at least in certain ρ0 recipient cells. Increasing the MELAS mtDNA population relative to WT mtDNA also resulted in increasingly impaired respiration, as anticipated for an increasingly mutant mtDNA heteroplasmic state (Supplementary Fig. S1). Overall, these data indicate that two independent MELAS recipient cells examined here do not retain exogenous mtDNA that can potentially improve respiration. This is different from 143BTK− ρ0 cells (Fig. 1, Supplementary Fig. S1) and suggests strong selective pressure to remove exogenous mtDNA and retain endogenous mutant mtDNA in these ρ + recipients despite potential respiratory advantages for retaining WT mtDNA.

Transfer of CAP-R mtDNA confers resistance to Δmt-ND4 cells. We addressed the inability of our standard transfer and selection protocol to isolate ρ + cells with stable exogenous mtDNA by using an antibiotic-resistant mitochondrial donor to apply additional selective pressure for exogenous mtDNA retention. Prior studies generated and used mtDNA mutations that confer resistance to the mitochondrial translation inhibitor, chloramphenicol (CAP). CAP-resistant (CAP-R) mitochondria first showed utility for mitochondrial transfer by microinjection and cybridization with CAP-S cells having WT respiratory profiles[25,43–45]. Since these studies showed exogenous mtDNA retention in WT ρ + cells, we examined whether this would work with our MitoPunch pipeline to permanently improve mitochondrial function in ρ + mutant cells (Fig. 3a). We used mouse fibroblast cell line CAP-R 501-1, which contains a mtDNA T2433C substitution resulting in chloramphenicol-resistance, as a mitochondrial donor. CAP-R 501-1 was derived from L929 mice with co-evolved C3H/An nucleus and mitochondrial haplotypes (Fig. 3b). In addition to antibiotic resistance, CAP-R 501-1 cells show increased OCR compared to the abolished OCR in L929 ρ0 fibroblasts, but less basal respiration, maximal respiration, and mitochondrial-derived ATP production compared to the unmodified L929 parental cells (Fig. 3c,

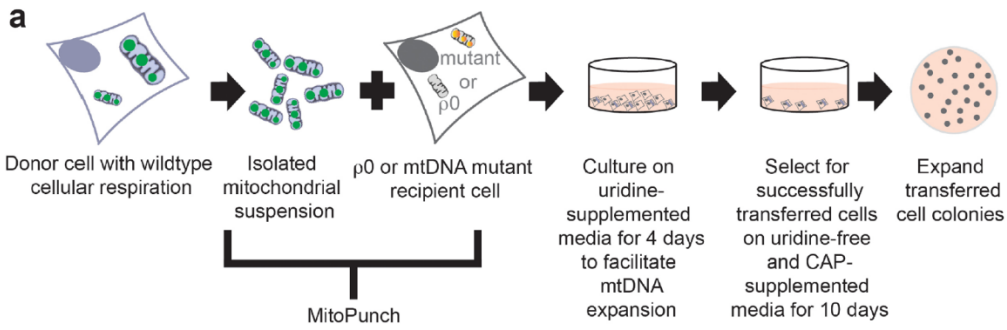

b

Cell Line	nDNA	mtDNA
CAP-R 501-1	C3H/An	C3H/An
L929 ρ0	C3H/An	-
Δmt-ND4	C3H/An	NIH3T3
Δmt-ND6	C3H/An	C3H/An

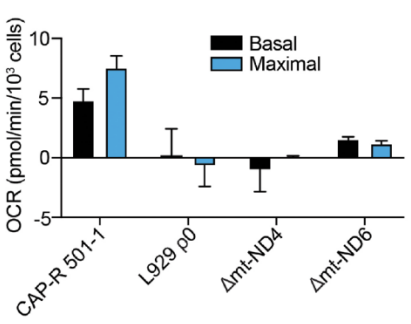

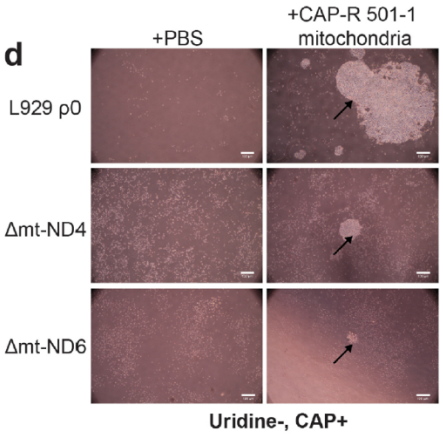

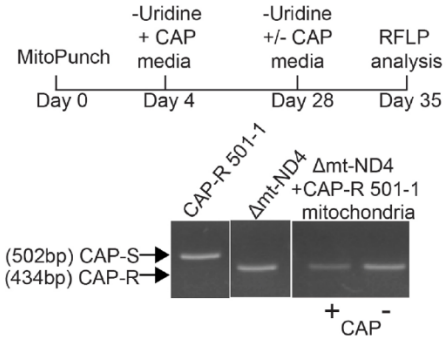

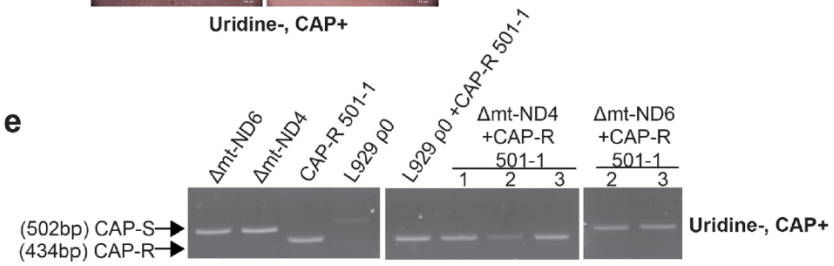

◂**Figure 3.** Chloramphenicol selection for transferred CAP-R mtDNA retention. (**a**) Selection of mouse ρ0 or ρ + mutant cells with successfully retained exogenous CAP-R 501-1 mtDNA. (**b**) Cell lines used with known nuclear and mitochondrial mouse backgrounds. (**c**) Seahorse Extracellular Flux analysis quantification of basal and maximal cellular respiration in Δmt-ND4, Δmt-ND6, CAP-R 501-1, and L929 ρ0 cells. Two-tailed, unpaired Student's t-test comparing samples to L929ρ0. * represents significance with * < 0.05, ** < 0.01, *** < 0.001, **** < 0.0001. Black * represents significance for Basal Respiration and Blue * represents significance for Maximal Respiration. The bar height denotes average of 3 replicates and the error bars are the standard deviation. (**d**) Phosphate buffered saline (PBS) or CAP-R 501-1 mitochondria were transferred into L929 ρ0, Δmt-ND4, and Δmt-ND6 recipient cells and were selected on uridine-deficient, CAP-supplemented media. Four weeks after mitochondrial transfer, colonies were imaged with an inverted microscope and 5 × objective. Scale bar denotes 100 µm. (**e**) RFLP analysis of CAP-R 501-1, L929 ρ0, L929 ρ0 + CAP-R 501-1, Δmt-ND4 + CAP-R 501-1, and Δmt-ND6 + CAP-R 501-1 bulk culture cells two weeks after mitochondrial transfer. (**f**) Following Δmt-ND4 + CAP-R 501-1 mitochondrial transfer, cells were cultured in (1) uridine-supplemented media for four days, (2) uridine-deficient, CAP-supplemented media for 24 days, and (3) uridine-supplemented media with or without CAP for 7 days. RFLP analysis of CAP-R 501-1, Δmt-ND4, and Δmt-ND4 + CAP-R 501-1 mitochondria. In (**e–f**), arrows denote the difference between CAP-S (502 bp) and CAP-R (434 bp) PCR products post-MaeII digestion on a 2.5% agarose gel electrophoresis. CAP-R 501-1 control is the same in each panel. Each of these panels were cropped from different parts of the same gel with the same exposure level.

Supplementary Fig. S3). To establish that this mitochondrial donor will work in a ρ0 background, we MitoPunch transferred isolated CAP-R 501-1 mitochondria into mouse L929 ρ0 cells (L929 ρ0 + CAP-R 501-1) that were grown in uridine-deficient, CAP-supplemented media (Fig. 3a). Four weeks post-transfer and sequential selection, tens of colonies were observed (Fig. 3d) and assessed as a bulk culture by restriction fragment length polymorphism (RFLP) analyses for retention of the CAP-R 501-1 mtDNA (Fig. 3e). L929 ρ0 + CAP-R 501-1 stably integrated the exogenous CAP-R mtDNA as shown by a 434 bp PCR product that results from cleavage by MaeII only when there is a T2433C substitution[46].

To attempt to extend this result for ρ+ mutant cells, we used two independent ρ+ recipient cybrid cells generated with different nuclear and mitochondrial DNA origins. A recent study showed that nucleus-mitochondrial genome (mtDNA-nDNA) interactions control mtDNA heteroplasmy[47]. Therefore, we tested whether recipient cells with mismatched or matched endogenous mtDNA-nDNA pair origins integrate exogenous mtDNA. For this, we used a recipient mouse cybrid cell line with a defect in complex 1 NADH dehydrogenase subunit 4 (delA10227, Δmt-ND4). Δmt-ND4 is a mismatched recipient cell line that originated from a cytoplasmic fusion between an L929 ρ0 cell (C3H/An mouse strain) and an enucleated cytoplast from the NIH3T3 mouse strain containing this deletion mutation[48]. We also used a second independent recipient mouse cybrid cell line with a defect in complex 1 NADH dehydrogenase subunit 6 (iC13887, Δmt-ND6). Δmt-ND6 is a matched recipient cell line that originated from a cytoplasmic fusion between an L929 ρ0 cell (C3H/An mouse strain) and an enucleated cytoplast from the L929 parental cell line (C3H/An mouse strain) containing this insertion mutation[49,50] (Fig. 3b). Both Δmt-ND4 and Δmt-ND6 recipient cells have severely impaired basal and maximal respiration in contrast to a robust respiratory profile for CAP-R 501–1 mitochondrial donor cells (Fig. 3c).

We MitoPunch transferred isolated CAP-R 501-1 mitochondria into Δmt-ND4 (Δmt-ND4 + CAP-R 501-1) and Δmt-ND6 (Δmt-ND6 + CAP-R 501-1) recipient cells. Following two weeks of sequential selection in uridine-deficient, CAP-supplemented media, up to 10 colonies were obtained (Fig. 3d). RFLP analysis of the bulk culture showed that Δmt-ND4 + CAP-R 501-1 cells retained exogenous CAP-R 501-1 mtDNA four weeks after mitochondrial transfer with an undetectable level of endogenous mtDNA (Fig. 3e, Supplementary Fig. S2). We were surprised by this result because Δmt-ND4 and CAP-R 501-1 are not of the same mitochondrial origins (Fig. 3b). Our data show that endogenous mutant mtDNA was completely replaced by a mtDNA sequence of interest using an additional selection step and without making cells ρ0 first. To address stability, following four weeks on uridine-deficient, CAP-supplemented media, Δmt-ND4 + CAP-R 501-1 cells were grown with or without CAP for one additional week (Fig. 3f, Supplementary Fig. S2). RFLP analyses of the bulk culture again showed no endogenous CAP-S mtDNA and instead exogenous CAP-R mtDNA five weeks after mitochondrial transfer. Thus, exogenous mtDNA stabilized in Δmt-ND4 cells without ongoing antibiotic selection, indicating permanent mtDNA replacement. In contrast, however, Δmt-ND6 + CAP-R 501-1 bulk cultures did not retain exogenous mtDNA by RFLP analyses (Fig. 3e, Supplementary Fig. S2), even though nucleus and mitochondrial origins were the same, another unanticipated result (Fig. 3b).

Stable transfer of CAP-R mtDNA restores respiration in ρ0 and Δmt-ND4 cells. Following permanent retention of exogenous CAP-R 501-1 mtDNA in L929 ρ0 and Δmt-ND4 ρ+ cells (Fig. 3e), we assessed changes in mitochondrial function. For this, we measured mitochondrial (ATPmito) and glycolytic (ATPglyco) ATP production using the Seahorse Extracellular Flux Analyzer. L929 ρ0 + CAP-R 501-1 bulk culture cells recovered ATPmito, basal and maximal respiration, in contrast to L929 ρ0 cells at levels comparable to CAP-R 501-1 parent donor cells (Fig. 4a, Supplementary Fig. S3). Repression of ATPglyco also accompanied increased ATPmito, basal and maximal respiration in Δmt-ND4 + CAP-R 501-1 bulk culture cells (Fig. 4b, Supplementary Fig. S3). In addition, the Δmt-ND4 + CAP-R 501-1 respiratory profile was comparable to the CAP-R 501-1 parent mitochondrial donor. However, Δmt-ND6 + CAP-R 501-1 bulk culture cells did not restore ATPmito, basal or maximal respiration (Fig. 4c, Supplementary Fig. S3). A lack of improvement in mitochondrial function in

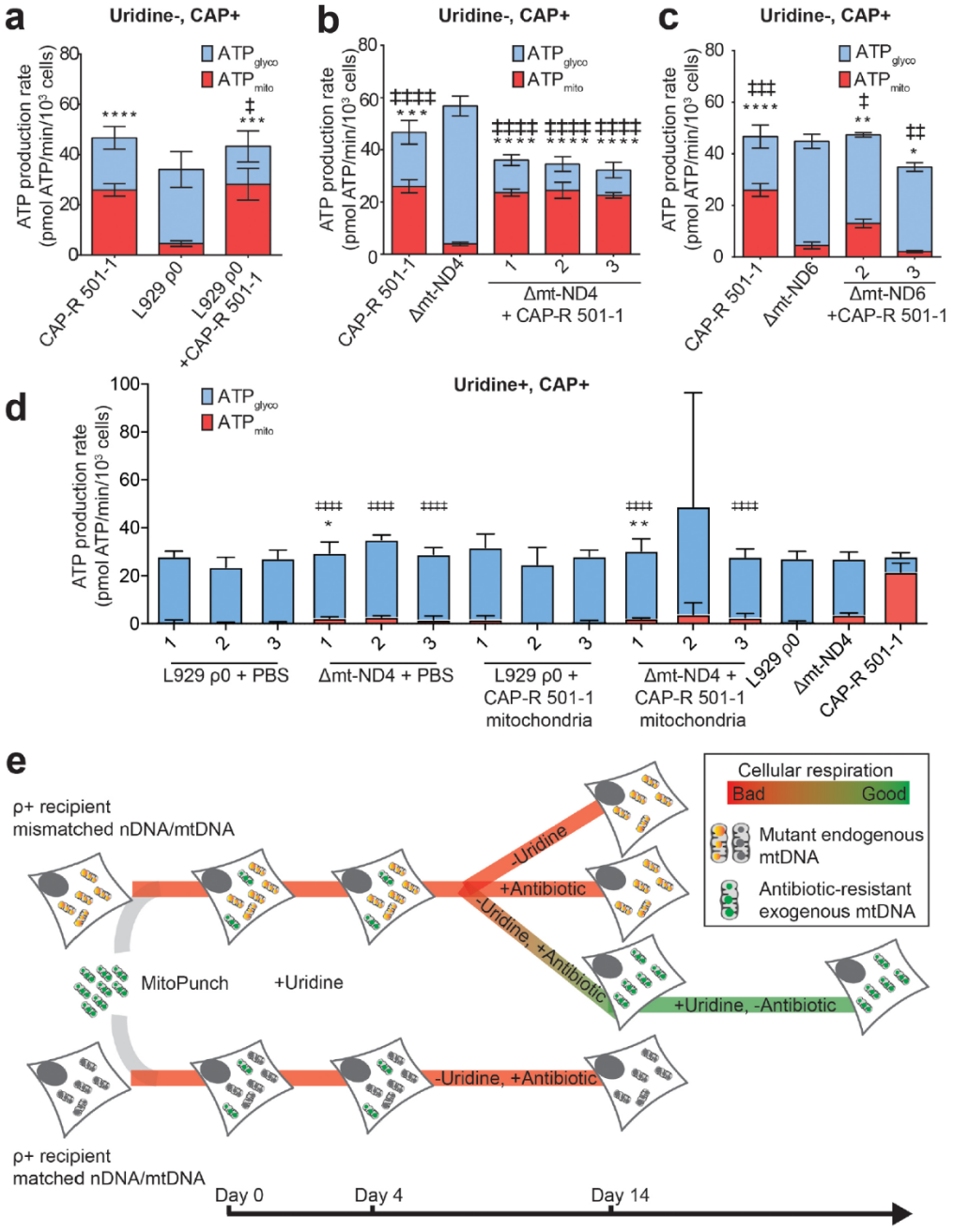
a
Uridine-, CAP+
ATP production rate (pmol ATP/min/10³ cells)
ATP glyco
ATP mito
CAP-R 501-1
L929 ρ0
L929 ρ0 +CAP-R 501-1
b
Uridine-, CAP+
CAP-R 501-1
Δmt-ND4
Δmt-ND4 + CAP-R 501-1
c
Uridine-, CAP+
CAP-R 501-1
Δmt-ND6
Δmt-ND6 +CAP-R 501-1
d
Uridine+, CAP+
L929 ρ0 + PBS
Δmt-ND4 + PBS
L929 ρ0 + CAP-R 501-1 mitochondria
Δmt-ND4 + CAP-R 501-1 mitochondria
L929 ρ0
Δmt-ND4
CAP-R 501-1
e
ρ+ recipient mismatched nDNA/mtDNA
MitoPunch
+Uridine
-Uridine
+Antibiotic
-Uridine, +Antibiotic
+Uridine, -Antibiotic
Cellular respiration
Bad
Good
Mutant endogenous mtDNA
Antibiotic-resistant exogenous mtDNA
ρ+ recipient matched nDNA/mtDNA
Day 0
Day 4
Day 14

◂**Figure 4.** ρ0 and ρ + mutant recipient cells have restored respiration with transferred CAP-R mitochondria. (**a–c**) Seahorse Extracellular Flux analysis and quantification of ATP levels contributed by mitochondria (ATPmito) and glycolysis (ATPglyco). Cells were cultured in uridine-deficient, CAP-supplemented media. (**a**) Analysis of CAP-R 501-1 mitochondrial donor, L929 ρ0 recipient, and L929 ρ0 + CAP-R 501-1 cells. (**b**) Analysis of CAP-R 501-1 mitochondrial donor, Δmt-ND4, and Δmt-ND4 + CAP-R 501-1 bulk culture cells from three independent transfers. (**c**) Analysis of Δmt-ND6, CAP-R 501-1, and Δmt-ND6 + CAP-R 501-1 bulk cultures from two independent transfers. (**a–c**) Two-tailed, unpaired Student's t-test comparing samples to L929 ρ0, Δmt-ND4, or Δmt-ND6. * represents significance for ATPmito and ‡ represents significance for ATPglyco. * < 0.05, ** < 0.01, *** < 0.001, **** < 0.0001. ‡ < 0.05, ‡ ‡ < 0.01, ‡ ‡ ‡ < 0.001, ‡ ‡ ‡ ‡ < 0.0001. The bar height denotes average of 4 replicates and the error bars are the standard deviation. (**d**) Seahorse Extracellular Flux analysis and quantification of ATPmito and ATPglyco in L929 ρ0, Δmt-ND4, CAP-R 501-1, L929 ρ0 + CAP-R 501-1 bulk cultures from three independent transfers, and Δmt-ND4 + CAP-R 501-1 bulk cultures from three independent transfers. Cells were cultured in uridine-supplemented, CAP-supplemented media. Two-tailed, unpaired Student's t-test comparing samples to Δmt-ND4. * represents significance for ATPmito and ‡ represents significance for ATPglyco. * < 0.05, ** < 0.01, *** < 0.001, **** < 0.0001. ‡ < 0.05, ‡ ‡ < 0.01, ‡ ‡ ‡ < 0.001, ‡ ‡ ‡ ‡ < 0.0001. There were no statistically significant differences when comparing the samples to L929 ρ0 cells. The bar height denotes average of 5 replicates and the error bars are the standard deviation. (**e**) Schematic showing summary of ρ + mitochondrial transfer efficiency in a given selection condition.

Δmt-ND6 + CAP-R 501-1 cells is likely from failed replacement of mutant mtDNA without exogenous mtDNA integration.

We note that in our studies Δmt-ND4 + CAP-R 501-1 mitochondrial transfer is only efficient with serial selection in uridine-deficient and CAP-supplemented media. Without double selection, or only CAP-supplemented media, exogenous CAP-R 501-1 mtDNA does not stably integrate into either the respiratory-incompetent L929 ρ0 or Δmt-ND4 ρ+ recipient cells as observed by continued lack of oxygen consumption (Fig. 4d, Supplementary Fig. S3). Currently, to transfer and permanently retain exogenous mtDNA in a ρ+, mutant recipient cell, our pipeline requires the transfer of mitochondria conferring antibiotic resistance and selection for stable hybrid cells in both uridine-deficient and antibiotic-supplemented media (Fig. 4e). Following five weeks of selection, transfer cells with permanently retained exogenous mtDNA do not require further selective growth conditions. However, and unexpectedly for the limited number of situations we have examined thus far, a recipient cell must have mismatched nDNA–mtDNA origins for exogenous mtDNA integration to occur using our MitoPunch mitochondrial transfer pipeline.

Discussion

Prior studies of mitochondrial transfer primarily used ρ0 cells as recipients due to the relative ease of integrating exogenous mtDNA[9,31,35]. However, DNA-intercalating and DNA polymerase chain terminating drugs used to deplete mtDNA to generate ρ0 cells can have off-target nDNA effects[33,51]. Although mtDNA diseases do correlate with reduced mtDNA copy numbers in cells, no ρ0 cells exist in vivo with the exception of red blood cells[34,52–55]. ρ0 tumor cells in experimental mouse systems acquire exogenous mtDNA from host cells, which stimulates tumor progression and aggression[36,56,57]. However, the majority of mitochondrial transfer events reported in vivo usually involve some form of tissue injury and ρ+ recipient cells[58,59]. The molecular mechanisms underpinning mitochondrial transfer and permanent exogenous mtDNA integration in ρ+ cells are currently unknown and require new systems to control and study this phenomenon[3,5,8,9,13,31,60,61].

Here, our mitochondrial transfer method improved respiration in metabolically impaired cells containing endogenous, mutant mtDNA. Other studies performed mitochondrial transplantation into ρ+ cells in vitro[29,62] and in vivo[63–68] for therapeutic purposes, but only observed short term changes that do not indicate permanent retention of exogenous mtDNA. For example, one study restored ATP production in an A3243G MELAS cell line using Pep-1 mediated mitochondrial transfer[62]. Mitochondrial function did improve in these dysfunctional cells after delivery, but the study was limited to four days in duration and the approach was unable to replace the endogenous detrimental mtDNA population. Another longer-term, four week study co-incubating mitochondria with WT cardiomyocytes reported only a temporary increase in mitochondrial function which, after two days, returned to the pre-transfer level of reduced respiration[28]. We observed that two weeks after transferring WT mitochondria into MELAS cells, whose respiration is similar to that of a ρ0 cell (Supplementary Fig. S1)[42], the recipient cells survive uridine-deficient media selection without stably integrating exogenous WT mtDNA. This occurred for two independent MELAS cell lines with either matched or mismatched mitochondrial donors. In our studies, mutant mtDNA recipient cells persisted from the lack of selective pressure to integrate exogenous mtDNA. Our findings support a prior cell-to-cell mitochondrial transfer study and indicate there is a fundamental inability to transfer mitochondria into mutant ρ+ recipient cells[69]. In addition, the transfer of equal amounts of HEK293T and MELAS mitochondria into a 143BTK− ρ0 recipient cell yields co-retention of both functional and dysfunctional mtDNA. Our data suggest for currently unknown reasons that the co-introduction of multiple mitochondrial sources into a ρ0 cell that did not co-adapt to either mtDNA population results in the retention of both populations. It may be that nDNA preferentially maintains co-adapted mtDNA due to metabolic requirements[3].

To circumvent a retention roadblock and apply an additional selective pressure to retain exogenous mtDNA, we used antibiotic-resistant mitochondria from CAP-R 501-1 cells. Previous studies have used cell fusion, co-incubation, and microinjection to deliver CAP-R mitochondria into WT cells[25,43,70]. We also achieved antibiotic-resistant mitochondrial transfer into mutant ρ+ cells. However, permanent exogenous mtDNA retention only

occurred for cells with mismatched, not co-adapted mtDNA-nDNA pairs. Exogenous mtDNA retention occurred for both a mismatched ρ+ recipient and also a ρ0 recipient. For Δmt-ND4 + CAP-R 501-1 cells, there was no detectable endogenous mtDNA five weeks after mitochondrial transfer. These unexpected results suggest that the endogenous mtDNA–nDNA co-evolution somehow influences mtDNA sequence retention[71,72]. How this correlates with the retention and function of non-native mtDNA sequences in humans is unclear. Mitochondrial replacement therapies and three-person in vitro fertilization technologies used to prevent the transmission of mtDNA disorders from affected mothers have resulted in live births, suggesting the successful retention of exogenous mtDNA[73,74]. However, pathogenic mtDNA sequences have been observed in ESCs derived from these embryos, which may indicate problems with permanent exogenous mtDNA retention[75]. Understanding the biological pathways necessary to retain transferred mtDNA in vitro may therefore provide insight into improving mitochondrial replacement therapies.

Our protocol, unlike cybridization which typically requires immortal or cancerous cell fusion, can utilize replication, or 'Hayflick',-limited cells, to permit reprogramming to induced pluripotent stem cells. Such 'primary' cell recipients have a limited number of cell divisions and cannot replicate long after mtDNA depletion to generate a ρ0 cell. Our future ability in MRT in cells capable of fate transitions is of great clinical significance. Further work is needed to uncover changes to the metabolome, transcriptome, and proteome with mitochondrial transfer, to determine the extent of functional restoration in recipient cells. Our ρ+, CAP-R mitochondrial transfer pipeline could be a tool for screening recipient cells for potential factors involved in exogenous mtDNA integration.

Methods

Cell culture. The A3243G MELAS cybrid cell line was obtained from Carlos Moraes (University of Miami)[76]. 143BTK− ρ0 human osteosarcoma cells, cybrid cell lines with the A3243G mutation or wildtype mtDNA from the same patient, and CAP-R mouse fibroblasts (501-1) were obtained from Douglas Wallace (University of Pennsylvania)[35,45,46,77]. L929 ρ0 and mouse cybrids with a mutation in the mitochondrial-encoded NADH dehydrogenase 4[48] (Δmt-ND4, delA10227) or mitochondrial-encoded NADH dehydrogenase 6[49,50] (Δmt-ND6, iC13887) were obtained from Jose Antonio Enriquez Dominguez (Centro Nacional de Investigaciones Cardiovasculares Carlos III (CNIC)). HEK293T cells expressing mitochondria-label dsRed protein (pMitoDsRed, Clontech Laboratories) were generated as previously published[38]. Cells were maintained in Dulbecco's Modified Eagle's Medium (DMEM; Gibco, Cat. #11966-025) supplemented with 10% Fetal Bovine Serum (FBS; Omega Scientific, FB-11), 0.7 mM non-essential amino acids (Gibco, Cat. #11140-050), GlutaMAX (Gibco, Cat. #35050061), penicillin and streptomycin antibiotics (ThermoFisher Scientific, Cat. #15070063), and 50 µg/mL uridine (Sigma, Cat. #U3003). Cultured cells were routinely tested for mycoplasma with the Lonza Mycoalert Mycoplasma Detection Kit. Cells were passaged every other day and incubated at 37 °C and 5% CO_2.

Mitochondrial transfer workflow. Mitochondria were isolated from ~ 5×10^6 donor cells using the Qproteome Mitochondria Isolation Kit (Qiagen, Cat. #37612). After isolation, around 15 µg of mitochondrial protein were suspended in 120 µL of 1 × phosphate-buffered saline (1 × PBS), pH 7.4, with calcium and magnesium and subsequently transferred into recipient cells by MitoPunch. After mitochondrial transfer, recipient cells that stably retained the exogenous mitochondria were obtained after a two-week selection in a uridine-free media that allows only cells with functional mitochondria to survive. For mitochondrial transfer experiments involving CAP-R mitochondria, transferred cell were selected in media lacking uridine and supplemented with 100 µg/mL CAP (Fisher Scientific, Cat. #22-055-125GM).

MitoPunch. The MitoPunch is a force-based delivery tool to transfer isolated mitochondria. Using a 5 V solenoid (Sparkfun, Cat. #ROB-11015) on a threaded plug (Thor Labs, Cat. #SM1PL) inside a threaded cage plate (Thor Labs, Cat. #CP02T), this solenoid will apply a force to a deformable PDMS (10:1 ratio of Part A base: Part B curing agent, 25 mm diameter, 0.67 mm height bottom circular layer, outer diameter, 22 mm; inner diameter, 10 mm; height, 1.30 mm upper circular layer) fluid reservoir containing approximately 120 µL of isolated mitochondrial suspension. This force propels the mitochondrial suspension into ~ 200,000 adherent cells seeded onto a porous membrane with 3 µm pores (Corning, Cat. #353181) and placed above the PDMS. The solenoid is controlled using a 5 V power supply mini board (Futurlec, Cat. #MINIPOWER) and a 12 V, 3 Amp DC power supply (MEAN WELL, Cat. #RS-35-12).

ImageStream. After MitoPunch mitochondrial transfer, cells were collected in 1.5 mL tubes and centrifuged at 1,000 × g for 5 min. The supernatant was aspirated and cells were washed 3 × with 0.5 mL PBS. After final wash, PBS was aspirated and cells were fixed with 100 µL of 4% paraformaldehyde (Thermo Fisher Scientific, Cat. #28906) for 15 min on ice. 1 mL of PBS with 5% FBS (Omega Scientific, FB-11) was added to fixative and centrifuged at 500 × g for 10 min. Supernatant was removed, cells were resuspended in PBS with 5% FBS and imaged on Amnis ImageStream^x MK II.

Oxygen consumption rate flux analysis. The Seahorse Extracellular Flux Analyzer measures cellular oxygen consumption rates (OCR) to quantify mitochondrial function. Cells were plated at ~ 15,000 cells/well density in a XF96 microplate (Seahorse Bioscience, Cat. #100882-004) 24 h prior to analysis. Prior to experiments, a drug titration experiment was performed to determine the optimal concentrations of oligomycin, FCCP, and antimycin A. Treatments of 1 µM oligomycin (ATP synthase inhibitor), 0.3 µM carbonyl cyanide-4-(trifluoromethoxy) phenylhydrazone (FCCP, uncoupling agent), and 1 µM antimycin A (ubiquinone inhibitor) were added to characterize specific ETC complexes. Estimations of ATP production rates were completed using the Agilent Seahorse XF ATP Real-Time rate assay[78]. Oligomycin-sensitive respiratory rates were con-

verted to rates of mitochondrial ATP production (ATPmito) assuming a P/O ratio of 2.73[79,80]. Glycolytic ATP rates (ATPglyco) production was estimated using the proton prediction rate (PPR) from lactate efflux provided by the XF96 Seahorse. PPR was corrected for respiratory CO_2 acidification and geometric assay volume using values provided by Agilent. ATPglyco was estimated using a 1:1 ratio between lactate efflux and ATP generation.

Restriction fragment length polymorphism (RFLP) analysis. Total mtDNA was isolated from cells using the DNeasy Blood and Tissue kit (Qiagen, Cat. #69504). mtDNA surrounding the CAP site were amplified by Polymerase Chain Reaction (PCR) using the following primers—forward: GAGGGTCCAACTGTCTCT TATC and reverse: TCCTTTCGTACTGGGAGAAATC. After PCR amplification, the product was digested with the MaeII restriction enzyme that cuts 5′-ACGT-3′ specifically at mtDNA sequence location 2501. The digested product was run on a 2.5% agarose gel at 100 V for 1 h and quantified using a Gene Genius bioimaging system. Last-cycle hot RFLP was not performed.

Microscopy. Cell morphology images were taken on an Olympus CKX31 (Cat. #CKX31SF5) inspection microscope with a 4× objective. Brightfield, DIC, and fluorescence images were obtained with a Zeiss Axio Observer Z1 microscope and Hamamatsu EM CCD camera (Cat. #C9100-02).

Sequencing of MELAS A3243G site. To detect presence of mtDNA containing the A3243G substitution, total DNA was isolated using the DNeasy Blood and Tissue kit (Qiagen, Cat. #69504). PCR amplification of MELAS region was performed using PCR primers: forward- CCTCGGAGCAGAACCCAACCT and reverse-CGAAGGGTTGTAGTAGCCCGT. PCR products were purified using the QIAquick PCR purification kit (Qiagen, Cat #28104) and were Sanger sequenced using the forward primer.

mtDNA qPCR quantification. Total DNA was extracted (Qiagen, Cat. # 69504) from cultured cells and mtDNA quantified using SYBR Select Master Mix for CFX (Life Technologies, Cat. # 4472942). mtDNA-encoded *MT-ND1* was amplified with the following primers: forward: CCCTAAAACCCGCCACATCT; reverse: CGA TGGTGAGAGCTAAGGTC. mtDNA levels were normalized to nucleus-encoded *36B4* gene (*RPLP0*) using the following primers: forward: TGGCAGCATCTACAACCCTGAAGT; reverse: TGGGTAGCCAATCTGAAG ACAGACA. qPCR was run on a BioRad CFX Thermal Cycler using the following protocol: (1) 50 °C for 2 min, (2) 95 °C for 2 min, and (3) 40 cycles at 95 °C for 10 s and 60 °C for 45 s. Samples were compared by calculating $\Delta\Delta CT$ and fold differences.

Received: 13 April 2020; Accepted: 10 August 2020
Published online: 31 August 2020

References

1. Caicedo, A., Aponte, P. M., Cabrera, F., Hidalgo, C. & Khoury, M. Artificial mitochondria transfer: Current challenges, advances, and future applications. *Stem Cells Int.* **2017**, 7610414. https://doi.org/10.1155/2017/7610414 (2017).
2. McBride, H. M., Neuspiel, M. & Wasiak, S. Mitochondria: more than just a powerhouse. *Curr. Biol.* **16**, R551-560. https://doi.org/10.1016/j.cub.2006.06.054 (2006).
3. Patananan, A. N., Sercel, A. J. & Teitell, M. A. More than a powerplant: The influence of mitochondrial transfer on the epigenome. *Curr. Opin. Physiol.* **3**, 16–24. https://doi.org/10.1016/j.cophys.2017.11.006 (2018).
4. Schon, E. A., DiMauro, S. & Hirano, M. Human mitochondrial DNA: Roles of inherited and somatic mutations. *Nat. Rev. Genet.* **13**, 878–890. https://doi.org/10.1038/nrg3275 (2012).
5. Greaves, L. C., Reeve, A. K., Taylor, R. W. & Turnbull, D. M. Mitochondrial DNA and disease. *J. Pathol.* **226**, 274–286. https://doi.org/10.1002/path.3028 (2012).
6. Khan, N. A., Govindaraj, P., Meena, A. K. & Thangaraj, K. Mitochondrial disorders: Challenges in diagnosis & treatment. *Indian J. Med. Res.* **141**, 13–26. https://doi.org/10.4103/0971-5916.154489 (2015).
7. Stewart, J. B. & Chinnery, P. F. The dynamics of mitochondrial DNA heteroplasmy: Implications for human health and disease. *Nat. Rev. Genet.* **16**, 530–542. https://doi.org/10.1038/nrg3966 (2015).
8. Schaefer, A. M. *et al.* Prevalence of mitochondrial DNA disease in adults. *Ann. Neurol.* **63**, 35–39. https://doi.org/10.1002/ana.21217 (2008).
9. Patananan, A. N., Wu, T. H., Chiou, P. Y. & Teitell, M. A. Modifying the mitochondrial genome. *Cell Metab.* **23**, 785–796. https://doi.org/10.1016/j.cmet.2016.04.004 (2016).
10. Elliott, H. R., Samuels, D. C., Eden, J. A., Relton, C. L. & Chinnery, P. F. Pathogenic mitochondrial DNA mutations are common in the general population. *Am. J. Hum. Genet.* **83**, 254–260. https://doi.org/10.1016/j.ajhg.2008.07.004 (2008).
11. Rebolledo-Jaramillo, B. *et al.* Maternal age effect and severe germ-line bottleneck in the inheritance of human mitochondrial DNA. *Proc. Natl. Acad. Sci. U S A* **111**, 15474–15479. https://doi.org/10.1073/pnas.1409328111 (2014).
12. Brambilla, A. *et al.* Clinical profile and outcome of cardiac involvement in MELAS syndrome. *Int. J. Cardiol.* **276**, 14–19. https://doi.org/10.1016/j.ijcard.2018.10.051 (2019).
13. DiMauro, S., Hirano, M. & Schon, E. A. Approaches to the treatment of mitochondrial diseases. *Muscle Nerve* **34**, 265–283. https://doi.org/10.1002/mus.20598 (2006).
14. Jinek, M. *et al.* A programmable dual-RNA-guided DNA endonuclease in adaptive bacterial immunity. *Science* **337**, 816–821. https://doi.org/10.1126/science.1225829 (2012).
15. Aiuti, A. *et al.* Correction of ADA-SCID by stem cell gene therapy combined with nonmyeloablative conditioning. *Science* **296**, 2410–2413. https://doi.org/10.1126/science.1070104 (2002).
16. Gammage, P. A., Moraes, C. T. & Minczuk, M. Mitochondrial genome engineering: The revolution may not be CRISPR-Ized. *Trends Genet.* **34**, 101–110. https://doi.org/10.1016/j.tig.2017.11.001 (2018).
17. Hashimoto, M. *et al.* MitoTALEN: A general approach to reduce mutant mtDNA loads and restore oxidative phosphorylation function in mitochondrial diseases. *Mol. Ther.* **23**, 1592–1599. https://doi.org/10.1038/mt.2015.126 (2015).

18. Bacman, S. R. *et al.* MitoTALEN reduces mutant mtDNA load and restores tRNA(Ala) levels in a mouse model of heteroplasmic mtDNA mutation. *Nat. Med.* **24**, 1696–1700. https://doi.org/10.1038/s41591-018-0166-8 (2018).
19. Bacman, S. R., Williams, S. L., Pinto, M. & Moraes, C. T. The use of mitochondria-targeted endonucleases to manipulate mtDNA. *Methods Enzymol.* **547**, 373–397. https://doi.org/10.1016/B978-0-12-801415-8.00018-7 (2014).
20. Gammage, P. A. & Minczuk, M. Enhanced manipulation of human mitochondrial DNA heteroplasmy in vitro using tunable mtZFN technology. *Methods Mol. Biol.* **43–56**, 2018. https://doi.org/10.1007/978-1-4939-8799-3_4 (1867).
21. Gammage, P. A. *et al.* Genome editing in mitochondria corrects a pathogenic mtDNA mutation in vivo. *Nat. Med.* **24**, 1691–1695. https://doi.org/10.1038/s41591-018-0165-9 (2018).
22. Peeva, V. *et al.* Linear mitochondrial DNA is rapidly degraded by components of the replication machinery. *Nat. Commun.* **9**, 1727. https://doi.org/10.1038/s41467-018-04131-w (2018).
23. Brooks, H. R. Mitochondria: Finding the power to change. *Cell* **175**, 891–893. https://doi.org/10.1016/j.cell.2018.10.035 (2018).
24. Kim, M. J., Hwang, J. W., Yun, C. K., Lee, Y. & Choi, Y. S. Delivery of exogenous mitochondria via centrifugation enhances cellular metabolic function. *Sci. Rep.* **8**, 3330. https://doi.org/10.1038/s41598-018-21539-y (2018).
25. King, M. P. & Attardi, G. Injection of mitochondria into human cells leads to a rapid replacement of the endogenous mitochondrial DNA. *Cell* **52**, 811–819. https://doi.org/10.1016/0092-8674(88)90423-0 (1988).
26. Heller, S. *et al.* Efficient repopulation of genetically derived rho zero cells with exogenous mitochondria. *Plos One* **8**, ARTN e73207. https://doi.org/10.1371/journal.pone.0073207 (2013).
27. Spees, J. L., Olson, S. D., Whitney, M. J. & Prockop, D. J. Mitochondrial transfer between cells can rescue aerobic respiration. *Proc. Natl. Acad. Sci. U S A* **103**, 1283–1288. https://doi.org/10.1073/pnas.0510511103 (2006).
28. Ali Pour, P., Kenney, M. C. & Kheradvar, A. Bioenergetics consequences of mitochondrial transplantation in cardiomyocytes. *J. Am. Heart Assoc.* **9**, e014501. https://doi.org/10.1161/JAHA.119.014501 (2020).
29. Kitani, T., Kami, D., Matoba, S. & Gojo, S. Internalization of isolated functional mitochondria: Involvement of macropinocytosis. *J. Cell Mol. Med.* **18**, 1694–1703. https://doi.org/10.1111/jcmm.12316 (2014).
30. Macheiner, T. *et al.* Magnetomitotransfer: An efficient way for direct mitochondria transfer into cultured human cells. *Sci. Rep.* **6**, 35571. https://doi.org/10.1038/srep35571 (2016).
31. Wu, T. H. *et al.* Mitochondrial transfer by photothermal nanoblade restores metabolite profile in mammalian cells. *Cell Metab.* **23**, 921–929. https://doi.org/10.1016/j.cmet.2016.04.007 (2016).
32. Caicedo, A. *et al.* MitoCeption as a new tool to assess the effects of mesenchymal stem/stromal cell mitochondria on cancer cell metabolism and function. *Sci. Rep.* **5**, 9073. https://doi.org/10.1038/srep09073 (2015).
33. Schubert, S. *et al.* Generation of rho zero cells: Visualization and quantification of the mtDNA depletion process. *Int. J. Mol. Sci.* **16**, 9850–9865. https://doi.org/10.3390/ijms16059850 (2015).
34. Nelson, I., Hanna, M. G., Wood, N. W. & Harding, A. E. Depletion of mitochondrial DNA by ddC in untransformed human cell lines. *Somat. Cell Mol. Genet.* **23**, 287–290. https://doi.org/10.1007/bf02674419 (1997).
35. King, M. P. & Attardi, G. Human cells lacking mtDNA: repopulation with exogenous mitochondria by complementation. *Science* **246**, 500–503. https://doi.org/10.1126/science.2814477 (1989).
36. Dong, L. F. *et al.* Horizontal transfer of whole mitochondria restores tumorigenic potential in mitochondrial DNA-deficient cancer cells. *Elife* **6**, e22187. https://doi.org/10.7554/eLife.22187 (2017).
37. Gregoire, M., Morais, R., Quilliam, M. A. & Gravel, D. On auxotrophy for pyrimidines of respiration-deficient chick embryo cells. *Eur. J. Biochem.* **142**, 49–55. https://doi.org/10.1111/j.1432-1033.1984.tb08249.x (1984).
38. Miyata, N. *et al.* Pharmacologic rescue of an enzyme-trafficking defect in primary hyperoxaluria 1. *Proc. Natl. Acad. Sci. U S A* **111**, 14406–14411. https://doi.org/10.1073/pnas.1408401111 (2014).
39. Gamba, J. *et al.* Nitric oxide synthesis is increased in cybrid cells with m.3243A > G mutation. *Int. J. Mol. Sci.* **14**, 394–410. https://doi.org/10.3390/ijms14010394 (2013).
40. Brunner, G. & Neupert, W. Turnover of outer and inner membrane proteins of rat liver mitochondria. *FEBS Lett.* **1**, 153–155. https://doi.org/10.1016/0014-5793(68)80045-6 (1968).
41. Lipsky, N. G. & Pedersen, P. L. Mitochondrial turnover in animal cells. Half-lives of mitochondria and mitochondrial subfractions of rat liver based on [14C]bicarbonate incorporation. *J. Biol. Chem.* **256**, 8652–8657 (1981).
42. Chomyn, A. *et al.* MELAS mutation in mtDNA binding site for transcription termination factor causes defects in protein synthesis and in respiration but no change in levels of upstream and downstream mature transcripts. *Proc. Natl. Acad. Sci. U S A* **89**, 4221–4225. https://doi.org/10.1073/pnas.89.10.4221 (1992).
43. Levy, S. E., Waymire, K. G., Kim, Y. L., MacGregor, G. R. & Wallace, D. C. Transfer of chloramphenicol-resistant mitochondrial DNA into the chimeric mouse. *Transgenic Res.* **8**, 137–145. https://doi.org/10.1023/a:1008967412955 (1999).
44. Wallace, D. C., Bunn, C. L. & Eisenstadt, J. M. Cytoplasmic transfer of chloramphenicol resistance in human tissue culture cells. *J. Cell Biol.* **67**, 174–188. https://doi.org/10.1083/jcb.67.1.174 (1975).
45. Bunn, C. L., Wallace, D. C. & Eisenstadt, J. M. Cytoplasmic inheritance of chloramphenicol resistance in mouse tissue culture cells. *Proc. Natl. Acad. Sci. U S A* **71**, 1681–1685. https://doi.org/10.1073/pnas.71.5.1681 (1974).
46. Blanc, H., Wright, C. T., Bibb, M. J., Wallace, D. C. & Clayton, D. A. Mitochondrial DNA of chloramphenicol-resistant mouse cells contains a single nucleotide change in the region encoding the 3' end of the large ribosomal RNA. *Proc. Natl. Acad. Sci. U S A* **78**, 3789–3793. https://doi.org/10.1073/pnas.78.6.3789 (1981).
47. Latorre-Pellicer, A. *et al.* Regulation of mother-to-offspring transmission of mtDNA heteroplasmy. *Cell Metab.* **30**, 1120–1130.e5. https://doi.org/10.1016/j.cmet.2019.09.007 (2019).
48. Perales-Clemente, E. *et al.* Five entry points of the mitochondrially encoded subunits in mammalian complex I assembly. *Mol Cell Biol* **30**, 3038–3047. https://doi.org/10.1128/MCB.00025-10 (2010).
49. Acin-Perez, R. *et al.* Respiratory complex III is required to maintain complex I in mammalian mitochondria. *Mol. Cell* **13**, 805–815. https://doi.org/10.1016/s1097-2765(04)00124-8 (2004).
50. Acin-Perez, R. *et al.* An intragenic suppressor in the cytochrome c oxidase I gene of mouse mitochondrial DNA. *Hum. Mol. Genet.* **12**, 329–339. https://doi.org/10.1093/hmg/ddg021 (2003).
51. Smiraglia, D. J., Kulawiec, M., Bistulfi, G. L., Gupta, S. G. & Singh, K. K. A novel role for mitochondria in regulating epigenetic modification in the nucleus. *Cancer Biol Ther* **7**, 1182–1190. https://doi.org/10.4161/cbt.7.8.6215 (2008).
52. El-Hattab, A. W. & Scaglia, F. Mitochondrial DNA depletion syndromes: review and updates of genetic basis, manifestations, and therapeutic options. *Neurotherapeutics* **10**, 186–198. https://doi.org/10.1007/s13311-013-0177-6 (2013).
53. Lesko, N. *et al.* Two novel mutations in thymidine kinase-2 cause early onset fatal encephalomyopathy and severe mtDNA depletion. *Neuromuscul. Disord.* **20**, 198–203. https://doi.org/10.1016/j.nmd.2009.11.013 (2010).
54. Mandel, H. *et al.* The deoxyguanosine kinase gene is mutated in individuals with depleted hepatocerebral mitochondrial DNA. *Nat. Genet.* **29**, 337–341. https://doi.org/10.1038/ng746 (2001).
55. Saada, A. *et al.* Mutant mitochondrial thymidine kinase in mitochondrial DNA depletion myopathy. *Nat. Genet.* **29**, 342–344. https://doi.org/10.1038/ng751 (2001).
56. Tan, A. S. *et al.* Mitochondrial genome acquisition restores respiratory function and tumorigenic potential of cancer cells without mitochondrial DNA. *Cell Metab.* **21**, 81–94. https://doi.org/10.1016/j.cmet.2014.12.003 (2015).
57. Lee, W. T. *et al.* Mitochondrial DNA plasticity is an essential inducer of tumorigenesis. *Cell Death Discov.* **2**, 16016. https://doi.org/10.1038/cddiscovery.2016.16 (2016).

58. Islam, M. N. *et al.* Mitochondrial transfer from bone-marrow-derived stromal cells to pulmonary alveoli protects against acute lung injury. *Nat. Med.* **18**, 759–765. https://doi.org/10.1038/nm.2736 (2012).
59. Prockop, D. J. Mitochondria to the rescue. *Nat. Med.* **18**, 653–654. https://doi.org/10.1038/nm.2769 (2012).
60. Taylor, R. W. & Turnbull, D. M. Mitochondrial DNA mutations in human disease. *Nat. Rev. Genet.* **6**, 389–402. https://doi.org/10.1038/nrg1606 (2005).
61. Wu, Y. C. *et al.* Massively parallel delivery of large cargo into mammalian cells with light pulses. *Nat. Methods* **12**, 439–444. https://doi.org/10.1038/nmeth.3357 (2015).
62. Chang, J. C. *et al.* Peptide-mediated delivery of donor mitochondria improves mitochondrial function and cell viability in human cybrid cells with the MELAS A3243G mutation. *Sci. Rep.* **7**, 10710. https://doi.org/10.1038/s41598-017-10870-5 (2017).
63. Bertero, E., Maack, C. & O'Rourke, B. Mitochondrial transplantation in humans: "magical" cure or cause for concern?. *J. Clin. Invest.* **128**, 5191–5194. https://doi.org/10.1172/JCI124944 (2018).
64. McCully, J. D. *et al.* Injection of isolated mitochondria during early reperfusion for cardioprotection. *Am. J. Physiol. Heart Circ. Physiol.* **296**, H94–H105. https://doi.org/10.1152/ajpheart.00567.2008 (2009).
65. Cowan, D. B. *et al.* Intracoronary Delivery of Mitochondria to the Ischemic Heart for Cardioprotection. *PLoS ONE* **11**, e0160889. https://doi.org/10.1371/journal.pone.0160889 (2016).
66. Masuzawa, A. *et al.* Transplantation of autologously derived mitochondria protects the heart from ischemia-reperfusion injury. *Am. J. Physiol. Heart Circ. Physiol.* **304**, H966-982. https://doi.org/10.1152/ajpheart.00883.2012 (2013).
67. Moskowitzova, K. *et al.* Mitochondrial transplantation enhances murine lung viability and recovery after ischemia-reperfusion injury. *Am. J. Physiol. Lung Cell Mol. Physiol.* **318**, L78–L88. https://doi.org/10.1152/ajplung.00221.2019 (2020).
68. Moskowitzova, K. *et al.* Mitochondrial transplantation prolongs cold ischemia time in murine heart transplantation. *J Heart Lung Transplant* **38**, 92–99. https://doi.org/10.1016/j.healun.2018.09.025 (2019).
69. Cho, Y. M. *et al.* Mesenchymal stem cells transfer mitochondria to the cells with virtually no mitochondrial function but not with pathogenic mtDNA mutations. *PLoS ONE* **7**, e32778. https://doi.org/10.1371/journal.pone.0032778 (2012).
70. Clark, M. A. & Shay, J. W. Mitochondrial transformation of mammalian cells. *Nature* **295**, 605–607. https://doi.org/10.1038/295605a0 (1982).
71. Sharpley, M. S. *et al.* Heteroplasmy of mouse mtDNA is genetically unstable and results in altered behavior and cognition. *Cell* **151**, 333–343. https://doi.org/10.1016/j.cell.2012.09.004 (2012).
72. Dunham-Snary, K. J. & Ballinger, S. W. GENETICS. Mitochondrial-nuclear DNA mismatch matters. *Science* **349**, 1449–1450. https://doi.org/10.1126/science.aac5271 (2015).
73. Wolf, D. P., Mitalipov, N. & Mitalipov, S. Mitochondrial replacement therapy in reproductive medicine. *Trends Mol. Med.* **21**, 68–76. https://doi.org/10.1016/j.molmed.2014.12.001 (2015).
74. Wolf, D. P., Mitalipov, P. A. & Mitalipov, S. M. Principles of and strategies for germline gene therapy. *Nat. Med.* **25**, 890–897. https://doi.org/10.1038/s41591-019-0473-8 (2019).
75. Kang, E. *et al.* Mitochondrial replacement in human oocytes carrying pathogenic mitochondrial DNA mutations. *Nature* **540**, 270–275. https://doi.org/10.1038/nature20592 (2016).
76. Srivastava, S. *et al.* PGC-1alpha/beta induced expression partially compensates for respiratory chain defects in cells from patients with mitochondrial disorders. *Hum. Mol. Genet.* **18**, 1805–1812. https://doi.org/10.1093/hmg/ddp093 (2009).
77. Picard, M. *et al.* Progressive increase in mtDNA 3243A>G heteroplasmy causes abrupt transcriptional reprogramming. *Proc. Natl. Acad. Sci. U S A* **111**, E4033-4042. https://doi.org/10.1073/pnas.1414028111 (2014).
78. Divakaruni, A. S. *et al.* Inhibition of the mitochondrial pyruvate carrier protects from excitotoxic neuronal death. *J. Cell Biol.* **216**, 1091–1105. https://doi.org/10.1083/jcb.201612067 (2017).
79. Brand, M. D. The efficiency and plasticity of mitochondrial energy transduction. *Biochem. Soc. Trans.* **33**, 897–904. https://doi.org/10.1042/BST20050897 (2005).
80. Watt, I. N., Montgomery, M. G., Runswick, M. J., Leslie, A. G. & Walker, J. E. Bioenergetic cost of making an adenosine triphosphate molecule in animal mitochondria. *Proc. Natl. Acad. Sci. U S A* **107**, 16823–16827. https://doi.org/10.1073/pnas.1011099107 (2010).

Acknowledgements

ERD is supported by the NIH (GM55052 and 5T34GM008563). ANP is supported by the NIH (T32CA009120) and American Heart Association (18POST34080342). AJS is supported by the NIH (T32GM007185 and T32CA009120). MAT is supported by the Air Force Office of Scientific Research (FA9550-15-1-0406), the NIH (R01GM114188, R01GM073981, R01CA185189, R21CA227480, R01GM127985, and P30CA016042), and by CIRM (RT3-07678). The authors acknowledge Brandon Desousa, Dr. Linsey Stiles, and Dr. Orian Shirihai of the UCLA Metabolism Core for assistance with Seahorse Extracellular Flux Analyzer assays.

Author contributions

Conceptualization: E.R.D., A.N.P., M.A.T. Methodology: E.R.D., A.N.P., A.J.S. Formal analysis: E.R.D., A.N.P., A.J.S. Investigation: E.R.D., A.N.P., A.J.S. Resources: E.R.D., A.N.P., A.J.S., M.A.T. Data curation: E.R.D., A.N.P. Writing-original draft: E.R.D., A.N.P. Writing-review and editing: E.R.D., A.N.P., A.J.S., M.A.T. Visualization: E.R.D., A.N.P. Supervision: A.N.P. Project administration: A.N.P., M.A.T. Funding acquisition: E.R.D., A.N.P., A.J.S., M.A.T.

Competing interests

M.A.T. is a co-founder, board member, shareholder, and consultant for NanoCav, LLC, a private start-up company working on mitochondrial transfer techniques and applications. The other authors do not have any conflicting interests to declare.

Additional information

Supplementary information is available for this paper at https://doi.org/10.1038/s41598-020-71199-0.

Correspondence and requests for materials should be addressed to M.A.T.

Reprints and permissions information is available at www.nature.com/reprints.

Publisher's note Springer Nature remains neutral with regard to jurisdictional claims in published maps and institutional affiliations.

Supplementary Information

Stable retention of chloramphenicol-resistant mtDNA to rescue metabolically impaired cells

Emma R. Dawson[1], Alexander N. Patananan[1], Alexander J. Sercel[2], Michael A. Teitell[1-6,*]

[1]Department of Pathology and Laboratory Medicine, University of California, Los Angeles, California 90095, United States

[2]Molecular Biology Institute Interdepartmental Program, University of California, Los Angeles, Los Angeles, CA 90095, USA

[3]Eli and Edythe Broad Center of Regenerative Medicine and Stem Cell Research University of California, Los Angeles, Los Angeles, CA 90095, USA

[4]California NanoSystems Institute, University of California, Los Angeles, Los Angeles, CA 90095, USA

[5]Department of Pediatrics, David Geffen School of Medicine, University of California, Los Angeles, Los Angeles, CA 90095, USA

[6]Jonsson Comprehensive Cancer Center, David Geffen School of Medicine, University of California, Los Angeles, Los Angeles, CA 90095, USA

[*]Correspondence: mteitell@mednet.ucla.edu

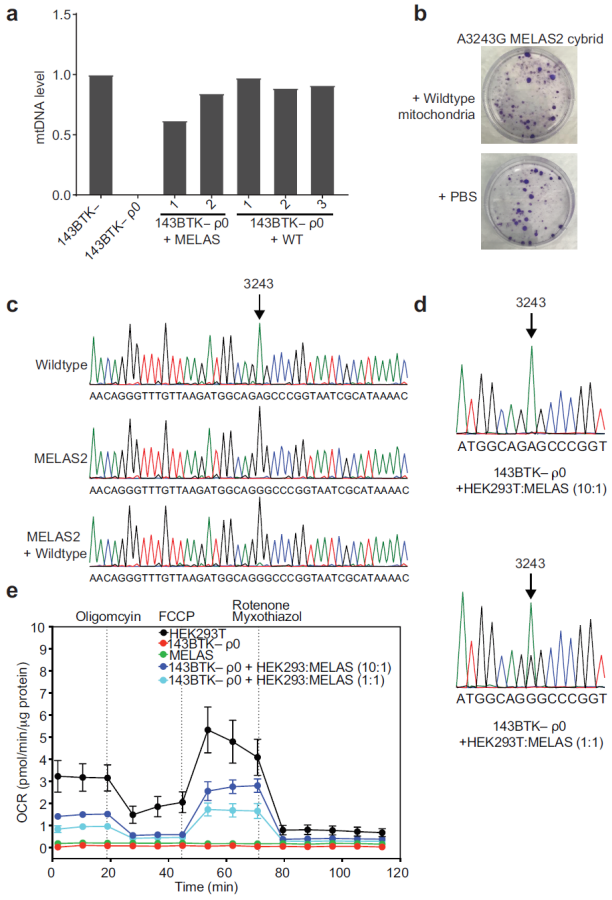

Figure S1. Selective pressure to retain mutant A3243G MELAS mtDNA.

(**a**) Quantification of mtDNA levels by qPCR in 143BTK– ρ0, 143BTK– ρ0 + MELAS clones 1 and 2, 143BTK– ρ0 + WT clones 1, 2, and 3, and the 143BTK– parent cell lines**.** The bar height denotes the average of three technical replicates. (**b**) MELAS2 + Wildtype and MELAS2 + PBS buffer cells were fixed with paraformaldehyde and stained with crystal violet to identify cell colonies. (**c**) Sanger sequencing of Wildtype, MELAS2, and MELAS2 + Wildtype. The arrow denotes mtDNA position 3243. (**d**) Sanger

sequencing of 143BTK– ρ0 + HEK293T:MELAS (10:1) and 143BTK– ρ0 + HEK293T:MELAS (1:1). Arrows denote mtDNA position 3243. (**e**) Seahorse Extracellular Flux analysis to quantify oxygen consumption rate of 143BTK– ρ0 + HEK293T:MELAS (10:1) and 143BTK– ρ0 + HEK293T:MELAS (1:1) cells. Oligomycin, FCCP, and rotenone/myxothiazol are an ATP synthase inhibitor, uncoupler, and complex I/III inhibitor, respectively. Each data point represents the average of three technical replicates and the error bar denotes standard deviation.

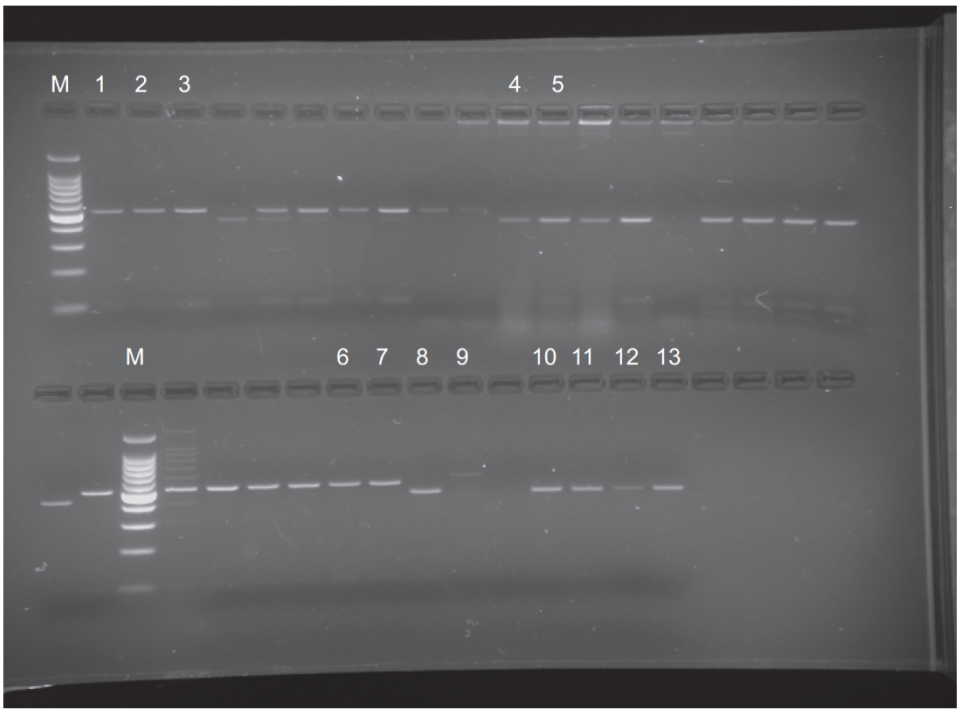

Figure S2. Uncropped gel for Figure 3e-f. PCR products post-MaeII digestion on a 2.5% agarose gel electrophoresis. Numbers on lanes correspond to the following samples: M) Marker, 1) Δmt-ND6 + CAP-R 501-1 bulk culture 2, 2) Δmt-ND6 + CAP-R 501-1 bulk culture 3, 3) Δmt-ND4 + PBS bulk culture, 4) Δmt-ND4 + CAP-R 501-1 bulk culture cultured for 5 weeks post-transfer in uridine-deficient, CAP-supplemented media, 5) Δmt-ND4 + CAP-R 501-1 bulk culture cultured for 4 weeks in uridine-deficient, CAP-supplemented media and one additional week in CAP-deficient media, 6) Δmt-ND6, 7) Δmt-ND4, 8) CAP-R 501-1, 9) L929 ρ0, 10) L929 ρ0 + CAP-R 501-1, 11) Δmt-ND4 + CAP-R 501-1 bulk culture 1, 12) Δmt-ND4 + CAP-R 501-1 bulk culture 2, 13)Δmt-ND4 + CAP-R 501-1 bulk culture 3. Unmarked lanes on the gel are the same

transfer cell lines (L929 ρ0 + CAP-R 501-1, ∆mt-ND4 + CAP-R 501-1, and ∆mt-ND6 + CAP-R 501-1) cultured in different media conditions (uridine-supplemented, complete, and galactose media) at different time points throughout the selection process to optimize our selection protocol.

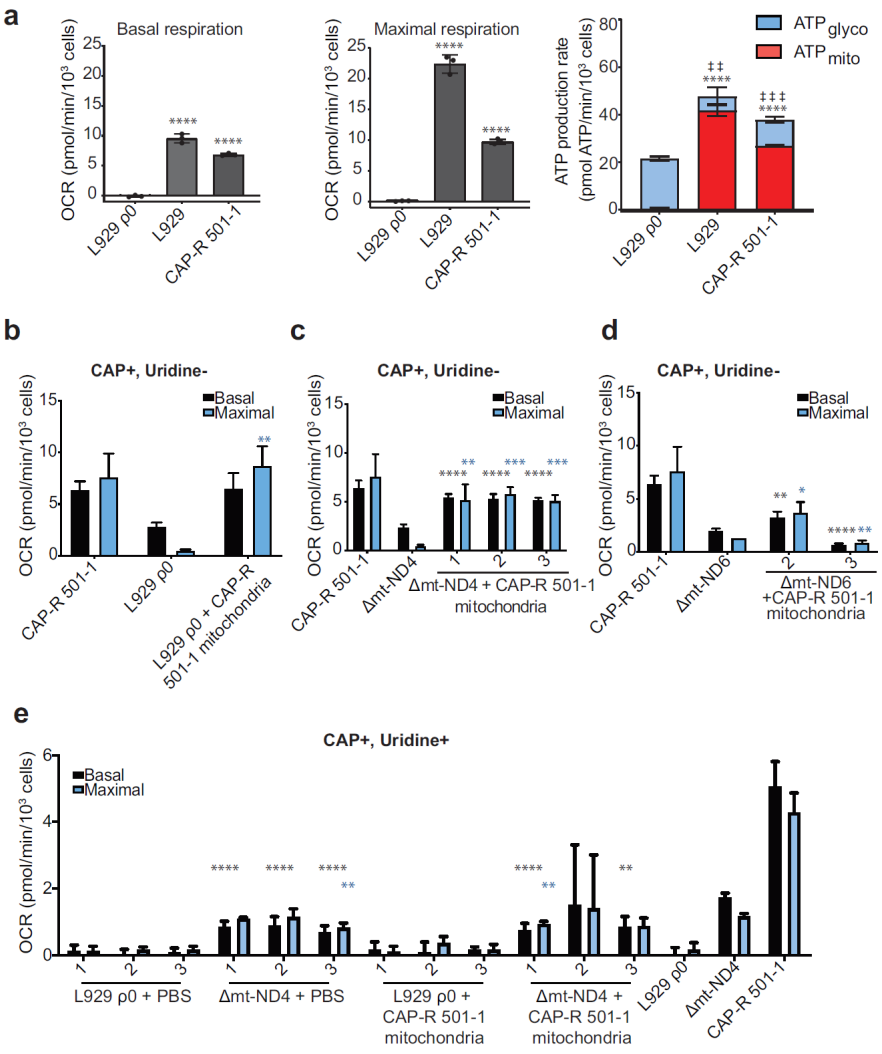

Figure S3. Basal and Maximal oxygen consumption rates corresponding to ATP production rates. (**a**) Seahorse Extracellular Flux analysis to quantify basal and maximal respiration and ATP production in L929 ρ0, L929 parent, and CAP-R 501-1 cell lines. Two-tailed, unpaired Student's t-test comparing samples to L929 ρ0. * represents

significance for ATPmito and ‡ represents significance for ATPglyco. * < 0.05, ** < 0.01, ***<0.001, ****<0.0001. ‡ <0.05, ‡ ‡ <0.01, ‡ ‡ ‡ <0.001, ‡ ‡ ‡ ‡ <0.0001. The bar height denotes the average of four replicates and the error bars are the standard deviation. (**b**) Seahorse Extracellular Flux analysis to quantify basal and maximal respiration in CAP-R 501-1, L929 ρ0, and L929 ρ0 + CAP-R 501-1. (**c**) Seahorse Extracellular Flux analysis to quantify basal and maximal respiration in CAP-R 501-1, ∆mt-ND4, and ∆mt-ND4 + CAP-R 501-1 clones 1, 2, and 3. (**d**) Seahorse Extracellular Flux analysis to quantify basal and maximal respiration in CAP-R 501-1, ∆mt-ND6, and ∆mt-ND6 + CAP-R 501-1 clones 2 and 3. For (b-d), cells had been previously cultured in uridine-deficient, CAP-supplemented media. Two-tailed, unpaired Student's t-test comparing samples to L929 ρ0, ∆mt-ND4, or ∆mt-ND6. The bar height denotes average of four replicates and the error bars are the standard deviation. (**e**) Seahorse Extracellular Flux analysis to quantify basal and maximal respiration in CAP-R 501-1, L929 ρ0, ∆mt-ND4, L929 ρ0 + CAP-R 501-1, and ∆mt-ND4 + CAP-R 501-1. Cells had been previously cultured in uridine-supplemented, CAP-supplemented media. Two-tailed, unpaired Student's t-test comparing samples to ∆mt-ND4. The bar height denotes average of five replicates and the error bars are the standard deviation. For (b-e), * represents significance with * < 0.05, ** < 0.01, ***<0.001, ****<0.0001. There were no statistically significant differences when comparing the samples to L929 ρ0. Black * represents significance for basal respiration and blue * represents significance for maximal respiration.

Chapter 6: Mitochondrial DNA Dynamics in Reprogramming to Pluripotency

Trends in
Cell Biology

CellPress
OPEN ACCESS

Review

Mitochondrial DNA Dynamics in Reprogramming to Pluripotency

Alexander J. Sercel,[1,11] Natasha M. Carlson,[2,3,11] Alexander N. Patananan,[3] and Michael A. Teitell[3,4,5,6,7,8,9,10,*]

Mammalian cells, with the exception of erythrocytes, harbor mitochondria, which are organelles that provide energy, intermediate metabolites, and additional activities to sustain cell viability, replication, and function. Mitochondria contain multiple copies of a circular genome called mitochondrial DNA (mtDNA), whose individual sequences are rarely identical (homoplasmy) because of inherited or sporadic mutations that result in multiple mtDNA genotypes (heteroplasmy). Here, we examine potential mechanisms for maintenance or shifts in heteroplasmy that occur in induced pluripotent stem cells (iPSCs) generated by cellular reprogramming, and further discuss manipulations that can alter heteroplasmy to impact stem and differentiated cell performance. This additional insight will assist in developing more robust iPSC-based models of disease and differentiated cell therapies.

Highlights

iPSCs can differentiate into clinically relevant cell types, but understanding how mtDNA changes with reprogramming and how these changes affect iPSC and progeny metabolism will help to maximize their disease modeling, drug screening, and therapeutic potential.

Reprogramming of somatic cells with mtDNA heteroplasmy can yield retained, evenly distributed, or skewed iPSC heteroplasmy ratios that will affect mitochondrial metabolism and potentially cell performance.

mtDNA manipulation techniques have potential for controlling the range of mtDNA genotypes within iPSCs and their differentiated progeny cells for desired applications.

iPSCs: Today and the Future

Induced pluripotent stem cells (iPSCs, see Glossary) and embryonic stem cells (ESCs) are promising cell types for *ex vivo* disease modeling, drug screening, and upcoming applications in regenerative medicine. iPSCs and ESCs self-renew without limit in tissue culture and can form any cell type. Since their introduction in 2006, iPSCs have become a major focus for both basic and applied research, in part, because of their unique growth characteristics and cellular properties, and their high potential in personalized medicine without the ethical implications carried by the derivation of ESCs [1]. Tremendous effort has been focused on mechanisms and manipulations that regulate and optimize stem cell pluripotency and differentiation. For example, autologous therapies from differentiated iPSCs can be made from any individual with the promise of reduced immunogenicity compared to allogeneic, non-self ESC-derived therapeutics [2]. As of August 2020, there were >600 active clinical trials involving stem cells of any type, which is an indication of strong and growing interest in applying these cells in future therapies. However, only seven of these trials utilized iPSCs in any manner, typically *ex vivo* (ClinicalTrials.gov). While there currently are no FDA-approved treatments involving iPSCs or their derivatives, a deeper understanding of their derivation, maintenance, and differentiation is needed to improve their efficacy and assure their safety in clinical and laboratory applications [3,4].

Among an array of potential impediments to overcome for bringing iPSCs into the clinic, the mitochondria and its genome, mtDNA, may play key roles. Recent findings indicate that iPSCs and ESCs depend on cellular metabolism, and especially upon mitochondria, to maintain **pluripotency** and develop functional, differentiated cell types. Beyond optimizing stem cell functions through improved basic understanding, recent studies of iPSCs show that mutations in mtDNA that develop during cellular reprogramming can facilitate transplanted cell immune rejection [5,6]. Therefore, we now evaluate and discuss what is known about mtDNA changes through somatic cell reprogramming to iPSCs, followed by differentiation into functional cell types. Understanding the dynamics and biology of mtDNA in reprogramming, pluripotency, and differentiation will enable

[1]Molecular Biology Interdepartmental Program, University of California, Los Angeles, Los Angeles, CA, USA 90095
[2]Department of Biology, California State University Northridge, CA, USA 91330
[3]Department of Pathology and Laboratory Medicine, David Geffen School of Medicine, University of California, Los Angeles, Los Angeles, CA, USA 90095
[4]Molecular Biology Institute, University of California, Los Angeles, Los Angeles, CA, USA 90095
[5]California NanoSystems Institute, University of California, Los Angeles, Los Angeles, CA, USA 90095
[6]Department of Bioengineering, University of California, Los Angeles, Los Angeles, CA, USA 90095
[7]Eli and Edythe Broad Center of Regenerative Medicine and Stem Cell Research University of California, Los Angeles, Los Angeles, CA, USA 90095
[8]Department of Pediatrics, David Geffen School of Medicine, University of California, Los Angeles, Los Angeles, CA, USA 90095

Trends in Cell Biology, April 2021, Vol. 31, No. 4 https://doi.org/10.1016/j.tcb.2020.12.009

improved disease modeling and drug screening *ex vivo*, and help to develop safer cell-based regenerative therapies of the future.

Mitochondria and mtDNA Genetics

Mitochondria exist within the cytoplasm of all nucleated mammalian cells as double-membrane-bound organelles that contain the circular, maternally inherited double-stranded mtDNA. Structurally, mitochondria exist on a spectrum that spans separate, punctate, ovoid organelles at one extreme to fused, elongated, and branching networks that appear to fill the cell cytoplasm at the other extreme. Each mitochondrion contains dozens to thousands of copies of mtDNA per cell. mtDNA replication occurs independently of nuclear DNA (nDNA) replication throughout the cell cycle. However, counter evidence also exists that suggests that the rate of mtDNA replication may vary with cell cycle stage [7,8]. The ~16.5-kbp mtDNA encodes 13 electron transport chain (ETC) proteins in addition to 22 tRNAs and 2 rRNAs for protein translation; all of which are essential for generating ATP by **oxidative phosphorylation** (OXPHOS). Reports estimating the *de novo* mtDNA mutation rate range in magnitude; however, this mutation rate is consistently 10× to 100× greater than similar reports for the nDNA [9–11]. mtDNA mutations typically present as deletions or SNPs that are either synonymous or nonsynonymous in protein-coding regions [12]. In general, cells may exclusively contain mitochondria with only single, identical mtDNA sequences, a condition termed **homoplasmy**, or they may contain a mixture of different, co-existing mtDNA genotypes, a condition termed **heteroplasmy** (Box 1) [13–17]. Heteroplasmy is quantified as the copy number ratio of a specific mtDNA sequence to the total mtDNA in a cell, notated as a percentage.

The heteroplasmy percentage of a cell can be dynamic and shift through several different mechanisms. Certain cell types experience reductions in mtDNA copy number during development leading to a **genetic bottleneck**, in which the proportion of specific mtDNA sequences can be reduced or enriched in the remaining mtDNA population [18]. Moreover, heteroplasmy can shift based on a **replicative advantage** of certain mtDNAs caused by the biochemical consequences of different mtDNA sequences [19–21]. Some mtDNA mutations cause respiratory dysfunction in cells and confer pathology in organisms, and such mutations were previously considered detrimental only

Box 1. Origins and Quantification of mtDNA Heteroplasmy

Unlike the diploid nDNA, mtDNA is polyploid and exists as dozens to thousands of copies per cell [107]. mtDNA is dispersed throughout each mitochondrion in tightly compacted nucleoprotein structures, known as nucleoids, that are associated with the matrix side of the mitochondrial inner membrane [108]. Because of the high rate of mtDNA mutation, estimated up to 100× higher than nDNA [10], a cell carrying a single mtDNA sequence (homoplasmy) is comparatively rare. Instead, a mixture of different mtDNA sequences and genotypes are typically present in each cell, creating a condition termed heteroplasmy. Most cells within healthy humans often have low levels of mtDNA mutations, which can remain low or expand and increase over time. These mutations can become significant for human health because mtDNA, which contains no intron sequences unlike nDNA, has coding and non-coding genes and regulatory regions that are essential for the function of OXPHOS.

mtDNA mutations and heteroplasmy are either maternally inherited or may accumulate during aging (see Figure 2 in main text). The mechanisms that cause sporadic mtDNA mutations are heavily debated. Because mtDNA is situated close to the ETC and its oxidative respiratory complexes, one potential mechanism is that ROS introduce base modifications and DNA breaks. However, some studies have concluded that ROS does not cause mtDNA mutations [49,109,110], but instead that mtDNA lesions are introduced by replication errors [111]. mtDNA replication is continuous even in senescent cells and requires the only nucleus-encoded, mitochondria-localized DNA polymerase, Pol γ. Replication errors may occur either by nucleotide imbalances, mutations to Pol γ, or low expression of mitochondrial transcription factor A [76,112,113].

To study the role of mtDNA mutations in human health requires robust tools to quantify heteroplasmy, which is defined as the percentage of total copies of a specific mtDNA sequence compared to all mtDNA copies within a cell. Common approaches to quantifying heteroplasmy due to point mutations and deletions include Southern blotting, restriction fragment length polymorphism, and allele refractory mutation system –quantitative PCR analyses. Advances in digital PCR and next generation sequencing potentially enable even more sensitive methods to quantify mtDNA heteroplasmy [114].

[9]Jonsson Comprehensive Cancer Center, David Geffen School of Medicine, University of California, Los Angeles, Los Angeles, CA, USA 90095
[10]https://teitell-lab.dgsom.ucla.edu/
[11]These authors contributed equally to the work

*Correspondence:
mteitell@mednet.ucla.edu (M.A. Teitell).

at high mutant heteroplasmy ratios. However, it is now recognized that even low mutant heteroplasmy ratios may result in an increased propensity for certain diseases, with different levels of mutant mtDNA causing **threshold effects** that lead to different outcomes in cell and organ function. As an example, the m.3243A>G mtDNA mutation is commonly associated with the metabolic disease mitochondrial encephalopathy, lactic acidosis, and stroke-like episodes (MELAS). At 20–30% mutant heteroplasmy, there is an association with type 1 or type 2 diabetes, whereas at 50–80% mutant heteroplasmy the mitochondrial ETC complex I may become dysfunctional and cause cardiomyopathies. Even higher mutant heteroplasmy ratios up to 90–100% are often perinatal lethal or may cause other diseases such as Leigh syndrome [22–24]. Combined observations over many years indicate that specific cell types, mtDNA mutations, and mutant burdens yield cellular and organismal phenotypes that range from unaffected to lethal pathophysiologies. Neurological disorders, cardiomyopathies, and muscle dysfunction may occur because specific mtDNA mutations and/or an elevated mutant burden impairs mitochondrial gene expression and/or ETC function, secondarily affecting energy production, the tricarboxylic acid (TCA) cycle, and a range of other essential mitochondrial activities [24,25]. Because of the importance of heteroplasmy in cellular fitness and disease penetrance, a deep understanding of mitochondria and mtDNA in PSCs is essential for effective utilization as research tools and potential therapeutic products.

PSC Mitochondria

The promise of PSC-derivative therapies is inextricably linked to mitochondrial function and intermediate cellular metabolism. Mitochondria in PSCs exist with lower density, perinuclear localization, and punctate morphology compared to mitochondrial features of typical somatic cells. These fragmented PSCs fuse into elongated, branching, filamentous networks with differentiation into cells of the three embryonic germ lineages, ectoderm, endoderm, and mesoderm (Figure 1). Conversely, the mitochondria of somatic cells revert to a lower density, perinuclear localization, and fragmented morphology with disordered mitochondrial cristae and a reduction in mtDNA copy number during cellular reprogramming to pluripotency [26–28]. This shift in mitochondrial morphology from fused networks to punctae upon reprogramming parallels a shift in the stoichiometry of glycolytic and mitochondrial proteins as well. Levels of enzymes and structural proteins that support glycolysis increase, along with ETC complex II, III, and V proteins, whereas the expression of ETC complex I and IV proteins decrease [29,30]. ETC complex I provides a large multisubunit protein structure that is essential for regulating OXPHOS. A reduction in the expression of ETC complex I proteins during somatic cell reprogramming shifts energy production and nucleotide biosynthesis for cell replication to an enhanced glycolytic nutrient flux [29] (Figure 1). Accordingly, iPSCs show a shift in nutrient utilization towards glycolysis and away from OXPHOS compared to differentiated cells [31]. However, iPSCs also remain dependent on mitochondrial metabolism and the TCA cycle for intermediate metabolites that modify the epigenome, which in turn regulates patterns of gene expression to control stem cell pluripotency and differentiation potential [32–41]. In addition, reactive oxygen species (ROS), often described as a cell damaging and unwanted byproduct of OXPHOS, have concentration- and species-specific roles in maintaining pluripotency, initiating somatic cell reprogramming, and facilitating iPSC differentiation; all of which depend upon metabolically active mitochondria [42–44]. Yet, despite the reduction in OXPHOS that occurs for iPSCs, mutant heteroplasmy can also reduce somatic cell reprogramming efficiency and affect iPSC performance [22] (Figure 1). Reversible shifts in mitochondrial structure and function associate with pluripotent and terminally differentiated cell states, but to what extent remodeling is a cellular response to, or an active driver of, cell state conversion and maintenance remains to be fully understood. Quantifying the changes in mitochondrial structure and function during cellular reprogramming helps to elucidate mechanisms of metabolic plasticity and 'rewiring' that occur during transitions between somatic cells and iPSCs.

Glossary

Biophotonic Laser Assisted Surgery Tool: high-throughput transmembrane delivery device that uses a 532 nm wavelength non-damaging laser pulse to enable the almost simultaneous transfer of up to micron-sized cargo directly into the cytoplasm of ~2 × 10^5 adherent mammalian cells.
Genetic bottleneck: phenomenon that occurs when the mtDNA copy number falls dramatically, leaving a smaller subset of the original mtDNA genotypes that were initially present remaining in a cell. After such an event, the proportions of different mtDNA genotypes can shift and may not recapitulate the same proportions found before the bottleneck.
Heteroplasmy: the state of more than one mitochondrial genotype existing within a cell. The greater the heteroplasmy of an mtDNA variant, the higher its copy number relative to other mtDNA genotypes within that cell.
Homoplasmy: the state of only having one mitochondrial genotype within a cell.
Induced pluripotent stem cell: a pluripotent stem cell derived from somatic cells that have undergone cellular reprogramming and reversion to pluripotency typically by viral transduction or mRNA transfection. iPSCs can be generated from the cells of different tissues of healthy or diseased individuals.
MitoPunch: high-throughput mitochondrial transfer device that uses pressure to deliver isolated mitochondria directly into the cytoplasm of ~2 × 10^5 cells simultaneously.
Oxidative Phosphorylation: this biochemical process utilizes the transport of elections sourced from biomolecule catabolism between the protein complexes of the mitochondrial electron transport chain to generate a hydrogen ion gradient and electrochemical potential across the mitochondrial inner membrane, which enables the activity of complex V ATP synthase.
Photothermal Nanoblade: single-cell intracellular delivery device that uses a 532-nm nondamaging laser pulse to enable delivery of up to micron-sized cargo into individual adherent cells.
Pluripotency: this state describes a cell that has the potential to differentiate into cells of all three embryonic germ layers and, thus, any cell within the body.

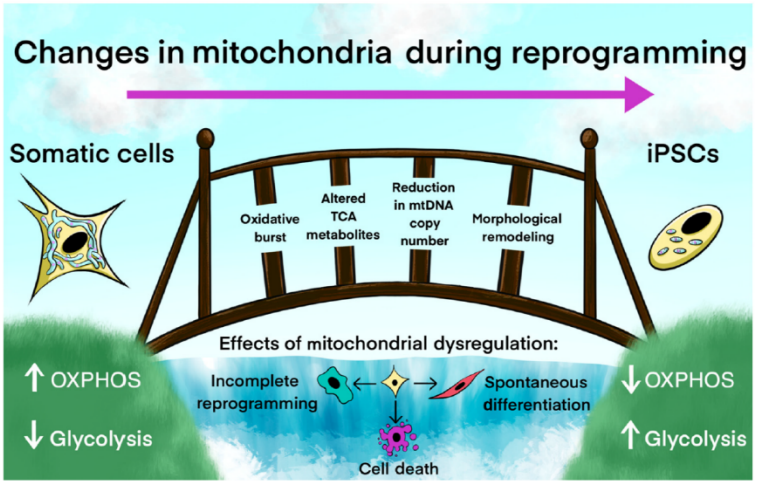

Figure 1. Remodeling of Mitochondrial Metabolism Is Required for Cellular Reprogramming to Pluripotency. Somatic cell reprogramming to iPSCs includes a transition in mitochondrial morphology from an elongated, filamentous, and branching network structure to a collection of small, punctate, and separate organelles. Concurrent with this morphologic shift, metabolism skews from mainly OXPHOS in somatic cells used in this illustration towards mainly glycolytic metabolism in reprogrammed iPSCs. Additional changes that occur during reprogramming include a reduction in mtDNA copy number, alterations in TCA cycle metabolite levels, changes in Ca^{2+} handling and the production of Fe–S clusters, and a required, time-coordinated oxidative burst. Mitochondrial dysfunction can disrupt these key metabolic transitions and may result in incomplete reprogramming, spontaneous differentiation [19], or cell death. Abbreviations: iPSC, induced pluripotent stem cell; mtDNA, mitochondrial DNA; OXPHOS, oxidative phosphorylation; TCA, tricarboxylic acid.

Replicative advantage: increase in replication rate of specific mtDNA genotypes relative to other mtDNA species in a cell. This may include mtDNA deletions that reduce the number of nucleotides that must be polymerized to increase the speed of mtDNA replication, and some mtDNA point mutations that can enhance replication by other biochemical means.
Threshold effect: phenomenon of mutant mtDNA causing different phenotypic effects based on the proportion of mutant to wild type mtDNA present. Many copies of mtDNA exists within cells, allowing wild type mtDNA to offset the deleterious effects of mutant mtDNA with progressively greater penetrance of the mutant phenotype in situations of greater representation within a cell.

Somatic Cell Reprogramming and mtDNA Heteroplasmy

Cellular reprogramming does not always generate iPSCs with heteroplasmy identical to the somatic source cells. Mutant mtDNA copy number can be enriched or reduced during somatic cell reprogramming, prolonged iPSC culture, and with iPSC differentiation [5,45–48]. Monitoring and controlling iPSC mutant heteroplasmy is important because mtDNA mutations can impact iPSC survival, proliferation, and differentiation potential, despite a higher reliance on glycolytic metabolism in pluripotency [49]. For example, iPSCs harboring the m.3243A>G mutation are viable despite decreased OXPHOS and elevated ROS levels; however, reprogramming efficiency was reduced and differentiation potential was impaired, particularly for high-energy-demanding cell types such as neurons and cardiomyocytes [22,50]. In addition, somatic cell reprogramming can cause increased levels and activity of telomerase, which supports indefinite mitotic division [51]. Mitochondrial dysfunction by mutation in somatic cells also reduces telomerase activity and shortens telomere regions [52]. It remains unclear whether increased mutant mtDNA heteroplasmy can affect iPSC telomeres; however, differentiated cells from iPSCs with an increased mutant mtDNA burden may show reduced longevity compared to low mutant heteroplasmy counterparts.

Few studies have investigated heteroplasmy changes with somatic cell reprogramming to pluripotency, but the results suggest outcomes with a high degree of variability (Table 1 and Figure 2). One study reported that fibroblasts with m.3243A>G mutant heteroplasmy of 77.7% yielded iPSCs with mutant heteroplasmy that ranged from undetectable to 99.4% after reprogramming, with most iPSC clones showing >80% mutant heteroplasmy [53]. A separate study also showed that fibroblasts with elevated mtDNA mutant heteroplasmy yielded iPSCs

Table 1. Heteroplasmy Shifts of mtDNA Mutations Following Cellular Reprogramming to Human iPSCs

Mutation	Initial heteroplasmy in fibroblasts	Heteroplasmy in iPSCs after reprogramming	Refs
m.3243A>G	77.70%	3.6–99.4%[a]	[53]
	69.67%	1.11%–85.05%[a]	[55]
	66.30%	0.67%–2.00%[a]	[55]
	29%	33–100%[a]	[54]
	50%	47.5–97.5%[b]	[22]
	80%	62.5%–92.5%[b]	[22]
	80%	67.5%–97.5%[a]	[22]
	50%	47.5%–92.5%[b]	[22]
	80%	72.5%–97.5%[b]	[22]
	80%	67.5%–97.5%[a]	[22]
m.13513G>A	84%	0–100%[a]	[54]
	50%	0–56%[a]	[48]
m.8993T>C	52%	0–87%[b]	[54]
	85%	88%	[104]
	55%	32%	[105]
m.11778G>C	100%	100%[c]	[106]
	100%	100%[c]	[106]
m.14484T>C + m.4160T>C	100%	100%[c]	[106]
m.8344A>G	90%	70%	[56]
	60%	60%	[56]

[a]Skewed distribution.
[b]Even distribution.
[c]From a homoplasmic cell line.

with extremely high or low mutant heteroplasmy [54]. In addition, fibroblasts from different individuals harboring the same mtDNA mutation with similar mutant heteroplasmy ratios may show dramatically different heteroplasmy shifts with reprogramming. In one case, dermal fibroblasts from two different individuals containing the m.3243A>G mutation at similar heteroplasmy levels (69.67% and 66.3%, respectively) showed either an even (1.11–85.05%) or a skewed mutant heteroplasmy distribution that contained almost all wild-type (WT) mtDNA in the iPSCs [55]. In a second case, fibroblasts isolated from three individual patients containing the same MELAS mutation similarly showed an extreme range of heteroplasmic shifts after reprogramming [62]. Reports of elevated mutant heteroplasmy for some iPSC clones do not guarantee that all somatic cells or specific mtDNA mutations with elevated heteroplasmy ratios survive reprogramming. In some cases, iPSCs with >80% mutant heteroplasmy become inviable, enabling iPSCs with more WT mtDNA sequences to overtake a reprogrammed population of cells to skew mutant heteroplasmy lower in the population [48]. Moreover, passaging iPSCs over time may decrease mutant heteroplasmy levels [48,56,57].

Altogether, three distinct distributions of mutant heteroplasmy appear to arise in populations of iPSCs generated from heteroplasmic fibroblasts (Figure 3). In one type, iPSCs retain the mutant heteroplasmy ratios of the source somatic cells. In the second, we call even distribution, iPSCs show an unbiased range of heteroplasmy from low to high. In the third, we call skewed distribution, mutant heteroplasmy copy number ratios exist as either low, high, or at both extremes relative to WT mtDNA sequences (Table 1). These three distributions suggest potentially different mechanisms of

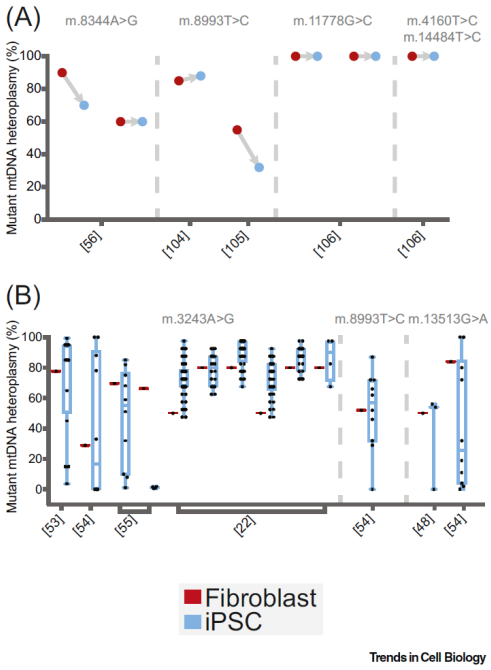

Figure 2. Meta-Analysis of Heteroplasmy Shifts During Reprogramming. Distributions of measured iPSC clone mutant heteroplasmy from studies listed in Table 1 are plotted alongside the heteroplasmy of the reprogrammed somatic source cells. Reprogrammed somatic cell heteroplasmy is indicated in red and resulting iPSC clone heteroplasmy is indicated in blue. (A) Heteroplasmy shifts measured in a single resulting iPSC clone derived from heteroplasmic starting cell materials. The single iPSC clones analyzed in each experiment are as follows: m.8344A>G from [56], m.8993T>C from [104] and [105], m.11778G>C from [106], and m.4160T>C and m.14484T>C from [106]. (B) Heteroplasmy shifts measured in multiple iPSC clones derived from heteroplasmic starting cell materials. The number of iPSC clones analyzed in each experiment are as follows: m.3243A>G from [53] (n=20, results sourced as averages taken from a binned bar chart and the text), [54] (n=10), [55] (listed from left to right: n=10, results sourced from a bar chart and the text, n=4, results sourced from a bar chart and the text), [22] (results sourced from a bar chart, listed from left to right: n=46, n=18, n=40, n=37, n=20, n=4); m.8993T>C from [54] (n=10); and m.13513G>A from [48] (n=3), and [54] (n=10). Abbreviations: iPSC, induced pluripotent stem cell.

shifting mutant heteroplasmy with reprogramming, which requires further studies to define molecular underpinnings. These observations motivate consideration of heteroplasmy when deriving iPSCs from patient cells and tissues with unknown mutant heteroplasmy levels, or when developing a disease model with iPSCs [46]. Despite the large number of known human mtDNA SNPs (~2000) and deletions [19,58], only seven have been studied in iPSCs. This small sample size makes generalizing these phenomena difficult; however, ignoring these shifts can potentially lead to poor reproducibility and differences in functional capabilities for iPSC clones used for developing personalized cell models and regenerative therapeutics.

Potential Mechanisms of Shifting Heteroplasmy with Reprogramming

The mechanisms regulating heteroplasmy shifts during somatic cell reprogramming are currently unknown and understanding them may facilitate the generation of iPSC lines that are functionally consistent. One study measured heteroplasmy in iPSC clones and clonally derived fibroblasts from the same clonal patient-derived fibroblast lines and reported similar heteroplasmic variance in both cell types [22]. This result suggests that heteroplasmy shifts are minimal during reprogramming and that any changes are due to heteroplasmic heterogeneity in the starting cell population. Further studies will help to confirm whether heteroplasmic drift is from stochastic fluctuations in reprogrammed somatic cells, or whether there are biological pressures that influence heteroplasmy shifts during iPSC derivations. In the absence of additional studies, an inference from work on somatic cells may provide some insight for potentially conserved mechanisms of heteroplasmy selection (Figure 2).

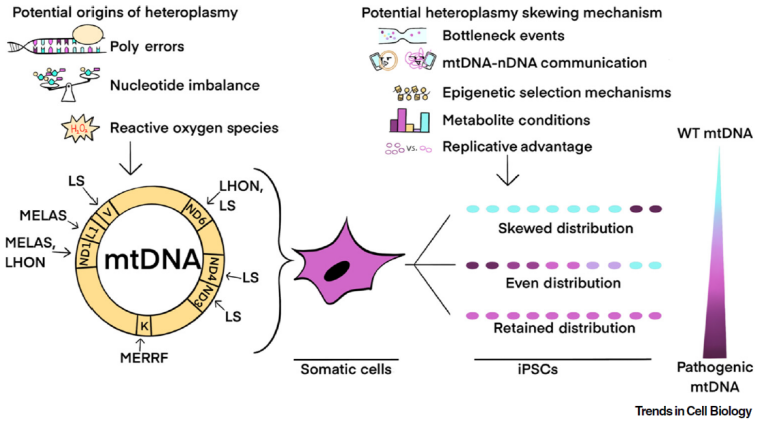

Figure 3. Potential Origins and Mechanisms of mtDNA Heteroplasmy Shifts During Reprogramming. Every nucleated somatic cell typically contains more than one mtDNA sequence. This situation, called heteroplasmy, can result from mtDNA point mutations and deletions due to several potential mechanisms, including Pol γ replication errors, nucleotide imbalances, and reactive-oxygen-species-induced mtDNA damage. Fibroblast cell lines with heteroplasmic mtDNA mutations that result in MELAS (mitochondrial encephalopathy and lactic acidosis syndrome), LS (Leigh syndrome), LHON (Leber's hereditary optic neuropathy), and MERRF (myoclonic epilepsy with ragged red fibers) human mtDNA diseases or syndromes have been reprogrammed to iPSCs. Resulting iPSCs can exhibit any of three different potential heteroplasmy patterns between WT and mutant mtDNA, including skewed, even, and retained mtDNA distributions. The mechanisms for generating these three distinct mtDNA distributions are not understood, although described mechanisms for somatic cell and germ cell shifts in heteroplasmy may operate during reprogramming and can include a genetic bottleneck, mtDNA–nDNA communication, epigenetic memory, metabolite conditions, and replicative advantages for certain mtDNA sequences. These factors, or their combinations, could lead to the heteroplasmy variations reported for individual iPSC clones. Abbreviations: mtDNA, mitochondrial DNA; nDNA, nuclear DNA; Pol, DNA polymerase; WT, wild type.

Heteroplasmy selection mechanisms seem to operate at different levels of complexity. mtDNA heteroplasmy is known to shift during reproduction and early development at the cellular level, which has been reviewed extensively elsewhere [59–61]. In these studies, an mtDNA bottleneck, or purifying selection, occurs during oogenesis with the mtDNA copy number and heteroplasmy ratio dramatically reduced, followed by subsequent re-expansion upon fertilization and implantation. This process can enrich for certain mtDNA sequences and skew heteroplasmy ratios [18]. mtDNA copy number reduction also occurs during cellular reprogramming and may give rise to a similar genetic bottleneck in iPSC generation [27,28,62–65]; however, the precise timing of this reduction and segregation during reprogramming remains unclear and warrants further investigation [22,50,54].

Recently reported observations show that selective pressure for specific heteroplasmy ratios is generated among tissue types with different metabolic requirements. Individual patients can demonstrate tissue-specific mutant heteroplasmy ratios potentially influenced by the unique metabolic demands of different tissues [66]. Specific mtDNA mutations and heteroplasmy ratios may provide a selection advantage through cellular fitness at the mitochondrial level by altering the epigenetic, metabolic, and/or energetic state of a cell. For example, the m.3243A>G mutation can promote tumorigenicity through altered ROS and TCA cycle metabolite concentrations that enhance the proliferation rate of transformed cells [67,68], and other tumor types show changes in mutant heteroplasmy levels with respect to normal tissue [69–71]. Specifically, work in human prostate cancer has shown strong heteroplasmy shifts in malignant cells relative to benign tissue, with higher heteroplasmy ratios correlating with greater metabolic rewiring and reduced patient

survival [72]. Similarly, iPSCs require certain metabolic conditions to sustain pluripotency (Figure 1). There may be mtDNA variants that enhance or impair the induction or maintenance of these metabolic states to provide a selective advantage or disadvantage for iPSC proliferation and survival. Reprogramming initiates metabolic rewiring in somatic cells and the energetic and metabolic demands particular to the iPSC fate may generate selective pressure for specific heteroplasmy ratios. Advances in single-cell sequencing approaches also help to enable the analysis of cell-to-cell genomic variation [73]. A recent study performed single cell sequencing on patient blood and showed that T cells harbor a reduced level of m.3243A>G heteroplasmy compared to other hematopoietic lineage cells [74]. Moreover, our literature meta-analysis suggests that the analysis of multiple clonal iPSC lines derived from clonal somatic cells are required to unravel heteroplasmy shifts due to reprogramming, which could provide insight into the mechanisms controlling these shifts (Figure 2). Altogether, cellular heterogeneity and tissue-type-specific selective pressures may influence heteroplasmy shifts during cellular reprogramming and suggest that single cell approaches to quantify these shifts will provide greater insight into the mechanisms and consequences thereof.

Heteroplasmy selection can occur at the level of mtDNA in individual cells. Mechanisms related to mtDNA replication may influence heteroplasmy, including expression levels and activity of the mitochondrial DNA polymerase, Pol γ, nucleotide imbalances, and selective replication of specific mtDNA sequences, such as those containing deletions [19,75,76]. mtDNA deletions and specific point mutations are known to generate a replicative advantage in mitochondrial biogenesis and mtDNA replication [20,77]. These effects may compound with potential heteroplasmy shifts that occur with cellular reprogramming, followed by mtDNA copy number expansion in iPSCs stimulated to differentiate. The cooperative regulation of mtDNA transcription from elements encoded within the nDNA and mtDNA may represent another genetic level of selective pressure that controls heteroplasmy. In studies of mother–offspring pairs, selection of the mtDNA variants present in the offspring were often influenced by the mother's nuclear genetic background [16], and the heteroplasmy of iPSCs may be affected by the parental cell source [47]. Additionally, patient fibroblasts with similar heteroplasmy for the same mutation can show unique ranges of iPSC heteroplasmy, perhaps from the influence of nDNA on mtDNA populations [55]. This phenomenon has also been observed in ESCs derived from somatic cell nuclear transfer embryos. ESCs from mtDNA corrected embryos were initially found to contain the donor mtDNA, suggesting that the disease would not arise in future generations [46]. However, these ESCs eventually reverted to the maternal haplotype, indicating likely residual native mtDNA and implying that the compatibility between the mtDNA and the germ-cell nDNA could affect mtDNA replication efficiency and the desired heteroplasmy shift. Mitochondrial metabolism may also affect heteroplasmy shifts by influencing the nuclear epigenome through alterations in the levels of α-ketoglutarate, succinate, *s*-adenosylmethionine, and other epigenetic-modifier levels in the cell [24,78,79]. Specific heteroplasmy states may poise cells to maintain pluripotency and provide a selective advantage during reprogramming.

Manipulating Heteroplasmy *In Vitro*

With our current lack of detailed mechanistic insight into the regulation of heteroplasmy during cellular reprogramming, methods that manipulate mtDNA sequences and heteroplasmy in somatic tissues may provide a path forward for specifying heteroplasmy ratios in iPSCs. Engineered endonucleases targeted to the mitochondria within cells have been used to degrade mutant mtDNA to enrich for WT heteroplasmy. Mitochondria-targeted transcription activator-like effector nucleases (mitoTALENs) degraded mutant mtDNA in fibroblasts prior to reprogramming to pluripotency and differentiation to progeny cells to reduce heteroplasmic levels of m.3243A>G, m.5024 C>T, and m.13513 G>A mutations [57,80,81]. To date, only mitoTALENs have shifted

the heteroplasmy of iPSCs; however, other endonucleases have the potential to manipulate levels of specific mtDNA sequences in iPSCs including mitochondrial zinc finger nucleases (mitoZFNs) and possibly the CRISPR/Cas gene editing system. mitoZFNs have successfully eliminated mutant mtDNA from human osteosarcoma cells [82], and two studies targeted mitoZFNs to the m.5024C>T mutation in mice, which showed a reduction of mutant mtDNA copy number in heart and skeletal muscle cells. However, neither study fully eliminated mutant heteroplasmy or measured the long-term effects of mitoZFN treatment on mutant heteroplasmy [83,84]. The CRISPR/Cas gene editing system has also been shown to degrade specific mtDNAs [85,86]. However, all endonuclease-enabled mtDNA manipulation tools are limited to eliminating specific mtDNA sequences and are unable to yield genetic knock-ins, which require the function of specific DNA repair mechanisms that are not as extensive or robust in the mitochondria as those in the nucleus. Some mtDNA repair mechanisms are well understood and characterized, such as base excision repair, whereas other mechanisms, such as double-stranded DNA and nucleotide excision repair, are poorly elucidated, as reviewed elsewhere [87,88]. In addition to our limited knowledge on the effects of endonucleases in stem cells, endonucleases have potential off-target effects, are time consuming to design for specific sequences, and must be engineered for import into the mitochondrial matrix [81,83]. Investigators have also looked beyond endonucleases to manipulate cellular pools of mtDNA. An exciting new study of a modified bacterial cytidine deaminase toxin showed direct editing of the mtDNA in transformed human cells, which shifted heteroplasmy and induced functional metabolic changes with minimal off-target activity [89]. This technology currently has a ~30% targeting efficiency and has promise for *in vitro* and *in vivo* mtDNA editing but has yet to be used in iPSCs or other stem cell types.

The transfer of mitochondria containing WT mtDNA sequences into somatic cells followed by reprogramming to iPSCs provides a potential route towards eliminating deleterious mtDNA mutations. Cytoplasmic hybrids, or 'cybrids', provide one type of widely used mitochondrial transfer approach almost exclusively applied to generating transformed, immortalized cells containing an mtDNA genotype of interest. In one study, cybridization corrected cells with homoplasmy for m.14484T>C and m.4160T>C mutations in a patient sample, producing one viable, nonimmortal cybrid fibroblast line out of 12 total lines that contained only nonmutant mtDNA [90]. Cells from this one successful line were later reprogrammed to iPSCs and differentiated into retinal ganglion cells that appeared to contain no mutant mtDNA. Currently this is the only study to successfully reprogram cybrids with a corrected mtDNA mutation, and further work is needed to assess the reproducibility, efficiency, or generality of this approach in iPSCs.

Additional approaches to stably introduce exogenous mtDNA sequences involve transferring isolated mitochondria into cells. A growing literature shows mitochondrial coincubation with mammalian cells yields efficient uptake of mitochondria from the culture medium with a range of changes to cell energetics and activity, but the majority of these studies report on effects seen within a limited time frame following transfer [91,92]. Several reports show stable integration of exogenous mtDNA from isolated mitochondrial co-incubation but require high levels of isolated mitochondria or antibiotic selection schemes that limit the mtDNA genotypes that can be transferred [93,94]. While co-incubation facilitates mitochondrial uptake, long-term maintenance of stably integrated exogenous mtDNA is difficult to achieve.

Microinjection has been used to directly transfer mitochondria into the cytoplasm of human cells to yield stable mitochondrial transfer [95]; however, the method is laborious and prone to damaging cells by disrupting the plasma membrane when inserting the glass microneedle. One recent technology that reduces the damage caused to recipient cells, called a '**photothermal nanoblade**', was used to transfer isolated mitochondria into transformed cells that lacked mtDNA to engineer

cellular metabolism [96]. However, this approach and its high throughput variant, the **Biophotonic Laser Assisted Surgery Tool**, have limited accessibility and have not been used directly with PSCs because of their requirement for expertise in lasers and advanced optics [97]. A variation of this technology, called **MitoPunch**, uses a solenoid driven piston to deliver isolated mitochondria into adherent mtDNA-depleted mammalian cells [98,99]. This method has been used to generate fibroblasts that stably express homoplasmic exogenous mtDNA and yield functional iPSCs after reprogramming [100]. These methods have not been used to alter heteroplasmy directly in iPSCs, but they represent the potential of altering the mtDNA content of somatic cells that are then reprogrammed for downstream applications. Isolated mitochondrial transfer into somatic cells using these and a range of other methods, including MitoCeption and Magnetomitotransfer, to promote mitochondrial uptake by recipient cells [91,101], is an exciting new area of research that holds promise for generating future cellular therapeutics for individuals living with mutant mtDNA-caused disorders (Figure 4).

Concluding Remarks

iPSCs hold promise for studies in development, physiology, and pathophysiology, and for future treatments of a wide array of diseases. Despite their therapeutic potential, several roadblocks have slowed the progress of iPSC products into clinical applications. Here, we evaluate and discuss one potential barrier that has been largely under the radar concerning mtDNA heteroplasmy shifts during somatic cell reprogramming and the importance of heteroplasmy ratios for iPSC functions and utility. We discuss the metabolic and mitochondrial demands of somatic cell reprogramming and put forth a conceptual framework based on the currently limited

Outstanding Questions

Will mtDNA heteroplasmy in iPSCs adversely affect differentiated cell therapies in regenerative medicine?

What are the metabolic and genetic regulators of mtDNA heteroplasmy?

What is the timing of mtDNA heteroplasmy shifts during reprogramming to pluripotency?

Does the reduction in mtDNA copy number during cellular reprogramming resemble the mtDNA bottleneck that occurs in oocyte development?

Can cytidine deaminase toxin enable efficient, on-target mtDNA editing in stem cells, including iPSCs and ESCs?

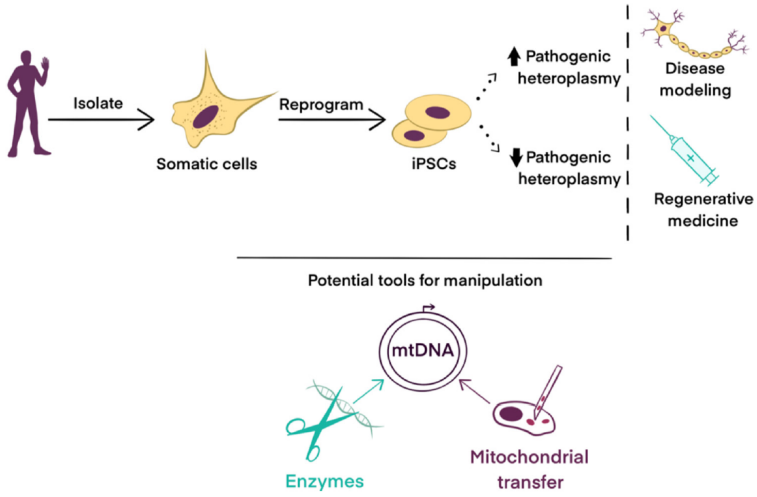

Figure 4. Controlling Heteroplasmy in iPSCs for Clinical Applications. The utility of reprogramming patient-derived somatic cells into iPSCs may become limited for many reasons including the uncontrolled generation of suboptimal mtDNA heteroplasmy ratios. Tools and approaches have been developed to controllably manipulate the mtDNA content in somatic cells that can then be converted to iPSCs, or in iPSCs themselves, including targeted endonucleases, somatic cell nuclear transfer, and engineered mitochondrial transfer modalities. Methodologies to specify heteroplasmy levels in iPSCs could improve applications in disease modeling, drug screening, and regenerative medicine by tailoring mtDNA populations for specific applications. Abbreviations: iPSC, induced pluripotent stem cell; mtDNA, mitochondrial DNA.

experimental data available to define three distinct heteroplasmy distributions identified within iPSC populations. We postulate mechanisms for these shifts based on evidence from studies of somatic and germ cells and encourage the community to expand on these experiments to enhance our understanding of mtDNA genetics in iPSCs. Finally, we explore current and future technologies and techniques to manipulate mtDNA sequences in order to model and possibly correct diseases of the mitochondria. Understanding the mechanisms that foster heteroplasmy shifts in somatic cell reprogramming should lead to the production of reproducible, consistent, and better-defined iPSC populations (see Outstanding Questions). An increased focus in this area of research is necessary to determine whether there are predictable shifts of heteroplasmy during cellular reprogramming, and careful time course experimentation using single cell -omics approaches will aid in understanding which selective pressures may be driving such changes. In addition, implementing recent advances in mitochondrial transfer and mtDNA genome editing techniques in tractable *in vitro* cell systems will enable studies of how heteroplasmy effects reprogramming, iPSC function, and iPSC differentiation into other cell types. This increased understanding will provide tools to manipulate mutant mtDNA levels in cells for disease modeling or therapeutic applications. Even simpler methods, such as partial mtDNA depletion or single cell expansions, may provide paths forward to remove deleterious mtDNA sequences from established or novel patient-derived iPSC lines [102].

There exist hundreds of documented disease-causing mutations to the mtDNA [103], and yet we do not know the rates at which specific mutations expand within cells of different fates, or how other sequences may become eliminated. Further advances in methods to control mtDNA sequences and the ratios of these sequences within cells are needed to minimize the risk of detrimental outcomes for patients treated in the future with stem cell-based products. The role of mitochondria as simple cellular 'power plants' is an oversimplification, and the broad range of mitochondrial functions, all of which are affected by mtDNA heteroplasmy, touch on most if not all aspects of cell and organismal biology, directly or indirectly. Perhaps the future of cell-based therapeutics depends on our ability to understand and manipulate this second, often overlooked, cellular genome.

Acknowledgments

A.J.S. has support from two NIH National Research Service Award fellowships (T32GM007185 and T32CA009120). N.M.C was supported by the California Institute for Regenerative Medicine Grant EDUC2-08411. A.N.P. has support from the NIH (T32CA009120) and American Heart Association (18POST34080342). M.A.T. is supported by the Air Force Office of Scientific Research (FA9550-15-1-0406), the NIH (R01GM114188, R01GM073981, R01CA185189, R21CA227480, R01GM127985, and P30CA016042), and by CIRM (RT3-07678).

References

1. Takahashi, K. and Yamanaka, S. (2006) Induction of pluripotent stem cells from mouse embryonic and adult fibroblast cultures by defined factors. *Cell* 126, 663–676
2. Guha, P. *et al.* (2013) Lack of immune response to differentiated cells derived from syngeneic induced pluripotent stem cells. *Cell Stem Cell* 12, 407–412
3. Liu, X. *et al.* (2017) The Immunogenicity and immune tolerance of pluripotent stem cell derivatives. *Front. Immunol.* 8, 645
4. Garreta, E. *et al.* (2018) Roadblocks in the path of iPSC to the clinic. *Curr. Transplant. Rep.* 5, 14–18
5. Deuse, T. *et al.* (2019) De novo mutations in mitochondrial DNA of iPSCs produce immunogenic neoepitopes in mice and humans. *Nat. Biotechnol.* 37, 1137–1144
6. Deuse, T. *et al.* (2015) SCNT-derived ESCs with mismatched mitochondria trigger an immune response in allogeneic hosts. *Cell Stem Cell* 16, 33–38
7. Magnusson, J. (2003) *Replication of mitochondrial DNA occurs throughout the mitochondria of cultured human cells.* 289 pp. 133–142
8. Sasaki, T. *et al.* (2017) Live imaging reveals the dynamics and regulation of mitochondrial nucleoids during the cell cycle in Fucci2-HeLa cells. *Sci. Rep.* 7, 11257
9. Ludwig, L.S. *et al.* (2019) Lineage tracing in humans enabled by mitochondrial mutations and single-cell genomics. *Cell* 176, 1325–1339 e1322
10. Stewart, J.B. and Chinnery, P.F. (2015) The dynamics of mitochondrial DNA heteroplasmy: implications for human health and disease. *Nat. Rev. Genet.* 16, 530–542
11. Lawless, C. *et al.* (2020) The rise and rise of mitochondrial DNA mutations. *Open Biol.* 10, 200061
12. Omasanggar, R. *et al.* (2020) Mitochondrial DNA mutations in Malaysian female breast cancer patients. *PLoS ONE* 15, e0233461
13. Temperley, R.J. *et al.* (2010) Human mitochondrial mRNAs–like members of all families, similar but different. *Biochim. Biophys. Acta* 1797, 1081–1085
14. Burgstaller, J.P. *et al.* (2014) MtDNA segregation in heteroplasmic tissues is common *in vivo* and modulated by haplotype differences and developmental stage. *Cell Rep.* 7, 2031–2041

15. Wallace, D.C. and Chalkia, D. (2013) Mitochondrial DNA genetics and the heteroplasmy conundrum in evolution and disease. *Cold Spring Harb. Perspect. Biol.* 5, a021220
16. Wei, W. *et al.* (2019) Germline selection shapes human mitochondrial DNA diversity. *Science* 364, eaau6520
17. Soares, P. *et al.* (2009) Correcting for purifying selection: an improved human mitochondrial molecular clock. *Am. J. Hum. Genet.* 84, 740–759
18. Zaidi, A.A. *et al.* (2019) Bottleneck and selection in the germline and maternal age influence transmission of mitochondrial DNA in human pedigrees. *Proc. Natl. Acad. Sci.* 116, 25172–25178
19. Russell, O.M. *et al.* (2018) Preferential amplification of a human mitochondrial DNA deletion *in vitro* and *in vivo*. *Sci. Rep.* 8, 1799
20. Yoneda, M. *et al.* (1992) Marked replicative advantage of human mtDNA carrying a point mutation that causes the MELAS encephalomyopathy. 89, 11164–11168
21. Wagner, J.T. *et al.* (2020) Mitochondrial DNA variation and selfish propagation following experimental bottlenecking in two distantly related caenorhabditis briggsae isolates. *Genes* 11, 77
22. Yokota, M. *et al.* (2015) Mitochondrial respiratory dysfunction caused by a heteroplasmic mitochondrial DNA mutation blocks cellular reprogramming. *Hum. Mol. Genet.* 24, 4698–4709
23. Matsubara, M. *et al.* (2018) Analysis of mitochondrial function in human induced pluripotent stem cells from patients with mitochondrial diabetes due to the A3243G mutation. *Sci. Rep.* 8, 949
24. Kopinski, P.K. *et al.* (2019) Regulation of nuclear epigenome by mitochondrial DNA heteroplasmy. *Proc. Natl. Acad. Sci. U. S. A.* 116, 16028–16035
25. Hirose, M. *et al.* (2018) Low-level mitochondrial heteroplasmy modulates DNA replication, glucose metabolism and lifespan in mice. *Sci. Rep.* 8, 5872
26. Seo, B. *et al.* (2018) Mitochondrial dynamics in stem cells and differentiation. *Int. J. Mol. Sci.* 19, 3893
27. Bonora, M. *et al.* (2012) ATP synthesis and storage. *Purinergic Signal* 8, 343–357
28. Krebs, H.A. (1940) The citric acid cycle and the Szent-Gyorgyi cycle in pigeon breast muscle. *Biochem. J.* 34, 775–779
29. Hansson, J. *et al.* (2012) Highly coordinated proteome dynamics during reprogramming of somatic cells to pluripotency. *Cell Rep.* 2, 1579–1592
30. Prigione, A. *et al.* (2014) HIF1alpha modulates cell fate reprogramming through early glycolytic shift and upregulation of PDK1-3 and PKM2. *Stem Cells* 32, 364–376
31. Cho, Y.M. *et al.* (2006) Dynamic changes in mitochondrial biogenesis and antioxidant enzymes during the spontaneous differentiation of human embryonic stem cells. *Biochem. Biophys. Res. Commun.* 348, 1472–1478
32. Zhang, J. *et al.* (2018) Metabolism in pluripotent stem cells and early mammalian development. *Cell Metab.* 27, 332–338
33. Zhang, H. *et al.* (2016) Distinct metabolic states can support self-renewal and lipogenesis in human pluripotent stem cells under different culture conditions. *Cell Rep.* 16, 1536–1547
34. Zhou, Z. *et al.* (2018) Mitochondrial metabolism in major neurological diseases. *Cells* 7, 229
35. Appling, D.R. (1991) Compartmentation of folate-mediated one-carbon metabolism in eukaryotes. *FASEB J.* 5, 2645–2651
36. Watson, J.A. and Lowenstein, J.M. (1970) Citrate and the conversion of carbohydrate into fat. Fatty acid synthesis by a combination of cytoplasm and mitochondria. *J. Biol. Chem.* 245, 5993–6002
37. Carey, B.W. *et al.* (2015) Intracellular alpha-ketoglutarate maintains the pluripotency of embryonic stem cells. *Nature* 518, 413–416
38. Guitart, A.V. *et al.* (2017) Fumarate hydratase is a critical metabolic regulator of hematopoietic stem cell functions. *J. Exp. Med.* 214, 719–735
39. Fang, Y. *et al.* (2019) Sirtuins in metabolic and epigenetic regulation of stem cells. *Trends Endocrinol. Metab.* 30, 177–188
40. Moussaieff, A. *et al.* (2015) Glycolysis-mediated changes in acetyl-CoA and histone acetylation control the early differentiation of embryonic stem cells. *Cell Metab.* 21, 392–402
41. Mews, P. *et al.* (2017) Acetyl-CoA synthetase regulates histone acetylation and hippocampal memory. *Nature* 546, 381–386
42. Zhou, G. *et al.* (2016) Optimal ROS signaling is critical for nuclear reprogramming. *Cell Rep.* 15, 919–925
43. Boland, M.J. *et al.* (2014) Epigenetic regulation of pluripotency and differentiation. *Circ. Res.* 115, 311–324
44. Ramakrishna, S. *et al.* (2014) Posttranslational modifications of defined embryonic reprogramming transcription factors. *Cell Reprogram* 16, 108–120
45. Hamalainen, R.H. (2016) Mitochondrial DNA mutations in iPS cells: mtDNA integrity as standard iPSC selection criteria? *EMBO J.* 35, 1960–1962
46. Kang, E. *et al.* (2016) Mitochondrial replacement in human oocytes carrying pathogenic mitochondrial DNA mutations. *Nature* 540, 270–275
47. Perales-Clemente, E. *et al.* (2016) Natural underlying mtDNA heteroplasmy as a potential source of intra-person hiPSC variability. *EMBO J.* 35, 1979–1990
48. Folmes, C.D. *et al.* (2013) Disease-causing mitochondrial heteroplasmy segregated within induced pluripotent stem cell clones derived from a patient with MELAS. *Stem Cells* 31, 1298–1308
49. Dahan, P. *et al.* (2019) Metabolism in pluripotency: both driver and passenger? *J. Biol. Chem.* 294, 5420–5429
50. Pickrell, A.M. and Youle, R.J. (2013) Mitochondrial disease: mtDNA and protein segregation mysteries in iPSCs. *Curr. Biol.* 23, R1052–R1054
51. Allsopp, R. (2012) Telomere length and iPSC re-programming: survival of the longest. *Cell Res.* 22, 614–615
52. Zhou, M.-C. *et al.* (2015) Analysis of association among clinical features and shorter leukocyte telomere length in mitochondrial diabetes with m.3243A>G mitochondrial DNA mutation. *BMC Med. Genet.* 16, 92
53. Kodaira, M. *et al.* (2015) Impaired respiratory function in MELAS-induced pluripotent stem cells with high heteroplasmy levels. *FEBS Open Bio* 5, 219–225
54. Ma, H. *et al.* (2015) Metabolic rescue in pluripotent cells from patients with mtDNA disease. *Nature* 524, 234–238
55. Chichagova, V. *et al.* (2017) Human iPSC disease modelling reveals functional and structural defects in retinal pigment epithelial cells harbouring the m.3243A > G mitochondrial DNA mutation. *Sci. Rep.* 7, 12320
56. Chou, S.J. *et al.* (2016) Impaired ROS scavenging system in human induced pluripotent stem cells generated from patients with MERRF syndrome. *Sci. Rep.* 6, 23661
57. Yahata, N. *et al.* (2017) TALEN-mediated shift of mitochondrial DNA heteroplasmy in MELAS-iPSCs with m.13513G>A mutation. *Sci. Rep.* 7, 15557
58. Ju, Y.S. *et al.* (2014) Origins and functional consequences of somatic mitochondrial DNA mutations in human cancer. *Elife* 3, e02935
59. Jackson, C.B. *et al.* (2020) Therapeutic manipulation of mtDNA heteroplasmy: a shifting perspective. *Trends Mol. Med.* 26, 698–709
60. Van Den Ameele, J. *et al.* (2020) Mitochondrial heteroplasmy beyond the oocyte bottleneck. *Semin. Cell Dev. Biol.* 97, 156–166
61. Hahn, A. and Zuryn, S. (2019) The cellular mitochondrial genome landscape in disease. *Trends Cell Biol.* 29, 227–240
62. Hamalainen, R.H. *et al.* (2013) Tissue- and cell-type-specific manifestations of heteroplasmic mtDNA 3243A>G mutation in human induced pluripotent stem cell-derived disease model. *Proc. Natl. Acad. Sci. U. S. A.* 110, E3622–E3630
63. Pessoa, L.V. *et al.* (2015) Mitochondrial DNA dynamics during *in vitro* culture and pluripotency induction of a bovine Rho0 cell line. *Genet. Mol. Res.* 14, 14093–14104
64. Latorre-Pellicer, A. *et al.* (2019) Regulation of mother-to-offspring transmission of mtDNA heteroplasmy. *Cell Metab* 30, 1120–1130 e1125
65. Floros, V.I. *et al.* (2018) Segregation of mitochondrial DNA heteroplasmy through a developmental genetic bottleneck in human embryos. *Nat. Cell Biol.* 20, 144–151
66. He, Y. *et al.* (2010) Heteroplasmic mitochondrial DNA mutations in normal and tumour cells. *Nature* 464, 610–614
67. Gammage, P.A. and Frezza, C. (2019) Mitochondrial DNA: the overlooked oncogenome? *BMC Biol.* 17, 53
68. Ishikawa, K. *et al.* (2008) ROS-generating mitochondrial DNA mutations can regulate tumor cell metastasis. *Science* 320, 661–664

69. Park, J.S. *et al.* (2009) A heteroplasmic, not homoplasmic, mitochondrial DNA mutation promotes tumorigenesis via alteration in reactive oxygen species generation and apoptosis. *Hum. Mol. Genet.* 18, 1578–1589
70. Qi, Y. *et al.* (2016) Heteroplasmy of mutant mitochondrial DNA A10398G and analysis of its prognostic value in non-small cell lung cancer. *Oncol. Lett.* 12, 3081–3088
71. Yuan, Y. *et al.* (2020) Comprehensive molecular characterization of mitochondrial genomes in human cancers. *Nat. Genet.* 52, 342–352
72. Schöpf, B. *et al.* (2020) OXPHOS remodeling in high-grade prostate cancer involves mtDNA mutations and increased succinate oxidation. *Nat. Commun.* 11, 1487
73. Gawad, C. *et al.* (2016) Single-cell genome sequencing: current state of the science. *Nat. Rev. Genet.* 17, 175–188
74. Walker, M.A. *et al.* (2020) Purifying selection against pathogenic mitochondrial DNA in human T cells. *N. Engl. J. Med.* 383, 1556–1563
75. Chiang, A.C.Y. *et al.* (2019) A genome-wide screen reveals that reducing mitochondrial dna polymerase Can Promote Elimination of Deleterious Mitochondrial mutations. *Curr. Biol.* 29, 4330–4336 e4333
76. Song, S. *et al.* (2005) DNA precursor asymmetries in mammalian tissue mitochondria and possible contribution to mutagenesis through reduced replication fidelity. *Proc. Natl. Acad. Sci. U. S. A.* 102, 4990–4995
77. Fukui, H. and Moraes, C.T. (2009) Mechanisms of formation and accumulation of mitochondrial DNA deletions in aging neurons. *Hum. Mol. Genet.* 18, 1028–1036
78. Picard, M. *et al.* (2014) Progressive increase in mtDNA 3243A>G heteroplasmy causes abrupt transcriptional reprogramming. *Proc. Natl. Acad. Sci.* 111, E4033–E4042
79. McManus, M.J. *et al.* (2019) Mitochondrial DNA variation dictates expressivity and progression of nuclear DNA mutations causing cardiomyopathy. *Cell Metab.* 29, 78–90 e75
80. Yang, Y. *et al.* (2018) Targeted elimination of mutant mitochondrial DNA in MELAS-iPSCs by mitoTALENs. *Protein Cell* 9, 283–297
81. Bacman, S.R. *et al.* (2018) Author Correction: MitoTALEN reduces mutant mtDNA load and restores tRNA(Ala) levels in a mouse model of heteroplasmic mtDNA mutation. *Nat. Med.* 24, 1940
82. Gammage, P.A. *et al.* (2016) Near-complete elimination of mutant mtDNA by iterative or dynamic dose-controlled treatment with mtZFNs. *Nucleic Acids Res.* 44, 7804–7816
83. Gammage, P.A. *et al.* (2018) Genome editing in mitochondria corrects a pathogenic mtDNA mutation *in vivo*. *Nat. Med.* 24, 1691–1695
84. Bacman, S.R. *et al.* (2018) MitoTALEN reduces mutant mtDNA load and restores tRNA(Ala) levels in a mouse model of heteroplasmic mtDNA mutation. *Nat. Med.* 24, 1696–1700
85. Jo, A. *et al.* (2015) Efficient mitochondrial genome editing by CRISPR/Cas9. *Biomed. Res. Int.* 2015, 1–10
86. Hussain, S.-R.A. *et al.* (2020) Adapting CRISPR/Cas9 System for Targeting Mitochondrial Genome. *BioRxiv* Published online February 12, 2020. https://doi.org/10.1101/2020.02.11.944819
87. Zinovkina, L.A. (2018) Mechanisms of mitochondrial DNA repair in mammals. *Biochem. Mosc.* 83, 233–249
88. Alexeyev, M. *et al.* (2013) The maintenance of mitochondrial DNA integrity – critical analysis and update. *Cold Spring Harb. Perspect. Biol.* 5, a012641-a012641
89. Mok, B.Y. *et al.* (2020) A bacterial cytidine deaminase toxin enables CRISPR-free mitochondrial base editing. *Nature* 583, 631–637
90. Wong, R.C.B. *et al.* (2017) Mitochondrial replacement in an iPSC model of Leber's hereditary optic neuropathy. *Aging (Albany NY)* 9, 1341–1350
91. Caicedo, A. *et al.* (2015) MitoCeption as a new tool to assess the effects of mesenchymal stem/stromal cell mitochondria on cancer cell metabolism and function. *Sci. Rep.* 5, 9073
92. Kesner, E.E. *et al.* (2016) Characteristics of mitochondrial transformation into human cells. *Sci. Rep.* 6, 26057
93. Clark, M.A. and Shay, J.W. (1982) Mitochondrial transformation of mammalian cells. *Nature* 295, 605–607
94. Patel, D. *et al.* (2017) Macropinocytic entry of isolated mitochondria in epidermal growth factor-activated human osteosarcoma cells. *Sci. Rep.* 7, 12886
95. King, M.P. and Attardi, G. (1988) Injection of mitochondria into human cells leads to a rapid replacement of the endogenous mitochondrial DNA. *Cell* 52, 811–819
96. Wu, T.H. *et al.* (2016) Mitochondrial transfer by photothermal nanoblade restores metabolite profile in mammalian cells. *Cell Metab.* 23, 921–929
97. Wu, Y.-C. *et al.* (2015) Massively parallel delivery of large cargo into mammalian cells with light pulses. *Nat. Methods* 12, 439–444
98. Dawson, E.R. *et al.* (2020) Stable retention of chloramphenicol-resistant mtDNA to rescue metabolically impaired cells. *Sci. Rep.* 10, 14326
99. Sercel, A.J. *et al.* (2020) Stable transplantation of human mitochondrial DNA by high-throughput, pressurized mitochondrial delivery. *BioRxiv* Published online September 15, 2020. https://doi.org/10.1101/2020.09.15.298174
100. Patananan, A.N. *et al.* (2020) Pressure-driven mitochondrial transfer pipeline generates mammalian cells of desired genetic combinations and fates. *Cell Reports* 33, 108562
101. Macheiner, T. *et al.* (2016) Magnetomitotransfer: an efficient way for direct mitochondria transfer into cultured human cells. *Sci. Rep.* 6, 35771
102. Kosanke, M. *et al.* (2020) iPSC culture expansion selects against putatively actionable mutations in the mitochondrial genome. *BioRxiv* Published online November 5, 2020. https://doi.org/10.1101/2020.11.05.369694
103. Tuppen, H.A.L. *et al.* (2010) Mitochondrial DNA mutations and human disease. *Biochim. Biophys. Acta Bioenerg.* 1797, 113–128
104. Grace, H.E. *et al.* (2019) mRNA reprogramming of T8993G Leigh's syndrome fibroblast cells to create induced pluripotent stem cell models for mitochondrial disorders. *Stem Cells Dev.* 28, 846–859
105. Galera, T. *et al.* (2016) Generation of a human iPSC line from a patient with Leigh syndrome. *Stem Cell Res.* 16, 63–66
106. Hung, S.S. *et al.* (2016) Study of mitochondrial respiratory defects on reprogramming to human induced pluripotent stem cells. *Aging (Albany NY)* 8, 945–957
107. Robin, E.D. and Wong, R. (1988) Mitochondrial DNA molecules and virtual number of mitochondria per cell in mammalian cells. *J. Cell. Physiol.* 136, 507–513
108. Gilkerson, R. *et al.* (2013) The mitochondrial nucleoid: integrating mitochondrial DNA into cellular homeostasis. *Cold Spring Harb. Perspect. Biol.* 5, a011080-a011080
109. Greaves, L.C. *et al.* (2014) Clonal expansion of early to mid-life mitochondrial DNA point mutations drives mitochondrial dysfunction during human ageing. *PLoS Genet.* https://doi.org/10.1371/journal.pgen.1004620
110. Kennedy, S.R. *et al.* (2013) Ultra-sensitive sequencing reveals an age-related increase in somatic mitochondrial mutations that are inconsistent with oxidative damage. *PLoS Genet.* 9, e1003794
111. Zheng, W. *et al.* (2006) Origins of human mitochondrial point mutations as DNA polymerase γ-mediated errors. *Mutat. Res. Fundam. Mol. Mech. Mutagen.* 599, 11–20
112. Nissanka, N. *et al.* (2018) The mitochondrial DNA polymerase gamma degrades linear DNA fragments precluding the formation of deletions. *Nat. Commun.* 9, 2491
113. Szczepanowska, K. and Trifunovic, A. (2015) Different faces of mitochondrial DNA mutators. *Biochim. Biophys. Acta Bioenerg.* 1847, 1362–1372
114. González, M.D.M. *et al.* (2020) Sensitivity of mitochondrial DNA heteroplasmy detection using Next Generation Sequencing. *Mitochondrion* 50, 88–93

Chapter 7: Pressure-Driven Mitochondrial Transfer Pipeline Generates Mammalian Cells of Desired Genetic Combinations and Fates

Cell Reports

Resource

Pressure-Driven Mitochondrial Transfer Pipeline Generates Mammalian Cells of Desired Genetic Combinations and Fates

Graphical Abstract

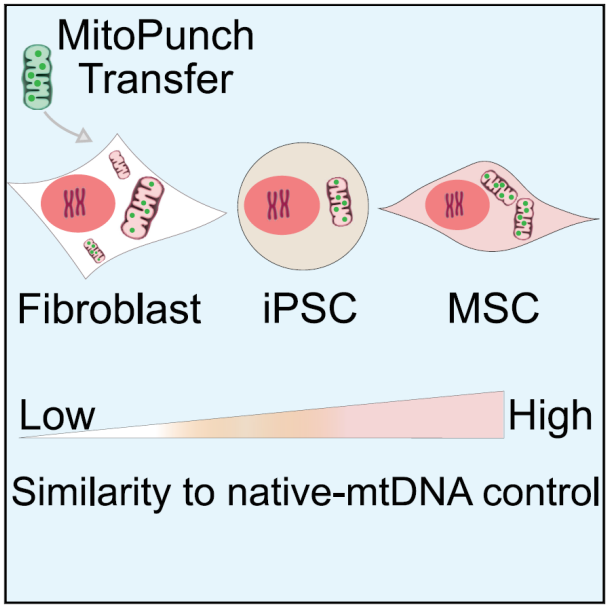

Authors

Alexander N. Patananan, Alexander J. Sercel, Ting-Hsiang Wu, ..., Kayvan R. Niazi, Pei-Yu Chiou, Michael A. Teitell

Correspondence

mteitell@mednet.ucla.edu

In Brief

Patananan and colleagues demonstrate a pipeline for transferring isolated mitochondria into mtDNA-deficient recipient cells. mtDNA-depleted fibroblasts permanently retain acquired non-native mtDNA through cell fate transitions. Initially, mitochondrial recipients show mtDNA-deficient cell transcriptome and metabolome profiles, with improvement to control profiles by reprogramming to pluripotency and subsequent differentiation.

Highlights

- We report a "proof-of-principle" mitochondrial transfer pipeline by MitoPunch
- MitoPunch generates cells with unique mtDNA-nDNA pairs, regardless of cell source
- Replacement mtDNA in non-immortal cells remains stable with cell fate conversions
- Enables studies of mtDNA-nDNA interactions with reprogramming and differentiation

Patananan et al., 2020, Cell Reports *33*, 108562
December 29, 2020
https://doi.org/10.1016/j.celrep.2020.108562

CellPress

Cell Reports

CellPress
OPEN ACCESS

Resource

Pressure-Driven Mitochondrial Transfer Pipeline Generates Mammalian Cells of Desired Genetic Combinations and Fates

Alexander N. Patananan,[1,16] Alexander J. Sercel,[2,16] Ting-Hsiang Wu,[3,16] Fasih M. Ahsan,[1] Alejandro Torres, Jr.,[1] Stephanie A.L. Kennedy,[1] Amy Vandiver,[4] Amanda J. Collier,[5,6,7] Artin Mehrabi,[3] Jon Van Lew,[3] Lise Zakin,[8] Noe Rodriguez,[8] Marcos Sixto,[8] Wael Tadros,[8] Adam Lazar,[8] Peter A. Sieling,[8] Thang L. Nguyen,[9] Emma R. Dawson,[1] Daniel Braas,[10] Justin Golovato,[11] Luis Cisneros,[11] Charles Vaske,[11] Kathrin Plath,[5,6,7] Shahrooz Rabizadeh,[3,8] Kayvan R. Niazi,[3,8] Pei-Yu Chiou,[9,12,13] and Michael A. Teitell[1,6,7,13,14,15,17,*]

[1]Department of Pathology and Laboratory Medicine, David Geffen School of Medicine, University of California, Los Angeles, Los Angeles, CA 90095, USA
[2]Molecular Biology Interdepartmental Program, University of California, Los Angeles, Los Angeles, CA 90095, USA
[3]NanoCav LLC, Culver City, CA 90232, USA
[4]Division of Dermatology, University of California, Los Angeles, Los Angeles, CA 90095, USA
[5]Department of Biological Chemistry, University of California, Los Angeles, Los Angeles, CA 90095, USA
[6]Molecular Biology Institute, University of California, Los Angeles, Los Angeles, CA 90095, USA
[7]Eli and Edythe Broad Center of Regenerative Medicine and Stem Cell Research, University of California, Los Angeles, Los Angeles, CA 90095, USA
[8]NantWorks, LLC, Culver City, CA 90232, USA
[9]Department of Bioengineering, University of California, Los Angeles, Los Angeles, CA 90095, USA
[10]UCLA Metabolomics Center, University of California, Los Angeles, Los Angeles, CA 90095, USA
[11]NantOmics, LLC, Culver City, CA 90232, USA
[12]Department of Mechanical and Aerospace Engineering, University of California, Los Angeles, Los Angeles, CA 90095, USA
[13]California NanoSystems Institute, University of California, Los Angeles, Los Angeles, CA 90095, USA
[14]Department of Pediatrics, David Geffen School of Medicine, University of California, Los Angeles, Los Angeles, CA 90095, USA
[15]Jonsson Comprehensive Cancer Center, David Geffen School of Medicine, University of California, Los Angeles, Los Angeles, CA 90095, USA
[16]These authors contributed equally
[17]Lead Contact
*Correspondence: mteitell@mednet.ucla.edu
https://doi.org/10.1016/j.celrep.2020.108562

SUMMARY

Generating mammalian cells with desired mitochondrial DNA (mtDNA) sequences is enabling for studies of mitochondria, disease modeling, and potential regenerative therapies. MitoPunch, a high-throughput mitochondrial transfer device, produces cells with specific mtDNA-nuclear DNA (nDNA) combinations by transferring isolated mitochondria from mouse or human cells into primary or immortal mtDNA-deficient (ρ0) cells. Stable isolated mitochondrial recipient (SIMR) cells isolated in restrictive media permanently retain donor mtDNA and reacquire respiration. However, SIMR fibroblasts maintain a ρ0-like cell metabolome and transcriptome despite growth in restrictive media. We reprogrammed non-immortal SIMR fibroblasts into induced pluripotent stem cells (iPSCs) with subsequent differentiation into diverse functional cell types, including mesenchymal stem cells (MSCs), adipocytes, osteoblasts, and chondrocytes. Remarkably, after reprogramming and differentiation, SIMR fibroblasts molecularly and phenotypically resemble unmanipulated control fibroblasts carried through the same protocol. Thus, our MitoPunch "pipeline" enables the production of SIMR cells with unique mtDNA-nDNA combinations for additional studies and applications in multiple cell types.

INTRODUCTION

Mammalian mitochondria are cellular power plants with additional roles in apoptosis, reactive oxygen species (ROS) and Fe-S cluster generation, Ca^{2+} regulation, and metabolite production (Patananan et al., 2018). Each mitochondrion contains >1,100 nucleus-encoded and imported proteins (Calvo et al., 2016) with numerous copies of a circular ~16.5-kilobase pair (kbp) mitochondrial genome (mtDNA) encoding 13 proteins required for electron transport chain (ETC) activity and

Cell Reports 33, 108562, December 29, 2020

respiration. As many as 1:5,000 people have mtDNA mutations that impair high-energy-demand tissues and contribute to debilitating diseases, including cancer, diabetes, and metabolic syndromes (Schaefer et al., 2004). In addition, cells may contain a mixture of different mtDNA sequences, a situation termed heteroplasmy, with up to 1 in 8 asymptomatic individuals carrying an unsuspected pathogenic mtDNA mutation (Elliott et al., 2008; Rebolledo-Jaramillo et al., 2014). Thus, an ability to controllably manipulate mtDNA sequences could enable studies of mitochondria and potentially develop disease models or therapies for mtDNA disorders.

In human reproduction, several types of mitochondrial replacement strategies were developed to exchange pathogenic mtDNA in a zygote with non-detrimental mtDNA from a healthy donor oocyte. These approaches have potential for preventing transmission of mtDNA disorders from carrier mothers to their children (Wolf et al., 2015; Wolf et al., 2019). However, *in vitro* methods to change mtDNA sequences within somatic cells and tissues remain limited (Patananan et al., 2016). Cell fusions that produce "cybrids" permanently retain donor mitochondria (Wong et al., 2017), although fusion partners are typically transformed cells that cannot be reprogrammed. Also, endonucleases imported into mitochondria can shift heteroplasmy ratios to alter mitochondria and cell functions by targeting specific sequences for destruction. However, these endonucleases are laborious to produce, are limited to certain mtDNA sequences, are inefficient, and do not yield homoplasmy (Campbell et al., 2018; Yahata et al., 2017; Yang et al., 2018). Of note, a recent and exciting development using a bacterial cytidine deaminase, DddA, to edit mtDNA single-base sequences is tempered by low efficiency and an undesirable off-target rate (Mok et al., 2020).

Several methods transfer isolated mitochondria into mtDNA-deficient cells, known as ρ0 (rho null) cells, to restore respiration (Kim et al., 2018; Nzigou Mombo et al., 2017). In addition, some studies reported endoyctosis of mitochondria by mammalian cells (Clark and Shay, 1982; Kesner et al., 2016). However, these studies were not concerned with rescuing ρ0 cells and generating stable isolated mitochondrial recipient (SIMR) clones that permanently retain donor mtDNA (Kesner et al., 2016; Kitani et al., 2014; Sun et al., 2019). A recent study did produce a limited number of SIMR clones by coincubating high concentrations of isolated HEK293T donor mitochondria with ρ0 osteosarcoma cells (Patel et al., 2017). We (Dawson et al., 2020) and others (Ali Pour et al., 2020) have recently reported similar findings in which cells are capable of endocytosing exogenous mitochondria and even altering metabolic functions for a limited period of time (~1 week), but these exogenous mtDNAs are lost over time. To address this problem, we previously developed a photothermal nanoblade to stably transfer small quantities of isolated mitochondria into ρ0 osteosarcoma cells (Wu et al., 2016). Unfortunately, the nanoblade is laborious and low throughput, and two of three SIMR clones reported did not reset the ρ0 cell metabolome. A technique that generates many non-transformed stable clones is desirable to examine novel mtDNA-nuclear DNA (nDNA) combinations through reprogramming to pluripotency and differentiation into multiple cell types.

Here, we describe a simple-to-use mitochondrial transfer technique called "MitoPunch" to rapidly generate numerous non-transformed SIMR clones. We apply MitoPunch to implement a pipeline that demonstrates donor mtDNA functions in recipient host primary cells at different cell fates. Our study establishes this resource pipeline to generate primary SIMR cells using non-immortalized materials. We also measure the status of the metabolome, transcriptome, and biophysical properties of SIMR cells with defined mtDNA-nDNA combinations to guide future studies generating somatic cells with desired mtDNA-nDNA combinations.

RESULTS

MitoPunch Generates SIMR Cells with a Range of Cell Types and mtDNAs

MitoPunch is a massively parallel, pressure-driven, large cargo transfer platform based on prior photothermal nanoblade and biophotonic laser-assisted cell surgery tool (BLAST) technologies (Sercel et al., 2020; Wu et al., 2016; Wu et al., 2015). MitoPunch uses a mechanical plunger to physically deform a pliable polydimethylsiloxane (PDMS) reservoir containing isolated mitochondria suspended in phosphate-buffered saline (1× PBS [pH 7.4]) (Figure 1A). Plunger activation propels the suspended cargo within the PDMS delivery chamber through a porous membrane containing numerous 3-μm-diameter holes on which a confluent layer of adherent cells is grown. This action directly forces isolated mitochondria into the cytosol of recipient cells.

To demonstrate MitoPunch generation of SIMR cells, we transferred isolated mitochondria from ~1.5 × 10^7 HEK293T cells into ~2 × 10^5 143BTK− ρ0 osteosarcoma cells. Post-transfer, we select for and isolate SIMR colony clones with permanently retained donor mtDNA using uridine-deficient media. This selection is enabling because respiration-defective ρ0 cells have inactive dihydroorate dehydrogenase and depend on exogenous uridine or restored respiration for pyrimidine biosynthesis (Grégoire et al., 1984). Compared to the coincubation of the same amount of isolated mitochondria with cells (Clark and Shay, 1982; Kesner et al., 2016), only 143BTK− ρ0 cells with HEK293T mitochondria from MitoPunch transfer (143BTK− ρ0+HEK293T) permanently retained donor mtDNA and survived uridine-deficient media selection (Figure 1B). In a representative set of mitochondrial transfer experiments, MitoPunch generated ~75 independent crystal-violet-stained SIMR clones in comparison to no clones obtained by coincubation (Figure 1B).

We next examined whether MitoPunch could generate SIMR clones with defined mtDNA-nDNA pairs that transfer features of mitochondrial disease. We isolated mitochondria from cybrid cells containing either an A3243G mtDNA substitution commonly associated with mitochondrial encephalopathy, lactic acidosis, and stroke-like episodes (MELAS) or wild-type (WT), non-mutant mtDNA from the same individual (Picard et al., 2014). The A3243G point mutation is in the $tRNA^{LEU}$ gene and results in altered production and assembly of ETC complexes with impaired oxidative phosphorylation (Chomyn et al., 1992; Sasarman et al., 2008). Following MitoPunch into 143BTK− ρ0 recipients and 2 weeks of selection, two of several dozen independent SIMR clones that permanently retained MELAS (143BTK− ρ0+MELAS) or WT (143BTK− ρ0+WT) mtDNA were tested for oxygen consumption rate (OCR) using the Seahorse

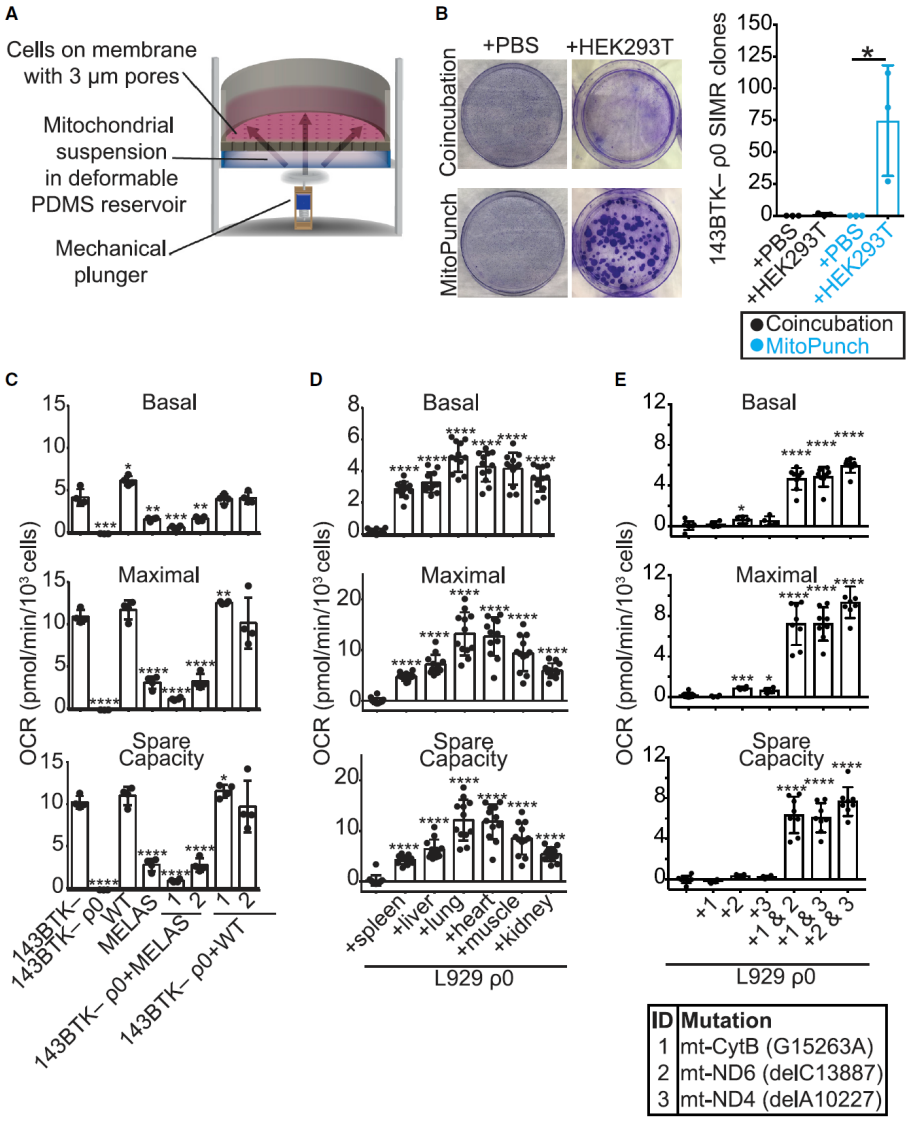

Figure 1. MitoPunch Is a Versatile Mitochondrial Transfer Technology

(A) Schematic representation of the MitoPunch mitochondrial transfer platform.

(B) Images of crystal-violet-stained SIMR colonies from coincubation or MitoPunch delivery of either 1× PBS (pH 7.4) (sham control) or isolated HEK293T cell mitochondria into 143BTK– ρ0 osteosarcoma cells after selection in uridine-depleted medium. Data are the means ± SD of three technical replicates.

(C) OCR measurements for ~1.5 × 10^4 143BTK–, 143BTK– ρ0, WT cybrid, MELAS cybrid, 143BTK– ρ0+MELAS SIMR, and 143BTK– ρ0+WT SIMR cells by Seahorse XF96 Extracellular Flux Analyzer. Values were calculated by standard procedures (see STAR Methods). Data are the means ± SD of four technical replicates.

(legend continued on next page)

Extracellular Flux Analyzer. Results showed 143BTK− ρ0+MELAS clones had significantly impaired basal respiration, maximal respiration, and spare respiratory capacity compared to patient-matched 143BTK− ρ0+WT and native 143BTK− control cells (Figure 1C), indicating stable mtDNA transfer of the primary metabolic deficit of the MELAS phenotype.

We then expanded mitochondrial donor and recipient cell pairings beyond these initial studies to demonstrate the versatility of MitoPunch. As examples, mitochondria were isolated from harvested C57BL/6 mouse tissues and MitoPunch transferred into C3H/An-derived L929 ρ0 immortalized fibroblasts. Two weeks of selection yielded dozens of SIMR clones from each mitochondrial source. SIMR clones generated with high-energy-demand heart, lung, or muscle-derived mitochondria showed the most robust respiratory profiles, in contrast to SIMR clones that received low-energy-demand spleen- or kidney-derived mitochondria (Figure 1D). We also evaluated MitoPunch delivery of heteroplasmic mtDNA mixtures into cells. Mitochondria isolated from mouse cybrid lines containing mtDNA mutations in the cytochrome B (*mt-Cytb*), NADH dehydrogenase subunit 4 (*mt-nd4*), and NADH dehydrogenase subunit 6 (*mt-nd6*) genes were MitoPunch transferred individually or in 1:1 mixtures by protein content into L929 ρ0 fibroblasts. SIMR cells with a single source of mutant mtDNA continued to show severe respiratory impairments (Figure 1E). In contrast, SIMR cells with a mixture of non-overlapping mutant mtDNAs showed markedly improved respiratory profiles, strongly suggesting that both mtDNAs were stably maintained (Figure 1E). Thus, MitoPunch and selection is a versatile approach for generating human or mouse SIMR cells with desired mtDNA-nDNA pairs. Co-transfer of multiple mtDNA types into the same recipient cell also provides a simple method to examine complementation for mutant mtDNA mixtures.

MitoPunch Generates Non-Transformed, Non-Malignant SIMR Cells

To obtain SIMR cells with mtDNA-nDNA combinations using non-immortalized recipient cells, we established a human fibroblast mitochondrial recipient pipeline. Hayflick-limited BJ foreskin (BJ) fibroblasts, neonatal dermal fibroblasts (NDFs), and adult dermal fibroblasts (ADFs) were treated for 3 weeks with FDA-approved 2′,3′-dideoxycytidine (ddC) (Nelson et al., 1997) to deplete endogenous mtDNA. Primary ρ0 human fibroblasts had undetectable mtDNA (Figures S1A and S1B) and cellular respiration (Figures S1C and S1D) by qPCR and Seahorse assay, respectively. Because ddC could cause nDNA alterations, we examined BJ ρ0 fibroblasts by whole-genome sequencing and identified only a few non-synonymous mutations at 0.6 mutations per megabase, on average, with no chromosomal breaks and no changes in DNA copy number (Table S1).

Subsequently, mitochondria isolated from a human peripheral blood mononuclear cell lot (PBMC1) were transferred into fresh ρ0 fibroblasts, followed by an empirical and reproducible selection protocol with uridine-deficient galactose medium. From 5–10 BJ fibroblasts, NDFs, or ADFs, ρ0+PBMC1 SIMR clones were isolated that showed the correct mtDNA-nDNA sequence pairs and human leukocyte antigen (HLA) recipient cell haplotypes (Figures 2A–2C). Primary, non-immortal SIMR clones were also obtained from independent PBMC2 and HEK293T cell mitochondrial transfers. We observed variable efficiencies for HEK293T cell and the PBMC2 mitochondrial transfers, whereas ADFs ρ0+PBMC2 did not yield clones (Figure S1E). Analysis of the bulk culture representing 23 BJ ρ0+HEK293T SIMR clones confirmed the correct mtDNA-nDNA pairing and HLA haplotype (Figures S1F and S1G).

We examined the respiratory function of BJ ρ0+PBMC1 and BJ ρ0+HEK293T SIMR fibroblasts by Seahorse assay, which showed statistically improved basal and maximal respiration and spare respiratory capacity for both SIMR cell types compared to BJ ρ0 fibroblasts, albeit remaining lower than levels for control BJ fibroblasts (Figures 2D and S1H). Immunofluorescence (IF) microscopy showed BJ ρ0 fibroblasts with a fragmented mitochondrial network morphology lacking mtDNA-containing nucleoids, as observed previously for ρ0 cells (Kukat et al., 2008) (Figure 2E). In contrast, native BJ fibroblasts showed a reticular mitochondrial network with dozens of nucleoids per cell (Figure 2E). By IF nucleoid speckle numbers, both BJ ρ0+PBMC1 and BJ ρ0+HEK293T SIMR cells appeared to restore mtDNA content to levels equivalent to or exceeding that of native BJ fibroblasts (Figures 2E and S1I). SIMR cell mitochondria showed a reticular mitochondrial network morphology similar to that of native BJ fibroblasts, although with denser and more swollen mitochondria (Figures 2E and S1I). Despite SIMR fibroblasts permanently retaining donor mtDNA, OCR and IF suggest that assimilation of transferred mtDNA results in cells with features in between those of BJ ρ0 and native BJ fibroblasts.

SIMR Fibroblasts Are Reprogrammable

We reprogrammed BJ ρ0+PBMC1 and BJ ρ0+HEK293T SIMR fibroblasts along with native BJ fibroblasts using *OCT4*, *SOX2*, *KLF4*, *cMYC*, *NANOG*, and *LIN28* RNAs and quantified for TRA-1-60$^+$ staining clones. In two independent experiments, native BJ fibroblasts yielded an average of 136 reprogrammed TRA-1-60$^+$ clones (0.068% efficiency), compared to 21 (0.011%) and three (0.0015%) clones for BJ ρ0+PBMC1 and BJ ρ0+HEK293T cells, respectively (Figures 3A and S1J). Three unique reprogrammed clones of BJ ρ0+PBMC1-iPSCs (1, 2, and 11) and BJ ρ0+HEK293T-iPSCs (1, 2, and 4) were tested for pluripotency biomarkers and stained positive for OCT3/4 and SOX2 transcription factors by flow cytometry, as did BJ-induced pluripotency stem cell (iPSC) control, but not native BJ fibroblasts, as expected (Figures 3B and S1K). Conversely, the differentiated cell biomarker CD44 (Quintanilla et al., 2014) was negative in all reprogrammed BJ ρ0+PBMC1-iPSC, BJ ρ0+HEK293T-iPSC, and control BJ-iPSC clones and immunostained only the native BJ fibroblasts

(D) OCR measurements for ~1.5 × 10^4 L929 ρ0 and L929 ρ0 SIMR cells generated with mitochondria from C57BL/6 mouse tissues. Data are the means ± SD of 12 technical replicates (L929 ρ0 cells had four technical replicates).
(E) OCR measurements for ~1.5 × 10^4 L929 ρ0 and L929 ρ0 SIMR cells generated by transferring isolated mitochondria alone or in combinations from mouse cybrids with non-overlapping mtDNA mutations (Mito 1, Mito 2, and Mito 3). Data are the means ± SD of eight technical replicates.
Statistical significance for (B)–(E) by unpaired, two-tailed Student's t test. *p ≱ 0.05; **p ≱ 0.01; ***p ≱ 0.001; ****p ≱ 0.0001. See also Figure S1.

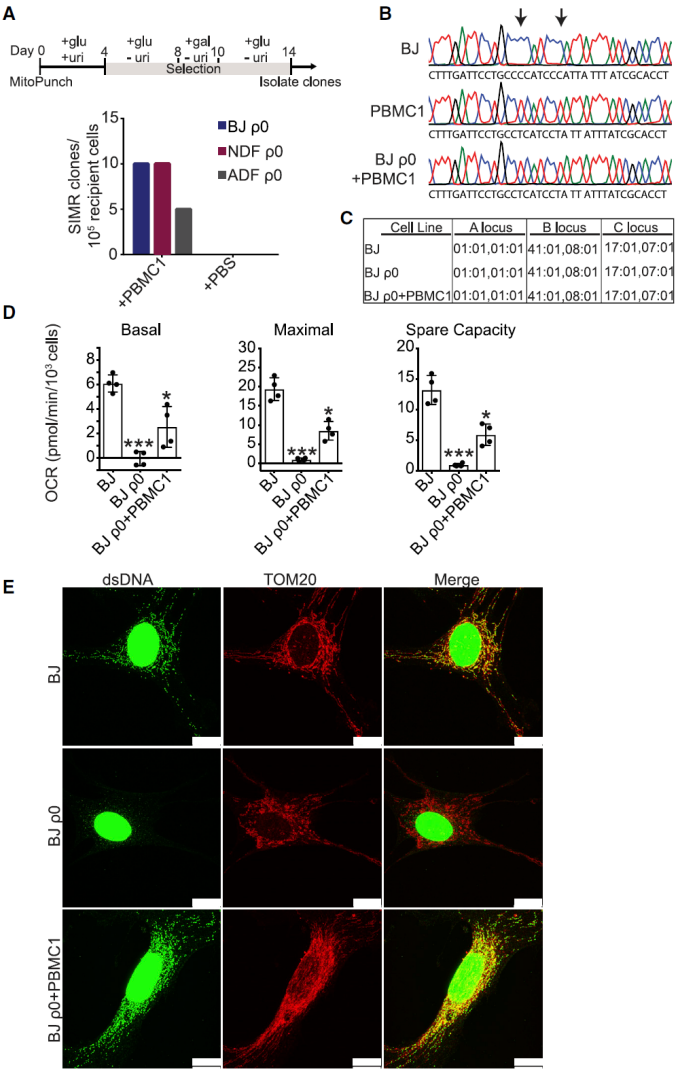

Figure 2. Generation of SIMR Fibroblasts

(A) Selection workflow (in days) for generating SIMR cells from ρ0 primary human fibroblasts and SIMR clone generation efficiency data. Mitochondria from ~3 × 10^7 peripheral blood mononuclear cells (PBMC1) were MitoPunch transferred into BJ ρ0, NDF ρ0, or ADF ρ0 recipient fibroblasts. After selection, SIMR colonies were stained with crystal violet and quantified. Clone counts from a single representative mitochondrial transfer into ~1 × 10^5 recipient ρ0 fibroblasts are indicated.

(B) D-loop hypervariable region mtDNA sequences from native BJ, PBMC1, and BJ ρ0+PBMC1 SIMR fibroblasts. Arrows denote single-nucleotide polymorphisms.

(C) Major histocompatibility complex (MHC) class I HLA A, B, and C locus genotyping using Opti-Type v.1.3.1 for native BJ, BJ ρ0, and BJ ρ0+PBMC1 SIMR fibroblasts.

(D) OCR measurements for ~1.5 × 10^4 native BJ, BJ ρ0, and BJ ρ0+PBMC1 SIMR fibroblasts by the Seahorse XF96 Extracellular Flux Analyzer. Values were calculated by standard procedures (see STAR Methods). Data are the means ± SD of four technical replicates. Statistical significance by unpaired, two-tailed Student's t test. *p ≤ 0.05; ***p ≤ 0.001

(E) Representative images of native BJ, BJ ρ0, and BJ ρ0+PBMC1 SIMR fibroblasts immunostained for double-stranded DNA (dsDNA) (green) and TOM20 (red) with colocalization indicated (yellow). Images (100×) were acquired on a Leica SP8 confocal microscope. Scale bars, 15 μm.

See also Figure S1 and Table S1.

(Figures 3B and S1K). BJ-iPSC and all SIMR-iPSC reprogrammed clones were also SSEA-4+ (Abujarour et al., 2013) and OCT4+ by IF (Figures 3C and S1L). Seahorse assays of BJ ρ0+PBMC1-iPSC and BJ ρ0+HEK293T-iPSC clones showed minimal or no statistical differences in basal respiration, maximal respiration, and spare respiratory capacity compared to the native BJ-iPSC control (Figures 3D and S1M). Thus, SIMR fibroblast reprogramming generated iPSCs with donor mtDNA.

Other studies have shown iPSC reprogramming of fibroblasts from individuals with pathogenic mtDNA mutations (Cherry et al., 2013; Folmes et al., 2013; Hämäläinen et al., 2013; Kang et al., 2016; Kodaira et al., 2015; Ma et al., 2015; Matsubara et al., 2018; Pek et al., 2019; Perales-Clemente et al., 2016; Russell et al., 2018; Yang et al., 2018), but this has not been attempted for SIMR fibroblasts with donated, non-native mutant mtDNA. Therefore, mitochondria containing an A3243G MELAS mtDNA mutation or WT mtDNA were isolated, followed by MitoPunch transfer into BJ ρ0 fibroblasts and selection. BJ ρ0+MELAS SIMR fibroblasts showed impaired proliferation during reprogramming and did not yield iPSCs (data not shown). Therefore, we switched to NDF ρ0 recipient fibroblasts and generated SIMR fibroblasts using isolated MELAS (NDF ρ0+MELAS), WT (NDF ρ0+WT), or NDF (NDF ρ0+NDF) mitochondria. Seahorse assays showed that NDF ρ0+MELAS fibroblasts had a significant reduction in basal respiration, maximal respiration, and spare respiratory capacity compared to native NDF, NDF ρ0+NDF, and NDF ρ0+WT

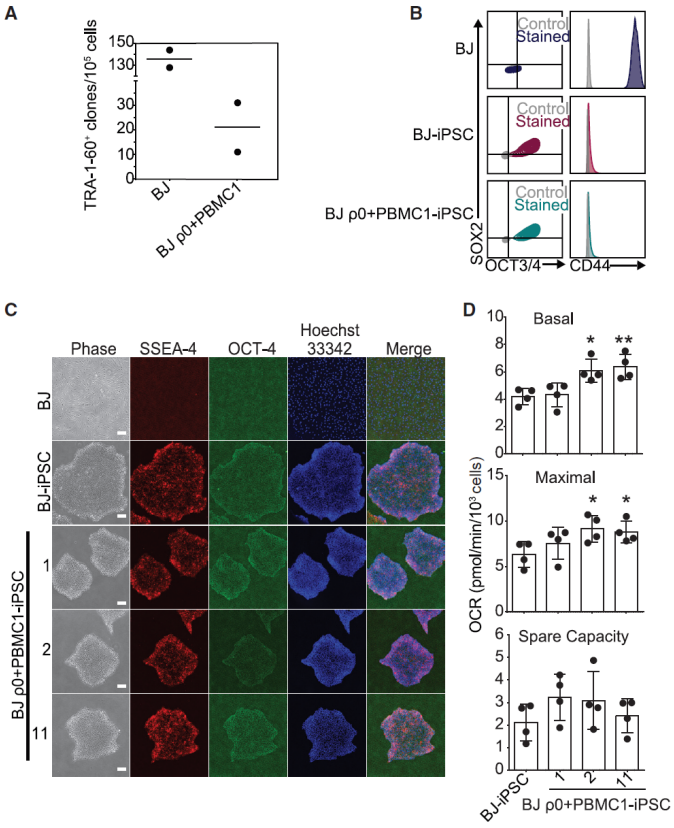

Figure 3. SIMR Fibroblasts Can Be Reprogrammed

(A) Native BJ and SIMR fibroblasts reprogrammed to iPSCs with TRA-1-60$^+$ clones counted by microscopy. Data are the means of biological duplicates. Data for BJ fibroblast control are the same data as in Figure S3A.

(B) Flow cytometry of pluripotency biomarkers SOX2 and OCT3/4, and fibroblast biomarker CD44. Immunostained samples are shown in color with isotype negative controls in gray. Representative data for native BJ fibroblasts and BJ-iPSCs, and for BJ ρ0+PBMC1-iPSC cells. Data for the native BJ fibroblasts and BJ-iPSCs shown here are the same as in Figure S3B.

(C) Representative phase contrast and IF microscopy images of native BJ fibroblast (negative control), BJ-iPSC (positive control), and three BJ ρ0+PBMC1-iPSC clones immunostained for pluripotency biomarkers SSEA-4 and OCT4. Scale bars, 100 μm.

(D) OCR measurements for ~1.5 × 10^4 native BJ-iPSCs and BJ ρ0+PBMC1-iPSC clones 1, 2, and 11. Data for BJ-iPSC control are the same as in Figure S3D. Data are the means ± SD of four technical replicates. Statistical significance by unpaired, two-tailed Student's t test. *p ≦ 0.05; **p ≦ 0.01

See also Figure S1 and Table S2.

fibroblasts (Figure S1N). Restriction fragment length polymorphism (RFLP) PCR analyses confirmed the generation of homoplasmic NDF ρ0+MELAS SIMR fibroblasts (Figure S1O). We also generated ~25%–50% heteroplasmic NDF ρ0+MELAS/WT fibroblasts, which was verified by RFLP analyses (Figure S1O). Homoplasmic NDF ρ0+MELAS fibroblasts underwent RNA-based reprogramming as described earlier, but all developing iPSC clones spontaneously differentiated (Figure S1P). Reprogramming of NDF ρ0+MELAS/WT heteroplasmic fibroblasts (Figures S1O) yielded 20 iPSC clones, but all clones retained only WT mtDNA by RFLP analysis (Figures S1P and S1Q). To examine whether the reprogramming method influenced mutant mtDNA SIMR-iPSC generation, NDF ρ0+MELAS fibroblasts underwent integrating DNA, lentiviral, and Sendai virus reprogramming strategies. In all cases, NDF ρ0+MELAS cells spontaneously differentiated despite early signs of reprogramming (Table S2). In addition, no NDF ρ0+MELAS-iPSCs were obtained when reprogramming was performed with additional uridine supplementation, antioxidant N-acetylcysteine, a Rho-associated protein kinase (ROCK) inhibitor, or low oxygen tension (data not shown). Similar results were also obtained with all four reprogramming strategies for NDF ρ0 SIMR fibroblasts containing additional mtDNA mutations including a cytochrome B deletion, a Kearns-Sayre common deletion, and A8344G or T8993G mtDNA substitutions (Table S2). Thus, SIMR fibroblasts readily maintain a large variety of mtDNA sequences, in contrast to SIMR-iPSCs, which can be generated only with non-detrimental mtDNA sequences. Further biochemical investigations are needed to determine how mtDNA sequences dictate SIMR reprogramming, whereas native mutant mtDNA fibroblasts can be reprogrammed (Hämäläinen et al., 2013; Ma et al., 2015; Pek et al., 2019).

SIMR-iPSCs Produce Functional, Differentiated Cell Types

We next determined whether SIMR-iPSCs with isogenic nuclei and non-native donor mtDNAs could differentiate. We chose to examine defined medium differentiation of mesenchymal stem cells (MSCs) because of their relevance to potential therapies and current use in over 850 clinical trials (Hsu et al., 2016). A BJ-iPSC control, BJ ρ0+PBMC1-iPSCs, and BJ ρ0+HEK293T-iPSCs were differentiated into MSCs and validated with an antibody panel against surface biomarkers established by the International Society for Cellular Therapy (ISCT) (Dominici et al., 2006). Flow cytometry verified that the BJ-MSC control, BJ

ρ0+PBMC1-MSC clones, and BJ ρ0+HEK293T-MSC clones were positive for MSC biomarkers CD73, CD90, and CD105, and negative for a cocktail of non-MSC biomarkers, including CD11b, CD19, CD34, CD45, and HLA-DR (Figures 4A and S1R). BJ-MSCs and all SIMR-MSC clones from both mtDNA donors adhered to plastic, consistent with ISCT criteria for MSCs (Figures 4B and S1S).

Seahorse assays of BJ-MSC control, BJ ρ0+PBMC1-MSC clones, and BJ ρ0+HEK293T-MSC clones revealed no or mild differences in basal respiration, maximal respiration, and spare respiratory capacity, indicating that respiratory changes are mutable for ρ0 fibroblasts after MitoPunch with reprogramming and differentiation (Figures 4C and S1T). Quantitative phase microscopy (QPM) was used to examine key cellular biophysical properties in SIMR MSCs and detected minimal to no differences in cell growth rate, area, and biomass among the BJ-MSC control, BJ ρ0+PBMC1-MSC clones, and BJ ρ0+HEK293T-MSC clones (Figures 4D and S1U). The function of SIMR-MSC clones and the BJ-MSC control was compared by co-culture with human PBMC-isolated T cells in a standard immunosuppression assay, which measures MSC clinical immunomodulatory performance (Djouad et al., 2003; Ghannam et al., 2010). All BJ ρ0+PBMC1-MSC and BJ ρ0+HEK293T-MSC clones repressed T cell proliferation (Figures 4E and S1V). BJ ρ0+PBMC1-MSC clone 11 showed the greatest immunosuppression and reduction in T cell proliferation, whereas no large differences were detected between the remaining SIMR-MSC clones and the BJ-MSC control. Finally, we performed directed trilineage differentiation of SIMR-MSCs into adipocytes, osteoblasts, and chondrocytes to demonstrate the clinical potential of MitoPunch-engineered lines. The BJ-MSC control, BJ ρ0+PBMC1-MSCs, and BJ ρ0+HEK293T-MSCs all formed these three MSC-differentiated lineages (Figures 4F and S1W). Adipocytes and chondrocytes were phenotypically similar between the BJ control and SIMR clones, whereas SIMR osteoblasts tended to qualitatively produce more calcium deposits. Thus, our mitochondrial transfer strategy enables the generation of iPSCs, MSCs, and further differentiated cell types from ρ0 fibroblasts by stable incorporation of specific, non-detrimental, and non-native donor mtDNAs.

SIMR Cell Metabolism and RNA Transcript Changes with Fate Transitions

We used ultra-high-performance liquid chromatography-mass spectrometry (UPHLC-MS) to quantify 154 steady-state metabolites in native BJ, BJ ρ0, BJ ρ0+PBMC1 clones, and BJ ρ0+HEK293T clones at fibroblast, iPSC, and MSC fates. Hierarchical clustering showed distinct, grouped profiles for fibroblasts, iPSCs, and MSCs independent of mitochondrial transfer status (Figures S2A and S2B; Table S3). Principal component analysis (PCA) of metabolite data also showed three main clusters representing fibroblast, iPSC, and MSC fates but no clear differences between SIMR and native control cells within each fate (Figures S2C and S2D). Metabolite set variation analysis (MSVA) and Euclidean distance analysis of the BJ ρ0+PBMC1-iPSC and BJ ρ0+PBMC1-MSC clones showed similar metabolite pathway profiles to themselves and to their respective BJ-iPSC and BJ-MSC controls (Figures S2A, S2E, and S2F). In contrast, BJ ρ0+HEK293T-iPSC clones 1 and 2 clustered separately from clone 4 and the BJ-iPSC control for several metabolic pathways, particularly purine, pyrimidine, glutathione, and ethanol metabolism (Figures S2B, S2E, and S2F). This separation in BJ ρ0+HEK293T-iPSC clones was no longer present upon further differentiation to BJ ρ0+HEK293T-MSC clones (Figures S2B, S2E, and S2F). In summary, steady-state metabolite analyses showed that SIMR cells are comparable to native control cells, with only a few differences that are resolved upon iPSC reprogramming and differentiation to MSCs.

We utilized RNA sequencing (RNA-seq) to evaluate whole-transcriptome profiles for SIMR cells at fibroblast, iPSC, and MSC fates. DESeq2 was used to identify significant differentially expressed genes (DEGs), defined as genes showing an absolute log 2-fold change > 0.5 and adjusted $p < 0.05$. For both BJ ρ0+PBMC1 and BJ ρ0+HEK293T SIMR cells, the greatest number of DEGs compared to native BJ control cells with an adjusted $p < 0.05$ occurred at the fibroblast fate (Figures 5A and S3A). RNA-seq identified 1741, 194, and 224 elevated and 1827, 68, and 115 repressed DEGs by comparing BJ ρ0+PBMC1 cells to native BJ parent cells at the fibroblast, iPSC, and MSC fates, respectively (Figure 5A; Table S4). Transcriptomic analysis of the independently generated BJ ρ0+HEK293T cells similarly identified 1,377, 537, and 239 elevated and 1,564, 648, and 210 repressed DEGs compared to native BJ parent cells at fibroblast, iPSC, and MSC fates, respectively (Figure S3A; Table S4).

Reactome pathway enrichment analysis of DEGs showed diverse pathways altered in SIMR fibroblast transcript profiles compared to those in native BJ fibroblasts, including those associated with extracellular matrix organization and the complement cascade (Figure S3B; Table S5). Differential expression and pathway enrichment analyses comparing all SIMR-iPSCs and SIMR-MSCs to native BJ-iPSC and BJ-MSC controls, respectively, identified a dramatically smaller number of DEGs, with overrepresented pathways driven primarily by a cluster of histone transcripts (Figures S3C and S3D; Table S5).

Further detailed transcriptome analyses uncovered metabolic pathway differences based on cell condition and fate. Somatic cell reprogramming to iPSCs requires a metabolic shift from predominantly oxidative phosphorylation to mainly glycolysis, which corresponds with all BJ ρ0+PBMC1-iPSC and BJ ρ0+HEK293T-iPSC clones showing elevated expression of glycolysis-associated transcripts by gene set variation analysis (GSVA) (Figures S4A and S4B). Additionally, GSVA showed increased expression of ETC transcripts in BJ ρ0, BJ ρ0+PBMC1, and BJ ρ0+HEK293T SIMR fibroblasts compared to that in native BJ fibroblasts (Figures S4A and S4B). However, immunoblots for succinate dehydrogenase (SDHB; complex II), ubiquinol-cytochrome *c* reductase core protein 2 (UUQCRC2; complex III), cytochrome C oxidase II (MT-COXII; complex IV), and ATP synthase F1 subunit alpha (ATP5A; complex V) demonstrated the opposite result, with ETC proteins in SIMR fibroblasts reduced compared to those in the native BJ fibroblast control (Figure S4C). Overall, whole-transcriptome data analysis showed that initial large differences between SIMR clones and native control cells at the fibroblast fate progressively dissipated during reprogramming and differentiation.

We examined the RNA transcript levels of 1,158 nuclear genes listed in the MitoCarta2.0 database that encode proteins that

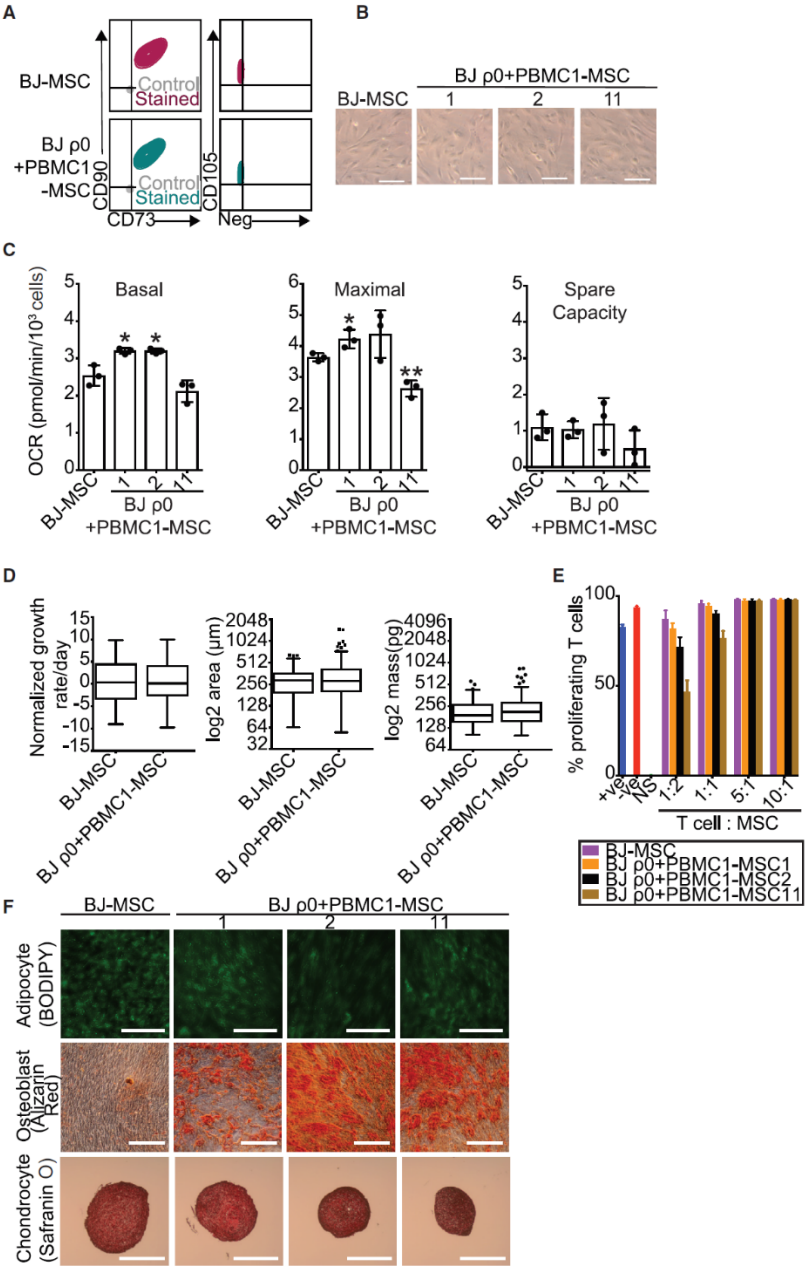

(legend on next page)

localize to the mitochondria. Hierarchical clustering analysis of transcripts from these genes identified a separation of BJ ρ0+PBMC1, BJ ρ0+HEK293T, and BJ ρ0 transcripts away from the native BJ transcripts at the fibroblast fate (Figures 5B and S3B). Pathway analysis of DEGs between these two groups showed an enrichment for genes encoding ETC proteins in the native BJ fibroblasts (Table S4). Of note, this differential clustering was not observed at the iPSC and MSC fates (Figures 5B and S5A).

Closer examination of mtDNA-encoded transcripts only demonstrated, as anticipated, that BJ ρ0 cells have dramatically lowered expression of all 13 coding gene transcripts compared to transcripts from SIMR and native fibroblast cells (Figures 5C and S5B). Additionally, both BJ ρ0+PBMC1 and BJ ρ0+HEK293T fibroblasts showed significantly reduced expression of the 13 mtDNA-encoded genes compared to native BJ fibroblasts (Figures 5C and S5B). By contrast, no significant difference was observed in mtDNA transcript levels after reprogramming SIMR and control fibroblasts to iPSCs, followed by differentiation to MSCs (Figures 5C and S5B).

We then used the MitoXplorer pipeline (Yim et al., 2020) to quantify the representation of 38 distinct mitochondrial processes within the identified DEGs. As anticipated from abolished respiration, BJ ρ0 fibroblasts showed DEGs for 29 mitochondrial processes compared to native BJ fibroblasts, especially within oxidative phosphorylation, mitochondrial genome translation, and amino acid metabolism processes (Figure 5D). Similarly, BJ ρ0+PBMC1 and BJ ρ0+HEK293T fibroblasts had altered gene expression profiles in 30 and 29 mitochondrial processes, respectively, in comparison to native BJ fibroblasts (Figures 5D and S5C). Further analysis at this fate using MitoXplorer highlighted differences between the two SIMR lines, as the BJ ρ0+PBMC1 had fewer DEGs for mtDNA-associated oxidative phosphorylation and mitochondrial genome translation compared to BJ ρ0+HEK293T fibroblasts. Furthermore, both SIMR fibroblast lines had more DEGs associated with nuclear-encoded mitochondrial translation and calcium signaling and transport than the BJ ρ0 line, when compared to native BJ fibroblasts. Of note, the number of affected mitochondrial processes was dramatically reduced by reprogramming, with only 7 and 16 processes exhibiting DEGs in BJ ρ0+PBMC1-iPSCs and BJ ρ0+HEK293T-iPSCs, respectively (Figures 5D and S5C). Finally, BJ ρ0+PBMC1-MSCs and BJ ρ0+HEK293T-MSCs exhibited only 3 and 8 mitochondrial processes with DEGs, respectively, with only ROS defense similarly altered between the two SIMR-MSC lines and MSC control (Figures 5D and S5C). These data uncover transcriptomic alterations to translation, among additional mitochondrial processes, at the fibroblast fate as a potential difference maker for exogenous mtDNA function in SIMR cells. Combined, the results show that, although SIMR cell mitochondrial function becomes more similar to that of the BJ control with reprogramming and differentiation, differences still exist that are based on the transferred mtDNA sequence.

DISCUSSION

Here, we use MitoPunch to report on a rapid, versatile pipeline to generate transformed or non-immortal cells with specific mtDNA-nDNA combinations, an advance with certain advantages over cybrid technology (Patananan et al., 2016; Wong et al., 2017), uncontrolled selection in physiologic mitochondrial "bottlenecks" (Latorre-Pellicer et al., 2019), or time-consuming screens for cells with desired mtDNA mutations (Fayzulin et al., 2015; Lorenz et al., 2017). We show that the transcriptome and metabolome of SIMR fibroblasts resemble those of ρ0 matched recipient cells and that reprogramming to pluripotency followed by differentiation resets these profiles to closely resemble those of unmanipulated control cells. Our studies would be difficult or impossible using other mitochondrial transfer approaches, such as those that use immortal cell lines incapable of reprogramming. Although it is also possible to generate SIMR cells with the nanoblade and microinjection, these low-throughput methods suffer practical and experimental limitations. In contrast, MitoPunch is an accessible approach to generate numerous clones with desired, stable mtDNA-nDNA combinations within 2 weeks.

SIMR clone formation was achieved for all ρ0 recipient fibroblasts studied. Of note, some mtDNA-nDNA combinations produced SIMR clones at lower efficiencies than other combinations, which could only be detected using a high-throughput platform like MitoPunch. In contrast to 143BTK− ρ0+HEK293T

Figure 4. SIMR iPSCs Produce MSCs with Trilineage Differentiation Potential

(A) Flow cytometry of MSC biomarkers CD73, CD90, and CD105, and a cocktail of negative MSC biomarkers. Immunostained samples are indicated in color, with isotype negative controls in gray. Data for BJ-MSC control are the same data as in Figure S5A. Representative clones for native BJ-MSCs and BJ ρ0+PBMC1-MSCs are indicated.

(B) Bright-field microscopy showing unmanipulated BJ-MSC and BJ ρ0+PBMC1-MSC clones 1, 2, and 11 adhering to plastic at 20× magnification (scale bars, 100 μm). Data for BJ-MSC control are the same data as in Figure S5B.

(C) OCR measurements for ~1.5 × 10^4 native BJ-MSCs and BJ ρ0+PBMC1-MSC clones 1, 2, and 11. Data for BJ-MSC control are the same as in Figure S5C. Data are the means ± SD of three technical replicates. Statistical significance by unpaired, two-tailed Student's t test. *$p \not\leq 0.05$; **$p \not\leq 0.01$.

(D) Quantitative phase microscopy of native BJ-MSCs and a 1:1:1 mix of BJ ρ0+PBMC1-MSC clones 1, 2, and 11. Data for BJ-MSC control are the same as in Figure S5D. Shown are box-and-whisker Tukey plots with outliers identified. Data were averaged from 77 and 172 cells for native BJ-MSCs and BJ ρ0+PBMC1-MSCs, respectively. Statistical significance by Welch's t test.

(E) T cells were added into native BJ-MSC or BJ ρ0+PBMC1-MSC clone 1, 2, or 11 cultures at 1:2, 1:1, 5:1, and 10:1 T cell:MSC ratios. After 5 days of co-culture, T cell proliferation was measured using a CFSE dye dilution assay by flow cytometry. The data labeled "NS" (no stimulus) denote T cells without CD3/CD28 bead activation. The data labeled "-ve" (negative) denote no addition of MSCs to stimulated T cells. The data labeled "+ve" (positive) denote a 1:1 addition of myeloid-derived suppressor cells to T cells. Data are the means ± SD of three technical replicates.

(F) Trilineage differentiation of native BJ-MSCs and BJ ρ0+PBMC1-MSC clones 1, 2, and 11. Representative sections were fixed and stained with 1 μM Bodipy 493/503, 1% alizarin red S, and 0.1% Safranin O, respectively. Shown are adipocytes (first row, 20×; scale bars, 100 μm), osteocytes (second row, 20×; scale bars, 200 μm), and chondrocytes (fourth row, 5×; scale bars, 500 μm).

See also Figure S1.

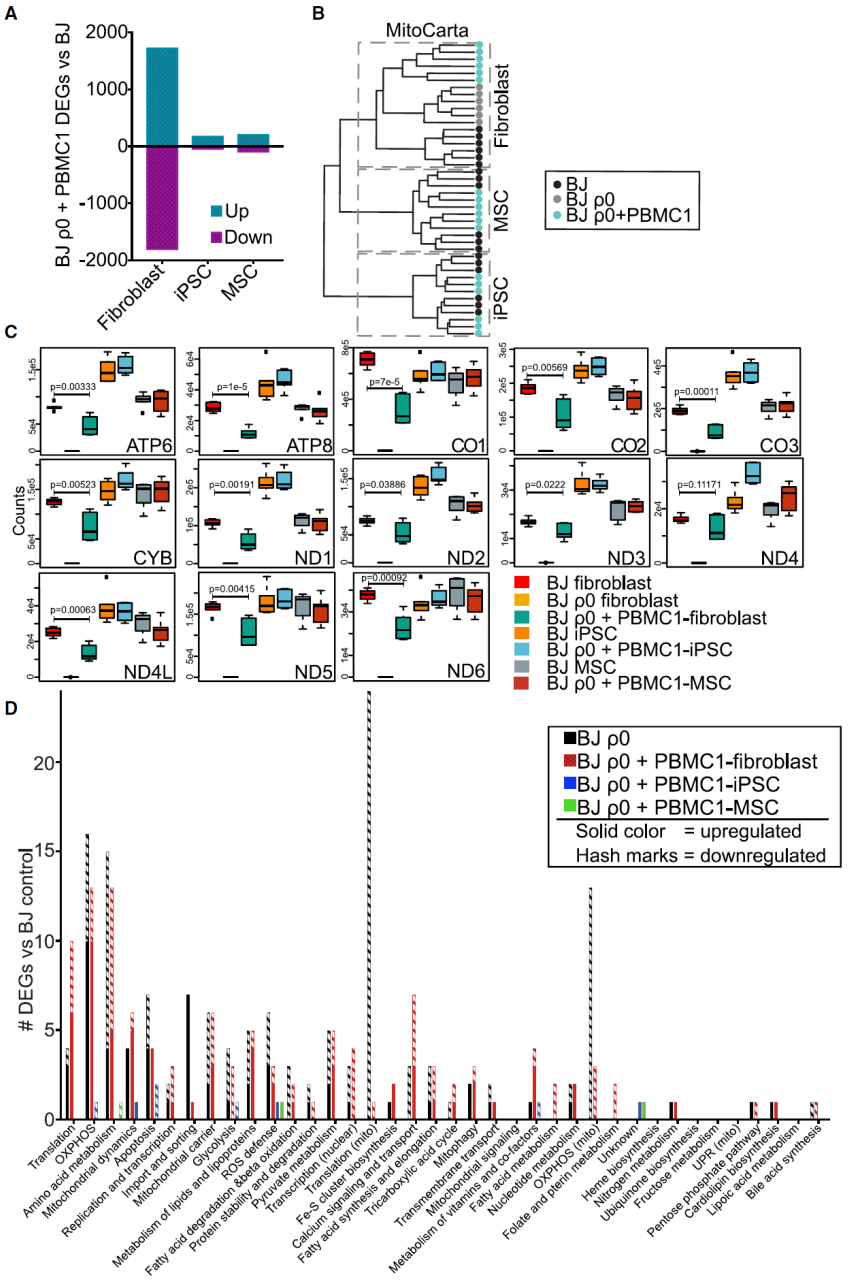

(legend on next page)

SIMR cells that produced ~75 clones, MitoPunch transfers into primary fibroblasts yielded fewer SIMR clones, possibly related to the Hayflick limit or a sub-optimal response to the MitoPunch procedure. For example, ADF ρ0 recipients grew the slowest, reached senescence shortly after mtDNA depletion (data not shown), and resulted in the fewest SIMR clones. On average, twice as many BJ ρ0+HEK293T clones were obtained compared to BJ ρ0+PBMC1 clones, which may be from a more compatible mtDNA-nDNA pairing and more favorable metabolic profile (Latorre-Pellicer et al., 2016). SIMR fibroblasts also showed a 10-fold reduction in reprogramming efficiency compared to native fibroblast controls. A similar reduction was observed in mouse embryo fibroblast reprogramming with non-native mtDNA, perhaps from a lower mtDNA-nDNA compatibility (Latorre-Pellicer et al., 2019).

Evidence for incomplete mtDNA-nDNA assimilation in SIMR fibroblasts was observed in transcriptome data that showed hundreds of DEGs between SIMR and unmanipulated fibroblasts. Also, MitoCarta2.0- and mtDNA-encoded transcripts were most similar for SIMR and ρ0 fibroblasts, despite SIMR cell culture in restrictive medium requiring ETC activity for growth and survival. These data suggest that exogenous mtDNA in SIMR fibroblasts do not fully communicate and influence the nDNA, despite being able to support a selectable level of ETC activity and adequate synthesis of metabolites for cell proliferation. Supporting evidence for this suggestion includes that ddC exposure yielded minimal nDNA damage and that the metabolome and transcriptome profiles of SIMR fibroblasts are mostly reset to unmanipulated BJ-iPSC profiles in SIMR-iPSCs. Our results agree with a report showing that ρ0 cells have altered metabolism and an epigenome that can only be partially reset by cybrid formation (Smiraglia et al., 2008). Our study provides a platform for investigating the resetting of ρ0 cell transcription and metabolism after stable mtDNA transplantation and subsequent cell fate changes. Further work is needed to determine whether cells that receive exogenous mtDNA by other forms of mitochondrial transfer also have disrupted mtDNA transcription profiles.

In summary, we provide a proof-of-principle mitochondrial transfer pipeline to generate cells of different fates with specific mtDNA-nDNA combinations, including clonal lines with genome pairings not found in nature. Future studies will generate SIMR-derived cells representing high-energy-demand tissues, such as cardiomyocytes or neurons, and will investigate the current inability to generate SIMR-iPSCs containing mutant mtDNAs to enable patient-specific disease and drug screening models with isogenic nuclei for mtDNA diseases. Furthermore, our results show that the interpretation of mitochondrial transfer experiments must consider that cells initially generated may not show complete mtDNA-nDNA integration and subsequent restoration of cellular pathways. This is particularly salient for cells that lack subsequent reprogramming potential, such as transient or transformed mitochondrial transfer cell lines, since our results show that reprogramming and differentiation are required for resetting the nDNA expression profile. Finally, this mitochondrial transfer pipeline bypasses the evolutionary pairwise selection of mtDNAs and nDNAs in cells to expand upon the repertoire of genomic combinations present in the human population and generates a library of cells at various fates with defined mtDNA-nDNA combinations and unique functional properties for research and potential therapeutic applications.

STAR★METHODS

Detailed methods are provided in the online version of this paper and include the following:

- KEY RESOURCES TABLE
- RESOURCE AVAILABILITY
  - Lead Contact
  - Materials Availability
  - Data and Code Availability
- EXPERIMENT MODEL AND SUBJECT DETAILS
  - Cell Lines
  - Human Tissues
- METHOD DETAILS
  - mtDNA Depletion and qPCR Verification
  - Mitochondrial Transfer into ρ0 Recipients
  - Confocal microscopy
  - Mitochondrial Oxygen Consumption Measurements
  - Mitochondrial Isolation from Mouse Tissues and Delivery
  - iPSC Reprogramming
  - MSC Differentiation
  - Human mtDNA D-Loop Sequencing
  - ROS Quantification
  - iPSC Flow Cytometry
  - MSC Flow Cytometry
  - Fluorescence Microscopy
  - MSC Immunosuppression Assay
  - Tri-lineage Differentiation
  - Tri-lineage Differentiation Analyses
  - UPHLC-MS Metabolomics Processing
  - RNA Extraction
  - RNA-Seq Library Preparation
  - Restriction-Fragment Length Polymorphism Heteroplasmy Assay

Figure 5. Transcriptome Features of SIMR and Native mtDNA Cells

(A) Number of DEGs for BJ ρ0+PBMC1 cells compared to native BJ cells at fibroblast, iPSC, and MSC fates.

(B) Hierarchical clustering of nuclear-encoded MitoCarta2.0 database genes from native BJ, BJ ρ0, and BJ ρ0+PBMC1 cells at fibroblast, iPSC, and MSC fates.

(C) Normalized, batch-adjusted read counts shown as box-and-whisker Tukey plots for 13 MitoCarta2.0-annotated mtDNA-encoded genes for native BJ, BJ ρ0, and BJ ρ0+PBMC1 cells at the fibroblast, iPSC, and MSC fates. Statistical significance was by Welch's t test.

(D) MitoXplorer-categorized DEGs for BJ ρ0+PBMC1 compared to native BJ cells at the fibroblast, iPSC, and MSC fates divided into the 38 mitochondrial processes.

See also Figures S2, S3, S4, and S5 and Tables S3, S4, and S5.

SUPPLEMENTAL INFORMATION

Supplemental Information can be found online at https://doi.org/10.1016/j.celrep.2020.108562.

ACKNOWLEDGMENTS

A.N.P. is supported by the NIH (T32CA009120) and American Heart Association (18POST34080342). A.J.S. is supported by the NIH (T32GM007185 and T32CA009120). K.P. is supported by the Broad Center of Regenerative Medicine and Stem Cell Research at UCLA, the David Geffen School of Medicine, the NIH (P01GM099134), and a Faculty Scholar grant from the HHMI. M.A.T. is supported by the Air Force Office of Scientific Research (FA9550-15-1-0406), the NIH (R01GM114188, R01GM073981, R01CA185189, R21CA227480, R01GM127985, and P30CA016042), and CIRM (RT3-07678). We thank Rebeca Acin-Perez, Linsey Stiles, and Orian Shirihai of the UCLA Metabolomics Core for help with Seahorse XF Analyzer assays. We thank Felicia Codrea from the UCLA Flow Cytometry Core, in addition to Laurent Bentolila and Matthew Schibler from the California Nanosystems Institute Advanced Light Microscopy/Spectroscopy Laboratory for their insight and assistance. We thank Jonathan Wanagat for his critical insights during manuscript preparation. We also acknowledge Drs. Idoya Lahortiga and Luk Cox for their Library of Science and Medical Illustrations (https://www.somersault1824.com/).

AUTHOR CONTRIBUTIONS

Conceptualization: A.N.P., A.J.S., T.-H.W., S.R., K.R.N., and M.A.T.; Methodology: A.N.P., A.J.S., T.-H.W., F.M.A., A.M., J.V.L., S.R., K.R.N., P.-Y.C., and M.A.T.; Software: T.L.N., F.M.A., A.V., J.G., and D.B.; Formal Analysis: A.N.P., A.J.S., F.M.A., A.V., T.L.N., and D.B.; Investigation: A.N.P., A.J.S., T.-H.W., F.M.A., A.V., S.A.L.K., T.N., A.T., A.J.C., E.R.D., A.M., J.V.L., L.Z., N.R., M.S., W.T., A.L., P.A.S., D.B., J.G., and C.V.; Resources: A.N.P., A.J.S., T.-H.W., and F.M.A.; Data Curation: A.N.P., F.M.A., A.V., D.B., and C.V.; Writing – Original Draft: A.N.P., A.J.S., and F.M.A.; Writing – Review & Editing: A.N.P., A.J.S., F.M.A., A.V., T.-H.W., K.R.N., and M.A.T.; Validation: A.N.P. and A.J.S.; Visualization: A.N.P., A.J.S., T.L.N., F.M.A., and A.V.; Supervision: A.N.P. and T.-H.W.; Project Administration: A.N.P. and T.-H.W.; Funding Acquisition: A.N.P., A.J.S., S.R., K.R.N., P.-Y.C., K.P., and M.A.T.

DECLARATION OF INTERESTS

M.A.T. and P.-Y.C. are co-founders, board members, shareholders, and consultants for NanoCav, a private start-up company working on mitochondrial transfer and quantitative phase microscopy techniques and applications. T.-H.W. was an employee of NanoCav and is employed by ImmunityBio, and S.R. and K.R.N. are board members of NanoCav and employed by ImmunityBio. The other authors report no competing interests.

Received: July 18, 2020
Revised: October 29, 2020
Accepted: December 6, 2020
Published: December 29, 2020

REFERENCES

Abujarour, R., Valamehr, B., Robinson, M., Rezner, B., Vranceanu, F., and Flynn, P. (2013). Optimized surface markers for the prospective isolation of high-quality hiPSCs using flow cytometry selection. Sci. Rep. *3*, 1179.

Ali Pour, P., Kenney, M.C., and Kheradvar, A. (2020). Bioenergetics Consequences of Mitochondrial Transplantation in Cardiomyocytes. J. Am. Heart Assoc. *9*, e014501.

Benjamini, Y., and Hochberg, Y. (1995). Controlling the false discovery rate - a practical and powerful approach to multiple testing. J. R. Stat. Soc. Series B Methodol. *57*, 289–300.

Calvo, S.E., Clauser, K.R., and Mootha, V.K. (2016). MitoCarta2.0: an updated inventory of mammalian mitochondrial proteins. Nucleic Acids Res. *44* (*D1*), D1251–D1257.

Campbell, J.M., Perales-Clemente, E., Ata, H., Vidal-Folch, N., Liu, W., Clark, K.J., Xu, X., Oglesbee, D., Nelson, T.J., and Ekker, S.C. (2018). Engineering targeted deletions in the mitochondrial genome. bioRxiv. https://doi.org/10.1101/287342.

Cherry, A.B., Gagne, K.E., McLoughlin, E.M., Baccei, A., Gorman, B., Hartung, O., Miller, J.D., Zhang, J., Zon, R.L., Ince, T.A., et al. (2013). Induced pluripotent stem cells with a mitochondrial DNA deletion. Stem Cells *31*, 1287–1297.

Chomyn, A., Martinuzzi, A., Yoneda, M., Daga, A., Hurko, O., Johns, D., Lai, S.T., Nonaka, I., Angelini, C., and Attardi, G. (1992). MELAS mutation in mtDNA binding site for transcription termination factor causes defects in protein synthesis and in respiration but no change in levels of upstream and downstream mature transcripts. Proc. Natl. Acad. Sci. USA *89*, 4221–4225.

Clark, M.A., and Shay, J.W. (1982). Mitochondrial transformation of mammalian cells. Nature *295*, 605–607.

Dawson, E.R., Patananan, A.N., Sercel, A.J., and Teitell, M.A. (2020). Stable retention of chloramphenicol-resistant mtDNA to rescue metabolically impaired cells. Sci. Rep. *10*, 14328.

Djouad, F., Plence, P., Bony, C., Tropel, P., Apparailly, F., Sany, J., Noël, D., and Jorgensen, C. (2003). Immunosuppressive effect of mesenchymal stem cells favors tumor growth in allogeneic animals. Blood *102*, 3837–3844.

Dominici, M., Le Blanc, K., Mueller, I., Slaper-Cortenbach, I., Marini, F., Krause, D., Deans, R., Keating, A., Prockop, D.j., and Horwitz, E. (2006). Minimal criteria for defining multipotent mesenchymal stromal cells. The International Society for Cellular Therapy position statement. Cytotherapy *8*, 315–317.

Elliott, H.R., Samuels, D.C., Eden, J.A., Relton, C.L., and Chinnery, P.F. (2008). Pathogenic mitochondrial DNA mutations are common in the general population. Am. J. Hum. Genet. *83*, 254–260.

Fayzulin, R.Z., Perez, M., Kozhukhar, N., Spadafora, D., Wilson, G.L., and Alexeyev, M.F. (2015). A method for mutagenesis of mouse mtDNA and a resource of mouse mtDNA mutations for modeling human pathological conditions. Nucleic Acids Res. *43*, e62.

Folmes, C.D.L., Martinez-Fernandez, A., Perales-Clemente, E., Li, X., McDonald, A., Oglesbee, D., Hrstka, S.C., Perez-Terzic, C., Terzic, A., and Nelson, T.J. (2013). Disease-causing mitochondrial heteroplasmy segregated within induced pluripotent stem cell clones derived from a patient with MELAS. Stem Cells *31*, 1298–1308.

Ghannam, S., Bouffi, C., Djouad, F., Jorgensen, C., and Noël, D. (2010). Immunosuppression by mesenchymal stem cells: mechanisms and clinical applications. Stem Cell Res. Ther. *1*, 2.

Grégoire, M., Morais, R., Quilliam, M.A., and Gravel, D. (1984). On auxotrophy for pyrimidines of respiration-deficient chick embryo cells. Eur. J. Biochem. *142*, 49–55.

Hämäläinen, R.H., Manninen, T., Koivumäki, H., Kislin, M., Otonkoski, T., and Suomalainen, A. (2013). Tissue- and cell-type-specific manifestations of

heteroplasmic mtDNA 3243A>G mutation in human induced pluripotent stem cell-derived disease model. Proc. Natl. Acad. Sci. USA *110*, E3622–E3630.

Hänzelmann, S., Castelo, R., and Guinney, J. (2013). GSVA: gene set variation analysis for microarray and RNA-seq data. BMC Bioinformatics *14*, 7.

Harrow, J., Frankish, A., Gonzalez, J.M., Tapanari, E., Diekhans, M., Kokocinski, F., Aken, B.L., Barrell, D., Zadissa, A., Searle, S., et al. (2012). GENCODE: the reference human genome annotation for The ENCODE Project. Genome Res. *22*, 1760–1774.

Hsu, P.J., Liu, K.J., Chao, Y.Y., Sytwu, H.K., and Yen, B.L. (2015). Assessment of the immunomodulatory properties of human mesenchymal stem cells (MSCs). J. Vis. Exp. (*106*), e53265.

Hsu, Y.C., Wu, Y.T., Yu, T.H., and Wei, Y.H. (2016). Mitochondria in mesenchymal stem cell biology and cell therapy: From cellular differentiation to mitochondrial transfer. Semin. Cell Dev. Biol. *52*, 119–131.

Huber, W., Carey, V.J., Gentleman, R., Anders, S., Carlson, M., Carvalho, B.S., Bravo, H.C., Davis, S., Gatto, L., Girke, T., et al. (2015). Orchestrating high-throughput genomic analysis with Bioconductor. Nat. Methods *12*, 115–121.

Husson, F. (2020). FactoMineR v2.2 (RDocumentation).

Kanehisa, M., Goto, S., Sato, Y., Furumichi, M., and Tanabe, M. (2012). KEGG for integration and interpretation of large-scale molecular data sets. Nucleic Acids Res. *40*, D109–D114.

Kang, E., Wang, X., Tippner-Hedges, R., Ma, H., Folmes, C.D., Gutierrez, N.M., Lee, Y., Van Dyken, C., Ahmed, R., Li, Y., et al. (2016). Age-related accumulation of somatic mitochondrial DNA mutations in adult-derived human iPSCs. Cell Stem Cell *18*, 625–636.

Kankainen, M., Gopalacharyulu, P., Holm, L., and Oresic, M. (2011). MPEA–metabolite pathway enrichment analysis. Bioinformatics *27*, 1878–1879.

Kassambara, A. (2017). R package ggpubr v0.1.6 (RDocumentation).

Kassambara, A. (2019). factoextra v1.0.6 (RDocumentation).

Kesner, E.E., Saada-Reich, A., and Lorberboum-Galski, H. (2016). Characteristics of Mitochondrial Transformation into Human Cells. Sci. Rep. *6*, 26057.

Kim, M.J., Hwang, J.W., Yun, C.K., Lee, Y., and Choi, Y.S. (2018). Delivery of exogenous mitochondria via centrifugation enhances cellular metabolic function. Sci. Rep. *8*, 3330.

Kitani, T., Kami, D., Matoba, S., and Gojo, S. (2014). Internalization of isolated functional mitochondria: involvement of macropinocytosis. J. Cell. Mol. Med. *18*, 1694–1703.

Kodaira, M., Hatakeyama, H., Yuasa, S., Seki, T., Egashira, T., Tohyama, S., Kuroda, Y., Tanaka, A., Okata, S., Hashimoto, H., et al. (2015). Impaired respiratory function in MELAS-induced pluripotent stem cells with high heteroplasmy levels. FEBS Open Bio *5*, 219–225.

Kolde, R. (2015). Package 'pheatmap' - Pretty Heatmaps (CRAN: R-Project).

Kukat, A., Kukat, C., Brocher, J., Schäfer, I., Krohne, G., Trounce, I.A., Villani, G., and Seibel, P. (2008). Generation of rho0 cells utilizing a mitochondrially targeted restriction endonuclease and comparative analyses. Nucleic Acids Res. *36*, e44.

Kumar, L., and Futschik, M.E. (2007). Mfuzz: a software package for soft clustering of microarray data. Bioinformation *2*, 5–7.

Latorre-Pellicer, A., Moreno-Loshuertos, R., Lechuga-Vieco, A.V., Sánchez-Cabo, F., Torroja, C., Acín-Pérez, R., Calvo, E., Aix, E., González-Guerra, A., Logan, A., et al. (2016). Mitochondrial and nuclear DNA matching shapes metabolism and healthy ageing. Nature *535*, 561–565.

Latorre-Pellicer, A., Lechuga-Vieco, A.V., Johnston, I.G., Hämäläinen, R.H., Pellico, J., Justo-Méndez, R., Fernández-Toro, J.M., Clavería, C., Guaras, A., Sierra, R., et al. (2019). Regulation of Mother-to-Offspring Transmission of mtDNA Heteroplasmy. Cell Metab. *30*, 1120–1130.e5.

Li, H., and Durbin, R. (2010). Fast and accurate long-read alignment with Burrows-Wheeler transform. Bioinformatics *26*, 589–595.

Lorenz, C., Lesimple, P., Bukowiecki, R., Zink, A., Inak, G., Mlody, B., Singh, M., Semtner, M., Mah, N., Auré, K., et al. (2017). Human iPSC-Derived Neural Progenitors Are an Effective Drug Discovery Model for Neurological mtDNA Disorders. Cell Stem Cell *20*, 659–674.e9.

Love, M.I., Huber, W., and Anders, S. (2014). Moderated estimation of fold change and dispersion for RNA-seq data with DESeq2. Genome Biol. *15*, 550.

Ma, H., Folmes, C.D., Wu, J., Morey, R., Mora-Castilla, S., Ocampo, A., Ma, L., Poulton, J., Wang, X., Ahmed, R., et al. (2015). Metabolic rescue in pluripotent cells from patients with mtDNA disease. Nature *524*, 234–238.

Matsubara, M., Kanda, H., Imamura, H., Inoue, M., Noguchi, M., Hosoda, K., Kakizuka, A., and Nakao, K. (2018). Analysis of mitochondrial function in human induced pluripotent stem cells from patients with mitochondrial diabetes due to the A3243G mutation. Sci. Rep. *8*, 949.

Miyata, N., Steffen, J., Johnson, M.E., Fargue, S., Danpure, C.J., and Koehler, C.M. (2014). Pharmacologic rescue of an enzyme-trafficking defect in primary hyperoxaluria 1. Proc. Natl. Acad. Sci. USA *111*, 14406–14411.

Mok, B.Y., de Moraes, M.H., Zeng, J., Bosch, D.E., Kotrys, A.V., Raguram, A., Hsu, F., Radey, M.C., Peterson, S.B., Mootha, V.K., et al. (2020). A bacterial cytidine deaminase toxin enables CRISPR-free mitochondrial base editing. Nature *583*, 631–637.

Mudge, J.M., and Harrow, J. (2015). Creating reference gene annotation for the mouse C57BL6/J genome assembly. Mamm. Genome *26*, 366–378.

Nelson, I., Hanna, M.G., Wood, N.W., and Harding, A.E. (1997). Depletion of mitochondrial DNA by ddC in untransformed human cell lines. Somat. Cell Mol. Genet. *23*, 287–290.

Nzigou Mombo, B., Gerbal-Chaloin, S., Bokus, A., Daujat-Chavanieu, M., Jorgensen, C., Hugnot, J.P., and Vignais, M.L. (2017). MitoCeption: Transferring isolated human MSC mitochondria to glioblastoma stem cells. J. Vis. Exp. (*120*), 55245.

Patananan, A.N., Wu, T.H., Chiou, P.Y., and Teitell, M.A. (2016). Modifying the mitochondrial genome. Cell Metab. *23*, 785–796.

Patananan, A.N., Sercel, A.J., and Teitell, M.A. (2018). More than a powerplant: the influence of mitochondrial transfer on the epigenome. Curr. Opin. Physiol. *3*, 16–24.

Patel, D., Rorbach, J., Downes, K., Szukszto, M.J., Pekalski, M.L., and Minczuk, M. (2017). Macropinocytic entry of isolated mitochondria in epidermal growth factor-activated human osteosarcoma cells. Sci. Rep. *7*, 12886.

Patro, R., Duggal, G., Love, M.I., Irizarry, R.A., and Kingsford, C. (2017). Salmon provides fast and bias-aware quantification of transcript expression. Nat. Methods *14*, 417–419.

Pek, N.M.Q., Phua, Q.H., Ho, B.X., Pang, J.K.S., Hor, J.H., An, O., Yang, H.H., Yu, Y., Fan, Y., Ng, S.Y., and Soh, B.S. (2019). Mitochondrial 3243A > G mutation confers pro-atherogenic and pro-inflammatory properties in MELAS iPS derived endothelial cells. Cell Death Dis. *10*, 802.

Perales-Clemente, E., Cook, A.N., Evans, J.M., Roellinger, S., Secreto, F., Emmanuele, V., Oglesbee, D., Mootha, V.K., Hirano, M., Schon, E.A., et al. (2016). Natural underlying mtDNA heteroplasmy as a potential source of intra-person hiPSC variability. EMBO J. *35*, 1979–1990.

Picard, M., Zhang, J., Hancock, S., Derbeneva, O., Golhar, R., Golik, P., O'Hearn, S., Levy, S., Potluri, P., Lvova, M., et al. (2014). Progressive increase in mtDNA 3243A>G heteroplasmy causes abrupt transcriptional reprogramming. Proc. Natl. Acad. Sci. USA *111*, E4033–E4042.

Quintanilla, R.H., Jr., Asprer, J.S.T., Vaz, C., Tanavde, V., and Lakshmipathy, U. (2014). CD44 is a negative cell surface marker for pluripotent stem cell identification during human fibroblast reprogramming. PLoS ONE *9*, e85419.

R Core Team (2017). R: A Language and Environment for Statistical Computing (R Foundation for Statistical Computing).

Rebolledo-Jaramillo, B., Su, M.S., Stoler, N., McElhoe, J.A., Dickins, B., Blankenberg, D., Korneliussen, T.S., Chiaromonte, F., Nielsen, R., Holland, M.M., et al. (2014). Maternal age effect and severe germ-line bottleneck in the inheritance of human mitochondrial DNA. Proc. Natl. Acad. Sci. USA *111*, 15474–15479.

Ritchie, M.E., Phipson, B., Wu, D., Hu, Y., Law, C.W., Shi, W., and Smyth, G.K. (2015). limma powers differential expression analyses for RNA-sequencing and microarray studies. Nucleic Acids Res. *43*, e47.

Russell, O.M., Fruh, I., Rai, P.K., Marcellin, D., Doll, T., Reeve, A., Germain, M., Bastien, J., Rygiel, K.A., Cerino, R., et al. (2018). Preferential amplification of a human mitochondrial DNA deletion in vitro and in vivo. Sci. Rep. *8*, 1799.

Sasarman, F., Antonicka, H., and Shoubridge, E.A. (2008). The A3243G tRNA-Leu(UUR) MELAS mutation causes amino acid misincorporation and a combined respiratory chain assembly defect partially suppressed by overexpression of EFTu and EFG2. Hum. Mol. Genet. *17*, 3697–3707.

Schaefer, A.M., Taylor, R.W., Turnbull, D.M., and Chinnery, P.F. (2004). The epidemiology of mitochondrial disorders–past, present and future. Biochim. Biophys. Acta *1659*, 115–120.

Sercel, A.J., Patananan, A.N., Man, T., Wu, T.-H., Yu, A.K., Guyot, G.W., Rabizadeh, S., Niazi, K.R., Chiou, P.-Y., and Teitell, M.A. (2020). Stable transplantation of human mitochondrial DNA by high-throughput, pressurized mitochondrial delivery. bioRxiv. https://doi.org/10.1101/2020.09.15.298174.

Smiraglia, D.J., Kulawiec, M., Bistulfi, G.L., Gupta, S.G., and Singh, K.K. (2008). A novel role for mitochondria in regulating epigenetic modification in the nucleus. Cancer Biol. Ther. *7*, 1182–1190.

Smith, A.C., and Robinson, A.J. (2016). MitoMiner v3.1, an update on the mitochondrial proteomics database. Nucleic Acids Res. *44* (*D1*), D1258–D1261.

Soneson, C., Love, M.I., and Robinson, M.D. (2015). Differential analyses for RNA-seq: transcript-level estimates improve gene-level inferences. F1000Res. *4*, 1521.

Sun, C., Liu, X., Wang, B., Wang, Z., Liu, Y., Di, C., Si, J., Li, H., Wu, Q., Xu, D., et al. (2019). Endocytosis-mediated mitochondrial transplantation: Transferring normal human astrocytic mitochondria into glioma cells rescues aerobic respiration and enhances radiosensitivity. Theranostics *9*, 3595–3607.

Szolek, A., Schubert, B., Mohr, C., Sturm, M., Feldhahn, M., and Kohlbacher, O. (2014). OptiType: precision HLA typing from next-generation sequencing data. Bioinformatics *30*, 3310–3316.

Warnes, G., Bolker, B., Bonebakker, L., Gentleman, R., Huber, W., Liaw, A., Lumley, T., Maechler, M., Magnusson, A., Moeller, S., et al. (2016). gplots: Various R Programming Tools for Plotting Data (CRAN: R-Project).

Wickham, H. (2019). ggplot2 v3.2.0 (RDocumentation).

Wolf, D.P., Mitalipov, N., and Mitalipov, S. (2015). Mitochondrial replacement therapy in reproductive medicine. Trends Mol. Med. *21*, 68–76.

Wolf, D.P., Mitalipov, P.A., and Mitalipov, S.M. (2019). Principles of and strategies for germline gene therapy. Nat. Med. *25*, 890–897.

Wong, R.C.B., Lim, S.Y., Hung, S.S.C., Jackson, S., Khan, S., Van Bergen, N.J., De Smit, E., Liang, H.H., Kearns, L.S., Clarke, L., et al. (2017). Mitochondrial replacement in an iPSC model of Leber's hereditary optic neuropathy. Aging (Albany NY) *9*, 1341–1350.

Wu, Y.C., Wu, T.H., Clemens, D.L., Lee, B.Y., Wen, X., Horwitz, M.A., Teitell, M.A., and Chiou, P.Y. (2015). Massively parallel delivery of large cargo into mammalian cells with light pulses. Nat. Methods *12*, 439–444.

Wu, T.H., Sagullo, E., Case, D., Zheng, X., Li, Y., Hong, J.S., TeSlaa, T., Patananan, A.N., McCaffery, J.M., Niazi, K., et al. (2016). Mitochondrial transfer by photothermal nanoblade restores metabolite profile in mammalian cells. Cell Metab. *23*, 921–929.

Xiao, G., Chan, L.N., Klemm, L., Braas, D., Chen, Z., Geng, H., Zhang, Q.C., Aghajanirefah, A., Cosgun, K.N., Sadras, T., et al. (2018). B-cell-specific diversion of glucose carbon utilization reveals a unique vulnerability in B cell malignancies. Cell *173*, 470–484.e18.

Yahata, N., Matsumoto, Y., Omi, M., Yamamoto, N., and Hata, R. (2017). TALEN-mediated shift of mitochondrial DNA heteroplasmy in MELAS-iPSCs with m.13513G>A mutation. Sci. Rep. *7*, 15557.

Yang, Y., Wu, H., Kang, X., Liang, Y., Lan, T., Li, T., Tan, T., Peng, J., Zhang, Q., An, G., et al. (2018). Targeted elimination of mutant mitochondrial DNA in MELAS-iPSCs by mitoTALENs. Protein Cell *9*, 283–297.

Yim, A., Koti, P., Bonnard, A., Marchiano, F., Dürrbaum, M., Garcia-Perez, C., Villaveces, J., Gamal, S., Cardone, G., Perocchi, F., et al. (2020). mitoXplorer, a visual data mining platform to systematically analyze and visualize mitochondrial expression dynamics and mutations. Nucleic Acids Res. *48*, 605–632.

Yu, G., and He, Q.Y. (2016). ReactomePA: an R/Bioconductor package for reactome pathway analysis and visualization. Mol. Biosyst. *12*, 477–479.

Yu, G., Wang, L.G., Han, Y., and He, Q.Y. (2012). clusterProfiler: an R package for comparing biological themes among gene clusters. OMICS *16*, 284–287.

STAR★METHODS

KEY RESOURCES TABLE

REAGENT or RESOURCE	SOURCE	IDENTIFIER
Antibodies		
OCT3/4	BD Bioscience	Cat#561628, RRID: AB_10895977
SOX2	BD Bioscience	Cat#561610, RRID: AB_10712763
Mouse IgG1 κ Isotype Control	BD Bioscience	Cat#557782, RRID: AB_396870
Mouse IgG1, κ Isotype Control	BD Bioscience	Cat#560373, RRID: AB_1645606
SSEA4	eBioscience	Cat#12-8843-42, RRID: AB_11151520
OCT4	eBioscience	Cat#53-5841-82, RRID: AB_1210530
TRA-1-60	Stemgent	Cat#09-0068, RRID: AB_2233143
TOMM20	Abcam	Cat#ab78547 RRID: AB_2043078
dsDNA	Abcam	Cat#ab27156 RRID: AB_470907
Biological Samples		
LP351 Human PBMCs (PBMC1)	HemaCare	Donor ID: D326351
LP298 Human PBMCs (PBMC2)	HemaCare	Donor ID: D316153
Chemicals, Peptides, and Recombinant Proteins		
2′,3′-dideoxycytidine	Sigma	D5782, CAS 7481-89-2
Dialyzed FBS	Life Technologies	Cat#26400-044
DMEM without glucose	GIBCO	Cat#11966025
Matrigel	Corning	Cat#356234
Lipofectamine RNAiMAX	ThermoFisher	Cat#13778100
mTeSR 1	StemCell Technologies	Cat#85850
Phusion high-fidelity PCR master mix with HF buffer	NEB	Cat#M0531S
Gentle Cell Dissociation Reagent	StemCell Technologies	Cat#07174
Accutase	BD Biosciences	Cat#561527
Hoechst 33342	ThermoFisher	Cat#R37605
Apa1	NEB BioLabs	Cat#R0114S
Critical Commercial Assays		
DNeasy Blood & Tissue kit	QIAGEN	Cat#69504
SYBR Select Master Mix for CFX	Life Technologies	Cat#4472942
Qproteome Mitochondria Isolation kit	QIAGEN	Cat#37612
StemRNA-NM Reprogramming kit		
ReproRNA-OKSGM	Stem Cell Technologies	Cat#05930
STEMCCA Constituitive Polycistronic (OKSM) Lentivirus Reprogramming kit	MilliporeSigma	Cat#SCR510
CytoTune-iPS 2.0 Sendai Reprogramming kit	Fisher Scientific	Cat#A16517
STEMdiff Mesenchymal Progenitor Kit	StemCell Technologies	Cat#05240
QIAGEN QIAQuick Gel Extraction kit	QIAGEN	Cat#28704
Fixation/Permeabilization Solution Kit with BD GolgiPlug	BD Bioscience	Cat#555028
Human MSC Analysis Kit	BD Bioscience	Cat#562245
V3 96-well plate	Agilent	Cat#101085-004
CD4+ T cell isolation kit	Miltenyi Biotec	Cat#130-096-533
Vybrant CFDA SE. Cell Tracer Kit	ThermoFisher	Cat#V12883

(*Continued on next page*)

Continued

REAGENT or RESOURCE	SOURCE	IDENTIFIER
Dynabeads Human T-activator CD3/CD28	ThermoFisher	Cat#11131D
MesenCult-ACF Basal Medium	StemCell Technologies	Cat#05449
MesenCult Adipogenic Differentiation Kit	StemCell Technologies	Cat#05412
MesenCult Osteogenic Differentiation medium	StemCell Technologies	Cat#05465
ACF Enzymatic Dissociation/Inhibition Solutions	StemCell Technologies	Cat#05426
MesenCult-ACF Chondrogenic Differentiation Medium	StemCell Technologies	Cat#05455
Y-27632	Stem Cell Technologies	Cat#72304
BCA protein assay	ThermoFisher	Cat#23225
CellROX Green Flow Cytometry Assay Kit	ThermoFisher	Cat#C10492
KAPA Stranded RNA-Seq Kit with Ribo-Erase	Kapa Biosystems, Roche	Cat#07962304001
Deposited Data		
RNaseq count matrices and raw reads	This paper	GEO: GSE115871
Metabolite relative amounts	This paper	N/A
Experimental Models: Cell Lines		
HEK293T	ATCC	Cat#CRL-3216
BJ Foreskin Fibroblast	ATCC	Cat#CRL-2522
Primary Dermal Fibroblast; Normal, Human, Adult	ATCC	Cat#PCS-201-012
Primary Dermal Fibroblast Normal; Human, Neonatal	ATCC	Cat#PCS-201-010
Leigh Syndrome ATP Synthase 6 (T8993G) Fibroblast	Coriell Institute	Cat#GM13411
Kearns-Sayre Syndrome (common deletion) Fibroblast	Coriell Institute	Cat#GM06225
MELAS (A3243G) Cybrid (CL3)	Gift from Douglas Wallace (Children's Hospital of Philadelphia Research Institute)	N/A
Wildtype Cybrid (CL9)	Gift from Douglas Wallace (Children's Hospital of Philadelphia Research Institute)	N/A
MELAS (A3243G) Cybrid	Gift from Carlos Moraes (University of Miami)	N/A
MERRF (A8344G) Cybrid	Gift from Carlos Moraes (University of Miami)	N/A
Δ Cytochrome B 3.0 Cybrid	Gift from Carlos Moraes (University of Miami)	N/A
L929 ρ0 Mouse Fibroblast	Gift from Jose Antonio Enriquez Dominguez (Centro Nacional de Investigaciones Cardiovasculares Carlos III (CNIC))	N/A
Oligonucleotides		
ND1 forward -CCCTA AAACCCGCCACATCT	IDT	N/A
ND1 reverse - CGAT GGTGAGAGCTAAGGTC	IDT	N/A
GAPDH Forward - TGCAC CACCAACTGCTTAGC	IDT	N/A
GAPDH Reverse - GGCA TGGACTGTGGTCATGAG	IDT	N/A
RPLP0 Forward -CGA CCTGGAAGTCCAACTAC	IDT	N/A

(*Continued on next page*)

Continued

REAGENT or RESOURCE	SOURCE	IDENTIFIER
RPLP0 Reverse -ATCT GCTGCATCTGCTTG	IDT	N/A
D Loop Forward - TTCCAA GGACAAATCAGAGAAAAAGT	IDT	N/A
D Loop Reverse - AGCC CGTCTAAACATTTTCAGTGTA	IDT	N/A
RFLP Forward - CCTC GGAGCAGAACCCAACCT	IDT	N/A
RFLP Reverse - CGAA GGGTTGTAGTAGCCCGT	IDT	N/A
Software and Algorithms		
FlowJo Software Version 10.4.2	FlowJo, LLC	N/A
Salmon v0.9.1	(Harrow et al., 2012; Mudge and Harrow, 2015; Patro et al., 2017)	https://github.com/COMBINE-lab/salmon/releases
Statistical Language R v3.6.0	(R Core Team, 2017)	https://www.r-project.org/
Bioconductor v3.9.0	(Huber et al., 2015)	https://bioconductor.org/news/bioc_3_3_release/
R Bioconductor package tximport v1.12.3	(Soneson et al., 2015)	https://support.bioconductor.org/p/106345/
R Bioconductor package DESeq2 v1.24.0	(Huber et al., 2015; Love et al., 2014)	https://bioconductor.org/packages/release/bioc/html/DESeq2.html
R package ggpubr v0.1.6	(Kassambara, 2017)	https://www.rdocumentation.org/packages/ggpubr/versions/0.1.6
R package pheatmap v1.0.12	(Warnes et al., 2016)	https://www.rdocumentation.org/packages/pheatmap/versions/1.0.8
R package gplots v3.0.1	(Kolde, 2015)	https://cran.r-project.org/web/packages/gplots/index.html
R package FactoMineR v2.2	(Husson, 2020)	https://www.rdocumentation.org/packages/FactoMineR/versions/1.34
R package factoextra v1.0.6	(Kassambara, 2019)	https://www.rdocumentation.org/packages/factoextra/versions/1.0.5
R Bioconductor package Mfuzz v2.38.0	(Kumar and Futschik, 2007)	https://bioc.ism.ac.jp/packages/3.6/bioc/html/Mfuzz.html
R package ggplot2 v3.2.0	(Wickham, 2019)	https://cran.r-project.org/web/packages/ggplot2/index.html
R Bioconductor package GSVA v1.32.0	(Hänzelmann et al., 2013)	https://anaconda.org/bioconda/bioconductor-gsva
R Bioconductor package limma v3.40.6	(Benjamini and Hochberg, 1995; Ritchie et al., 2015)	https://www.bioconductor.org/install/
R Bioconductor package clusterProfiler v3.12.0	(Yu and He, 2016)	https://bioconductor.org/packages/3.7/bioc/vignettes/clusterProfiler/inst/doc/clusterProfiler.html
R Bioconductor package ReactomePA v1.28.0	(Yu et al., 2012)	https://anaconda.org/bioconda/bioconductor-reactomepa
TraceFinder v3.3	ThermoFisher	Cat#OPTON-30493
MitoXplorer 1.0	(Yim et al., 2020)	http://mitoxplorer.ibdm.univ-mrs.fr

RESOURCE AVAILABILITY

Lead Contact

Further information and requests for resources and reagents should be directed to and will be fulfilled by the Lead Contact, Dr. Michael A. Teitell (mteitell@mednet.ucla.edu).

Materials Availability

All materials generated in this study are available upon reasonable request to the Lead Contact, Dr. Michael A. Teitell.

Data and Code Availability

All raw RNA-Seq reads, transcript abundance values, and processed gene count matrices are submitted to the NCBI Gene Expression Omnibus (GEO). The accession number for the RNA-seq reads reported in this paper is GEO: GSE115871. All other data are available upon request. All software used is available either commercially or as freeware. All custom code is available on GitHub at https://bitbucket.org/ahsanfasih/mitoDesigner/src/master/.

EXPERIMENT MODEL AND SUBJECT DETAILS

Cell Lines

HEK293T cells expressing mitochondria-targeted DsRed protein (pMitoDsRed, Clontech Laboratories) were made as previously described (Miyata et al., 2014). Primary, non-transformed human fibroblast sources include BJ (ATCC, Cat. # CRL-2522), ADF (ATCC, Cat. # PCS-201-012), and NDF (ATCC, Cat. # PCS-201-010). Isogenic cybrid cell lines derived from the same patient containing either the homoplasmic A3243G MELAS substitution or homoplasmic WT sequence were obtained from Douglas Wallace (Children's Hospital of Philadelphia Research Institute). An alternative A3243G MELAS cybrid cell line, in addition to A8344G MERRF and Δcytochrome B 3.0 cybrid cell lines, were from Carlos Moraes (University of Miami). Two primary A3243G MELAS fibroblast lines were from Anu Suomalainen Wartiovaara (University of Helsinki). Primary fibroblasts associated with Leigh Syndrome (T8993G, Cat. # GM13411) and Kearns Sayre Syndrome (common deletion, Cat. # GM06225) were obtained from the Coriell Repository.

BJ, NDF, ADF, and HEK293T-DsRed cells were grown at 37°C and 5% CO_2 in complete media containing DMEM (Corning, Cat. # 10013CV) supplemented with 10% Fetal Bovine Serum (FBS, Hyclone, Cat. # SH30088.03HI0), penicillin-streptomycin (Corning, Cat. # 30-002-CI), GlutaMax (ThermoFisher, Cat. # 35050-061), and non-essential amino acids (MEM NEAA, ThermoFisher, Cat. # 11-140-050). BJ ρ0, NDF ρ0, ADF ρ0, MELAS, MERRF, Δcytochrome B 3.0, Leigh Syndrome, and Kearns Sayre Syndrome cells were grown in complete media supplemented with 50 μg/ml uridine (Sigma, Cat. # U3003). iPSCs were grown on matrigel (Corning, Cat. # 356234) coated plates in mTeSR1 media (StemCell Technologies, Cat. # 85850) according to the manufacturer's protocol. MSCs were grown in defined, MesenCult-ACF media (StemCell Technologies, Cat. # 05449) following the manufacturer's protocol. Cells tested negative repeatedly for mycoplasma using a universal mycoplasma detection kit (ATCC, Cat. # 30-1012K).

Human Tissues

The following human tissues were used: PBMC1 (PBMCs from leukopak donor 351, Caucasian female, 42 year old, Donor ID: D326351, HemaCare Corp) and PBMC2 (PBMCs from leukopak donor 298, Hispanic/Latino male, 25 year old, Donor ID: D316153, HemaCare Corp).

METHOD DETAILS

mtDNA Depletion and qPCR Verification

A 1000x stock of ddC (Sigma, Cat. # D5782) was prepared in water and added to BJ, ADF, and NDF cells grown in complete media with 50 μg/ml uridine to an appropriate final concentration. Cells were passaged every 3-4 d with fresh ddC added over 3 weeks. Following ddC treatment, total DNA was extracted (QIAGEN, Cat. # 69504) and mtDNA quantified using SYBR Select Master Mix for CFX (Life Technologies, Cat. # 4472942). mtDNA-encoded *MT-ND1* was amplified with the following primers: forward: CCCTAAAACCCGCCACATCT; reverse: CGATGGTGAGAGCTAAGGTC. mtDNA levels were normalized to nucleus-encoded *GAPDH* using the following primers: forward: TGCACCACCAACTGCTTAGC; reverse: GGCATGGACTGTGGTCATGAG. RPLP0 served as an alternative nucleus-encoded gene for normalization using the following primers: forward: CGACCTGGAAGTCCAACTAC; reverse: ATCTGCTGCATCTGCTTG. qPCR was run on a BioRad CFX Thermal Cycler using the following protocol: 1) 50°C for 2 min, 2) 95°C for 2 min, and 3) 40 cycles at 95°C for 10 s and 60°C for 45 s. Samples were compared by calculating ΔΔCT and fold differences.

Mitochondrial Transfer into ρ0 Recipients

Mitochondria were harvested from HEK293T-DsRed cells, PBMCs (PBMC1 or PBMC2), or other cell types using a Qproteome Mitochondria Isolation Kit (QIAGEN, Cat. # 37612) following the manufacturer's protocol. Mitochondrial pellets were re-suspended in 1x PBS, pH 7.4, at 1 mg total protein/ml. Mitochondrial suspensions were delivered into ρ0 cells using MitoPunch.

The MitoPunch platform is a force-based mitochondrial transfer device. Briefly, a 5V solenoid (Sparkfun, Cat. # ROB-11015) is mounted on a threaded plug (Thor Labs, Cat. # SM1PL) and inserted into a threaded cage plate (Thor Labs, Cat. # CP02T). Above the solenoid, assembly rods (Thor Labs, Cat. # ER3) support an upper plate (Thor Labs, Cat. # CP02). The upper plate holds a custom machined aluminum washer (outer diameter, 25 mm; inner diameter, 10 mm) that supports a deformable PDMS (10:1 ratio of Part A base: Part B curing agent) fluid reservoir above the solenoid. The PDMS reservoir is composed of a bottom circular layer (25 mm diameter, 0.67 mm height) chemically bonded to an upper circular ring layer (outer diameter, 25 mm; inner diameter, 10 mm; height,

1.30 mm) and can hold approximately 120 μl of isolated mitochondrial suspension. Cells are seeded onto a porous membrane with 3 μm pores (Corning, Cat. # 353181) 24 h prior to mitochondrial transfer.

To perform mitochondrial transfer, this membrane with adherent cells is secured on top of the PDMS reservoir using an upper plate (Thor Labs, Cat. # CP02). The solenoid is controlled by a 5V power supply mini board (Futurlec, Cat. # MINIPOWER) and powered by a 12V, 3 Amp DC power supply (MEAN WELL, Cat. # RS-35-12). The activated solenoid strikes the center of the PDMS chamber, deforming the bottom circular layer by approximately 1.3 mm. This deformation rapidly injects the mitochondrial suspension through the membrane and into the monolayer cell culture on the opposite side. A tunable MitoPunch prototype was developed by NanoCav LLC with variable plunger force which improves SIMR generation efficiency especially in replication-limited fibroblasts.

As a comparison to MitoPunch, we performed isolated mitochondria coincubation control experiments. An equal number of coincubation recipient cells were seeded alongside MitoPunch recipients in 12 well dishes instead of the porous membrane. After ~24 h, an equal volume of mitochondrial isolate as loaded into the PDMS reservoir for MitoPunch was pipetted into the cell medium of each coincubation recipient well and incubated at 37°C for 2 h before being released, collected, and plated on 10 cm dishes for selection as described below.

For human fibroblasts and mouse recipients, cells were grown in complete media with 50 μg/mL uridine for 4 d following mitochondria delivery and on day 5 post-delivery, cells were shifted to uridine-free complete media prepared with 10% dialyzed FBS (Life Technologies, Cat. # 26400-044). On day 8 post-delivery, cells were shifted to glucose-free, galactose-containing medium (DMEM without glucose, GIBCO, Cat. # 11966025) supplemented with 10% dialyzed FBS and 4.5 g/l galactose. Colonies emerged at approximately 10 d post-delivery and cells were shifted back to uridine-free medium before colonies were counted by microscopy or isolated using cloning rings. For human 143BTK– ρ0 recipients, cells were grown in complete media with 50 μg/mL uridine following mitochondria delivery and shifted to uridine-free complete media prepared with 10% dialyzed FBS on day 3 post-delivery, and clones emerged approximately 10 d post-delivery and were quantified.

Confocal microscopy

Cells, ~1x10^5, were plated on glass coverslips (Zeiss, Cat. # 474030-9000) in 6 well dishes in 2 mL of media and cultured for approximately 24 h. The media was aspirated and cells then fixed by incubation of 1 mL freshly diluted 4% paraformaldehyde (Thermo Fisher Scientific, Cat. # 28906) in 1x PBS, pH 7.4, for 15 min at RT. Paraformaldehyde was removed and cells were washed 3x with PBS, and then washed 3x with PBS with 5 min RT incubation during each wash. Cells were permeabilized by a 10 min RT incubation with 0.1% Triton X-100 (Sigma, Cat. # X100). Permeabilized cells were washed 3x with PBS and then blocked by incubation for 1 h at RT with 2% bovine serum albumin (BSA) dissolved in PBS. After blocking, cells were incubated with primary antibodies at 1:1000 dilution in 2% BSA blocking buffer against dsDNA (Abcam, Cat. # ab27156) and TOM20 (Abcam, Cat. # ab78547), and then washed 3x with 5 min RT incubation with PBS. After washing, cells were incubated for 1 h with secondary antibodies (Invitrogen, Cat. #'s A31573 and A21202) diluted 1:100 in 2% BSA blocking buffer protected from light at RT, and washed 3x with 5 min incubations with PBS. To mount coverslips on slides, samples were removed from the 6 well dish, dipped in deionized water, dried with a Kimwipe, and mounted using ProLong Gold Antifade Mountant with DAPI (Invitrogen, Cat. # P3691) on microscope slides (VWR, Cat. # 48311-601). Mounted samples were allowed to dry protected from light at RT for 48 h prior to imaging with a Leica SP8 confocal microscope.

Mitochondrial Oxygen Consumption Measurements

OCR was measured using a Seahorse XF96 Extracellular Flux Analyzer (Agilent). For fibroblasts or MSCs, 1 – 2 x10^5 cells per well were seeded onto a V3 96-well plate (Agilent, Cat. # 101085-004) and grown overnight before analysis. iPSCs were treated similarly but plated on matrigel-coated V3 plates. A mitochondrial stress test quantified OCR at basal respiration and after the sequential addition of mitochondrial inhibitors oligomycin, carbonyl cyanide-p-trifluoromethoxyphenylhydrazone (FCCP), and rotenone.

Mitochondrial Isolation from Mouse Tissues and Delivery

Spleen, liver, lung, bone marrow, heart, skeletal muscle, and kidney were harvested from an ~8 month-old female C57BL/6 mouse. Briefly, tissue was dissociated by passage through a cell strainer using the plunger of a syringe, and mitochondria were isolated from dissociated tissue using the Qproteome Mitochondria Isolation Kit (QIAGEN, Cat. # 37612) following the manufacturer's protocol. Mitochondrial suspensions were delivered into L929 ρ0 fibroblasts using MitoPunch. L929 ρ0 recipient cells were grown in complete media supplemented with 50 μg/mL uridine for 4 d following mitochondria delivery. On day 5 post-delivery, cells were shifted to uridine-free complete media prepared with 10% dialyzed FBS (Life Technologies, Cat. # 26400-044). On day 8 post-delivery, cells were shifted to glucose-free, galactose-containing medium (DMEM without glucose, GIBCO, Cat. # 11966025) supplemented with 10% dialyzed FBS and 4.5 g/l galactose. Colonies emerged at approximately 10 d post-delivery and cells were shifted back to uridine-free medium before colonies were counted by microscopy or isolated using cloning rings.

iPSC Reprogramming

Reprogramming of fibroblast lines to iPSCs was done using the StemRNA-NM Reprogramming kit (Stemgent, Cat. # 00-0076) following the manufacturer's protocol. Briefly, fibroblasts were plated on a matrigel (Corning, Cat. # 356234) coated 6-well plate at 2x10^5 cells/well on 0 d. Daily transfections of non-modified (NM)-RNA reprogramming cocktail were performed for 4 d using Lipofectamine RNAiMAX (ThermoFisher, Cat. # 13778100). On 10-12 d, iPSC colonies were identified by staining with TRA-1-60

antibody (Stemgent, Cat. # 09-0068). TRA-1-60^{+} iPSC colonies were picked and re-plated on matrigel coated 12-well plates and maintained in mTeSR 1 medium (StemCell Technologies, Cat. # 85850). Alternative reprogramming strategies for fibroblasts included using ReproRNA-OKSGM (Stem Cell Technologies, Cat. # 05930), STEMCCA Lentiviral (MilliporeSigma, Cat. #SCR510), and CytoTune-iPS 2.0 Sendai (Fisher Scientific, Cat. # A16517) kits according to the manufacturers' protocols.

MSC Differentiation

MSC lines were generated from iPSCs using the STEMdiff Mesenchymal Progenitor Kit (StemCell Technologies, Cat. # 05240) following the manufacturer's protocol over the course of 21 d. Briefly, iPSCs were dispersed as single cells, plated at ~5 × 10^4 cells/cm^2, and cultured for 2 d on Matrigel with mTeSR1 medium before the medium was changed to STEMdiff -ACF Mesenchymal Induction Medium. STEMdiff -ACF Mesenchymal Induction Medium was changed daily for 3 d, and on day 4, the medium was changed to MesenCult -ACF Plus Medium. Cells were fed again with MesenCult -ACF Plus Medium on day 5. On day 6, cells were collected with Gentle Cell Dissociation Reagent (StemCell Technologies, Cat. # 07174) and passaged onto plastic plates with MesenCult -ACF Plus Medium with 10 μM ROCK inhibitor (Y-27632; Stem Cell Technologies, Cat. # 72304). Daily half-medium changes were made for ~1 week when cells were ~80% confluent. Cells were further passaged by dissociation with ACF Enzymatic Dissociation Solution and resuspended in MesenCult -ACF Plus Medium before further analysis.

Human mtDNA D-Loop Sequencing

Total DNA was extracted from 1x10^6 cells using the QIAGEN DNasy Blood and Tissue kit. PCR was performed using Phusion high-fidelity PCR master mix with HF buffer (NEB, Cat. # M0531S) and the following primers: forward – TTCCAAGGACAAATCAGAGAAAAAGT, reverse – AGCCCGTCTAAACATTTTCAGTGTA. PCR was run on an Eppendorf vapo.protect thermal cycler at 1) 98°C for 2 min, 2) 30 cycles at 98°C for 15 s, 58°C for 30 s, 72°C for 30 s, and 3) 72°C for 5 min. PCR products were run on a 0.8%–1% agarose TAE gel, extracted with the QIAGEN QIAQuick Gel Extraction kit (QIAGEN, Cat. # 28704), and Sanger sequenced using the same PCR primers.

ROS Quantification

CellROX Green Flow Cytometry Assay Kit (ThermoFisher, Cat. # C10492) was used according to the manufacturer's protocol. Briefly, 7.5x10^4 cells were plated in a 6-well plate ~24 h prior to measurements. 250 μM tert butyl hydroperoxide (TBHP) and 750 μM CellROX reagent were added to the cells ~2 h and 1 h prior to quantification, respectively. Cells were released using Accutase, washed once with FACS buffer (5% FBS in 1x DPBS, pH 7.4), and quantified using a LSRFortessa flow cytometer (BD Bioscience).

iPSC Flow Cytometry

iPSCs were harvested by 15 min RT incubation with Gentle Cell Dissociation Reagent. Cells were centrifuged at 300 x g for 5 min, washed in 1ml DPBS + 10% FBS, and re-suspended in 100 μL BD Perm/Fix Buffer (BD Bioscience). Cells were incubated at 4°C for 15 min and washed twice in DPBS + 10% FBS. Following the second wash, cells were incubated in 50μl DPBS + 10% FBS containing conjugated antibodies. Antibodies used were OCT3/4 AlexaFluor488 (BD Bioscience 561628 1:10), SOX2 V450 (BD Bioscience 561610 1:10), Mouse IgG1 κ Isotype Control AlexaFluor488 (BD Biosciences 557782 1:10), Mouse IgG1, κ Isotype Control V450 (BD Bioscience 560373 1:10), and CD44 PE (BD Bioscience 562245 1:21). Cells were incubated with conjugated antibodies for 30 min and then washed twice in DPBS + 10% FBS. Data was acquired on a LSRFortessa flow cytometer (BD Bioscience) and analyzed using FlowJo software (FlowJo, LLC).

MSC Flow Cytometry

MSCs were harvested by 5 min, 37°C incubation with Accutase (BD Biosciences). Cells were centrifuged at 300 x g for 5 min, washed in 1ml DPBS + 10% FBS, and re-suspended in DPBS + 10% FBS at 5x10^6 cells/ml. Cells were incubated in 100μl DPBS + 10% FBS for 30 min at 4°C with the antibodies provided in the Human MSC Analysis Kit (BD Biosciences, Cat. # 562245) for 30 min and then washed twice in DPBS + 10% FBS. Data was acquired on a LSRFortessa flow cytometer (BD Bioscience) and analyzed using FlowJo software (FlowJo, LLC).

Fluorescence Microscopy

iPSCs were cultured on matrigel-coated 6-well plates and fixed with 4% paraformaldehyde for 10 min. Blocking was done for 1 h in 1x PBS, pH 7.4, with 5% FBS and 0.3% Triton X-100. Cells were stained with SSEA4 (eBioscience, Cat. # 12-8843-42) and OCT4 (eBioscience, Cat. # 53-5841-82) antibodies, and Hoechst 33342 dye (ThermoFisher, Cat. # R37605) overnight at 4°C in blocking buffer. Phase contrast and fluorescence images were obtained with a Zeiss Axio Observer Z1 microscope and Hamamatsu EM CCD camera (Cat. # C9100-02).

MSC Immunosuppression Assay

MSC inhibition of T cell proliferation was performed as described previously (Hsu et al., 2015). Briefly, MSCs were plated in a 12-well plate the day before assay. PBMCs were isolated by Ficoll gradient from a healthy de-identified leukopak donor. CD4^{+} T cells were isolated from PBMCs using the CD4^{+} T cell Isolation Kit (Miltenyi Biotec, Cat. # 130-096-533) and labeled with CFDA SE

(ThermoFisher, Cat. # V12883). Labeled $CD4^+$ T cells were stimulated with Dynabeads Human T-activator CD3/CD28 (ThermoFisher, Cat. # 11131D) at a ratio of one bead per T cell. T cells were added into MSC cultures at the following T cell:MSC ratios: 1:2, 1:1, 5:1, and 10:1. After 5 d of co-culture, T cell proliferation was measured using CFSE signature dye dilution by flow cytometry.

Tri-lineage Differentiation

Adipocytes, osteoblasts, and chondrocytes were generated from MSCs. For adipocyte differentiation, MSCs between passages 3 – 4 were plated on 6-well plates with MesenCult-ACF Basal Medium (StemCell Technologies, Cat. # 05449) at $4 – 5 \times 10^5$ cells per well. Differentiation was performed using the MesenCult Adipogenic Differentiation Kit (StemCell Technologies, Cat. # 05412) according to the manufacturer's protocol. Media changes were done every 3 – 4 d until 13 d. For osteogenic lineage differentiation, MSCs between passages 3 – 4 were plated on a 6-well plate with MesenCult-ACF Basal Medium (StemCell Technologies) at $3 – 4 \times 10^4$ cells per well. Differentiation was performed using MesenCult Osteogenic Differentiation medium (StemCell Technologies, Cat. # 05465) according to the manufacturer's protocol. Medium changes were done every 3 – 4 d until 13 d. For 3-D pellet chondrogenic differentiation, MSCs were first released from T25 flasks using ACF Enzymatic Dissociation/Inhibition Solution (StemCell Technologies, Cat. # 05426) and collected in polypropylene tubes at $2.5 – 3 \times 10^6$ cells per tube with MesenCult-ACF Chondrogenic Differentiation Medium (StemCell Technologies, Cat. # 05455) according to the manufacturer's protocol. Medium changes were done every 3 – 4 days until 13 d.

Tri-lineage Differentiation Analyses

Osteogenic differentiation was assayed by staining cells with 1% Alizarin Red solution. Medium was removed from cells grown on 6-well plates and cells were washed 3 times with 1X DPBS. Cells were fixed in 4% PFA in 1X DPBS at 4°C for 15 min prior to 15 min incubation with 1% alizarin red at RT. Alizarin red solution was aspirated and the cells were imaged using a standard inverted microscope.

Adipogenic differentiation was assayed by staining cells with 0.1% Bodipy solution. Medium was removed from cells grown on 6-well plates and cells were washed 3x with 1X DPBS. Cells were fixed in 4% PFA in 1X DPBS at 4°C for 15 min and washed twice with 1X DPBS prior to a 10 min incubation with 0.1% Bodipy at RT. Bodipy solution was aspirated and the cells were washed with 1X DPBS prior to acquiring phase contrast and fluorescence images with a Zeiss Axio Observer Z1 microscope and Hamamatsu EM CCD camera (Cat. # C9100-02).

Chondrocyte differentiation was assayed by staining chondrogenic spheroids and spheroid sections with 0.1% Safranin O solution. For staining whole spheroids, the medium was removed from the spheroids and they were fixed in 4% PFA for 15 min at RT. The spheroids were washed twice with 1x PBS, pH 7.4, before 15 min incubation with 0.1% Safranin O solution at RT. The stained spheroids were washed twice with 1ml water and transferred by serological pipette to a 48-well dish for imaging. For spheroid section staining, spheroids were fixed in 10% formalin for 18 h, washed twice in water, and placed in 70% ethanol. Spheroids were microtome sectioned by the UCLA Translational Pathology Core Laboratory, tissue placed on microscope slides. Sections were deparaffinized and rehydrated by washes in xylenes, ethanol, and water. Unstained sections were stained with hematoxylin and eosin or 0.1% Safranin O for 10 min at RT prior to washing in ethanol. Sections were imaged under a standard inverted microscope.

UPHLC-MS Metabolomics Processing

Ultra-high-performance liquid chromatography mass spectrometry (UHLPC-MS) was performed as described previously (Xiao et al., 2018) to quantify metabolites from ~$7x10^5$ cells. Briefly, cells were rinsed with cold 150 mM ammonium acetate, pH 7.3, followed by addition of ice-cold 80% methanol. Cells were detached with scrapers, transferred into microcentrifuge tubes, and 1 nmol D/L-norvaline added. After vortexing, the suspension was centrifuged at 4°C at maximum speed. The supernatant was transferred into a glass vial, metabolites dried down under vacuum using an EZ-2Elite evaporator at 30°C, and re-suspended in 70% acetonitrile. To normalize samples, pellets were re-suspended in 58 mM Tris-HCl, pH 6.8, 5% glycerol, and 17 mg/ml sodium dodecyl sulfate and quantified by BCA protein assay (ThermoFisher, Cat. # 23225).

Metabolites were separated on a Luna NH2 (150 mm x 2 mm, Phenomenex) column using 5 mM NH_4AcO, pH 9.9 (buffer A), acetonitrile (buffer B), and the following gradient: initially at 15% buffer B, 18 min gradient to 90% buffer B, 9 min isocratic at 90% buffer B, 7 min isocratic at 15% buffer B. Samples were analyzed with an UltiMate 3000RSLC (Thermo Scientific) coupled to a Q Exactive mass spectrometer (Thermo Scientific) run with polarity switching (+3.50 kV / −3.50 kV) in full scan mode and m/z range of 65-975. Metabolites were quantified with TraceFinder 3.3 using accurate mass measurements ($\leq$3 ppm) and retention times of pure standards.

RNA Extraction

Fibroblasts, iPSCs, and MSCs were grown in biological triplicates and technical duplicates to 70 – 80% confluence and purified using the RNeasy Mini Kit (QIAGEN, Cat. # 74104) and RNase-free DNase (QIAGEN, Cat. # 79254) following the manufacturer's protocols. All samples showed a A260/280 ratio > 1.99 (Nanodrop; Thermo Scientific). Prior to library preparation, quality control of the RNA was performed using the Advanced Analytical Technologies Fragment Analyzer (Advanced Analytical, Inc.) and analyzed using PROSize 2.0.0.51 software. RNA Quality Numbers (RQNs) were computed per sample between 8.1 and 10, indicating intact total RNA per sample prior to library preparation.

RNA-Seq Library Preparation

Strand-specific ribosomal RNA (rRNA) depleted RNA-Seq libraries were prepared from 1 μg of total RNA using the KAPA Stranded RNA-Seq Kit with Ribo-Erase (Kapa Biosystems, Roche). Briefly, rRNA was depleted from total RNA samples, the remaining RNA was heat fragmented, and strand-specific cDNA was synthesized using a first strand random priming and second strand dUTP incorporation approach. Fragments were then A-tailed, adapters were ligated, and libraries were amplified using high-fidelity PCR. All libraries were prepared in technical duplicates per sample (n = 60 samples, 120 libraries total), and resulting raw sequencing reads merged for downstream alignment and analysis. Libraries were paired-end sequenced at 2x150 bp on an Illumina NovaSeq 6000.

Restriction-Fragment Length Polymorphism Heteroplasmy Assay

To quantify relative levels of mtDNA containing the A3243G substitution, total DNA was isolated from cells using the DNeasy Blood and Tissue kit (QIAGEN, Cat. # 69504). PCR amplification of the MELAS region to generate a 634 bp product was performed using the following primers: forward – CCTCGGAGCAGAACCCAACCT and reverse – CGAAGGGTTGTAGTAGCCCGT. ApaI digestion (NEB Biolabs, Cat. # R0114S) of the PCR product was performed according to manufacturer's protocol for 2 h at 25°C, and deactivated at 65°C for 20 min. Sample was separated on a 2.5% agarose gel at 100V for 1 h.

QUANTIFICATION AND STATISTICAL ANALYSIS

mtDNA Depletion and qPCR Verification

Statistical details are provided in each figure legend.

Mitochondrial Oxygen Consumption Rate Measurements

Statistical details are provided in each figure legend.

Metabolomics Data Analysis

Data analysis, including principal components analysis (PCA) and clustering, was performed using the statistical language R v3.6.0 and Bioconductor v3.9.0 packages (Huber et al., 2015; R Core Team, 2017). Metabolite abundance was normalized per μg of protein content per metabolite extraction, and metabolites not detected were set to zero. Metabolite normalized amounts were log transformed and then scaled and centered into Z-scores for relative comparison using R base function *scale()* with parameters *"scale = TRUE, center = TRUE"*. Heatmaps and Euclidean distance similarity plots were created using the Z-scores in R package pheatmap v1.0.12, and hierarchical clustering was performed using the Euclidean distance measure.

PCA was performed using R packages FactoMineR v2.2 and factoextra v1.0.6. PC scores computed from normalized metabolite counts with function *PCA()* using parameters *"scale.unit = TRUE, ncp = 10, graph = FALSE"*.

Pathway-level metabolite set enrichment analysis was performed using R Bioconductor package GSVA v1.32.0 (Hänzelmann et al., 2013). Metabolite normalized abundances were standardized using a log2(normalized amounts + 1) transformation, and metabolites per sample were converted to a pathways per sample matrix using function *gsva()* with parameters *"method = gsva, maseq = FALSE, abs.ranking = FALSE, min.sz = 5, max.sz = 500"*. GSVA pathway enrichment scores were then extracted and significance testing for multiple transfer conditions was calculated using R Bioconductor package limma v3.40.6, as described above. Pathway metabolite sets were constructed using the KEGG Compound Database and derived from the existing Metabolite Pathway Enrichment Analysis (MPEA) toolbox (Kanehisa et al., 2012; Kankainen et al., 2011).

RNA-Seq Pre-Processing

Fibroblasts, iPSCs, and MSCs were each sequenced in biological triplicates and technical duplicates (n = 60 total samples) to account for variation in extraction and culturing. Raw sequencing reads were converted into fastq files and filtered for low quality reads and Illumina sequencing adaptor contamination using bcl2fastq (Illumina). Reads were then quasi-mapped and quantified to the *Homo sapiens* GENCODE 28 (GRCh38.p12, Ensembl 92, April 2018) transcriptome using the alignment-free transcript level quantifier Salmon v0.9.1 (Harrow et al., 2012; Mudge and Harrow, 2015; Patro et al., 2017). A quasi-mapping index was prepared using parameters *"salmon index -k 31 –type quasi"*, and comprehensive transcript level estimates were calculated using parameters *"salmon quant -l A –seqBias –gcBias–discardOrphansQuasi"*. Transcript level counts were collapsed to gene level (HGNC) counts, transcripts per million abundances (TPM) and estimated lengths using R Bioconductor package tximport v1.12.3 (Soneson et al., 2015).

Differential Gene Expression Analysis

The resulting sample gene count matrix was size factor normalized and analyzed for pairwise differential gene expression using R Bioconductor package DESeq2 v1.18.1. Expression changes were estimated using an empirical Bayes procedure to generate moderated fold change values with design "~ Batch + Sample," modeling batch effect variation due to day of RNA extraction (Huber et al., 2015; Love et al., 2014). Significance testing was performed using the Wald test, and resulting *P values* were adjusted for multiple testing using the Benjamini-Hochberg procedure (Benjamini and Hochberg, 1995). DEGs were filtered using an adjusted false discovery rate (FDR) q value < 0.05 and an absolute $\log_2$ transformed fold-change > 0.05.

MitoXplorer Analysis

Differential expression analysis was performed using DESeq2, specifying an absolute log2 transformed fold change threshold > 0.5. Result lists including all genes were uploaded to the MitoXplorer 1.0 pipeline (http://mitoxplorer.ibdm.univ-mrs.fr/index.php) comparing SIMR-fibroblasts, -iPSCs, or -MSCs to the corresponding cell fate of the BJ control. DEGs were filtered using a $\log_2$ transformed fold-change threshold of 0.05. Subsequently, the number of upregulated and downregulated DEGs for each mitochondrial process were counted.

Gene Expression PCA and hierarchal clustering

Variance stabilized transform (VST) values in the gene count matrix were calculated and plotted for PCA using R Bioconductor packages DESeq2, FactoMineR, and factoextra, as described in the metabolomics methods (Huber et al., 2015; Love et al., 2014). For PCA of nucleus-encoded mitochondrial protein and mtDNA transcripts, relevant transcripts were extracted using localization evidence derived from MitoMiner v4.0, subsetting VST matrices using genes listed in MitoCarta 2.0 (Calvo et al., 2016; Smith and Robinson, 2016). Clonal heatmaps were prepared using R Bioconductor packages pheatmap v1.0.8 and gplots v3.0.1 (Warnes et al., 2016; Kolde, 2015). Heirarchal clustering was performed using R based function hclust and plotted using the dendextend package.

Metabolic Transcript Gene Set Variation Analysis (GSVA)

GSVA on metabolic transcripts was performed similarly to metabolomics data as noted above. Pathway-level metabolic gene set enrichment analysis was performed using R Bioconductor package GSVA v1.32.0 function *gsva()* with parameters *"method = gsva, rnaseq = FALSE, abs.ranking = FALSE, min.sz = 5, max.sz = 500"* using a $\log_2$(TPM + 1) transformed gene expression matrix (Hänzelmann et al., 2013). GSVA pathway enrichment scores per sample were extracted and assessed for significance using R Bioconductor package limma v3.40.0, as described above except with a Benjamini-Hochberg adjusted *P value* threshold = 0.01. Pathway metabolite sets were constructed using the KEGG PATHWAY Database, utilizing gene sets annotated to the metabolic pathways overview map HSA01100 (Kanehisa et al., 2012). Significance testing across clones and conditions for each gene set were calculated using Kruskal-Wallis ANOVA.

Gene Set Overrepresentation Analysis (ORA)

DEGs were extracted and analyzed for pathway/gene ontology (GO) term overrepresentation using the R Bioconductor package clusterProfiler v3.12.0 and ReactomePA v1.28.0, using a background gene set of all genes expressed with at least one read count in the sample gene count matrix (Yu and He, 2016; Yu et al., 2012). Overrepresented Reactome/KEGG pathways and GO terms were identified across DEG lists and conditions using clusterProfiler function *compareCluster()* with significance testing cutoffs of $p < 0.05$, and an adjusted FDR < 0.25.

HLA Class I Genotyping

MHC Class I HLA genotypes were identified using OptiType v1.3.1(Szolek et al., 2014). All raw RNA-Seq sample FASTQs were aligned to the HLA Class I reference transcriptome packaged in OptiType using BWA MEM v0.7.17 with standard parameters (Li and Durbin, 2010). HLA subset reads were then analyzed for Class I genotype using OptiType in paired-end RNA mode with standard parameters.

Cell Reports, Volume *33*

Supplemental Information

Pressure-Driven Mitochondrial Transfer Pipeline Generates Mammalian Cells of Desired Genetic Combinations and Fates

Alexander N. Patananan, Alexander J. Sercel, Ting-Hsiang Wu, Fasih M. Ahsan, Alejandro Torres Jr., Stephanie A.L. Kennedy, Amy Vandiver, Amanda J. Collier, Artin Mehrabi, Jon Van Lew, Lise Zakin, Noe Rodriguez, Marcos Sixto, Wael Tadros, Adam Lazar, Peter A. Sieling, Thang L. Nguyen, Emma R. Dawson, Daniel Braas, Justin Golovato, Luis Cisneros, Charles Vaske, Kathrin Plath, Shahrooz Rabizadeh, Kayvan R. Niazi, Pei-Yu Chiou, and Michael A. Teitell

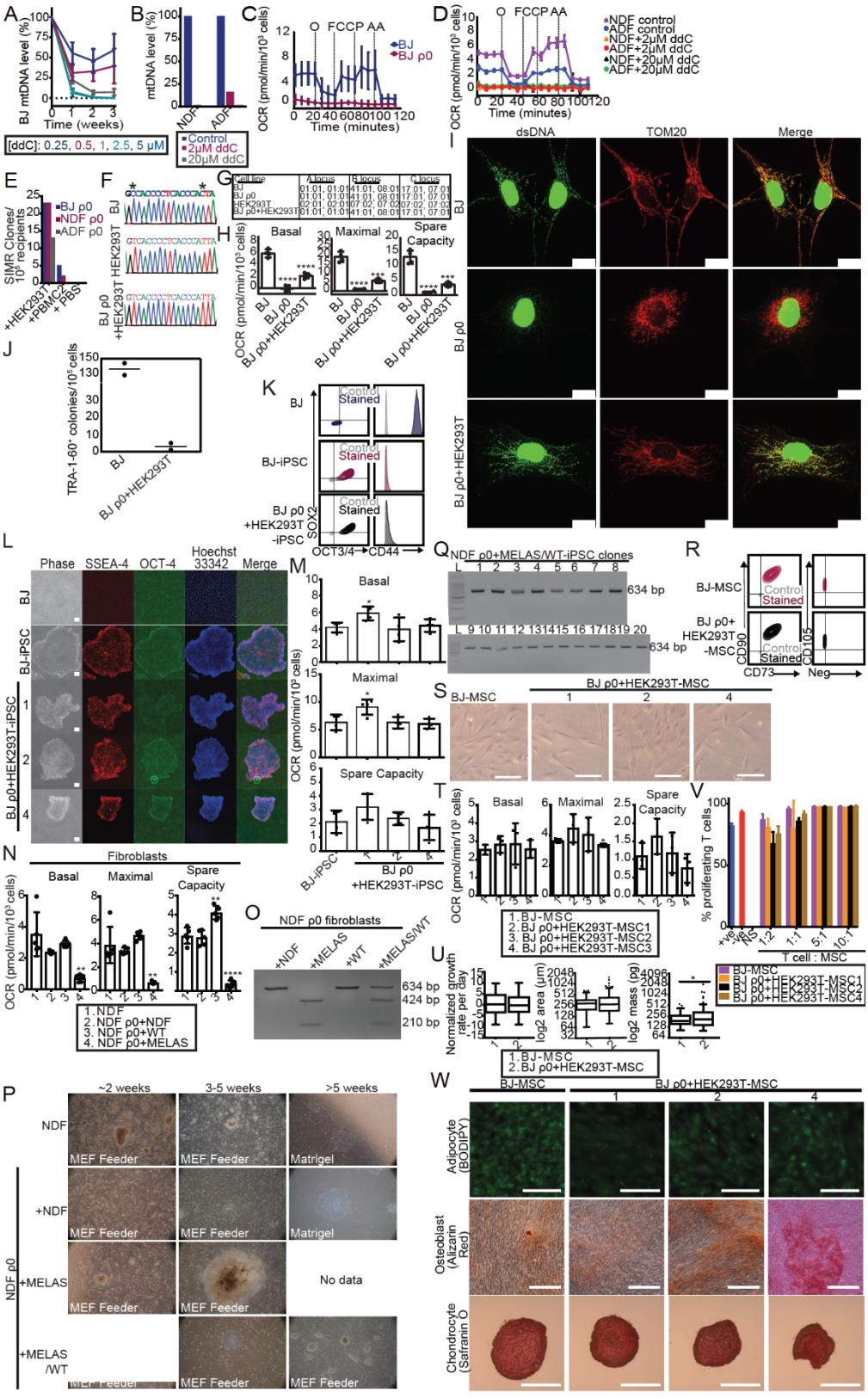
A
BJ mtDNA level (%)
Time (weeks)
[ddC]: 0.25, 0.5, 1, 2.5, 5 μM
B
mtDNA level (%)
NDF
ADF
Control
2μM ddC
20μM ddC
C
OCR (pmol/min/10³ cells)
O FCCP AA
BJ
BJ ρ0
Time (minutes)
D
OCR (pmol/min/10³ cells)
O FCCP AA
NDF control
ADF control
NDF+2μM ddC
ADF+2μM ddC
NDF+20μM ddC
ADF+20μM ddC
Time (minutes)
E
SIMR Clones/ 10⁶ recipients
BJ ρ0
NDF ρ0
ADF ρ0
+HEK293T
+PBMC2
+PBS
F
BJ
HEK293T
BJ ρ0 +HEK293T
G
Cell line
A locus
B locus
C locus
BJ
BJ ρ0
HEK293T
BJ ρ0+HEK293T
H
Basal
Maximal
Spare Capacity
OCR (pmol/min/10³ cells)
BJ
BJ ρ0
BJ ρ0+HEK293T
I
dsDNA
TOM20
Merge
BJ
BJ ρ0
BJ ρ0+HEK293T
J
TRA-1-60⁺ colonies/10⁵ cells
BJ
BJ ρ0+HEK293T
K
BJ
BJ-iPSC
BJ ρ0 +HEK293T -iPSC
Control
Stained
SOX2
OCT3/4
CD44
L
Phase
SSEA-4
OCT-4
Hoechst 33342
Merge
BJ
BJ-iPSC
BJ ρ0+HEK293T-iPSC
1
2
4
M
Basal
Maximal
Spare Capacity
OCR (pmol/min/10³ cells)
BJ-iPSC
BJ ρ0 +HEK293T-iPSC
N
Fibroblasts
Basal
Maximal
Spare Capacity
OCR (pmol/min/10³ cells)
1.NDF
2.NDF ρ0+NDF
3. NDF ρ0+WT
4. NDF ρ0+MELAS
O
NDF ρ0 fibroblasts
+NDF
+MELAS
+WT
+MELAS/WT
634 bp
424 bp
210 bp
P
~2 weeks
3-5 weeks
>5 weeks
NDF
+NDF
+MELAS
+MELAS /WT
NDF ρ0
MEF Feeder
Matrigel
No data
Q
NDF ρ0+MELAS/WT-iPSC clones
634 bp
634 bp
R
BJ-MSC
BJ ρ0+ HEK293T -MSC
Control
Stained
CD90
CD105
CD73
Neg
S
BJ-MSC
BJ ρ0+HEK293T-MSC
1
2
4
T
Basal
Maximal
Spare Capacity
OCR (pmol/min/10³ cells)
1.BJ-MSC
2.BJ ρ0+HEK293T-MSC1
3. BJ ρ0+HEK293T-MSC2
4. BJ ρ0+HEK293T-MSC3
U
Normalized growth rate per day
log2 area (μm²)
log2 mass (pg)
1.BJ-MSC
2.BJ ρ0+HEK293T-MSC
V
% proliferating T cells
+ve
-ve
NS
1:2
1:1
5:1
10:1
T cell : MSC
BJ-MSC
BJ ρ0+HEK293T-MSC1
BJ ρ0+HEK293T-MSC2
BJ ρ0+HEK293T-MSC4
W
BJ-MSC
BJ ρ0+HEK293T-MSC
1
2
4
Adipocyte (BODIPY)
Osteoblast (Alizarin Red)
Chondrocyte (Safranin O)

Figure S1. The MitoPunch Pipeline Generates Functional Cells with Unique mtDNA-nDNA Pairings, Related to Figures 1, 2, 3, and 4.
(A) Native BJ fibroblasts were exposed to the indicated doses of ddC for three weeks. mtDNA levels were quantified by qPCR using primers for MT-ND1 and normalized to GAPDH. Data are the mean ± SD of three independent biological replicates.
(B) Native ADF and NDF cells were exposed to the indicated doses of ddC for three weeks. mtDNA levels were quantified by qPCR using primers for MT-ND1 and normalized to RPLP0. Data represents the mean of three technical replicates.
(C) OCR measurements for ~$2.0x10^4$ native BJ and BJ ρ0 fibroblasts. Agents injected were oligomycin (O), Carbonyl cyanide-p-trifluoromethoxyphenylhydrazone (FCCP), and antimycin A (AA) at the indicated time points. Data are the mean ± SD of five technical replicates.
(D) OCR measurements for 1.5 – $2.0x10^4$ NDF, ADF, NDF ρ0, and ADF ρ0 (by exposure to the indicated amounts of ddC) fibroblasts. Data are the mean ± SD of four technical replicates.
(E) Mitochondria from HEK293T cells and from ~$3x10^7$ peripheral blood mononuclear cells (PBMC2) were MitoPunch transferred into BJ ρ0, NDF ρ0, or ADF ρ0 recipient fibroblasts. Following selection, SIMR colonies were stained with crystal violet and quantified. Clone counts from a single representative mitochondria transfer into ~$1x10^5$ recipient ρ0 fibroblasts are shown.
(F) D-loop hypervariable region mtDNA sequences from native BJ, HEK293T cell, and BJ ρ0+PBMC2 SIMR fibroblasts. Stars denote single nucleotide polymorphisms.
(G) MHC Class I HLA A, B, and C locus genotyping using OptiType v1.3.1 for native BJ, BJ ρ0, HEK293T, and BJ ρ0+HEK293T SIMR cells.
(H) OCR measurements for ~$1.5x10^4$ native BJ, BJ ρ0, and BJ ρ0+HEK293T SIMR fibroblasts. Data are the mean ± SD of four technical replicates. Statistical significance for by unpaired, two-tailed Student's t test. ***$p \leq 0.001$; ****$p \leq 0.0001$
(I) Representative images of native BJ, BJ ρ0, and BJ ρ0+HEK293T SIMR fibroblasts immunostained for dsDNA (green) and TOM20 (red) with co-localization indicated (yellow). Images (100X) acquired on a Leica SP8 confocal microscope. Scale bars are 15 μm.
(J) Native BJ and BJ SIMR fibroblasts reprogrammed to iPSCs with TRA-1-60^+ clones counted by microscopy. Data is the mean of biological duplicates. BJ fibroblast control shows the same data used in Figure 3A.
(K) Flow cytometry of pluripotency biomarkers SOX2 and OCT3/4, and fibroblast biomarker CD44. Immunostained samples are shown in color with isotype negative controls in grey. Representative data for native BJ fibroblasts and BJ-iPSCs, and for BJ ρ0+HEK293T-iPSC cells. The native BJ fibroblast and BJ-iPSC data shown here is the same as in Figure 3B.
(L) Representative phase contrast and IF microscopy images of unmodified BJ fibroblast (negative control), BJ-iPSCs (positive control), and three BJ ρ0+HEK293T-iPSC clones immunostained for pluripotency biomarkers SSEA-4 and OCT4. Scale bar is 100 μm.
(M) OCR measurements for ~$1.5x10^4$ native BJ-iPSCs and BJ ρ0+HEK293T-iPSC clones 1, 2, and 4. BJ-iPSC control shows the same data used in Figure 3D. Data are the mean ± SD of four technical replicates. Statistical significance was by unpaired, two-tailed Student's t test. *$p \leq 0.05$
(N) OCR measurements for ~$1.5x10^4$ native NDF, NDF ρ0+NDF, NDF ρ0+WT, and NDF ρ0+MELAS SIMR fibroblasts. Data are the mean ± SD of five technical replicates.
Statistical significance was by unpaired, two-tailed Student's t test. **$p \leq 0.01$; ****$p \leq 0.0001$
(O) RFLP analysis of mtDNA from homoplasmic NDF ρ0+NDF, NDF ρ0+MELAS, and NDF ρ0+WT SIMR fibroblasts, and 1:1 heteroplasmic NDF ρ0+MELAS/WT SIMR fibroblasts. ApaI restriction enzyme cleaves the 634 bp amplicon into 424 bp and 210 bp bands when the MELAS A3243G sequence is present.
(P) Representative phase contrast images (4X) of native NDF, NDF ρ0+NDF, NDF ρ0+MELAS, and NDF ρ0+MELAS/WT cells during reprogramming to iPSCs. Exposure and tint adjusted for subpanel consistency.
(Q) RFLP analysis of mtDNA from 20 independent, 1:1 heteroplasmic NDF ρ0+MELAS/WT-iPSC clones. ApaI restriction enzyme cleaves the 634 bp amplicon into 424 bp and 210 bp bands when the MELAS A3243G sequence is present.
(R) Flow cytometry of MSC biomarkers CD73, CD90, CD105, and a mix of negative MSC biomarkers. Immunostained samples are shown in color with isotype negative controls in grey. BJ-MSC control shows the same data used in Figure 4A. Representative clones for native BJ-MSCs and BJ ρ0+HEK293T-MSCs are shown.
(S) Brightfield microscopy showing native BJ-MSC, BJ ρ0+HEK293T-MSC clones 1, 2, and 4 adhering to plastic at 20X (scale bar, 100 μm) magnifications. BJ-MSC control shows the same data used in Figure 4B.

(T) OCR measurements for ~$1.5x10^4$ native BJ-MSCs and BJ ρ0+HEK293T-MSC clones 1, 2, and 4. BJ-MSC control shows the same data used in Figure 4C. Data are the mean ± SD of three technical replicates. Statistical significance was by unpaired, two-tailed Student's t test. *$p \leq 0.05$
(U) Quantitative phase microscopy of unmodified BJ-MSCs and a 1:1:1 mix of BJ ρ0+HEK293T-MSC clones 1, 2, and 4. BJ-MSC control shows the same data used in Figure 4D. Shown are box-and-whisker Tukey plots with outliers identified. Data was averaged from 77 and 124 cells for native BJ-MSCs and BJ ρ0+HEK293T-MSCs, respectively. Statistical significance was by Welch's T test. *$p \leq 0.05$
(V) T cells were added into native BJ-MSC or BJ ρ0+HEK293T-MSC clone 1, 2, or 4 cultures at 1:2, 1:1, 5:1, and 10:1 T cell: MSC ratios. After 5 days of co-culture, T cell proliferation was measured using a CFSE dye dilution assay by flow cytometry. The data labeled "NS" (no stimulus) denotes T cells without CD3/CD28 bead activation. The data labeled "-ve" (negative) denotes no addition of MSCs to stimulated T cells. The data labeled "+ve" (positive) denotes a 1:1 addition of MDSCs to T cells. Data are the mean ± SD of three technical replicates.
(W) Tri-lineage differentiation of native BJ-MSCs and BJ ρ0+HEK293T-MSC clones 1, 2, and 4. Representative sections were fixed and stained with 1 μM Bodipy 493/503, 1% alizarin red S, and 0.1% Safranin O, respectively. Shown are adipocytes (first row 20X; scale bar 100 μm), osteocytes (second row 20X; 200 μm), and chondrocytes (third row 5X; 500 μm).

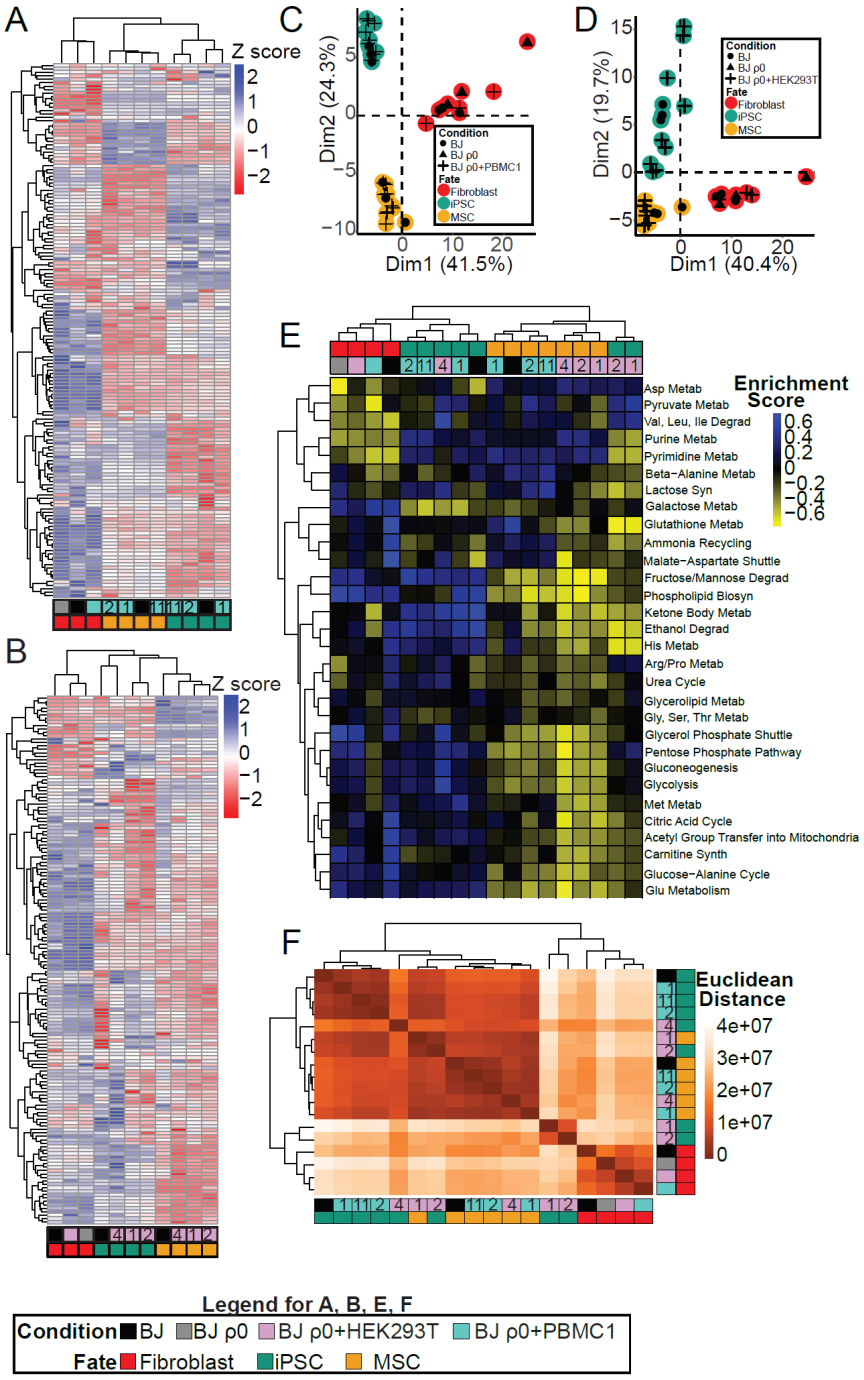

Figure S2. SIMR Metabolome Tracks Mainly with Cell Fate, Related to Figure 5.
(A) Quantification of 154 metabolites in native BJ, BJ ρ0, and BJ ρ0+PBMC1 cells by UHPLC-MS. Z-scores were calculated from the normalized, log transformed abundance of metabolites across averaged samples. Samples were clustered by similarity using an unbiased approach.

(B) Quantification of 154 metabolites in native BJ, BJ ρ0, and BJ ρ0+HEK293T cells by UHPLC-MS. Z-scores were calculated from the normalized, log transformed abundance of metabolites across averaged samples. Samples were clustered by similarity using an unbiased approach.
(C) PCA of normalized metabolite abundance. Colors denote fibroblasts (red), iPSCs (green), and MSCs (yellow), whereas shapes denote native BJ control (•), BJ ρ0 (▲), and BJ ρ0+PBMC1 (+) cells. Scatter plot shows the first (Dim1) and second (Dim2) principal components along the x- and y- axes, respectively.
(D) PCA of normalized metabolite abundance. Colors denote fibroblasts (red), iPSCs (green), and MSCs (yellow), whereas shapes denote native BJ control (•), BJ ρ0 (▲), and BJ ρ0+HEK293T (+) cells. Scatter plot shows the first (Dim1) and second (Dim2) principal components along the x- and y- axes, respectively.
(E) Metabolite set variation analysis (MSVA) indicating metabolite pathway enrichment across averaged samples. Rows indicate independent KEGG metabolic pathways analyzed. Higher MSVA enrichment scores indicate elevated pathway enrichment relative to all samples, lower MSVA enrichment scores indicate reduced pathway enrichment relative to all samples. Samples annotation is by cell fate (top row) and by mtDNA transfer condition (second row). Clone number for BJ ρ0+PBMC1 and BJ ρ0+HEK293T SIMR cells are indicated by a number in the transfer condition row.
(F) Euclidean distance similarity matrix of whole metabolite profiles across all sample comparisons. Heatmap values indicate the Euclidean distance between the two indicated samples (n = 54).

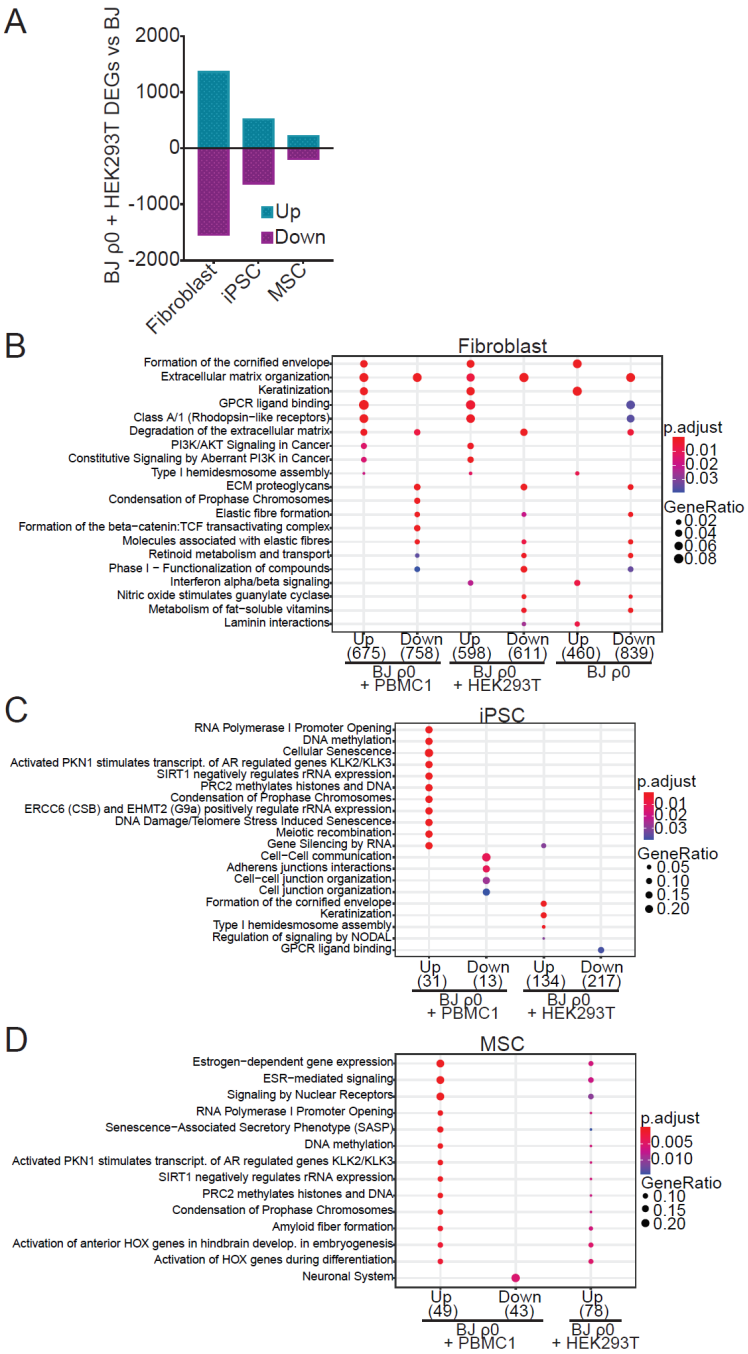

Figure S3. SIMR Fibroblast Transcriptome Homeostasis Reset by Cell Fate Transitions, Related to Figure 5.
(A) Number of DEGs for BJ ρ0+HEK293T cells compared to native BJ cells at fibroblast, iPSC, and MSC fates.
(B) Reactome pathway database overrepresentation analyses (ORA) of BJ ρ0+PBMC1, BJ ρ0+HEK293T, and BJ ρ0 compared to native BJ fibroblasts.

(C) Reactome pathway database ORA of BJ ρ0+PBMC1, BJ ρ0+HEK293T, and BJ ρ0 compared to native BJ iPSCs.
(D) Reactome pathway database ORA of BJ ρ0+PBMC1, BJ ρ0+HEK293T, and BJ ρ0 compared to native BJ MSCs.

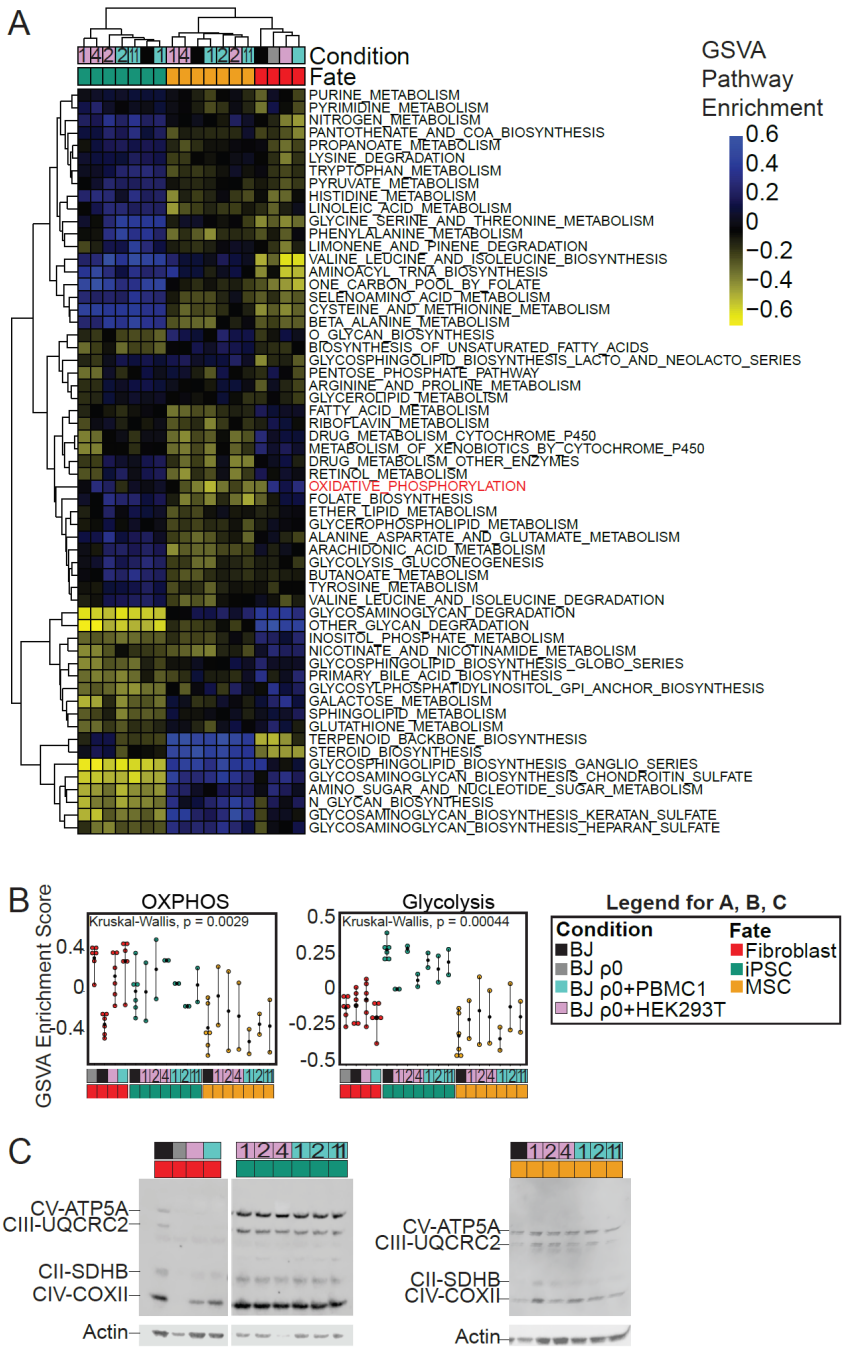

Figure S4. SIMR Cell Pathway Analysis Through Fate Transition, Related to Figure 5.
(A) Heatmap of gene set variation analysis (GSVA) showing enrichments for transcripts that encode metabolic pathways between averaged clones. Rows indicate independent KEGG metabolic pathways analyzed (HSA01100).

(B) Means of individual GSVA scores averaged for all 18 sample and clone fates and conditions (n = 6 for BJ samples; n = 2 for each SIMR clone) for enrichments of oxidative phosphorylation and glycolysis-gluconeogenesis encoding pathway genes.
(C) Immunoblots of ETC complex proteins for native BJ and BJ ρ0 control cells with BJ ρ0+PBMC1 and BJ ρ0+HEK293T SIMR cells at fibroblast, iPSC, and MSC fates.

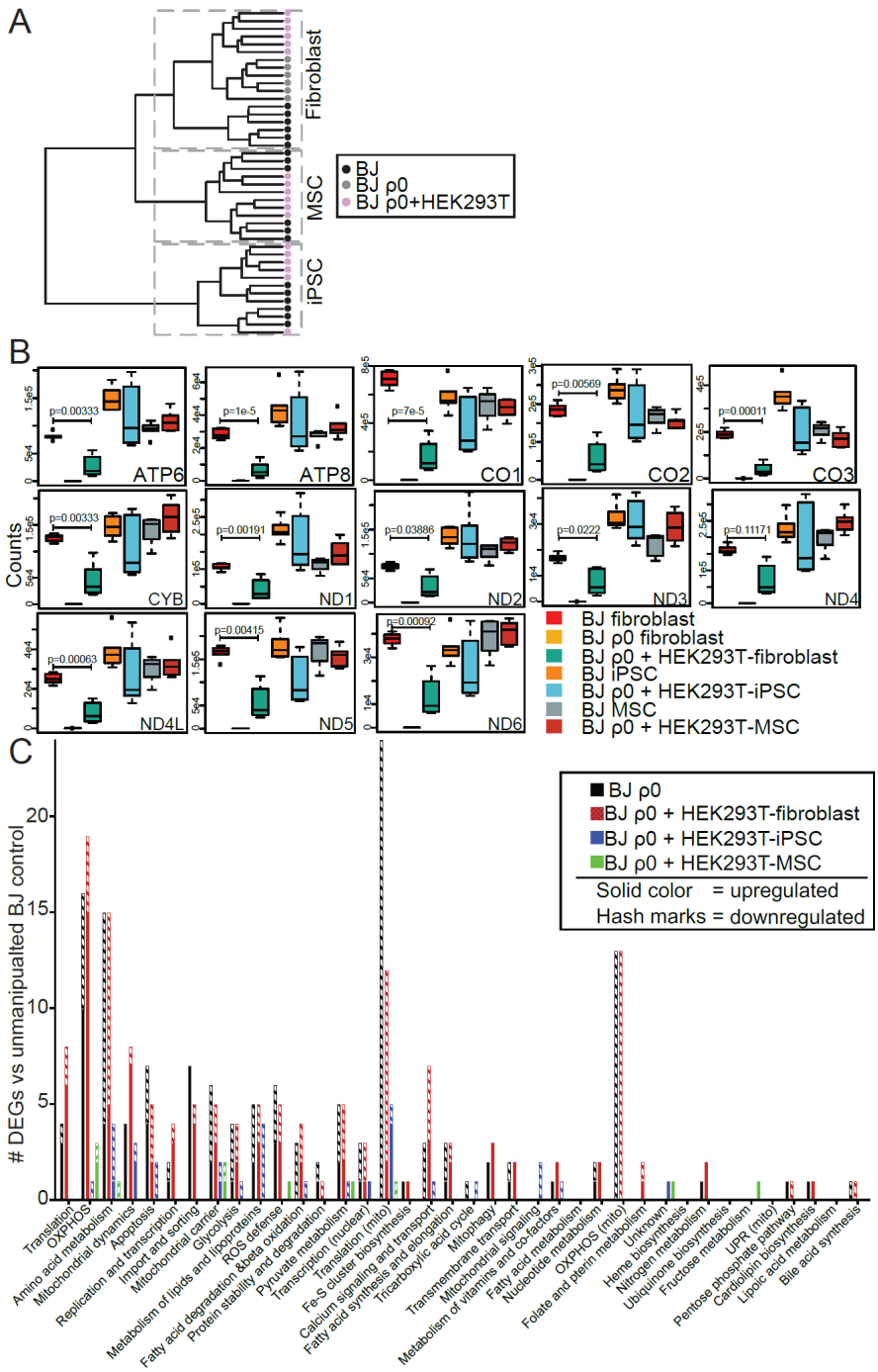

Figure S5. Mitochondrial-Associated Transcriptional Changes, Related to Figure 5.
(A) Hierarchical clustering of MitoCarta 2.0 database genes from native BJ, BJ ρ0, and BJ ρ0+HEK293T cells at fibroblast, iPSC, and MSC fates.

(B) Normalized, batch adjusted read counts shown as box-and-whisker Tukey plots for 13 MitoCarta annotated mtDNA-encoded genes for native BJ, BJ ρ0, and BJ ρ0+HEK293T cells at the fibroblast, iPSC, and MSC fates. Statistical significance was by Welch's T test.
(C) MitoXplorer categorized DEGs for BJ ρ0+HEK293T compared to native BJ cells at the fibroblast, iPSC, and MSC fates divided into the 38 mitochondrial processes.

Chapter 8: Conclusion

Mitochondrial activity is key to the function and fate of mammalian cells and depends upon coordination of the mtDNA and nDNA. Given the bi-genomic composition of the mitochondria, proteins encoded in both the mtDNA and the nDNA must work together in intricate and highly regulated superstructures. Therefore, control over the expression and interactions of the gene products of these two genomes is essential for maintaining mitochondrial respiration and metabolism (Mottis et al., 2019; Quiros et al., 2016). Mutations in the mtDNA that result in loss of function of ETC subunits can cause loss of respiration, aberrant metabolism, and redox stress which can result in disease (Taylor and Turnbull, 2005). Detailed genetic and biochemical experimentation of specific mtDNA sequences in fixed nDNA genetic backgrounds is key to understanding the relationship between the two genomes found in nucleated mammalian cells. It is for this reason that the current limitations in mtDNA gene editing severely restrict our understanding of mtDNA genetics and the relationship between the mtDNA and the nDNA in maintaining cellular metabolism and energetic homeostasis.

The work presented in this thesis represents our efforts to develop the MitoPunch apparatus into a platform for efficient stable mitochondrial transfer to enable tractable studies of mtDNA-nDNA interactions in human cells. While tools that facilitate direct gene editing of the mtDNA with the ease and flexibility that the CRISPR-Cas9 system has enabled for the nDNA are yet to be developed (Patananan et al., 2016), MitoPunch for the first time provides a means to efficiently produce large numbers of SIMR clones with specified mtDNA and nDNA combinations in both transformed and replication-limited, reprogrammable cell types using a wide array of mitochondrial sources. This thesis provides a conceptual framework for mitochondrial transfer as an important tool to study mtDNA-nDNA interactions, a detailed

protocol for constructing the MitoPunch apparatus, and proof of principle studies for the application of MitoPunch in the fields of mitochondrial genetics and tissue engineering.

Mitochondrial metabolism and cell identity

Mitochondria are far more than powerhouses dedicated to producing ATP. The mitochondrial network is a hub of metabolism that generates the organic and inorganic building blocks necessary for cell growth and function (Chen et al., 2016). In addition to providing energy and materials for many cellular processes, the compounds produced in the mitochondria also act as signaling molecules that cue cellular responses to nutrient and environmental stress (Picard et al., 2018). Additionally, many of these metabolites serve as substrates and regulators of key epigenetic marking enzymes, placing mitochondrial function at the nexus of maintaining cell function and fate (Matilainen et al., 2017; Patananan et al., 2018).

In Chapter 2 of this thesis, we review in detail the specific mitochondrial metabolites that contribute to epigenetic regulation of the nuclear genome (Patananan et al., 2018). Among them are compounds that influence levels of DNA methylation and histone acetylation which are key epigenetic marks that maintain the integrity of nuclear gene expression. A growing literature suggests that the integrity of epigenetic patterning is essential to prevent premature cellular aging, and that this patterning depends, at least in part, upon mitochondrial metabolism (Jones et al., 2015; Kane and Sinclair, 2019; Zhang et al., 2018). Additionally, perturbations in the levels of these metabolites can induce phenotypic switching in several cell types and drive differentiation in pluripotent stem cells (Patananan et al., 2018; TeSlaa et al., 2016). Thus, alterations in mitochondrial function caused by mtDNA genotypic and heteroplasmic variation

can have profound effects on cellular function and identity. Such changes in cell fate are of key importance to the fields of pluripotent stem cell maintenance and differentiation, as well as somatic cell reprogramming. We provide a review and meta-analysis of work conducted to measure shifts in mtDNA heteroplasmy when somatic cells are reprogrammed to pluripotency in Chapter 6 of this thesis (Sercel et al., 2021a). Few reports exist measuring changes in heteroplasmy during somatic cell reprogramming, but what has been reported demonstrates that mtDNA heteroplasmy can change dramatically with the selective pressures and genetic bottlenecking that occurs when producing iPSCs. Advances in iPSC technology promise to enable the next generation of personalized and regenerative therapies. Ensuring the integrity of the mtDNA in therapeutic iPSC-derived cells is an underappreciated, but potentially critically important, factor the field must consider.

Studies of the influence of mtDNA sequence and heteroplasmy on mitochondrial metabolism, and, by extension, regulation of the nuclear epigenome, in physiologically relevant isogenic nuclear contexts is severely hindered by the lack of mtDNA editing tools (Patananan et al., 2016). MitoPunch provides an avenue to study the effects of specific mtDNA sequences and heteroplasmy on the metabolism of replication limited, reprogrammable cell types. Moreover, reprogrammed SIMR clones are tractable systems to investigate the contribution of specific mtDNA sequences to cell metabolism, function, and identity in patient-derived, physiologically relevant cell types. Such studies will further our understanding of human development, aging, gene regulation, and tissue engineering by leveraging the models that MitoPunch can generate.

Mitochondrial transfer

Mitochondrial transfer is a rapidly growing field that encompasses several distinct phenomena which are yet to be fully understood. Within the last two decades, the literature has reported mitochondrial trafficking between cells *in vivo* and *in vitro* as an active biological process via several distinct mechanisms (Hayakawa et al., 2016; Kesner et al., 2016; Kitani et al., 2014; Spees et al., 2006). Additionally, genetic evidence of stable mitochondrial transfer from mouse host to mtDNA depleted cancer cells and from canine to a horizontally transmitted tumor implies that cancer cells uptake mitochondria from the tumor microenvironment (Dong et al., 2017; Strakova et al., 2020). These reports together suggest that mitochondrial transfer occurs in physiologic contexts and potentially plays a role in protecting cells from metabolic, oxidative, and other forms of stress. Additionally, cancer cells may upregulate this phenomenon to overcome the challenging tumor microenvironment.

While these studies provide evidence for the phenomenon of cell-to-cell mitochondrial transfer and investigate the mechanisms that influence these transfer events to a limited degree, the field lacks a deep understanding of how to control these transfers or of what, if any, long term effects they have on recipient cells. Despite this, some clinical efforts show beneficial effects of infusing isolated mitochondria into ischemic cardiac tissue on patient outcomes following heart attack (Emani et al., 2017; Shin et al., 2017). Recent reports show cell free mtDNA, and potentially whole mitochondria, are present in human blood and that their levels can increase with stress and other factors (Cushen et al., 2020; Trumpff et al., 2019; Trumpff et al., 2021). It is unclear if these mitochondria are trafficked into cells to aid with stress or serve some other

purpose. The phenomenon of naturally occurring *in vivo* mitochondrial transfer warrants further investigation.

In parallel to this work, effort has been placed on developing tools to facilitate mitochondrial transfer to study mtDNA-nDNA interactions and to model the effects of exogenous mitochondria on cell function. The approaches used to produce clones with specified mtDNA-nDNA include cybridization (Wilkins et al., 2014), microinjection of isolated mitochondria (King and Attardi, 1988), delivery by photothermal nanoblade (Wu et al., 2016), and now MitoPunch (Dawson et al., 2020; Patananan et al., 2020; Sercel et al., 2021b), and all can stably rescue the mtDNA content and respiration of ρ0 cells with ranging technical limitations.

In addition to these techniques to stably rescue ρ0 cells with exogenous mitochondria, the field has developed various means to promote interaction between cells and isolated mitochondria in tissue culture to measure the resulting effects on metabolism and cell function (Caicedo et al., 2015; Kitani et al., 2014; Macheiner et al., 2016). Unfortunately, this area of research suffers from a lack of clarity in objective. Reports describing new approaches to induce isolated mitochondria-recipient cell interactions focus on demonstrating uptake and measuring short term changes to recipient cell function after coincubation with highly concentrated isolated mitochondrial suspensions. However, there are many observations of this occurring without any outside intervention, obviating the need for technology to enable mitochondria-recipient cell interactions. These studies suggest that uptake depends on macropinocytosis (Kitani et al., 2014), but the majority do not investigate the mechanisms underlying the changes in recipient cell metabolism, the long-term effects of these uptake events, or whether recipient cells stably

retain exogenous mtDNA. There are two reports of coincubation producing stable rescue clones from ρ0 cells (Clark and Shay, 1982; Patel et al., 2017), however, the conditions required to produce those rescue clones are almost impossible to achieve with patient-derived tissues, limiting the possible mtDNA-nDNA combinations that can be studied and their *in vivo* relevance. Moreover, little effort is made to represent physiologically relevant levels of cell-free mitochondria in these studies, and the applicability of these findings to *in vivo* responses to isolated mitochondria is unclear. This branch of mitochondrial transfer work would be strengthened by defining more physiologically relevant conditions and questions to investigate the potential implications of the cell-free mitochondria observed in recent animal and human studies.

SIMR clone gene expression and reprogramming

An understudied question in this space is whether respiration-incompetent ρ0 recipient cells, which are known to show altered transcription and metabolism, regain normal gene expression and metabolic function after stably integrating exogenous mtDNA. One report looking at nDNA methylation patterns in transformed cybrids suggests that the former ρ0 cells did not recover the parental epigenetic patterning (Smiraglia et al., 2008). Chapter 7 of this thesis investigates this phenomenon in SIMR clones generated from Hayflick-limited cells that we reprogrammed to IPSC and further differentiated to mesenchymal stem cells by measuring the whole transcriptome at each cell fate (Patananan et al., 2020). We found that SIMR fibroblasts shared more transcriptomic similarity with ρ0 cells than with the unmanipulated matched parental control as measured by differential gene expression. In particular, mtDNA encoded genes were expressed at lower levels in SIMR fibroblasts than in the parental fibroblast lines.

However, following reprogramming and differentiation, the number of differentially expressed genes among the control and SIMR groups was dramatically reduced, and the respiratory profiles became insignificantly different.

This finding is of critical importance to the field of mtDNA genetics as much work has been done using cybrid models of mtDNA-nDNA interactions and diseases caused by mtDNA mutants (Kopinski et al., 2019; Picard et al., 2014; Wilkins et al., 2014). As previously discussed, the fact that the mitochondria are composed of gene products from two genomes necessitates precise coordination of transcription and translation to ensure proper mitochondrial function. If we assume that SIMR and cybrid lines share similar transcriptomic deficiencies, as evidenced by prior work in the literature (Smiraglia et al., 2008) and the findings from Chapter 7, then we must consider the possibility that investigations of respiration, metabolism, transcription, and epigenetics in mtDNA mutant and heteroplasmic cybrid lines suffer from artifacts caused by using previously $\rho 0$ starting material. We observed recovery of SIMR cell transcription following somatic cell reprogramming and differentiation, and it stands to reason that studies of specific mtDNA-nDNA combinations using reprogrammed and differentiated SIMR lines bear more physiological relevance to the interactions between these two genomes than can be achieved using cybrid or SIMR lines that have not undergone fate transition. Therefore, it is critical to generate models of specific mtDNA-nDNA in reprogrammable cells, and MitoPunch is uniquely suited to produce such lines for these studies.

A key finding from the work in Chapter 7 of this thesis is that we were unable to successfully reprogram SIMR fibroblasts generated using homoplasmic mutant mtDNA-bearing

mitochondria. We attempted to reprogram SIMR fibroblasts containing heteroplasmic mutant mtDNA which resulted in viable iPSC clones, however, all recovered clones were homoplasmic wildtype. This is not likely to be a result of the mtDNA mutations themselves inhibiting reprogramming as many reports show successful reprogramming of primary human cells bearing mtDNA mutations to iPSC fate as discussed in Chapter 6 of this thesis (Sercel et al., 2021a). Moreover, our lab has recently successfully reprogrammed patient-derived mtDNA mutant fibroblasts using the same methods we employed while attempting to reprogram mtDNA mutant SIMR fibroblasts (Data not shown). Our results suggest that there is something unique about mtDNA mutant SIMR fibroblasts that renders them unfit for reprogramming.

We present two hypotheses for this observation that depend upon the fact that somatic cell reprogramming requires a 'burst' of mitochondrial OXPHOS as an early step of the reprogramming process (Hawkins et al., 2016; Kida et al., 2015). This burst is thought to generate the ATP and metabolites necessary for remodeling the nuclear chromatin to facilitate fate transition. First, we hypothesize that the mtDNA depletion process disrupts key mitonuclear communication pathways that make somatic cell reprogramming more difficult for cells to achieve. Under this model, wildtype SIMR cells can overcome the disrupted mitonuclear communication induced by prior mtDNA depletion and generate iPSCs because they contain functional mtDNA. Also, patient-derived mtDNA mutant cells can initiate reprogramming despite their reduced mitochondrial function because their mitonuclear communication is unchanged by mtDNA depletion. mtDNA mutant SIMR cells, which suffer from impaired mitochondrial function from mtDNA mutations and mitonuclear coordination caused by the mtDNA depletion process, are unable to accomplish the respiratory burst and fail to generate

iPSCs. This reasoning is supported by our results showing that we can produce iPSCs from heteroplasmic SIMR fibroblasts, however, we only recover iPSC clones that contain homoplasmic wildtype mtDNA. We hypothesize that the mutant mtDNA is selected against during the reprogramming process as it is unable to provide sufficient respiration to facilitate reprograming after mtDNA depletion.

As an alternative, we hypothesize that the foreign mutant mtDNA is rejected by the cell due to mitonuclear incompatibility resulting from the fact that the two genomes were not co-evolved. Under this model, the evolved coordination of the mtDNA and the nDNA is the primary driver of the oxidative burst that enables reprogramming. Wildtype SIMR fibroblasts are sufficiently fit to compensate for the inefficiencies caused by mtDNA-nDNA mismatch, and mutant mtDNA-containing patient fibroblasts can overcome the metabolic demands of reprogramming because their mitonuclear interactions are established through evolutionary time. However, the combined deficiencies of respiration incompetent mtDNA and mitonuclear mismatch render reprogramming impossible. Ongoing work in the Teitell laboratory aims to address this question and will provide key insights into the reliance of reprogramming on mitonuclear co-evolution and mitochondrial function.

Concluding remarks

The field of mitochondrial transfer is young but rapidly growing and aims to elucidate mtDNA-nDNA interactions by generating novel pairings of nuclear and mitochondrial genomes. This thesis presents MitoPunch as an enabling technology to develop tractable models of mitonuclear communication in physiologically relevant cell types that are challenging or

impossible to achieve with current methodology. While MitoPunch is uniquely suited to generate such cell systems, it is limited by requiring ρ0 recipient cell starting material unless antibiotic resistant mtDNA sequences are delivered to recipient cells as shown in Chapter 5 of this thesis (Dawson et al., 2020). Future advances in this field using mitochondrial transfer techniques will require the means to reprogram mtDNA mutant SIMR fibroblasts to produce physiological models of mtDNA diseases in relevant cell models, or the capability to efficiently replace existing mtDNA species in cells with a wide range of exogenous mtDNA without mtDNA depletion. Further investigation into the nature of mitonuclear communication and the development of tools to manipulate it will be key to fully understanding the contribution of our second genome to human life and generating future therapies for presently incurable mitochondrial diseases.

References

Caicedo, A., Fritz, V., Brondello, J.M., Ayala, M., Dennemont, I., Abdellaoui, N., de Fraipont, F., Moisan, A., Prouteau, C.A., Boukhaddaoui, H., et al. (2015). MitoCeption as a new tool to assess the effects of mesenchymal stem/stromal cell mitochondria on cancer cell metabolism and function. Sci Rep *5*, 9073.

Chen, W.W., Freinkman, E., Wang, T., Birsoy, K., and Sabatini, D.M. (2016). Absolute Quantification of Matrix Metabolites Reveals the Dynamics of Mitochondrial Metabolism. Cell *166*, 1324-1337 e1311.

Clark, M.A., and Shay, J.W. (1982). Mitochondrial transformation of mammalian cells. Nature *295*, 605-607.

Cushen, S.C., Sprouse, M.L., Blessing, A., Sun, J., Jarvis, S.S., Okada, Y., Fu, Q., Romero, S.A., Phillips, N.R., and Goulopoulou, S. (2020). Cell-free mitochondrial DNA increases in maternal circulation during healthy pregnancy: a prospective, longitudinal study. Am J Physiol Regul Integr Comp Physiol *318*, R445-R452.

Dawson, E.R., Patananan, A.N., Sercel, A.J., and Teitell, M.A. (2020). Stable retention of chloramphenicol-resistant mtDNA to rescue metabolically impaired cells. In Sci Rep (Springer Science and Business Media LLC).

Dong, L.F., Kovarova, J., Bajzikova, M., Bezawork-Geleta, A., Svec, D., Endaya, B., Sachaphibulkij, K., Coelho, A.R., Sebkova, N., Ruzickova, A., et al. (2017). Horizontal transfer of whole mitochondria restores tumorigenic potential in mitochondrial DNA-deficient cancer cells. Elife *6*.

Emani, S.M., Piekarski, B.L., Harrild, D., Del Nido, P.J., and McCully, J.D. (2017). Autologous mitochondrial transplantation for dysfunction after ischemia-reperfusion injury. The Journal of Thoracic and Cardiovascular Surgery *154*, 286-289.

Hawkins, K.E., Joy, S., Delhove, J.M., Kotiadis, V.N., Fernandez, E., Fitzpatrick, L.M., Whiteford, J.R., King, P.J., Bolanos, J.P., Duchen, M.R., et al. (2016). NRF2 Orchestrates the Metabolic Shift during Induced Pluripotent Stem Cell Reprogramming. Cell Rep *14*, 1883-1891.

Hayakawa, K., Esposito, E., Wang, X., Terasaki, Y., Liu, Y., Xing, C., Ji, X., and Lo, E.H. (2016). Transfer of mitochondria from astrocytes to neurons after stroke. Nature *535*, 551-555.

Jones, M.J., Goodman, S.J., and Kobor, M.S. (2015). DNA methylation and healthy human aging. Aging Cell *14*, 924-932.

Kane, A.E., and Sinclair, D.A. (2019). Epigenetic changes during aging and their reprogramming potential. Crit Rev Biochem Mol Biol *54*, 61-83.

Kesner, E.E., Saada-Reich, A., and Lorberboum-Galski, H. (2016). Characteristics of Mitochondrial Transformation into Human Cells. In Sci Rep (Springer Science and Business Media LLC), p. 26057.

Kida, Y.S., Kawamura, T., Wei, Z., Sogo, T., Jacinto, S., Shigeno, A., Kushige, H., Yoshihara, E., Liddle, C., Ecker, J.R., et al. (2015). ERRs Mediate a Metabolic Switch Required for Somatic Cell Reprogramming to Pluripotency. Cell Stem Cell *16*, 547-555.

King, M.P., and Attardi, G. (1988). Injection of mitochondria into human cells leads to a rapid replacement of the endogenous mitochondrial DNA. Cell *52*, 811-819.

Kitani, T., Kami, D., Matoba, S., and Gojo, S. (2014). Internalization of isolated functional mitochondria: involvement of macropinocytosis. J Cell Mol Med *18*, 1694-1703.

Kopinski, P.K., Janssen, K.A., Schaefer, P.M., Trefely, S., Perry, C.E., Potluri, P., Tintos-Hernandez, J.A., Singh, L.N., Karch, K.R., Campbell, S.L., et al. (2019). Regulation of nuclear epigenome by mitochondrial DNA heteroplasmy. Proc Natl Acad Sci U S A *116*, 16028-16035.

Macheiner, T., Fengler, V.H.I., Agreiter, M., Eisenberg, T., Madeo, F., Kolb, D., Huppertz, B., Ackbar, R., and Sargsyan, K. (2016). Magnetomitotransfer: An efficient way for direct mitochondria transfer into cultured human cells. In Sci Rep (Springer Science and Business Media LLC), p. 35571.

Matilainen, O., Quiros, P.M., and Auwerx, J. (2017). Mitochondria and Epigenetics - Crosstalk in Homeostasis and Stress. Trends Cell Biol *27*, 453-463.

Mottis, A., Herzig, S., and Auwerx, J. (2019). Mitocellular communication: Shaping health and disease. Science *366*, 827-832.

Patananan, A.N., Sercel, A.J., and Teitell, M.A. (2018). More than a powerplant: the influence of mitochondrial transfer on the epigenome. Curr Opin Physiol *3*, 16-24.

Patananan, A.N., Sercel, A.J., Wu, T.H., Ahsan, F.M., Torres, A., Jr., Kennedy, S.A.L., Vandiver, A., Collier, A.J., Mehrabi, A., Van Lew, J., et al. (2020). Pressure-Driven Mitochondrial Transfer Pipeline Generates Mammalian Cells of Desired Genetic Combinations and Fates. Cell Rep *33*, 108562.

Patananan, A.N., Wu, T.H., Chiou, P.Y., and Teitell, M.A. (2016). Modifying the Mitochondrial Genome. Cell Metab *23*, 785-796.

Patel, D., Rorbach, J., Downes, K., Szukszto, M.J., Pekalski, M.L., and Minczuk, M. (2017). Macropinocytic entry of isolated mitochondria in epidermal growth factor-activated human osteosarcoma cells. In Sci Rep (Springer Science and Business Media LLC).

Picard, M., McEwen, B.S., Epel, E.S., and Sandi, C. (2018). An energetic view of stress: Focus on mitochondria. Front Neuroendocrinol *49*, 72-85.

Picard, M., Zhang, J., Hancock, S., Derbeneva, O., Golhar, R., Golik, P., O'Hearn, S., Levy, S., Potluri, P., Lvova, M., et al. (2014). Progressive increase in mtDNA 3243A>G heteroplasmy causes abrupt transcriptional reprogramming. Proc Natl Acad Sci U S A *111*, E4033-4042.

Quiros, P.M., Mottis, A., and Auwerx, J. (2016). Mitonuclear communication in homeostasis and stress. Nat Rev Mol Cell Biol *17*, 213-226.

Sercel, A.J., Carlson, N.M., Patananan, A.N., and Teitell, M.A. (2021a). Mitochondrial DNA Dynamics in Reprogramming to Pluripotency. Trends Cell Biol *31*, 311-323.

Sercel, A.J., Patananan, A.N., Man, T., Wu, T.H., Yu, A.K., Guyot, G.W., Rabizadeh, S., Niazi, K.R., Chiou, P.Y., and Teitell, M.A. (2021b). Stable transplantation of human mitochondrial DNA by high-throughput, pressurized isolated mitochondrial delivery. Elife *10*.

Shin, B., Cowan, D.B., Emani, S.M., Del Nido, P.J., and McCully, J.D. (2017). Mitochondrial Transplantation in Myocardial Ischemia and Reperfusion Injury. (Springer International Publishing), pp. 595-619.

Smiraglia, D.J., Kulawiec, M., Bistulfi, G.L., Gupta, S.G., and Singh, K.K. (2008). A novel role for mitochondria in regulating epigenetic modification in the nucleus. Cancer Biol Ther *7*, 1182-1190.

Spees, J.L., Olson, S.D., Whitney, M.J., and Prockop, D.J. (2006). Mitochondrial transfer between cells can rescue aerobic respiration. Proc Natl Acad Sci U S A *103*, 1283-1288.

Strakova, A., Nicholls, T.J., Baez-Ortega, A., Ni Leathlobhair, M., Sampson, A.T., Hughes, K., Bolton, I.A.G., Gori, K., Wang, J., Airikkala-Otter, I., et al. (2020). Recurrent horizontal transfer identifies mitochondrial positive selection in a transmissible cancer. Nat Commun *11*, 3059.

Taylor, R.W., and Turnbull, D.M. (2005). Mitochondrial DNA mutations in human disease. Nat Rev Genet *6*, 389-402.

TeSlaa, T., Chaikovsky, A.C., Lipchina, I., Escobar, S.L., Hochedlinger, K., Huang, J., Graeber, T.G., Braas, D., and Teitell, M.A. (2016). alpha-Ketoglutarate Accelerates the Initial Differentiation of Primed Human Pluripotent Stem Cells. Cell Metab *24*, 485-493.

Trumpff, C., Marsland, A.L., Basualto-Alarcon, C., Martin, J.L., Carroll, J.E., Sturm, G., Vincent, A.E., Mosharov, E.V., Gu, Z., Kaufman, B.A., et al. (2019). Acute psychological stress increases serum circulating cell-free mitochondrial DNA. Psychoneuroendocrinology *106*, 268-276.

Trumpff, C., Michelson, J., Lagranha, C.J., Taleon, V., Karan, K.R., Sturm, G., Lindqvist, D., Fernstrom, J., Moser, D., Kaufman, B.A., et al. (2021). Stress and circulating cell-free mitochondrial DNA: A systematic review of human studies, physiological considerations, and technical recommendations. Mitochondrion *59*, 225-245.

Wilkins, H.M., Carl, S.M., and Swerdlow, R.H. (2014). Cytoplasmic hybrid (cybrid) cell lines as a practical model for mitochondriopathies. Redox Biol *2*, 619-631.

Wu, T.H., Sagullo, E., Case, D., Zheng, X., Li, Y., Hong, J.S., TeSlaa, T., Patananan, A.N., McCaffery, J.M., Niazi, K., et al. (2016). Mitochondrial Transfer by Photothermal Nanoblade Restores Metabolite Profile in Mammalian Cells. Cell Metab *23*, 921-929.

Zhang, H., Menzies, K.J., and Auwerx, J. (2018). The role of mitochondria in stem cell fate and aging. Development *145*.